# The Institute of Paper Science and Technology

Atlanta, Georgia

## Doctor's Dissertation

**The Role of Carbon Dioxide in the Combustion of Kraft Black Liquor Char**

**Stacy Ray Lee**

**November, 1993**

# THE ROLE OF CARBON DIOXIDE IN THE COMBUSTION OF KRAFT BLACK LIQUOR CHAR

A Thesis Submitted by

Stacy Ray Lee

B.S., 1988, North Carolina State University

M.S., 1990, Institute of Paper Science and Technology

in partial fulfillment of the requirements
of the Institute of Paper Science and Technology
for the degree of Doctor of Philosophy,
Atlanta, Georgia



November 22, 1993

TABLE OF CONTENTS

LIST OF FIGURES

LIST OF TABLES

## ABSTRACT

The $CO_2$ gasification rate of kraft black liquor char was studied using a fixed bed reactor at temperatures of 600°C, 700°C, and 800°C. The rate and the activation energy compared well to rate and activation energies reported previously from thermogravimetric measurements of kraft char gasification. Mass transfer limitations on the observed rate were determined to be negligible by changing both carrier gas and flowrates. Application of the rate derived from the fixed bed reactor to a recovery furnace char bed at typical operating conditions predicts that the rate of $CO_2$ gasification on the bed is mass transfer controlled at temperatures as low as 850°C.

A study of two distinct procedures for preheating kraft black liquor char prior to heterogeneous reaction indicated that the elemental composition of kraft black liquor char is dependent on the devolatilization temperature. Heating partially devolatilized black liquor char to various temperatures (600°C, 700°C, or 800°C) resulted in temperature dependency for C, H, O, and S char compositions. In contrast, heating partially devolatilized black liquor char to 950°C and cooling down to a specified temperature (600°C, 700°C, or 800°C) resulted in no composition change with cool down temperature. A comparison of gasification rates with $CO_2$ for chars prepared according to the two methods indicated a difference in rates, frequency factors, and activation energies.

The oxidation rate of kraft black liquor char in $O_2$ was studied using a fixed bed reactor at 700°C. The observed rate was controlled by film mass transfer. Based on material balances around the gas stream and char bed, the concentrations of CO, $CO_2$, and $O_2$ in the product gas were lower than expected. This was shown by material balances on oxygen, carbon, sulfur, sodium, and hydrogen to be a result of $O_2$ and $CO_2$ consuming reactions in the exhaust line.

The combination of oxidation and gasification of kraft black liquor char was studied using the same fixed bed reactor at 700°C. The combination $CO_2$ gasification and $O_2$ combustion results suggest

that the rate is not equivalent to the sum of the individual rates. Product stream concentration profiles for CO and $CO_2$ indicated that a portion of the CO from $CO_2$ gasification reacted with $O_2$ to form $CO_2$. This conversion was represented by $\chi$. Oxygen, carbon, sulfur, and sodium balances implied that $O_2$ and $CO_2$ were consumed in the exhaust line.

The combined rate of oxidation/gasification can be expressed with the following rate expression:

$$R_C = R_{O2} + (1-\chi)R_{CO2}$$

where $R_C$ = total carbon depletion rate,
$R_{O2}$ = reaction rate for oxidation,
$R_{CO2}$ = reaction rate for gasification, and
$\chi$ = experimental conversion parameter.

Experimental results compared well to the calculated values.

The bulk density and organic carbon concentration of kraft black liquor char during the char burning stage of combustion were determined following the completion of devolatilization and gasification of a packed bed of char particles. The specific volume of char was also determined from single particle swelling experiments in various gas atmospheres, temperatures, and velocities. The organic carbon concentration in kraft char averaged 7.8-12.5 $kg/m^3$ and was independent of fractional burnout of organic carbon at burnout levels greater than 10%. The bulk density of char went through a minimum value of 25 $kg/m^3$ at 10% conversion of organic carbon and gradually increased as the organic carbon was depleted. The specific volume was found to be independent of the heating flux to the char particle and dependent on temperature. Particles burned in an atmosphere of $O_2$ had higher specific volumes than particles gasified or pyrolyzed in $CO_2$ or CO. In each gas environment, the specific volume stabilized as the experimental residence time exceeded 10-15 seconds for the single particle experiments.

# INTRODUCTION

The kraft recovery cycle has contributed to the economic success of the kraft pulping process. In the kraft pulping process, a solution of NaOH and $Na_2S$ is mixed with wood chips at an elevated pressure and temperature resulting in the degradation of lignin compounds and the liberation of cellulosic and hemicellulosic fibers. The dissolved lignin, degraded carbohydrates, and residual pulping chemicals, recovered as weak black liquor (12-15% solids), are washed from the wood pulp and concentrated in multiple effect evaporators. The concentrated black liquor, known as strong black liquor (65-75% solids), is burned in a Tomlinson recovery furnace. The recovery furnace is a multipurpose reactor which evaporates the remaining water in the concentrated black liquor, disposes of the organic waste through combustion, recovers the spent pulping chemicals (inorganics), and recovers energy generated during combustion. The energy generated during combustion is used as steam and electricity throughout an integrated pulp and paper mill. The spent pulping chemicals are discharged from the furnace as a molten smelt that flows freely from the bottom of the furnace. Pulping chemicals are formed by dissolving the smelt and processing the product through causticizing and calcining stages.

Strong black liquor burns in air in three stages known as drying, devolatilization, and char burning.[1-3] Drying involves the evaporation of most of the water present in black liquor. During devolatilization the organic compounds in black liquor solids are thermally degraded to yield combustible gases and residual char. This black liquor char (BLC) is a black, porous, and friable material consisting primarily of organic carbon and the inorganic salts $Na_2CO_3$, $Na_2SO_4$, and $Na_2S$. Approximately one-half of the carbon and most of the sodium contained in the incoming black liquor are found in the BLC.[4] On a molar basis, carbon is the dominant species and excess reactant in the BLC.

Char burning consists of heterogeneous reactions that can occur either in-flight or on the char bed in which the residual carbon is oxidized to CO and $CO_2$. During char burning, the primary oxidizer is $O_2$

in the combustion air. The $O_2$ depletes the carbon in the char through direct oxidation and through the sulfate/sulfide cycle.[2,4,5] Blackwell and King[6] have reported $O_2$ concentrations from 2 to 4% immediately above the bed, and from 14-18% at a height of twenty to thirty inches above the bed. The low $O_2$ concentrations next to the char bed suggest that other oxidizer species such as $CO_2$ and $H_2O$ may play an important role in carbon oxidation. This is supported by results from a recent effort in three-dimensional mathematical modeling of the kraft recovery furnace by Grace *et al.*[7] Addition of the $CO_2$ and $H_2O$ gasification reactions to the char bed portion of the model altered the predicted result from one in which there was substantial buildup of carbon on the bed to one where the carbon burning rate was approximately equivalent to the rate of the carbon reaching the bed.

Several researchers have invested many efforts into understanding the chemistry and kinetics of kraft BLC combustion. Attempts at developing this understanding have involved direct measurements within and above the furnace char bed. However, direct measurements are difficult to obtain because of the high temperature and corrosive nature of the combustion zone. In addition, assigning a given measurement from *in situ* sampling of a furnace to a specific reaction is questionable considering the complex and simultaneous occurrences of drying, devolatilization, char burning, and smelt reaction. Also, flue gas concentrations are not always dependable for predicting char bed behavior because of interference in gas concentration by secondary reactions in the region between the char bed and point of measurement.

A more fundamental understanding of the kraft recovery process has been gained through laboratory studies. The greatest advantage of the laboratory studies is the ability to isolate specific combustion processes. Research has resulted in an understanding of several specific parts of kraft BLC combustion. For example, areas of research at IPST have included single droplet combustion,[8] pyrolysis studies,[9] char combustion kinetics,[2,4,5,10-16] sulfur release mechanisms,[17] fume deposition mechanisms,[18,19]

black liquor spray studies,[20,21] measurement of $CO/CO_2$ concentrations and temperature with FTIR,[22,23] $NO_x$ destruction mechanisms,[24] and $NO_x$ emission mechanism.[25]

Despite the work which has already been accomplished, many areas of kraft black liquor combustion are not well understood. The consumption of char carbon on the char bed is a complicated process which is not fully understood. As noted earlier, carbon is consumed on the char bed through combustion with $O_2$, gasification with $H_2O$ and $CO_2$, and depletion through the sulfate/sulfide cycle.[2,4,5] Kinetic rate data for many of these individual processes are available, however, an understanding of the interaction between these reactions is not currently available. More specifically, the relationship between $CO_2$, $O_2$, and Char-C is not completely understood.

The general goal of this thesis was to gain a better understanding of the role $CO_2$ has in the combustion of kraft BLC. The first specific objective of the thesis was to determine the inherent kinetics of the $CO_2$ gasification of kraft black liquor char using a fixed bed reactor to verify earlier published results using thermogravimetric analysis. The second objective was to determine the transition temperature where the $CO_2$ gasification reaction goes from kinetic control to mass transfer control. The final objective was to determine if the combination $CO_2$ gasification and $O_2$ combustion of kraft black liquor char was equivalent to the sum of the individual rates and to develop a rate expression for this reaction.

# BACKGROUND

The following literature review will provide general information regarding kraft black liquor and coal combustion that pertains to $CO_2$ gasification, $O_2$ combustion, and the interaction of $CO_2$ and $O_2$ in heterogeneous combustion. The characteristics of kraft black liquor combustion, drying, devolatilization, char burning, and inorganic smelt reactions, will be discussed briefly. The BLC burning stage will be discussed in greater detail with an emphasis on $O_2$ combustion and $CO_2$ gasification studies. In addition, alkali-catalyzed $CO_2$ gasification of coal char will be reviewed because it provides a good explanation of some of the results found in this study. Finally, the studies of combination oxidation/gasification of kraft BLC will be reviewed.

Appendix I contains a glossary of terms associated with the processes of BLC combustion as used in this discussion.

## KRAFT BLACK LIQUOR CHAR COMBUSTION

As noted earlier, laboratory experiments have contributed significantly to the understanding of black liquor combustion processes and chemistry. At Abo Akademi[1] and the Institute of Paper Science and Technology (IPST),[8,9] single droplet combustion in laboratory reactors was used to determine the stages of black liquor combustion. These studies concluded that black liquor drop combustion occurred in four stages characterized as drying, devolatilization, char burning, and inorganic smelt reactions. Several researchers have expanded upon this initial research to provide a more comprehensive understanding of black liquor combustion, through the use of single particle reactors (SPR), thermogravimetric analysis (TGA), and fixed bed reactors.

Drying

The drying stage of black liquor drop combustion is a complex process which occurs predominantly in-flight. Hupa *et al.*[1] studied drop drying in a radiant environment at 800°C. Drops with an initial diameter of 1-2 mm dried in 1-2 seconds, indicating that drying times were linearly related to initial drop diameter. The drop diameter increased slightly within the first few tenths of a second. As the drop continued to dry, the production of water vapor caused the drop to inflate and rupture, resulting in a period of rapid swelling and shrinking. Hupa *et al.*[1] noted that the end of the drying stage was marked by the appearance of a bright yellow diffusion flame. The heat transferred to the drop evaporates the water and raises the temperature of the drop. Once the black liquor solids are at pyrolysis temperature, volatiles evolution starts.

Devolatilization

The black liquor devolatilization stage is characterized by rapid particle swelling, the appearance and disappearance of a surrounding yellow diffusion flame, volatiles' evolution, and a continuously increasing particle temperature. As the black liquor approaches the end of drying and reaches approximately 200°C, organic components of the black liquor begin to decompose and gas phase volatiles are released. The gas evolution is most predominant as the particle temperature is increased from 250°C to 500°C. Frederick[26] noted that the escaping volatiles ignite and form a visible flame around the swelling particle if the temperature of the gaseous environment is above 550°C and the $O_2$ content is greater than 10%. Noopila and Hupa[27] noted that extinction of the visible flame is commonly used to mark the end of the devolatilization stage.

Hupa *et al.*[1] and Crane[28] found that the bulk gas temperature had little effect on the time required for volatilization. According to Hupa *et al.*,[1] the lack of interaction between the reactor temperature and the volatilization rate was due to the burning of volatiles in an envelope around the particle. This reaction temperature was determined by this phenomena regardless of the bulk temperature. Crane[28] noted a greater increase in the rates of volatilization with increasing oxygen which is consistent with Hupa *et al.*'s observations. Adams and Frederick[3] noted that the duration of the devolatilization stage depends primarily on heating rate and the volatiles' yield.

Swelling During Devolatilization

Spent pulping liquor droplets characteristically swell extensively during combustion.[29-33] Frederick, Noopila, and Hupa[31] summarized individual black liquor droplet swelling as follows: The droplet swells slightly as it enters the furnace, but then the diameter remains nearly constant for the remainder of the drying stage. During devolatilization, the droplet swells rapidly to a maximum value. Maximum swelling coincides with the end of devolatilization. In the char burning stage, the droplet diameter decreases as char is converted to gases; only a smelt bead remains at the end of this stage.

Traditionally, the extent of swelling has been quantified by a swelling factor or by a specific swollen volume. Frederick *et al.*[31] suggested that the swelling factor, defined as the ratio of the diameter of a swollen particle to its initial diameter, is commonly used when referring to swelling during drying. In addition, specific swollen volume, the maximum volume achieved by the droplet during swelling divided by the initial dry solids mass of the droplet, is used when referring to swelling during devolatilization.

Miller[9] investigated the swelling of kraft black liquor during the drying and devolatilization stages of combustion. The effect of process variables such as pyrolysis temperature, solids content,

heating rate, and particle size were investigated. Black liquor particles were heated by a hot flowing $N_2$ gas stream. For the investigated range of 300-900°C, maximum swollen volume occurred at a temperature of 500°C. The period of black liquor swelling corresponded to the evolution of pyrolysis gases; however, there was no correlation found between the amount of pyrolysis gases evolved and the change in char volume. The initial solids content of black liquor had a small influence on the swelling of black liquor (liquors below 80% initial solids content swelled more than liquors above 85% solids). The heating rate was found to affect the rate of swelling but not the final volume. Initial particle size (1-4mm in diameter) had no effect on the swollen volume per unit particle weight.

Frederick *et al.*[31] also studied swelling during drying and devolatilization. Swelling during drying was found to be insensitive to furnace conditions and droplet size. Swelling during drying was, on average, constant for all liquors for which data were available. Although swelling during devolatilization was clearly liquor dependent, this swelling was not dependent on droplet size or, for two of the three liquors measured, on the initial dry solids content. Under otherwise identical conditions, droplets swelled to approximately the same extent in air or high concentrations of $CO_2$ or $H_2O$ vapor in $N_2$ as noted in Table 1. Swelling was greater in $N_2$ and greatest at low $O_2$ concentrations in $N_2$. The enhanced swelling at low oxygen content was not discussed.

Frederick *et al.*[31] stated that low-temperature swelling measurements (400-500°C) were not relevant when dealing with recovery boiler combustion problems. For example, analysis showed that there was no correlation between the swelling measurements at 420°C and those made at recovery furnace temperatures (800°C). Similar data at 700°C and 800°C correlated well with each other. Therefore, swelling measurements should be made at temperatures representative of actual furnace conditions. Frederick *et al.*[31] noted that swelling decreases with increasing furnace temperatures, over the range

600-900°C, for three different liquors. They concluded that droplets swell less at the higher temperatures encountered in recovery furnaces.

**Table 1.** The Effect of Gas Atmosphere on the Swelling of Black Liquor Droplets at 800°C for a Softwood Kraft Liquor.[31]

| Gas Composition | Swollen Volume,[31] ($cm^3/g$) | Bulk Density for a Bed Void Fraction of 0.40, ($kg/m^3$) |
|---|---|---|
| $N_2$ | 100-166 | 3.6-6.0 |
| 4-12% $O_2$/88-96% $N_2$ | 113-355 | 1.7-5.3 |
| 21% $O_2$/79% $N_2$ | 45-87 | 6.9-13.3 |
| 20% $CO_2$/80% $N_2$ | 39-47 | 12.8-15.4 |
| 20% $H_2O$/80% $N_2$ | 41-81 | 7.4-14.6 |

Char Burning

Char is the solid product of the devolatilization stage. Kraft BLC is a black, porous, and friable material consisting primarily of organic carbon and the inorganic salts $Na_2CO_3$, $Na_2SO_4$, and $Na_2S$. Approximately one-half of the carbon and most of the sodium contained in the incoming black liquor are found in the BLC.[4] The specific composition of the chars used in this study will be presented later.

Hupa *et al.*[1] identified the char burning stage as the longest stage of black liquor combustion which extends from extinction of the volatiles' flame to the sudden collapse of the residue into a molten smelt bead. The char burning occurs as heterogeneous reactions in which the residual carbon is oxidized and the inorganics are reduced and coalesced. Char burning can occur either in-flight or on the char bed.

Frederick *et al.*[31] noted that liquor particles contracted during char burning. The particles shrink as carbon at the surface is burned away and the remaining inorganic smelt contracts under surface tension forces. Experimental data showing particle diameter decreasing with combustion time agreed well with model predictions made by assuming that external mass transfer controls the rate of char combustion. These heterogeneous reactions will be reviewed in the following sections.

During char burning, the primary oxidizer is the $O_2$ in the entering air. The $O_2$ depletes the carbon in the BLC by direct oxidation and the sulfate/sulfide cycle.[2, 4, 5] Blackwell and King[6] reported measurements of the $O_2$ concentration in the gas above the char bed from 2-4% immediately above the bed, and from 14-18% twenty to thirty inches above the bed. These measurements were supported by a bed imaging system,[6] which showed that the flame began about 20-30 inches above the top of the char bed. The low $O_2$ concentration next to the char bed suggests that the carbon may have other paths for the oxidation. For example, other oxidizers such as $H_2O$ and $CO_2$ exist in the boundary above a char bed. Borg *et al.*[33] determined the gas composition above a char bed using a sampling probe. From their observations, the $CO_2$ concentration was 13%. This high level of $CO_2$ in the gas phase above the bed suggests that the gasification of kraft char with $CO_2$ may be an important reaction pathway for carbon depletion.

Grace *et al.*[13] have summarized that there are four carbon oxidation reactions with $Na_2SO_4$, $O_2$, $CO_2$, and $H_2O$ acting as oxidants. The stoichiometry of the first two reactions is difficult to define since CO and $CO_2$ can be products. Grace *et al.*[13] noted that the reaction with sulfate involves only bed constituents and acts as a homogeneous reaction. Therefore, the three heterogeneous reactions of importance are with $O_2$, $CO_2$, and $H_2O$. Grace *et al.*[13] noted that the role of the gasification reactions can be clarified by treating them in terms of mass transfer and chemical reaction at the surface in series. They assumed that the concentrations of $O_2$, $H_2O$, and $CO_2$ are 10%, 20%, and 12%, respectively; therefore, the relative reaction rates would be about 1 to 2.6 to 1 if the temperature is high enough for mass transfer control. Thus the gasification reactions, if fully active, have the potential of removing more than three times as much carbon from the bed as direct oxidation alone.

Char Carbon-$O_2$ Reaction

Grace *et al.*[13] and Brown *et al.*[11] used a batch reactor to obtain quantitative data on char bed burning. Char burning rates were obtained under conditions which simulate char bed burning in recovery boiler furnaces. Bed burning was concluded to be an oxygen mass transfer limited rate process based on the burning rate data. The burning rate proved to be directly proportional to $O_2$ concentration and dependent on velocity to the order of 0.8-1.0. Measured burning rates were of the approximate magnitude predicted by mass transfer coefficient correlations. The data provide a quantitative estimate of the amount of burning that could take place on the char bed of a recovery furnace. Brown *et al.*[11] noted that it is not unreasonable to expect that about 45% of the char carbon could be burned on the char bed representing about 15% of the total burning load.

Sulfate-Sulfide Cycle

Grace *et al.*[2, 4, 5] have noted that kraft BLC burns via a sulfate-sulfide cycle. Oxygen enters from the combustion air and oxidizes $Na_2S$ to $Na_2SO_4$. The $Na_2SO_4$ carries the oxygen over to the carbon, where $CO_2$ and CO are formed. The $Na_2SO_4$, in turn, is reduced back to sulfide, completing the cycle. Two reactions are considered to take place. The only reaction between char species and $O_2$ is:

$$Na_2S + 2O_2 \leftrightarrow Na_2SO_4 \qquad \text{rxn. 1}$$

Char carbon is oxidized by sulfate according to the reaction:

$$C + \left[\frac{(2-f)}{4}\right] Na_2SO_4 \leftrightarrow \left[\frac{(2-f)}{4}\right] Na_2S + fCO + (1-f)CO_2 \qquad \text{rxn. 2}$$

where $f$ is the mole fraction of CO in the product gas. Grace *et al.*[2, 4, 5] noted that the sulfate-sulfide cycle permits two apparently contradictory processes, carbon burn-up and sulfate reduction, to occur simultaneously in the furnace. This cycle allows char carbon burn-off in an oxygen-containing atmosphere while still achieving high degrees of sulfur reduction. The rate of the carbon-sulfate reaction

must exceed the rate of oxygen supply for this to occur. Sulfide oxidation is oxygen mass transfer controlled under almost any circumstance.[2,4,5] Control shifts to inherent chemical kinetics only when the sulfide is essentially depleted. Simultaneous carbon burning and sulfate reduction can occur if the rate-limiting step is the oxidation.

Char Carbon-$H_2O$ Reaction

Li and van Heiningen[34, 35] completed the first study of $H_2O$ gasification kinetics of kraft BLC using a thermogravimetric analysis (TGA) system. The effect of $H_2O$ and $H_2$ concentration on the gasification rate can be described by Langmuir-Hinshelwood type kinetics as follows

$$-r_w = \frac{K'\left[C_{H_2O}\right]}{\left[C_{H_2O}\right] + K'_{H_2}\left[C_{H_2}\right]}$$

An activation energy of 50.0 kcal/mol was obtained. Methane formation was negligible, and $H_2S$ was the major gaseous sulfur-containing product obtained over the temperature range studied, 873-973 K. The rate of BLC gasification is 2 or 3 orders of magnitude higher than the rate for activated carbon, respectively, with or without alkali-metal carbonate impregnation. Similarly, it is 3 or 4 orders of magnitude higher than the rate for coal char, respectively, with or without alkali-metal carbonate impregnation. Li and van Heiningen[34,35] concluded that the extremely fine dispersion of sodium in the carbon matrix results in the high reactivity.

van Heiningen *et al.*[36] measured the $H_2O$ gasification rate at 700°C of different black liquor chars with a TGA system. They concluded that the gasification rate of slow pyrolysis char is lower than that of the corresponding rapid pyrolysis chars. The gasification rate of the slow pyrolysis chars is first order in carbon, while the rapid pyrolysis chars show a rate behavior closer to zero order in carbon, at least for carbon conversions less than about 50%. The reactivity order of the slow and rapid pyrolysis chars is best correlated by the BET surface of the chars and the Na/C molar ratio during $H_2O$ gasification,

respectively. These results are explained by a better dispersion of the catalytically active sodium containing species in the rapid pyrolysis chars compared to that of the slow pyrolysis chars.

Whitty *et al.*[37] investigated the kinetics of the $H_2O$ gasification of BLC by using a pressurized TGA system over the range 600-675°C, 1-30 bar total pressure. The experiments were performed either with or without one of the reaction products ($H_2$, CO) present and under conditions such that film mass transfer and pore diffusion did not affect the overall rate. The rate of gasification was found to decrease with increasing pressure, by a factor of 3.5 over the pressure range 2-30 bar. This decrease is presumably due to the increase of inhibiting effects of the products, $H_2$ and CO, with increasing pressure. At constant total pressure and $H_2$ partial pressure, the rate was found to increase with increasing $H_2O$ partial pressure. The presence of $H_2$ slowed the reaction, with the inhibiting effect being a function of the $H_2$ partial pressure. Carbon monoxide was found to be a much stronger inhibitor than $H_2$, and exhibited the same behavior of decreasing the rate as a function of the CO partial pressure. The activation energy was found to be 55.5 kcal/mol, which corresponds to an increase in the rate by a factor of 27 over the temperature range 600-700°C.

Grace *et al.*[13] and Brown *et al.*[11] used a batch reactor to determine the effect of $H_2O$ on the rate of char burning. As noted earlier, char burning rates were measured with fully pyrolyzed char and $O_2$-$N_2$ mixtures to allow determination of $O_2$ mass transfer rates and measurements of $O_2$ mass transfer coefficients. Steam was added to the gas supply to obtain information on bed burning with simultaneous oxidation and gasification. Addition of $H_2O$ did not increase the carbon flux. The increased carbon removal due to the $H_2O$ gasification reaction was counterbalanced by the decrease in the $O_2$-C reaction, since $O_2$ reacts with CO and $H_2$ in the boundary layer.

Char Carbon-$CO_2$ Reaction

Li and van Heiningen[38-41] used a TGA system to study the $CO_2$ gasification rate of small quantities (5 mg) of slow and fast pyrolysis BLC between 600°C and 800°C. The fast pyrolysis char was made by pyrolyzing black liquor solids for twenty minutes under $N_2$ with 10% CO in a tube furnace preheated to 580°C. The slow pyrolysis char was prepared by raising the temperature from 20°C to 775°C at a rate of 25°C per minute. The reported gasification rate of BLC was 10-20 times greater than that obtained for activated carbon or coal chars impregnated with $Na_2CO_3$. The high loading and fine distribution of sodium in BLC were responsible for the high gasification rates. The rate of BLC gasification was also influenced by the method of black liquor drying because drying influenced the sodium dispersion. The influences of gas composition on BLC gasification were modeled using Langmuir-Hinshelwood type kinetics; activation energies (44.7 kcal/mol for slow pyrolysis char, 60.0 kcal/mol for fast pyrolysis char) were similar to activation energies for burning alkali metal impregnated porous carbon. The CO inhibition was relatively small and the gasification rate was first order in carbon up to 80% conversion. The internal surface area of the BLC appeared to have an influence on the gasification rate.

Frederick and Hupa[42, 43] studied the kinetics of $CO_2$ gasification of small quantities of BLC (100 mg) at similar temperatures but used a pressurized TGA system to produce pressures between 1 and 30 bars. The rate of gasification was found to be slightly less than first order in $CO_2$ and strongly inhibited by CO at higher pressures. At constant gas composition and temperature, the rates of gasification of BLC with $CO_2$ were reduced as pressure was increased. Frederick and Hupa[42, 43] reported an activation energy of 44.4 kcal/mol for the $CO_2$ gasification reaction. The rate varied by a factor of two at identical gasification conditions for experiments with BLC from three different liquors.

Frederick, Wag, and Hupa[44] studied the kinetics of $CO_2$ gasification of small quantities of BLC (100 mg) in a pressurized TGA system at 700°C, 0.1-25 bar $CO_2$ partial pressure, and 0-6 bar CO partial pressure. The rate of gasification was an order of magnitude or more higher than the rate of gasification of potassium-impregnated activated carbon and several orders of magnitude greater than for alkali-impregnated coal chars. In addition, the rate was less than first order in $CO_2$, strongly inhibited by CO, and strongly temperature dependent. Although there were large differences in the carbon source, catalyst type and loading, the gasification kinetics followed the Kapteijn *et al.*[45] mechanism for potassium-catalyzed $CO_2$ gasification of activated carbon. The Kapteijn *et al.*[45] mechanism will be discussed in detail later. Frederick, Wag, and Hupa[44] reported that the rate of gasification initially increased with increasing carbon conversion, but decreased with increasing conversion over most of the range of conversion. The change in rate with carbon conversion is apparently related to changes in the number of active carbon sites and catalyst sites. Finally, no loss of sodium from the char was observed during gasification.

Goerg and Cameron[14, 46] studied the $CO_2$ gasification of a kraft char (1.0 g) and $Na_2CO_3$ (81.62 g) mixtures using a fixed bed purge reactor. Goerg and Cameron suggested that the inhibiting effect of CO caused the rate of reaction to be less than first order in carbon concentration. A Langmuir-Hinshelwood model of the gasification reaction agreed closely with the experimental results. From the experimental results the following were concluded by Goerg and Cameron: the rate decreases as the CO concentration increases, the rate levels off as the $CO_2$ concentration increases, and the rate is proportional to the $CO_2$ concentration as the CO and $CO_2$ concentrations are lowered. Based on the high activation energy (46.8 kcal/mol) and experimental results, Goerg and Cameron concluded that the $CO_2$ gasification reaction is kinetically controlled rather than mass transfer controlled for the range of experimental temperatures (927-1010°C) tested.

The rates from Goerg and Cameron[14,46] were much lower than the rates reported by Li and van Heiningen,[38-41] Frederick and Hupa,[42,43] and Frederick, Wag, and Hupa.[44] However, the activation energies reported by each group of investigators were in agreement.

Grace *et al.*[13] and Brown *et al.*[11] used a batch reactor to determine the effect of $CO_2$ on the rate of char burning. As noted earlier, char burning rates were measured with fully pyrolyzed char and $O_2$-$N_2$ mixtures to allow determination of $O_2$ mass transfer rates and measurements of $O_2$ mass transfer coefficients. Grace *et al.*[11] noted that the addition of 10% $CO_2$ increased the burning rate by about 25%. The effect of $CO_2$ was significantly less when $H_2O$ was present.

Characteristic Temperature for $CO_2$ Gasification of Kraft Black Liquor Char

A specific objective of this thesis was to determine the transition temperature where the $CO_2$ gasification of kraft BLC goes from kinetic control to mass transfer control. The characteristic temperature can be defined as the temperature where the reaction rate is controlled equally by mass transfer and inherent chemical kinetics. Therefore, the reaction rate will be 1/2 the rate for complete mass transfer control at this temperature.

Grace *et al.*[13] estimated the characteristic temperature range for $CO_2$ gasification from the combined $CO_2$ gasification/$O_2$ combustion data. The characteristic temperature for the laboratory char bed reactor tests was about 930°C for $CO_2$ gasification. Using an activation energy of 48 kcal/mole, the temperature for 90% mass transfer control, $T_{90}$, was determined to be about 1080°C. Grace *et al.*[13] concluded that the temperature range over which reaction kinetics affects gasification rates is broad and encompasses the normal range of bed temperatures.

However, a check of the calculations indicates that $T_{50}$ is actually 912°C. However, the actual value of $T_{50}$ is probably lower because of two factors. First, Grace *et al.*[13] determined that for the

temperature range of 800-990°C for the char bed reactor the Arrhenius activation energy for the $CO_2$ gasification reaction was 24 kcal/mole. This value is considerably lower than the chemical kinetic activation energy of approximately 47 kcal/mole. Therefore, this would suggest the characteristic temperature is lower than the 800-990°C for the char bed reactor experiments. Second, Grace *et al.*[13] determined the $CO_2$ gasification at the higher temperature (970°C) by subtracting the preestablished oxidation rate from the total burning rate. Therefore, any gas reaction in the gas phase between the incoming oxygen and the CO from char gasification was neglected. In addition, the higher temperatures are probably lower than the actual rate because the actual oxidation rate is less than the oxidation rate used in the calculations. If the $CO_2$ rate was actually higher than the one reported, the characteristic temperature would be lower. Therefore, the characteristic temperature for $CO_2$ gasification of kraft BLC has not been defined.

Inorganic Smelt Reactions

Hupa *et al.*[1] have identified the inorganic reactions stage as the elapsed time from collapse of the char particle to visible cooling of the smelt bead. Grace *et al.*[4] noted that the inorganics coalesce only when the organic carbon content approaches 2-3%. $Na_2S$ remaining at the end of char burning is oxidized to $Na_2SO_4$ after most of the carbon has been consumed in char burning. The conversion of $Na_2S$ to $Na_2SO_4$ is an exothermic reaction that increases the smelt temperature approximately 100°C.

## COAL CHAR GASIFICATION WITH $CO_2$

Numerous studies of the carbon-$CO_2$ reaction with coal have been completed. A review of these studies has been presented by Laurendaeu.[47] The rate of carbon gasification by $CO_2$ is generally much lower than the rate of reaction of carbon with $O_2$. For example, Harris and Smith[48] concluded that the relative intrinsic reaction rates of brown coal char at 700°C and 0.2 atm with $CO_2$, $H_2O$, and $O_2$ were 1, 2, and 1.0E4 respectively.

Through an evaluation of the rate data from the coal literature, it must be noted that temperature and reactant concentrations are not the only variables which influence the reaction rates. Smoot and Smith[49] have suggested that the composition of the feed material, internal and external surface areas, and catalytic impurities are important. In general, chars from lower rank coals are more reactive than those from higher rank coals. Furthermore, an increase in internal surface area leads to a higher reaction rate. Finally, the presence of salts of the alkali and transition metals act as catalysts for the combustion and gasification reactions.

Grace *et al.*[4] have reported the inorganic content of kraft char as $Na_2CO_3$, $Na_2S$, and $Na_2SO_4$ at weight percents of 59.8, 2.9, and 1.8, respectively. In addition, a comparison of kraft BLC[15] versus coal char[49] reveals that black liquor chars have a lower carbon content, higher oxygen content, higher sodium content, equal or greater hydrogen content, and approximately equal sulfur and potassium contents. The high weight percent of inorganic salts and the elemental differences would lead one to expect the rates of these reactions to be greater for black liquor chars versus coal chars.

Alkali Catalyzed Carbon $CO_2$ Gasification

Kraft black liquor char and alkali catalyzed carbon are similar in that both have appreciable levels of alkali species ($Na_2CO_3$, $K_2CO_3$, etc.). Meijer[50] has provided an excellent review of mechanisms for alkali-catalyzed gasification of carbon with $CO_2$. These mechanisms and recent accomplishments will be briefly reviewed.

Rao *et al.*[51] and McKee *et al.*[52-56] proposed a cyclic mechanism for the alkali-catalyzed gasification of carbon with $CO_2$ consisting of three steps involving gaseous intermediates M(g), CO(g), and $CO_2$(g), as follows:

$$M_2CO_3(s,l) + 2\ C(s) \Leftrightarrow 2\ M(g) + 3\ CO(g) \qquad \text{rxn. 3}$$

$$2\ M(g) + CO_2(g) \Leftrightarrow M_2O(s,l) + CO(g) \qquad \text{rxn. 4}$$

$$M_2O(s,l) + CO_2(g) \Leftrightarrow M_2CO_3(s,l) \qquad \text{rxn. 5}$$

According to Rao *et al.*,[51] reactions 4 and 5 are expected to proceed rapidly and reaction 3 is the rate-controlling step. However, Saber *et al.*[57] and Kapteijn *et al.*[58] noted that when a mixture of carbon and $K_2CO_3$ is heated in He, $CO_2$ evolves below 1000K as a result of desorption from the carbon surface. Saber *et al.*[57] note that this $CO_2$ is not due to carbonate decomposition; $K_2CO_3$ in the presence of carbon does not decompose to a large extent below 1000K. Above 1000K, $K_2CO_3$ decomposes and carbon-surface oxygens stabilize the potassium and decrease the rate of potassium volatilization. These results suggest that the mechanism in reactions 3-5 is not likely.

Spiro *et al.*[59] proposed a redox mechanism based on alkali hydride intermediates to account for the differences between coal char and graphite reactivity. The major differences between coal chars and graphite were identified as the presence of indigenous mineral matter, variations in porosity, surface area, and the presence of residual hydrogen and heteroatoms. Although mineral matter, porosity, and surface

area are not entirely without influence, Spiro *et al.*[59] concluded that these variables did not dominate the gasification process. Therefore, the McKee *et al.*[52-56] cyclic mechanism was modified for coal chars to include an influence of residual hydrogen via alkali hydride catalytic intermediates.

Mims and Pabst[60, 61] favor a mechanism where surface phenoxides associated with the catalyst are gasification intermediates. Through the use of $^{13}$C-NMR and methylation with $CH_3I$, Mims and Pabst postulated the presence of alkali phenolate groups on the carbon surface. The methylation experiments showed that the active species on the carbon surface consisted of 4 to 5 potassium atoms and were independent of $K_2CO_3$ loading, thereby showing the high dispersion of the alkali catalyst. Mims and Pabst concluded that the catalytically active sites are stable intermediate products in the reduction of alkali salts by carbon and may be present before gasification. The proposed mechanism suggests that the surface salt (phenoxides) complexes are the active sites, and gasification proceeds by a rapid reversible oxidation of these sites followed by a slower decomposition step yielding CO. The mechanism is electrochemical with the catalyst phase acting as an electrolyte. The basic salt phase stabilizes the surface phenoxides analogs, thereby providing a suitable precursor for CO evolution.

Several researchers[52, 62, 63] have suggested the presence of intercalation compounds (i.e., $C_8K$, $C_{24}K$, etc.) in the alkali-catalyzed gasification mechanism. However, Tromp and Cordfunke[64] used high temperature *in situ* X-ray diffraction to show that alkali metal intercalation compounds are not stable under steady state gasification conditions. Tromp and Cordfunke concluded that an interaction occurs between the two physically mixed components ($K_2CO_3$ or $Na_2CO_3$ and activated carbon) at the gasification temperatures (925-1125K). The interaction is stronger with potassium than with sodium. The alkali-carbon interaction might take place via the functional groups on the carbon surface since the interaction decreases with increasing pretreatment temperature of the activated carbon. Moulijn *et al.*[65] also concluded that bulk intercalation compounds are not present under gasification conditions.

Kapteijn and Moulijn,[45] Moulijn *et al.*,[65] and Sams and Shadman[66] postulated a two-step oxidation-reduction cycle for the potassium catalyzed-$CO_2$ gasification of carbon. In the oxidation-reduction cycle, oxygen is transferred from $CO_2$ via the alkali metal to carbon under the formation of CO as follows:

$$[K_xO_y] + CO_2 \Leftrightarrow [K_xO_{y+1}] + CO \qquad \text{rxn. 6}$$

$$[K_xO_{y+1}] + C \Leftrightarrow [K_xO_y] + CO \qquad \text{rxn. 7}$$

Reaction 6, considered to be in chemical equilibrium, determines the ratio of the active potassium species in a lower and a higher oxidation state which is dependent on the $CO/CO_2$ ratio in the feed. The equilibrium in the first step shifts until nearly all the potassium is in the higher oxidation state when pure $CO_2$ is present in the feed. Therefore, the overall reaction rate is independent of $CO_2$ pressure. In contrast, CO addition generates sites of lower oxidation state and determines the rate of reaction 7, which is considered to be rate determining. This explains the pressure independence and the CO inhibition. Kapteijn, Cerfontain, and Moulijn[45, 65] conclude that the $CO/CO_2$ ratio is the controlling factor in the dependency of the gasification rate on the gas phase composition.

Cerfontain and Moulijn[67, 68] used *in situ* fourier transform infrared (FTIR) spectroscopy to study the alkali carbonate gasification of an activated carbon. C(O) complexes are formed when $CO_2$ interacts with the alkali carbonate-carbon system above 773K. The number of C(O) complexes increase in the range Na<K<Cs, but did not decrease in a CO atmosphere. Finally, Cerfontain and Moulijn concluded the C(O) complexes formed during gasification originate from stable C(O) complexes such as alkali phenolates.

Several researchers[45, 68-72] have supported the two-step model described in reactions 6 and 7. Kapteijn *et al.*[72] studied the influence of different alkali metals (Na, K, Rb and Cs) on the kinetics of the $CO_2$ gasification. The main role of the catalyst was described as increasing the steady state concentration

of oxygen at the carbon surface by increasing the total number of active sites. The activation energy for the second step (the rate determining step) was 5-10 kcal/mol lower for the catalyzed reaction versus the uncatalyzed reaction. The decrease in activation energy was explained by the increased oxygen concentration at the carbon surface or the inhibiting effect of CO. The reaction rate was shown to increase with catalyst loading and with specific catalyst in the periodic order Na<K<Rb<Cs. Mims and Pabst[60] explained that the difference in rates of the alkali metals was due in large part to differences in dispersion.

Several researchers[60, 73-76] have applied labeled molecules to the alkali-catalyzed gasification reaction to show that the two-step mechanism proposed by Kapteijn, Cerfontain, and Moulijn[45, 65, 75] is a simplified description of the mechanism occurring during alkali-catalyzed gasification. Cerfontain *et al.*[75] used $^{13}CO_2$ to propose an extended model for oxygen exchange and carbon gasification in $CO/CO_2$ atmospheres over alkali/carbon systems. The extended model is as follows:

$$CO_2 + *(CO_2) \Leftrightarrow *(CO_3) + CO \qquad \text{rxn. 8}$$

$$*(CO_3) + C_f \Leftrightarrow *(CO_2) + C(O) \qquad \text{rxn. 9}$$

$$C(O) \Leftrightarrow CO \qquad \text{rxn. 10}$$

$$CO + C(O) \Leftrightarrow CO_2 + C_f \qquad \text{rxn. 11}$$

The catalytically active alkali cluster is represented by *. Cerfontain *et al.*[75] noted that oxygen exchange occurs by reaction of gaseous CO with the chemisorbed $CO_2$ accompanied by the formation of $CO_2$, followed by a back reaction with another $CO_2$ molecule (rxn. 9). Cerfontain *et al.* concluded that the oxygen exchange occurs on alkali catalyst sites without direct involvement of the carbon itself. The gasification phenomena proceed at a much lower rate. Cerfontain *et al.* proposed that the oxidized catalyst site is able to oxidize the carbon in its vicinity, thereby assisted by $CO_2$ (rxn. 9). The oxidized carbon sites either slowly decompose with formation of CO (gasification, rxn. 10) or are reduced by

gas-phase CO (inhibition, rxn. 11). In addition, Cerfontain *et al.* found that the alkali-catalyzed oxygen exchange rate is only dependent on the CO pressure, suggesting that the C(O) concentration is independent of the $CO/CO_2$ ratio.

Cerfontain *et al.*[75, 76] used $^{13}C$- and $^{18}O$-labeled $CO_2$ to determine that the alkali catalyst contains chemisorbed $CO_2$ in alkali oxide clusters. The strong interaction of $CO_2$ with the alkali system results in chemisorption being nearly temperature and pressure independent. Chemisorbed $CO_2$ is easily exchanged with gas phase $CO_2$ in the alkali/carbon system as follows:

$$*(CO_3) + {}^{13}CO_2 \Leftrightarrow *({}^{13}CO_3) + CO_2. \qquad \text{rxn. 12}$$

The amount of chemisorbed $CO_2$ increases with increasing catalyst loading. Meijer[50] noted that the role of this chemisorbed $CO_2$ in the alkali-catalyzed gasification mechanism is not fully understood.

Meijer *et al.*[77] observed substantial catalyst loss at low carbon burn-off of 10%. During potassium-catalyzed $CO_2$ gasification, initially 20-40% of the potassium was lost and the balance remained present throughout gasification. From the results of temperature-programmed desorption experiments, the amount of catalyst (K) that can be stabilized on the carbon is independent of the initial catalyst loading. Sodium shows less interaction with the carbon matrix when compared to potassium, resulting in less sodium that can be stabilized on the carbon. The amount of catalyst that can be stabilized on the carbon is dependent on the amount of oxygen in the carbon increasing in the order Na<K<Cs. The alkali metal's ability to migrate into the carbon matrix and the interaction with lattice oxygen accounts for the differences between the alkali metals. Meijer *et al.* explained that the migration of Cs and K into the carbon matrix explains the burn-off profiles. Initially, only part of the catalyst is active for gasification, but gradually more catalyst becomes available, resulting in an increasing gasification rate.

Sams and Shadman[78] investigated the effect of catalyst concentration (K/C) and the internal porous structure of the solid on the rate of char-$CO_2$ gasification. Initially, the change in rate with conversion was slow and increased or decreased depending on the initial catalyst concentration. Eventually, the rate decreased dramatically after a certain carbon conversion was achieved. In contrast, Mims and Pabst[60, 61] suggested that the rate remained constant between 20-70% conversion. Sams and Shadman suggested that this was incorrect since the rate is a complex function of catalyst concentration and internal surface area, parameters which vary with conversion. In addition, the discrepancies may be due to the use of average rates by Mims and Pabst versus intrinsic rates by Sams and Shadman. Sams and Shadman explained that the sharp drop in rate prior to full carbon conversion was a result of blocking of carbon pores by catalyst deposition. Sams and Shadman divided the effect of catalyst concentration on the rate in three regions. In region I, the rate increased sharply with increasing K/C ratio for low levels of catalyst loading. In region II, the rate became insensitive to the addition of more catalyst and increased <10% while the K/C ratio more than doubled. Finally, a decrease in the rate with the addition of catalyst was observed in region III. The activity in the three regions was also explained by the blocking of carbon pores by catalyst deposition. Sams and Shadman explained that the increased rate in region I was associated with the increased concentration of catalytic sites as K is added. At some level (region II), the surface becomes saturated with catalyst and few new catalytic sites are generated. As more catalyst is added to the char surface, the deposits begin to block some of the pores and restrict $CO_2$ access to the reaction sites; thereby, the rate decreases as described in region III.

The extended model by Cerfontain *et al.*[75] was expanded by Kapteijn *et al.*[79] and Meijer[50] to include the following sequence of elementary processes.

$$CO_2 + * \Leftrightarrow *CO_2 \qquad \text{rxn. 13}$$

$$*CO_2 \Leftrightarrow *O + CO \qquad \text{rxn. 14}$$

$$C_f + *O \Leftrightarrow * + C(O) \qquad \text{rxn. 15}$$

$C(O) \Leftrightarrow CO$ rxn. 16

The distribution of the active sites between *, O*, and $CO_2$* is determined by the gas atmosphere composition. Experiments with $C^{18}O_2$ showed that the chemisorbed $CO_2$ retained its chemical identity at lower temperatures (600K); however, an exchange with oxygen in the alkali cluster is observed at higher temperatures. Cerfontain *et al.*[75] and Meijer[50] noted that all the oxygen present in the catalyst cluster can be exchanged in this manner under gasification conditions. Kapteijn *et al.*[79] suggested that catalyzed $CO_2$ gasification takes place only above 800K for two reasons:

(i) C(O) complexes only decompose at high temperatures and
(ii) *$CO_2$ complexes, necessary to produce the reactive O* sites that oxidize the carbon, only decompose at high temperatures.

Even at the high temperatures necessary for gasification, the catalyst remained on the carbon surface. Mims and Pabst,[60] as noted earlier, have suggested that the alkali catalyst is anchored to the carbon surface via a phenolate type of bonding. In agreement, Kapteijn *et al.*[79] concluded that all potassium is trapped via phenolate bonds at low potassium catalyst loadings. As noted earlier by Meijer,[77] only part of the catalyst was initially active for gasification, but gradually more catalyst becomes available, resulting in an increasing gasification rate. Kapteijn *et al.*[79] concluded that 3-5 potassium atoms are involved in the chemisorption of one $CO_2$ molecule.

Meijer[50] suggested that the composition of the catalytically active species changed with increasing gasification temperature. Meijer noted that at 1000K the cluster was composed of several potassium phenolate species and contained a considerable amount of chemisorbed $CO_2$ and reactive oxygen; whereas, merely highly reactive potassium phenolate species were present at 1200K.

COMBINED OXIDATION/GASIFICATION OF KRAFT BLACK LIQUOR CHAR

Grace *et al.*[13] have noted that simultaneous oxidation/gasification can occur when the char bed is contacted with a gas stream containing $O_2$, $H_2O$, and $CO_2$. Grace *et al.* evaluated combined oxidation/gasification mathematically by defining two parameters as follows:

$\alpha$ = the fraction of $O_2$ that could react in the boundary layer with CO evolving off the char bed that does react, and

$f$ = stoichiometric factor for direct carbon oxidation defined by the reaction.

$$\left[1 - \frac{f}{2}\right] O_2 + C \Leftrightarrow fCO + (1-f)CO_2 \qquad \text{rxn. 17}$$

Grace *et al.* expressed the net oxygen flux to the surface as:

$$R'_{O_2} = \frac{\left[R_{O_2} - \alpha\left(R_{CO_2} + R_{H_2O}\right)\right]}{\left[1 + \frac{\alpha f}{(2-f)}\right]} \text{ for } R'_{O_2} > 0 \qquad \text{eqn. 1}$$

$$R'_{O_2} = 0 \text{ for } R'_{O_2} < 0. \qquad \text{eqn. 2}$$

Then, the carbon removal flux, $R_C$, is defined as:

$$R_C = R_{CO_2} + R_{H_2O} + \left[\frac{2}{2-f}\right] R'_{O_2} \qquad \text{eqn. 3}$$

Grace *et al.*[13] discussed the special case where oxidation proceeds to completion in the boundary layer above the bed, $\alpha = 1$. In this case, $R'_{O_2}$ is reduced as follows:

$$R'_{O_2} = \left[\frac{2-f}{2}\right]\left(R_{O_2} - R_{CO_2} - R_{H_2O}\right) \qquad \text{eqn. 4}$$

$$R_C = R_{O_2} \text{ if } R_{O_2} > R_{H_2O} + R_{CO_2} \qquad \text{eqn. 5}$$

and if

$$R'_{O_2} = 0 \qquad \text{eqn. 6}$$

$$R_C = R_{H_2O} + R_{CO_2} \text{ if } R_{O_2} < R_{H_2O} + R_{CO_2} \qquad \text{eqn. 7}$$

In this case, the oxidation and gasification effect on carbon removal is mutually exclusive with the burning rate determined by whether the oxygen flux or effective $H_2O + CO_2$ fluxes are in excess.

Grace *et al.*[13] also discussed the opposite special case where no oxidation occurs in the gas phase boundary layer above the char bed. In this case, $R'_{O_2}$ is reduced as follows:

$$R'_{O_2} = R_{O_2} \qquad \text{eqn. 8}$$

and $$R_C = R_{O_2} + R_{H_2O} + R_{CO_2}. \qquad \text{eqn. 9}$$

Therefore, the overall stoichiometry will be the net result of the stoichiometry of all three reactions and is dependent on the value of *f*.

Grace *et al.*[13] completed a series of experiments on combined oxidation/gasification utilizing the Institute of Paper Science and Technology/Department of Energy char bed reactor. The bed was contacted with a gas mixture of $N_2$, $CO_2$, $H_2O$, and $O_2$. The char oxidation rate was subtracted from the total burning rate to determine the char gasification rate. Therefore, any gas reaction in the gas phase between the incoming oxygen and the CO and $H_2$ from char gasification was neglected.

Grace *et al.*[13] concluded that the rate of carbon removal in simultaneous oxidation and gasification is normally equal to the rate of oxygen mass transfer or to the sum of the effective $CO_2$ and $H_2O$ transfer rates, whichever is greater. Consumption of $O_2$ in the boundary layer by combustibles which evolve from the bed surface inhibit parallel oxidation and gasification at the bed surface.

Frederick[80] compared a droplet combustion model versus experimental results for single particles exposed to $O_2$ and $CO_2$ at 800°C. Results clearly showed that char combustion times decreased as oxygen content increased for constant $CO_2$ concentration (20%). The model far underestimated the char burning times at all levels of oxygen when both $CO_2$ and $O_2$ were assumed to contribute to the oxidation of char carbon. When the rate of $CO_2$ gasification was assumed to be negligible, the model accurately predicted the char burning times. Frederick explained this by noting that the predicted $CO_2$ gasification reaction proceeds too slowly at 800°C.

## REVIEW OF EXPERIMENTAL REACTORS

Previous laboratory studies have provided a great amount of information regarding the fundamentals of black liquor combustion. However, several challenges remain. For example, the gasification of black liquor char with $CO_2$ and $H_2O$ is not fully understood. Most research on the gasification reactions have involved the use of thermogravimetric analysis (TGA).[34-44] The thermobalance used in TGA has been recognized as a useful and simple tool for measuring heterogeneous reaction rates. However, sources of error in thermogravimetry can lead to considerable inaccuracies in the temperature and mass-change data obtained; thereby resulting in unreliable intrinsic reaction kinetics under certain conditions. Wendlandt[81] noted that accurate thermogravimetry requires that a correction be applied for these errors or that at least some recognition be made of their magnitude. Many of the errors are interrelated and cannot be considered separately; therefore, full consideration must be given to all these factors in thermogravimetry. Wendlandt[81] summarized the possible sources of error in thermogravimetry as follows:

1. Sample-container air buoyancy.
2. Furnace convection currents and turbulence.
3. Random fluctuations in the recording mechanism and balance.
4. Furnace induction effects.
5. Electrostatic effects on balance mechanism.
6. Environment of the thermobalance.
7. Condensation on sample support.
8. Temperature measurement and calibration.
9. Weight calibration of recording balance.
10. Reaction of the sample with sample container.
11. Temperature fluctuations.
12. Momentum-transfer effects in vacuum TG.

Buoyancy cannot be neglected for accurate TG measurements. The effect of buoyancy on the sample and certain parts of the thermobalance decrease as a function of temperature. Also, the density of the gas phase decreases with temperature. Wendlandt[81] illustrates the effect of gas density and buoyancy by noting that at 300°C the density, and therefore the buoyancy exerted on the sample, is about one half

as great as at 25°C. In air, this results in an apparent mass variation of about 0.6 mg/cm$^3$. Buoyancy not only affects parts of the balance system and sample crucible, but it also affects a sample that changes its mass and volume during its thermal decomposition reaction.

Newkirk[82] and Lukaszewski[83] studied the apparent mass-gain or mass-loss due to convection currents in the furnace. The apparent mass-loss caused by the upflowing stream of gas on the sample container and the apparent mass-gain due to gas turbulence are determined largely by the sample crucible size and shape. It was discovered that except for a large opening, there was always an initial mass-gain even when on further heating there was an overall mass-loss. It was not possible to choose an opening that would give no apparent mass-gain on heating over the entire temperature range. In addition, Newkirk[82] found an additional apparent mass-gain as the gas velocity increased with the magnitude of the gain governed by the molecular mass of the gas employed.

The sample temperature during reaction is difficult to measure since a thermocouple implanted directly in the solid disrupts weight measurement. Wendlandt[81] suggested that if the temperature of the sample is taken as the temperature measured by a thermocouple located just above or below the sample container, then the true sample temperature will either lead or lag behind the furnace temperature. The magnitude of this difference depends on factors such as the nature of the reaction (whether it is endothermic or exothermic), the heating rate, the sample thermal conductivity, and the geometry of the sample holder.

Major transport resistances, such as gas phase mass transfer external to and within the solid sample, can obscure measurement of intrinsic reaction kinetics since the reactant gas passes around the sample pan and exchanges mass with the sample only by diffusion via the top exposed surface.

Wendlandt[81] noted that a well designed thermobalance should reduce several of the other errors to negligible values. Wendlandt[81] explained that the errors caused by random fluctuations of the recording mechanism, furnace induction effects, electrostatic effects, changes in thermobalance environment, and so on can be eliminated by proper thermobalance design, construction, and location in the laboratory.

Verification of the earlier $CO_2$ kraft BLC gasification research with an alternate reactor is desirable. Table 2 reviews some of the experimental reactors considered for this study. For this study, a fixed bed reactor was utilized because the sample temperature can be measured directly and the reactant gas can flow through the char in a manner similar to that of an actual furnace bed. Weekman[84] noted that the fixed bed reactor is an excellent reactor for sampling and analysis of product composition. In addition, several researchers[48, 50, 69, 77, 85-88] have utilized fixed bed reactors to study the gasification kinetics of alkali catalyzed carbons. In fact, Meijer's[50] Ph.D. thesis included a comparative study on the kinetics of the alkali-catalyzed gasification reactivity in $CO_2$ of a bituminous coal char (Westerholt) at elevated pressures in a fixed-bed reactor and a thermobalance. Meijer[50] concluded that both apparati essentially yield the same kinetic description. Finally, the fixed bed reactor is relatively easy to construct and fairly inexpensive to operate.

**Table 2:** Summary of Reactor Ratings for Heterogeneous Oxidation of Kraft Black Liquor Char

| Reactor Type | Product Gas Sampling | Residual Solids Recovery | Bed Temp. Measurement | Isothermality | Construction Cost | Ease of Operation | Time Required per Experiment | Operating Cost | Application to Actual Bed Burning |
|---|---|---|---|---|---|---|---|---|---|
| Fixed Bed Reactor | Good | Good | Good<br>Thermocouples inserted directly into char bed without disturbing reaction | Good<br>Depending on bed depth, bed width and level of organic carbon conversion | Low<br>Equipment (i.e., furnace, gas analyzers, flow meters, char retorts) readily available | Fair<br>However, deviation from plug flow may be possible | Poor<br>Each experiment requires at least one day to accomodate reactor heat-up and cool-down | Low<br>Experimental costs include gases and residual solids analysis | Good<br>Allows simulation of reaction gas flowing upward through char bed |
| Cross Flow Reactor employed by Grace *et al.*[11,13] | Fair<br>Experience indicates difficulty in closing mass balances | Fair | Good<br>Thermocouples inserted directly into char bed without disturbing reaction | Fair<br>Wetting of lower layers of char with coalesced smelt from top layer results in localized hot spots | Moderate<br>Equipment requires modification to achieve desired temperatures | Fair<br>Difficult to control bed height and temperature, stangnant regions may exist above char bed | Poor<br>Each experiment requires at least one day to accomodate reactor heat-up and cool-down | Low<br>Experimental costs include gases and residual solids analysis | Good<br>Allows simulation of reaction gas flowing across char bed top as bed is constantly replenished |
| Single Particle Reactor employed by Verrill[19] | Poor<br>Negligible concentration due to low solids mass | Poor<br>Residual solids fall off of platinum wire | Poor<br>Unable to directly determine solids temperature | Poor<br>Rapid temperature increase occurs when particle is inserted into furnace | Low<br>Equipment readily available | Poor<br>Tedious to recovery residual char particles, difficult to duplicate experiments | Good<br>Several particles can be exposed to various conditions in a few hours | Low<br>Experimental costs include gases and residual solids analysis | Poor<br>Allows simulation of single particle char burning |
| Thermogravimetric Anaylsis | Poor<br>Negligible concentration due to low solids mass | Good | Poor<br>Unable to directly determine solids temperature | Good | High<br>Custom Designed Equipment which must be ordered | Poor<br>Several sources of error must be addressed | Fair<br>Char must be cooled prior to elemental analysis, this may require a few hours per sample | Low<br>Experimental costs include gases and residual solids analysis | Poor<br>Gas does not flow through char bed, only across char surface |

## THESIS OBJECTIVES

The objectives of this thesis include the following:

1. Determine the inherent kinetics of the $CO_2$ gasification of kraft black liquor char using a fixed bed reactor to verify the earlier results of thermogravimetric analysis,

2. Determine the transition temperature where the $CO_2$ gasification reaction goes from kinetic control to mass transfer control for typical gas velocities, gas concentrations, char particle sizes, and char densities for a char bed geometry.

3. Determine if the combination $CO_2$ gasification and $O_2$ combustion of kraft black liquor char is equivalent to the sum of the individual rates, and

4. If there is a significant interaction such that the rates are not additive, develop a rate expression for the reaction of kraft black liquor char with $CO_2$ and $O_2$.

# EXPERIMENTAL

To accomplish the thesis objectives, a unique experimental reactor was designed for gasification and combustion of kraft black liquor char (BLC). This section provides a description of the reactor, procedures, and materials used in the experimental study. A detailed list of the major equipment is provided in Appendix II.

## BLACK LIQUOR SAMPLES AND ANALYSIS

Two different samples of black liquor were utilized to manufacture the char for this study. The elemental composition of the black liquors used to manufacture the reacting chars is provided in Table 3. The samples were obtained "as fired" after the addition of precipitator dust, hopper catch, and make-up chemicals.

**Table 3.** Elemental Analysis of Black Liquor Used to Manufacture Char

| Characteristic or Element | Weight % | |
|---|---|---|
| Liquor Number | I* | II** |
| Liquor Solids | 69.8 | 67.2 |
| Carbon | 37.3 | 37.8 |
| Hydrogen | 3.8 | 3.6 |
| Oxygen | 33.4 | 35.4 |
| Sulfur | 4.6 | 5.4 |
| Chlorine | 0.68 | 0.45 |
| Sodium | 18.7 | 19.3[b] |
| Carbonate C | N/A | 0.71 |
| Potassium | 1.1 | 1 |

a Standard black liquor analyses by Huffman Laboratories, Golden, Colorado unless otherwise noted; elemental composition reported as percent of black liquor solids.

b Average of 20 ICP determinations of acid-digested samples by Verrill.[19]

* Kraft black liquor, Softwood/Hardwood mixture, New Bern, NC, Weyerhaeuser Paper Company, collected January, 1989

** Kraft black liquor, Softwood/Hardwood mixture, New Bern, NC, Weyerhaeuser Paper Company, collected March, 1991

## HETEROGENEOUS REACTION PROCEDURES

The major objectives of this thesis require the gasification and/or oxidation of BLC. The following sections review the methods of char formation from black liquor, procedures for completing char pyrolysis, and the method of heterogeneous reaction.

### Char Formation and Devolatilization

Partially devolatilized char particles were formed by injecting single black liquor droplets downward into upward flowing $N_2$ using a drop tube furnace as described by Clay *et al.*[12] The particles are defined as partially devolatilized since volatiles evolved during the heat-up stage of the gasification/oxidation experiments. The drop tube furnace consisted of a vertical tube furnace placed above a char bed furnace. Liquor of approximately 65-70% solids was converted to droplets by a vibrating feed mechanism on top of the tube furnace. The droplets fell downward through upward flowing air and devolatilization product gases. The droplets were heated by convection from the gases and radiation from the furnace walls. Drying, swelling, partial devolatilization, and limited char burning occurred as the droplets descended through the tube furnace. The swollen char particles were collected in the char bed furnace, where 95%$N_2$/5%CO was directed across the bed surface to quench any combustion. The char particles were removed from the char bed furnace and stored in sealed plastic bags. The drop tube furnace temperature was approximately 950°C, the initial black liquor droplet diameter was 2 mm, the particle retention time was approximately 2 seconds, and the mean char particle diameter was 7.7±2.2 mm.

The partially devolatilized particles were fully devolatilized by further heating in a cylindrical fixed bed reactor (7.1 cm diameter by 15.2 cm depth), shown in Fig. 1. This was accomplished at atmospheric pressure with a mixture of 95%$N_2$/5%CO flowing through the fixed bed at a flowrate of

approximately 5 slpm. Li[39] suggested that $Na_2CO_3$ will react with organic carbon at 550°C yielding products such as gaseous Na, CO, and some $CO_2$. Therefore, CO was included in the preheat gas to suppress the $Na_2CO_3$-char C reaction. Li showed that the addition of CO leads to the suppression of the decomposition of $Na_2CO_3$ at 775°C. The CO and $CO_2$ concentrations in the product gases were measured continuously using an infrared analyzer. Devolatilization was considered to be complete when the CO and $CO_2$ concentrations in the product gas approached 5% and 0% (the levels of CO and $CO_2$ in the feed).

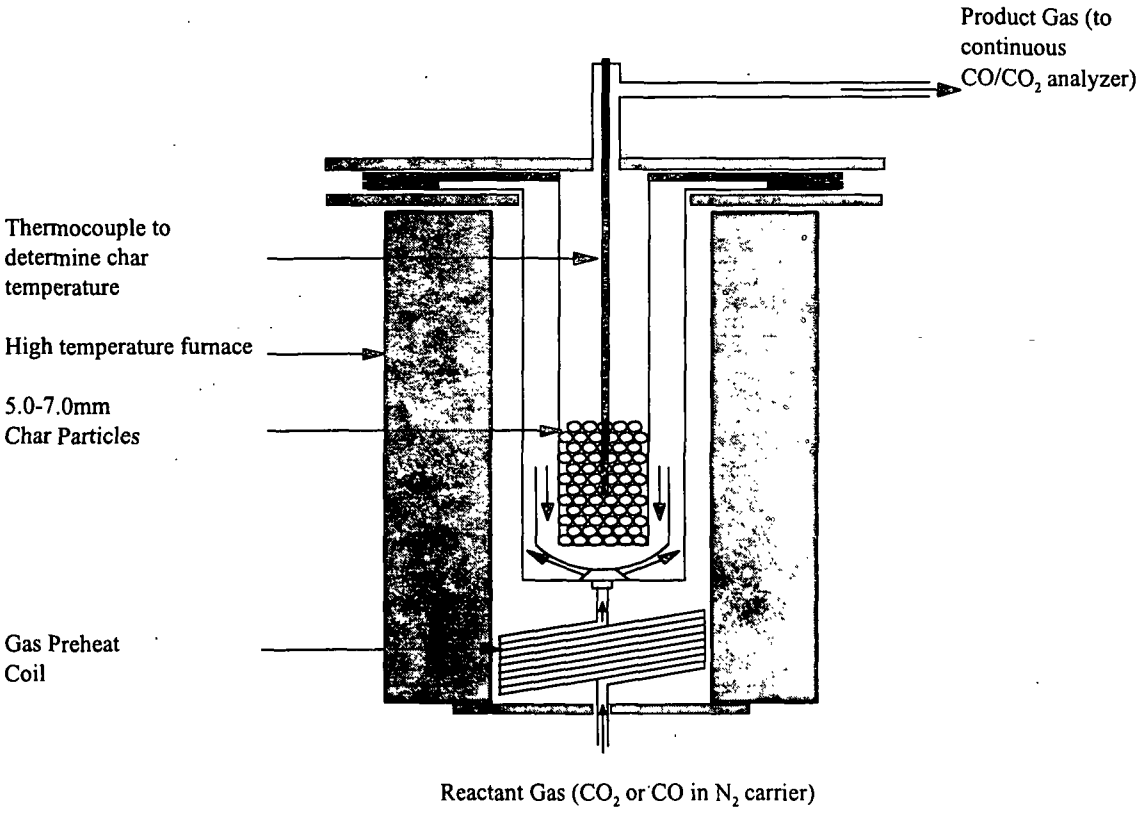


**Figure 1.** Schematic for Fixed Bed Reactor Used for $CO_2$ Gasification of Black Liquor Char.

Procedures for Preheating BLC Prior to Heterogeneous Reaction

The composition of char prior to gasification or combustion influences the kinetics of the heterogeneous reactions.[41, 49] The temperature of devolatilization has been shown to influence the composition of kraft black liquor char.[9] Smoot and Smith[49] noted that coal char composition following devolatilization was dependent on the devolatilization temperature. Smoot and Smith summarize several devolatilization models which were dependent on temperature.

For the gasification experiments in this study, two different procedures were used to preheat black liquor char prior to heterogeneous combustion since the elemental composition of the resulting chars were significantly affected by the devolatilization temperature. The reaction temperature preheat procedure (RTPP) involved heating partially devolatilized char particles in an atmosphere of 95%$N_2$/5%CO to various temperatures (600°C, 700°C, or 800°C), achieving complete devolatilization at the given temperature, and upon complete devolatilization, maintaining the char at the given temperature for one hour. This procedure is similar to the one used by Frederick and Hupa[42-44] and Li and van Heiningen.[38-41] In addition, this devolatilization temperature was chosen primarily for convenience, as gasification of the char was initiated immediately upon completion of devolatilization. The maximum temperature preheat procedure (MTPP) involved heating partially devolatilized char particles in an atmosphere of 95%$N_2$/5%CO to a temperature of 950°C, and then upon complete devolatilization, maintaining the char at 950°C for one additional hour, and then cooling down to the predetermined reaction temperature (600°C, 700°C, or 800°C) to begin the gasification experiment. The differences in elemental composition of the chars from these two preheat procedures will be discussed.

Comparison of the Elemental Composition of Chars Prepared According to the RTPP and the MTPP

A series of experiments was conducted to determine the effects of the two procedures on the elemental composition of char. For the RTPP, partially devolatilized kraft black liquor char particles were fully devolatilized by heating in a cylindrical fixed bed reactor (7.1 cm diameter by 15.2 cm depth), shown in Fig.1. The char beds were heated to temperatures of 600°C, 700°C, or 800°C. Each experiment began with 15.7 g of char. For the MTPP, partially devolatilized kraft black liquor char particles were fully devolatilized by heating in a muffle furnace reactor, shown in Fig. 2. The gas entrance region of the U-tube was partially packed with stainless steel shavings to increase heat transfer to the gas. The muffle furnace reactor allowed char to be packed in a stainless steel basket which was secured at the end of a thermocouple. The thermocouple was used to insert the char bed into the reactor, determine the temperature of the char bed, and withdraw the char bed from the reactor. After char had been packed into the basket and inserted into the furnace, it was heated to 950°C at atmospheric pressure with a mixture of 95%$N_2$/5%CO flowing through the furnace at a flowrate of approximately 3.0 slpm. A maximum temperature of 950°C was chosen because this represented a temperature above that expected for subsequent gasification experiments. The CO and $CO_2$ concentrations in the product gases were measured continuously using an infrared analyzer which was calibrated before and after each experiment. Devolatilization was considered to be complete when the CO and $CO_2$ concentrations in the product gas approached 5% and 0%, respectively (the levels of CO and $CO_2$ in the feed). The char beds were held at 950°C for an additional hour after devolatilization was completed, and then allowed to cool to reaction temperature (600°C, 700°C, or 800°C). The char beds were held at 600°C, 700°C, or 800°C for approximately 20-30 minutes, and then rapidly cooled to 25°C. Each experiment began with 7.75 g of char. The preheat reactor included a cool-down zone that allowed the char bed to be cooled rapidly from the reaction temperature to room temperature under an atmosphere of 95%$N_2$/5%CO.

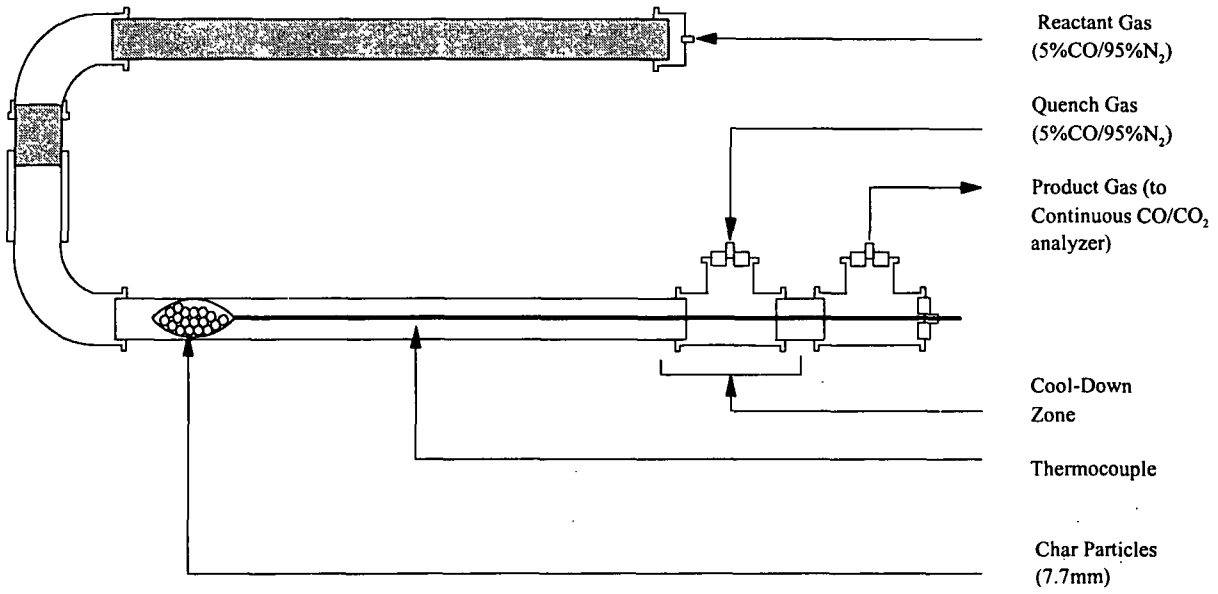


**Figure 2.** Schematic for Muffle Furnace Reactor Used for Preparing Black Liquor Char for Elemental Analysis Through the Maximum Temperature Preheat Procedure.

The ratio of initial char (partially devolatilized char) elemental mass to residual char (completely devolatilized char) elemental mass for char prepared according to the RTPP is shown in Fig. 3. The initial elemental composition of carbonate C, sulfate S, and thiosulfate S in the partially devolatilized char was not determined. The residual masses of these elements are available in Table 4. The elemental analysis data for the initial char and residual chars prepared according to the RTPP are available in Appendix III. The elemental composition of the resulting char from the RTPP was significantly affected by the devolatilization temperature used in the fixed bed. For example, an analysis of variance test at the 99% confidence level on the C, H, O, and S data determined that the concentration of these elements were affected by the devolatilization temperature. However, an analysis of variance test at the 99% confidence level on the Na, Carbonate C, Sulfate S, and Thiosulfate S data determined that the concentrations of these elements were not affected by the devolatilization temperature. This would suggest that the $Na_2CO_3$, $Na_2SO_4$, and $Na_2S_2O_3$ compositions did not change with temperature. In addition, the compounds that were volatilized from the char during heat-up were likely of the form $C_xH_yO_z$. This is supported by the decrease in C, H, O, and residual char mass as the devolatilization

temperature increased. The increase in S with devolatilization temperature may be because S was converted to some fixed form as the char bed temperature was increased from 25-800°C. Since the char beds were held at the temperature for 1 hour after devolatilization was completed, these results suggest that the net S release is greatest at the lower temperatures of this study.

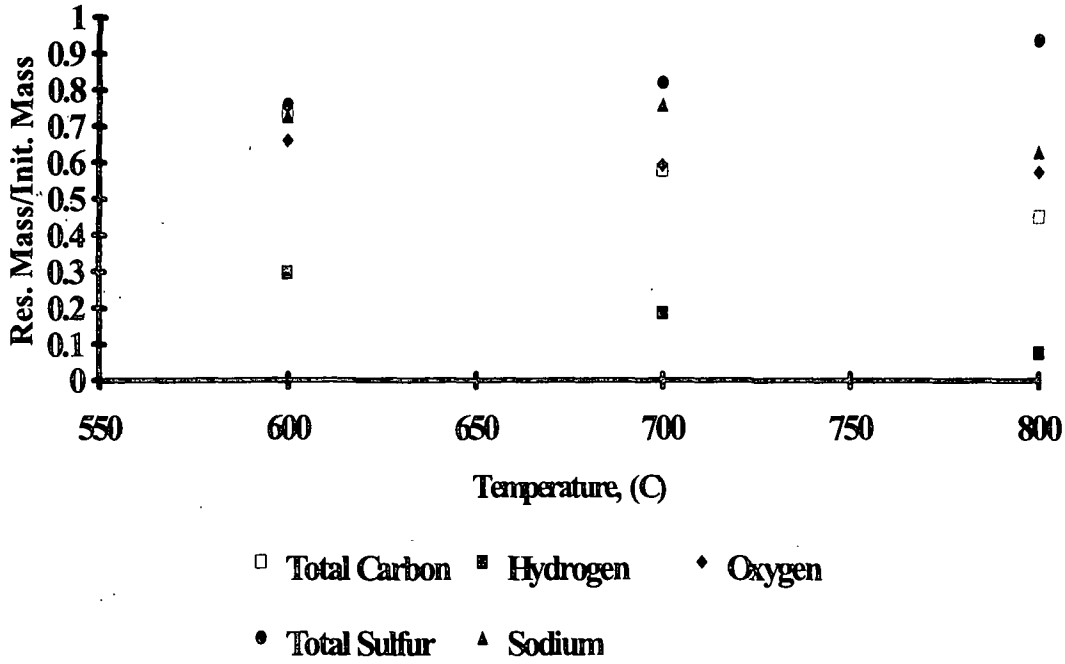


**Figure 3.** Char Element Mass/Initial Char Element Mass as a Function of Temperature for Char Prepared According to the Reaction Temperature Preheat Procedure.

**Table 4.** Composition (Mass, g) of Residual BLC Prepared According to the Reaction Temperature Preheat Procedure.

| | Devolatilization Temperature | | |
|---|---|---|---|
| **Element** | 600°C | 700°C | 800°C |
| Carbonate C | 0.59 | 0.74 | 0.64 |
| Sulfate S | 0.21 | 0.15 | 0.21 |
| Thiosulfate S | 0.03 | 0.07 | 0.02 |

The ratio of initial char (partially devolatilized char) elemental mass to residual char (completely devolatilized char) elemental mass for char prepared according to the MTPP is shown in Fig. 4. The initial elemental composition of Sulfate S and Thiosulfate S in the partially devolatilized char was not determined. The residual masses of these elements are available in Table 5. The elemental analysis data for the initial char and residual chars prepared according to the MTPP are available in Appendix III. The elemental composition of the resulting char from the MTPP was not affected by the cool-down temperature. The total C and Carbonate C values shown in Fig. 4 are averages of three experiments. Using analysis of variance and studentized range statistic at the 99% confidence level, the values over the entire temperature range cannot be judged different. In addition, the elemental mass of H, O, Na, S, Sulfate S, Thiosulfate S, or residual char mass did not increase or decrease with devolatilization temperature. Although experiments were conducted in triplicate at each cool-down temperature, only one residual sample at each temperature was processed for these elements.

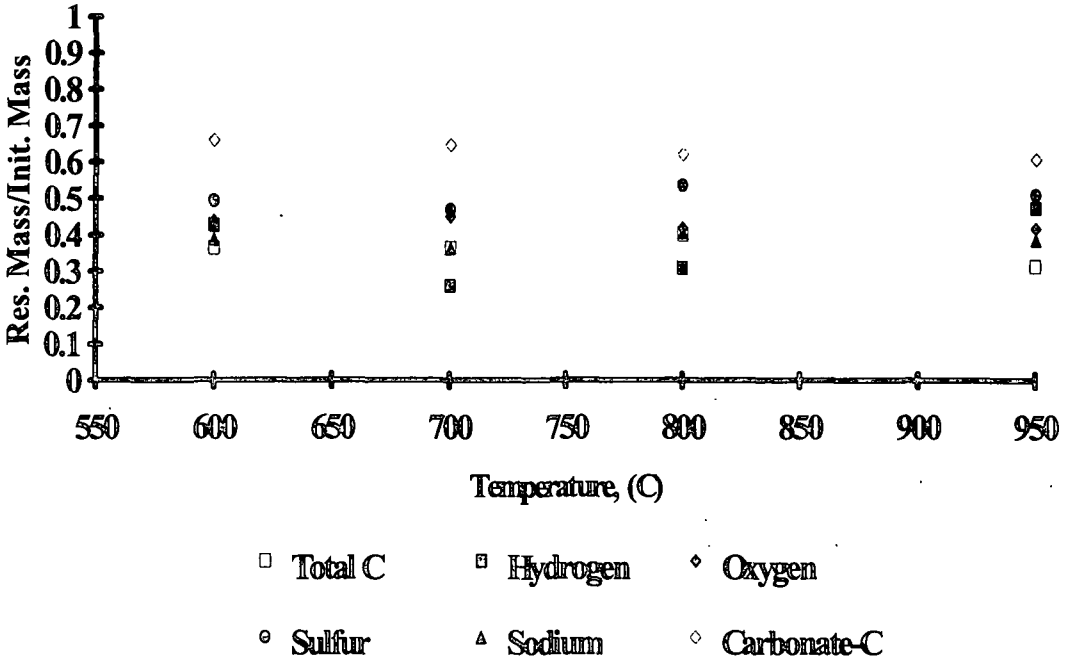


**Figure 4.** Char Element Mass/Initial Char Element Mass as a Function of Temperature for Char Prepared According to the Maximum Temperature Preheat Procedure.

**Table 5.** Composition (Mass, g) of Residual BLC Prepared According to the Maximum Temperature Preheat Procedure.

| | Devolatilization Temperature | | | |
|---|---|---|---|---|
| **Element** | 600°C | 700°C | 800°C | 950°C |
| Sulfate S | 0.01 | 0.03 | 0.03 | 0.01 |
| Thiosulfate S | 0.06 | 0.05 | 0.04 | 0.08 |

Heterogeneous Reaction of BLC

Gasification, oxidation, and gasification/oxidation experiments were initiated by replacing the CO in the carrier gas with the desired level of $CO_2$ and/or $O_2$. The product gas was monitored continuously for CO, $CO_2$, and $O_2$ concentrations. The initial and residual char mass was recorded for mass balance purposes and kinetic rate determination. Tables 6-9 contain the range of conditions used in the experimental phases. The rationale for using different carrier gases and carrier gas flowrates was to test mass transfer effects on the measured rates. Control experiments showed that $CO_2$ was not depleted significantly by the reactor walls. Appendix IV contains the results of the control experiments.

**Table 6.** Range of Conditions in the $CO_2$ Gasification Phase I Experiments Using the Reaction Temperature Preheat Procedure and Char Manufactured from Black Liquor I.

| Parameter | Value |
|---|---|
| Temperature | 600°C, 700°C, 800°C |
| Pressure | 1 atmosphere |
| $CO_2$ Concentration | 4.3%-10.1% |
| Carrier Gases | He, $N_2$ |
| Gas Flow Rate | 5.32 slpm, 10.10 slpm |
| Initial Organic Carbon Mass | 2.4-3.7 g |
| Char Mass | 10-15 g |
| Preheat Procedure | RTPP |

**Table 7.** Range of Conditions in the $CO_2$ Gasification Phase II Experiments Using the Maximum Temperature Preheat Procedure and Char Manufactured from Black Liquor II.

| Parameter | Value |
|---|---|
| Temperature | 600°C, 700°C, 800°C, 950°C |
| Pressure | 1 atmosphere |
| $CO_2$ Concentration | 4.7%-5.1% |
| Carrier Gases | He, $N_2$ |
| Gas Flow Rate | 2.71 slpm, 5.32 slpm |
| Initial Organic Carbon Mass | 5.5-6.7 |
| Char Mass | 18-22 g |
| Preheat Procedure | MTPP |

**Table 8.** Range of Conditions in the $O_2$ Oxidation Phase III Experiments Using the Maximum Temperature Preheat Procedure and Char Manufactured from Black Liquor II.

| Parameter | Value |
|---|---|
| Temperature | 700°C |
| Pressure | 1 atmosphere |
| $O_2$ Concentration | 2.0%-2.4%, 4.5%-4.7% |
| Carrier Gases | $N_2$ |
| Gas Flow Rate | 5.3-5.5 |
| Initial Organic Carbon Mass | 6.1 g |
| Char Mass | 20 g |
| Preheat Procedure | MTPP |

**Table 9.** Range of Conditions in the $CO_2/O_2$ Combination Phase IV Experiments Using the Maximum Temperature Preheat Procedure and Char Manufactured from Black Liquor II.

| Parameter | Value |
|---|---|
| Temperature | 700°C |
| Pressure | 1 atmosphere |
| $CO_2$ Concentration | 4.8%-4.9% |
| $O_2$ Concentration | 2.0%-2.2%, 4.7%-4.9% |
| Carrier Gases | $N_2$ |
| Gas Flow Rate | 5.3-5.6 slpm |
| Initial Organic Carbon Mass | 6.1 g |
| Char Mass | 20 g |
| Preheat Procedure | MTPP |

## KRAFT BLACK LIQUOR CHAR DENSITY

Although the bulk density of kraft char during devolatilization and gasification was not originally of interest in achieving the thesis objectives, it became clear that this information would provide tremendous insight into this study. Swelling data from the applicable literature was used to determine the bulk density of char during the devolatilization stage. To verify the swelling data, single droplet experiments completed at IPST[24] were reviewed. In addition, char mass and volume measurements made during $CO_2$ gasification and $O_2$ oxidation experiments were used to illustrate how char density changes during the char burning stage of combustion.

### Fixed Bed Experiments to Determine Kraft Black Liquor Char Density

Using the fixed bed reactor described earlier, the char prepared according to the RTPP and MTPP was exposed to $CO_2$ and/or $O_2$. The organic carbon concentrations and bulk densities of the black liquor char were determined from the volume, mass, and weight fraction of carbon in the residual chars from the preheat experiments and the $CO_2$ gasification experiments. The analysis of the data allowed the char density to be determined as a function of organic carbon depletion.

### Single Particle Experiments to Determine Kraft Black Liquor Char Density

Data obtained from Verrill[19] were used to arrive at values of specific volume for single char particles. Individual droplets of kraft black liquor were exposed in a single particle reactor, to various gas conditions ($CO_2/CO/N_2$, $CO/N_2$, $O_2/N_2$), temperature (500°C, 600°C, 750°C, and 900°C), residence times (3,7,10,15,20,30, and 40 seconds), and gas velocities (0.61 m/s and 1.83 m/s). During these experiments, individual droplets of black liquor were formed on nichrome wires and inserted into the quartz reaction chamber of the furnace. After the specified residence time, the resulting char was withdrawn from the pyrolytic environment into a quench stream and allowed to cool. A constant average

velocity in the quartz reaction chamber was maintained for different furnace temperatures by adjusting the gas flow rate. Each experiment typically consisted of two replicate weight loss determinations at three different particle residence times. Composite samples of five fully-intact char particles were accumulated for each weight determination. Control of the exposure time was very good; for a given determination, the standard deviation of the average exposure time ranged from 0.1 to 0.3 seconds.

Droplet combustion and pyrolysis behavior recorded on videotape by Verrill,[19] were further analyzed for this thesis. A Tracor Northern TN-8502 image analyzer was used to determine the char particle size. The image analysis procedure was initiated by acquiring the image directly from the video. This original image consisted of a continuously varying gray picture. The image was then sampled at discrete points and the light intensity was converted to an integer value varying from black (0) to white (255). Next, the original gray level image was processed to reduce the background to a more uniform gray level. The next step involved a process called binary thresholding which created a two-state map resulting in a binary image which is defined as a black and white representation of the gray image. The droplet volume was then calculated from the average droplet diameter.

It should be noted that the swelling reported in this study is on a different basis than earlier work.[34-38] Swelling has been traditionally expressed as a swelling factor or as the specific swollen volume; however, these definitions do not allow the specific volume per mass of char to be determined throughout the stages of combustion. Knowing the specific volume of char allows the data to be converted to density as a function of time. In this study, specific volume was defined as the particle volume divided by the particle mass at the time of measurement.

## EXPERIMENTAL EQUIPMENT

The fixed bed reactor was designed to study the gasification and oxidation of BLC at elevated temperatures. The following section describes the components of the fixed bed reactor.

### Fixed Bed Reactor Components

A schematic diagram depicting the major components of the fixed bed reactor is illustrated in Fig. 1. The gas preheat coil was constructed from 1/4-in. ID stainless steel tubing. Heat transfer calculations (Appendix V) indicated that 12.5 ft of tube was necessary to heat the gas mixture to 1200°C. To ensure adequate heat transfer, the actual tube length was 40 ft. The preheat coil was connected to an AISI Type 304 (16 gage) stainless steel exterior retort by a 3/8 in. fitting. Upon entering the exterior retort, the gas mixture was dispersed by a baffle directly above the connection point.

The char was contained in a char retort (7.6 cm diameter by 38 cm length) which was constructed of Haynes HR-160 alloy. The char rested on a Nichrome screen which rested in the bottom of the char retort. The char retort allowed the char bed to rest at the center of the furnace. In addition, another Nichrome screen was placed on top of the char bed to prevent the light, friable char from flying out of the char containing retort and plugging the exit lines.

An alumina crucible was placed on the baffle and served as a lower sleeve for the char containing retort. This location was selected to prevent molten smelt from plugging the gas inlet. Alumina crucibles can withstand exposure to molten salts above the temperature range of the experiments and are not reactive with the gases and inorganics in char and smelt.

The retorts were capped with a 1.0 in. thick stainless steel plate. Commercial gaskets used for steam lines were used between the flanges to ensure no gas loss from the system. Gas flow balances at

room temperature and the reaction temperature indicated minimal gas loss (<5%) with these gaskets. After product gas exited the top of the furnace, CO, $CO_2$, and $O_2$ concentrations were determined with gas analyzers. An NDIR analyzer was used to determine CO and $CO_2$ concentration and a Teledyne Hastings microfuel cell detector was used to determine $O_2$ concentration. During each experiment, the gas analyzers were calibrated before char preheat and prior to reactant gas addition. The product gas passed through a packed tube of glass wool before entering the gas analyzers to prevent particulate contamination of the detectors.

The high temperature tube furnace had a maximum rated temperature of 1093°C (2000°F). The furnace temperature was controlled automatically with an electronic proportional controller to ± 1°C. The wall temperature control thermocouple was implanted in the midpoint of the furnace wall. A type-K thermocouple implanted in the center of the char bed was used to control the bed (reaction) temperature. This thermocouple was calibrated against a standardized thermocouple over the temperature range of this study. The furnace temperature was manually adjusted to achieve the desired bed temperature. Thermo-12™ block insulation was used to reduce heat losses from the top and bottom of the furnace.

Gas ($N_2$, He, CO, $CO_2$, and $O_2$) flow was regulated by needle valves and monitored by Hastings digital mass flow meters. The flow meters were calibrated against wet flow meters. The mass flow meters measure flow with no correction for temperature and pressure as with traditional flow meters. The manufacturer's calibration for the flow meters was for air; therefore, the measurements for the reactant gases were corrected with appropriate conversion factors.

# RESULTS AND DISCUSSION

The experimental data and a discussion of results are presented in the following five sections and basically follow the order of the original objectives. In Section 1, the kinetics of the $CO_2$ gasification of kraft black liquor char using the fixed bed reactor are presented. Furthermore, the effect of the different preheat methods on the gasification rate are discussed. Finally, the results of the thesis are compared to the earlier $CO_2$ gasification results. In Section 2, the transition temperature where the $CO_2$ gasification reaction goes from kinetic control to mass transfer control is established for a char bed geometry. In Section 3, the results of $O_2$ combustion of kraft black liquor char using the fixed bed reactor are presented. In Section 4, the results of $O_2/CO_2$ char burning of kraft black liquor char are discussed. In Section 5, data are presented which determine the bulk density and organic carbon concentration of kraft black liquor char during the char burning stage of combustion.

## 1. $CO_2$ GASIFICATION OF KRAFT BLACK LIQUOR CHAR IN A FIXED BED REACTOR

### Thermodynamic Feasibility

Prior to a discussion of the kinetics of $CO_2$ gasification, the thermodynamic feasibility of the $CO_2$ gasification reaction was explored. Appendix VI reviews the thermodynamics of this reaction. Over the temperature range explored in this study, the reaction is thermodynamically feasible.

Determination of Kinetic Parameters

Regression Analysis

Typical sets of CO and $CO_2$ concentration profiles obtained at the reactor outlet are shown in Figs. 5 and 6 for chars preheated according to the Reaction Temperature Preheat Procedure and the Maximum Temperature Preheat Procedure, respectively. Complete sets of CO and $CO_2$ concentration profiles recorded at the various experimental conditions outlined in Tables 3 and 4 (of the EXPERIMENTAL section) are provided in Appendices VII and VIII. In addition, the elemental analyses of residual chars gasified by $CO_2$ and prepared according to the RTPP and MTPP are available in Appendix IX. The rate of gasification was determined from the $CO_2$ concentration profiles according to a method outlined by Smith[89] for a fixed bed in which the solid particles contain one reactant and the second reactant is in the fluid phase. The $CO_2$ concentration decreased along the reactor length, and this variation of concentration with length was a function of time. Thus, the process did not operate at a steady state. For isothermal plug-flow, a mass conservation equation for $CO_2$ is written as:

$$-u\frac{\partial(C_{CO_2})}{\partial z} = r\rho_{bed} + \varepsilon_{bed}\frac{\partial(C_{CO_2})}{\partial t} \qquad \text{eqn. 10}$$

where $\rho_{bed}$ = density of char bed, (kg organic C/$m^3$ char)
(both organic carbon mass and char volume were dependent on char bed height, z)
$r\rho_{bed}$ = global rate of disappearance of $CO_2$ per unit volume of reactor, (gmole/$m^3$/s)
u = superficial velocity in the direction of flow, (m/s)
$\varepsilon_{bed}$ = void fraction of char bed, (0.40)
z = axial position in the char bed, (m)
t = time, (s)

An energy balance, available in Appendix X, suggests that the temperature difference from the bottom to the top of the bed is approximately -4.5°C. Therefore, it is reasonable to assume that the fixed bed reactor is essentially isothermal. Levenspiel[90] notes that the vessel dispersion number represents flow

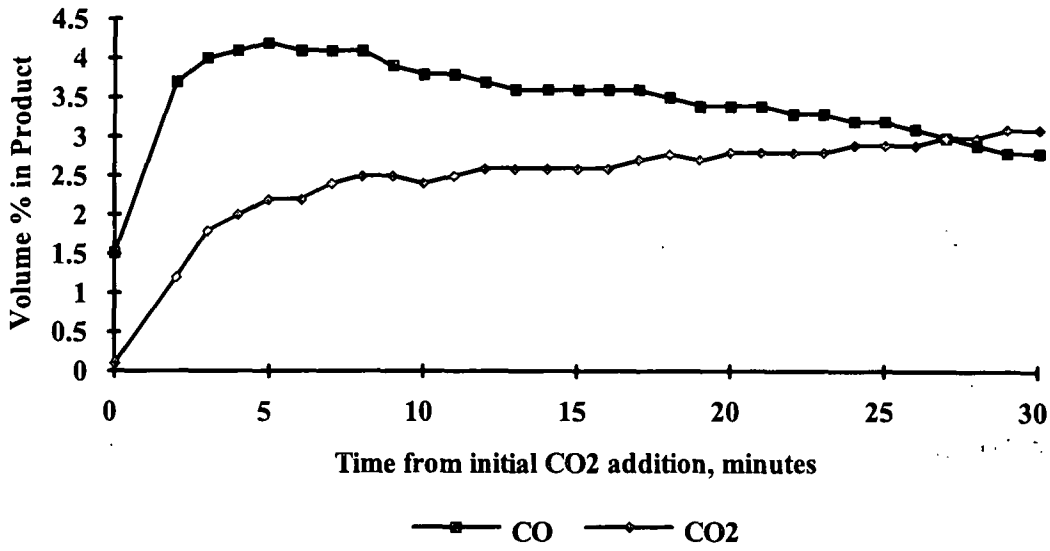


**Figure 5.** %CO and $\%CO_2$ in Product Gas as a Function of Time for a Typical Gasification Experiment for Char Prepared According to the Reaction Temperature Preheat Procedure (702°C, 4.3% $CO_2$, 5.3 slpm, $N_2$ Carrier Gas).

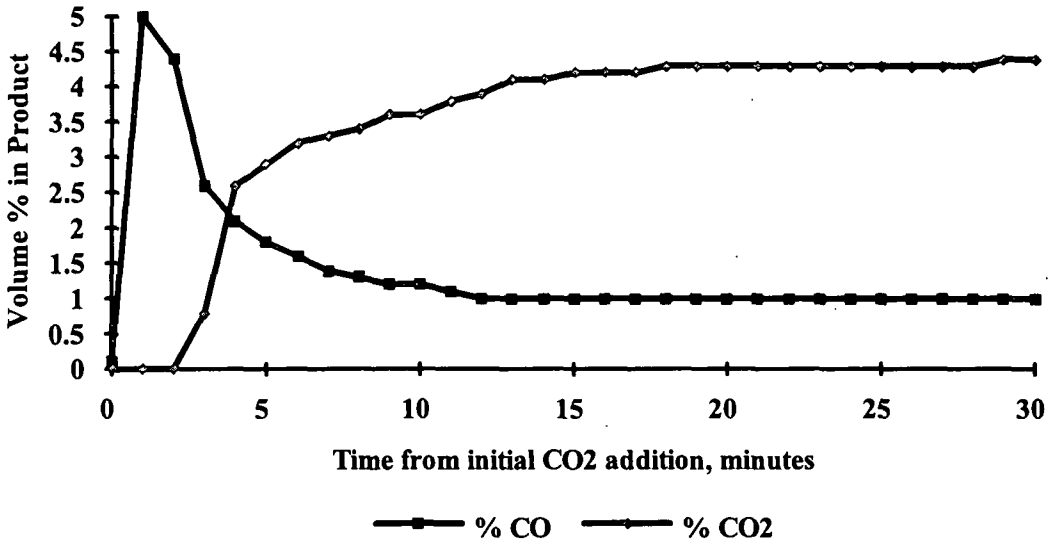


**Figure 6.** %CO and $\%CO_2$ in Product Gas as a Function of Time for a Typical Gasification Experiment for Char Prepared According to the Maximum Temperature Preheat Procedure (712°C, 4.8%$CO_2$, 5.5 slpm, $N_2$ Carrier Gas).

that deviates not too greatly from plug flow. The vessel dispersion number for the fixed bed reactor, available in Appendix XI, was determined at room temperature using a step test. The results indicate that there is an intermediate level of dispersion in the fixed bed reactor. However, experimental observations suggest that dispersion is negligible since the residual char beds are uniform in appearance and the product gas concentrations do not show any unusual peaks or dips.

Over small increments of time (1 to 2 minutes in Figs. 5 and 6), the $CO_2$ concentration is approximately constant and the time component in eqn. 10 can be considered negligible. For example, an order of magnitude calculation shows that the rate component is at least three orders of magnitude greater than the time component (~1700:1). Assuming a global rate for $CO_2$ gasification of BLC (i.e., $r = k(C_{CO_2})^n$ where n is the reaction order), eqn. 10 can be integrated and rearranged to solve for the rate constant.

For all values of n except n = 1,

$$k = \frac{u}{L\rho_{bed}}\left[\frac{(C_{CO_2})_{feed}^{(1-n)} - (C_{CO_2})_{exit}^{(1-n)}}{(1-n)}\right] = \frac{uA}{m}\left[\frac{(C_{CO_2})_{feed}^{(1-n)} - (C_{CO_2})_{exit}^{(1-n)}}{(1-n)}\right] \qquad \text{eqn. 11}$$

where A = total cross sectional area of the fixed bed reactor, ($m^2$)
m = mass of organic carbon in the fixed bed reactor, (kg)
L = char bed height, (m)
k = reaction rate constant.

For first order (n=1),

$$k = \frac{u}{L\rho_{bed}} \ln \frac{(C_{CO_2})_{feed}}{(C_{CO_2})_{exit}} = \frac{uA}{m} \ln \frac{(C_{CO_2})_{feed}}{(C_{CO_2})_{exit}}. \qquad \text{eqn. 12}$$

Evaluation of eqn. 12 at $\Delta$ t increments of one minute yields the rate constant (for a first order global rate (n=1)) as a function of fractional conversion of organic carbon. Figs. 7 and 8 show the results

for the experimental data shown in Figs. 5 and 6. Complete sets of rate constant results for the various experimental conditions are available in Appendices XII and XIII. Fig. 7 shows that for a typical experiment at 700°C the rate constant is independent of fractional conversion of organic carbon. However, a typical fractional conversion profile at 800°C shows several distinguishable regions (Figs. 9 and 10). Initially, a high rate constant is observed (for conversions of 0-10%), which decreases at higher conversion and passes through a minimum between 15-40% fractional conversion. Depending on the experimental parameters, either a constant or a continuously increasing rate constant is observed from 40% up to 65-85% conversion. The reasons for this will be discussed later. No observations were recorded at higher conversions.

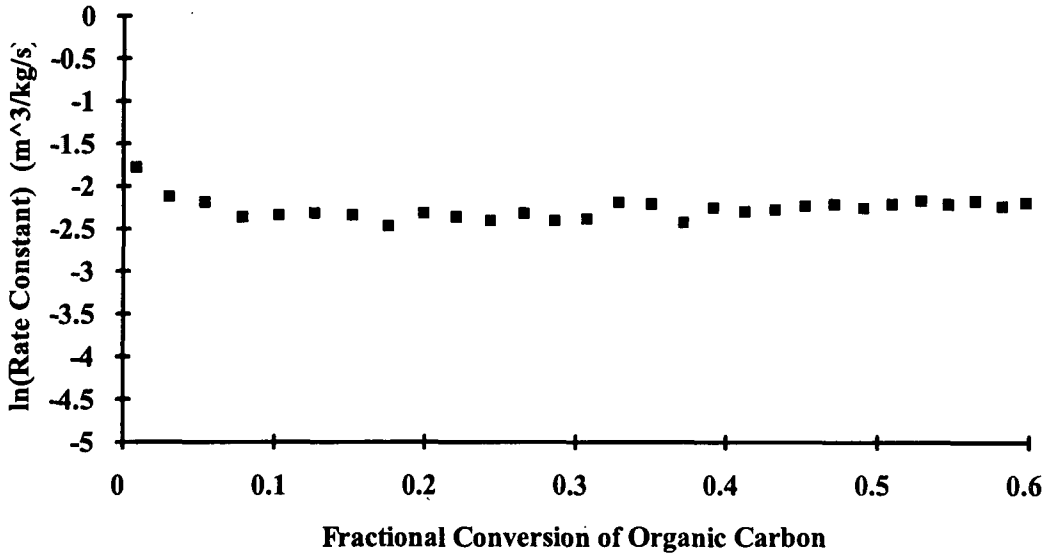


**Figure 7.** Rate Constant vs. Fractional Burnout of Organic Carbon for a Typical Gasification Experiment for Char Prepared According to the Reaction Temperature Preheat Procedure (702°C, 4.3% $CO_2$, 5.3 slpm, $N_2$ Carrier Gas).

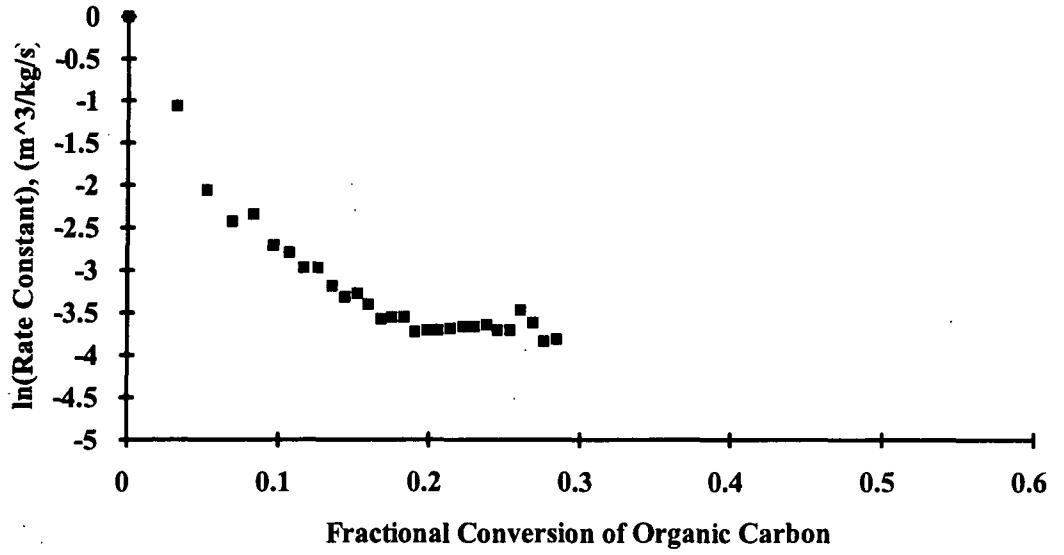


**Figure 8.** Rate Constant vs. Fractional Burnout of Organic Carbon for a Typical Gasification Experiment for Char Prepared According to the Maximum Temperature Preheat Procedure (712°C, 4.8%$CO_2$, 5.5 slpm, $N_2$ Carrier Gas).

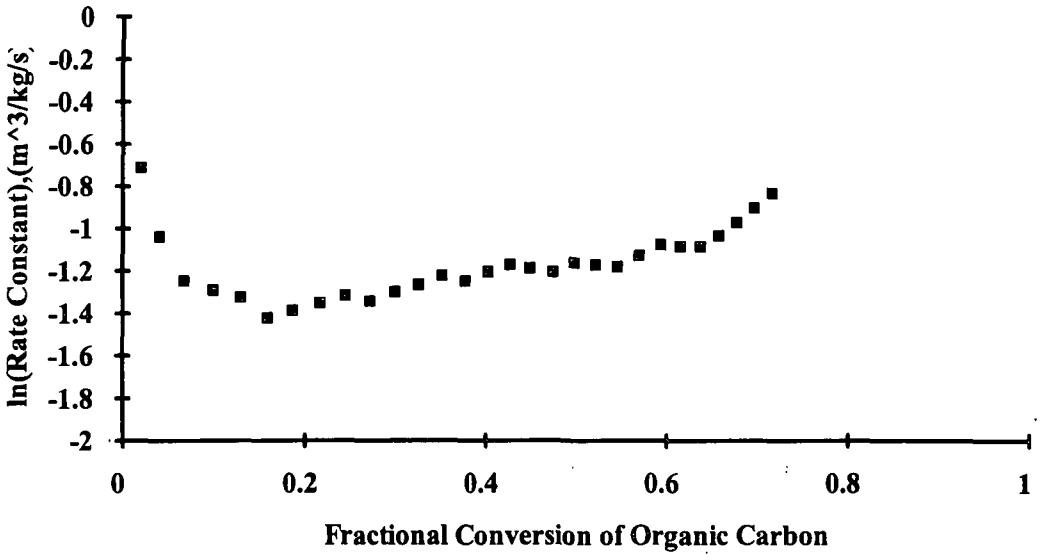


**Figure 9.** Rate Constant vs. Fractional Burnout of Organic Carbon for a Typical Gasification Experiment for Char Prepared According to the Reaction Temperature Preheat Procedure (800°C, 4.4% $CO_2$, 5.4 slpm, $N_2$ Carrier Gas).

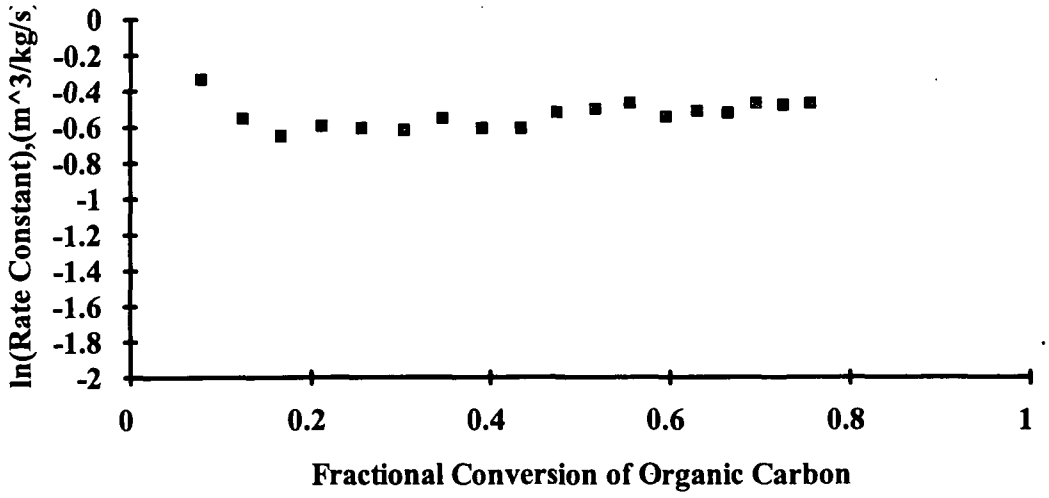


**Figure 10.** Rate Constant vs. Fractional Burnout of Organic Carbon for a Typical Gasification Experiment for Char Prepared According to the Maximum Temperature Preheat Procedure (801°C, 5.1%$CO_2$, 5.2 slpm, $N_2$ Carrier Gas).

To determine the reaction order, the reaction order was guessed and the differential equation (eqn. 10) used to model the fixed bed reactor was integrated. If the rate is expressed as $r = k\left(C_{CO_2}\right)^n$, eqn. 11 can be expressed as follows for any value of n other that n=1.

$$\frac{\left(C_{CO_2}^{(1-n)}\right)_{feed} + \left(C_{CO_2}^{(1-n)}\right)_{exit}}{(1-n)} = k\left(\frac{m}{uA}\right) \qquad \text{eqn. 13}$$

For first order (n=1), eqn. 12 becomes:

$$\ln\frac{(C_{CO_2})_{feed}}{(C_{CO_2})_{exit}} = k\left(\frac{m}{uA}\right). \qquad \text{eqn. 14}$$

If the assumed order is correct, a plot of the left side of the equation versus the right side should be linear. For values of n = 0, 0.5, 1, 1.5, and 2, the concentration terms on the left side of eqns. 13 and 14 were plotted versus $\left(\frac{m}{uA}\right)$. Table 10 summarizes the $R^2$ values for the respective orders. From this analysis, it is difficult to conclude that one value of n adequately represents all of the data.

**Table 10:** Summary of $R^2$ Values to Test for Different Orders for $CO_2$ Gasification Data

| Exp. Num. | Temp. (°C) | $CO_2$ Conc., (%) | Gas Flow | Carrier Gas | Preheat Procedure | $R^2$ n=0 | $R^2$ n=.5 | $R^2$ n=1 | $R^2$ n=1.5 | $R^2$ n=2 |
|---|---|---|---|---|---|---|---|---|---|---|
| 4909 | 601 | 4.3 | 5.3 | $N_2$ | RTPP | 0.94 | 0.94 | 0.94 | 0.93 | 0.92 |
| 4910 | 600 | 4.3 | 5.3 | $N_2$ | RTPP | 0.74 | 0.74 | 0.73 | 0.73 | 0.72 |
| 4911 | 604 | 4.4 | 5.3 | $N_2$ | RTPP | 0.74 | 0.59 | 0.41 | 0.34 | 0.27 |
| 4902 | 702 | 4.3 | 5.3 | $N_2$ | RTPP | 0.68 | 0.76 | 0.88 | 0.85 | 0.87 |
| 4903 | 700 | 4.4 | 5.3 | $N_2$ | RTPP | 0.97 | 0.96 | 0.96 | 0.95 | 0.95 |
| 4904 | 701 | 4.3 | 5.3 | $N_2$ | RTPP | 0.82 | 0.85 | 0.9 | 0.87 | 0.88 |
| 4905 | 801 | 4.4 | 5.3 | $N_2$ | RTPP | 0.94 | 0.95 | 0.95 | 0.95 | 0.95 |
| 4906 | 800 | 4.4 | 5.4 | $N_2$ | RTPP | 0.96 | 0.96 | 0.96 | 0.95 | 0.93 |
| 4907 | 799 | 4.3 | 5.3 | $N_2$ | RTPP | 0.73 | 0.76 | 0.77 | 0.74 | 0.73 |
| 4913 | 800 | 4.9 | 5.4 | He | RTPP | 0.98 | 0.97 | 0.97 | 0.81 | 0.68 |
| 4914 | 800 | 4.8 | 5.4 | He | RTPP | 0.97 | 0.95 | 0.91 | 0.84 | 0.77 |
| 4915 | 803 | 4.9 | 5.4 | He | RTPP | 0.98 | 0.96 | 0.87 | 0.73 | 0.58 |
| 4916 | 801 | 4.7 | 10.6 | $N_2$ | RTPP | 0.88 | 0.88 | 0.89 | 0.88 | 0.88 |
| 4917 | 805 | 4.8 | 10.6 | $N_2$ | RTPP | 0.94 | 0.93 | 0.91 | 0.88 | 0.85 |
| 4918 | 803 | 4.7 | 10.6 | $N_2$ | RTPP | 0.98 | 0.98 | 0.98 | 0.97 | 0.95 |
| 4979 | 604 | 4.8 | 5.4 | $N_2$ | MTPP | 0.68 | 0.68 | 0.69 | 0.69 | 0.69 |
| 4982 | 602 | 4.7 | 5.5 | $N_2$ | MTPP | 0.31 | 0.33 | 0.34 | 0.34 | 0.35 |
| 4972 | 712 | 4.8 | 5.5 | $N_2$ | MTPP | 0.89 | 0.9 | 0.9 | 0.91 | 0.91 |
| 4973 | 712 | 4.8 | 5.5 | $N_2$ | MTPP | 0.79 | 0.77 | 0.75 | 0.75 | 0.73 |
| 4975 | 699 | 4.8 | 5.4 | $N_2$ | MTPP | 0.87 | 0.85 | 0.81 | 0.82 | 0.8 |
| 4976 | 799 | 4.8 | 5.5 | $N_2$ | MTPP | 0.62 | 0.9 | 0.89 | 0.87 | 0.85 |
| 4977 | 795 | 4.8 | 5.5 | $N_2$ | MTPP | 0.94 | 0.94 | 0.94 | 0.93 | 0.91 |
| 4989 | 801 | 5.1 | 5.2 | $N_2$ | MTPP | 0.94 | 0.98 | 0.98 | 0.95 | 0.88 |
| 4985 | 696 | 4.8 | 2.7 | $N_2$ | MTPP | 0.92 | 0.89 | 0.87 | 0.81 | 0.77 |
| 4990 | 699 | 5.1 | 2.6 | $N_2$ | MTPP | 0.95 | 0.92 | 0.84 | 0.86 | 0.82 |
| 4991 | 693 | 5.1 | 2.7 | $N_2$ | MTPP | 0.92 | 0.9 | 0.88 | 0.84 | 0.81 |
| 4974 | 697 | 5 | 5.3 | He | MTPP | 0.68 | 0.67 | 0.54 | 0.65 | 0.64 |
| 4983 | 698 | 4.8 | 5.5 | He | MTPP | 0.57 | 0.56 | 0.52 | 0.53 | 0.52 |

Next, the following equations were generated by taking the natural logarithm of each side of eqns. 13 and 14. For any value of n other than n=1,

$$\ln\left[\frac{\left(C_{CO_2}^{(1-n)}\right)_{feed}-\left(C_{CO_2}^{(1-n)}\right)_{exit}}{(1-n)}\right]=\ln\left(\frac{m}{uA}\right)+\ln k \text{ , and} \qquad \text{eqn. 15}$$

for first order (n=1),

$$\ln\left[\ln\frac{(C_{CO_2})_{feed}}{(C_{CO_2})_{exit}}\right]=\ln\left(\frac{m}{uA}\right)+\ln k \text{ .} \qquad \text{eqn. 16}$$

Again, if the assumed order is correct, a plot of the left side versus the $\ln\left(\frac{m}{uA}\right)$ term would be linear. For values of n = 0, 0.5, 1, 1.5, and 2, the concentration terms on the left side of eqns. 15 and 16 where plotted versus $\ln\left(\frac{m}{uA}\right)$. Table 11 summarizes the $R^2$ values and the resultant slopes for the respective orders. Obviously, $R^2$ values closest to 1.0 and the slopes closest to 1.0 indicate the best value of n. From this analysis, it is again difficult to conclude that one value of n adequately represents all of the data.

**Table 11:** Summary of $R^2$ Values and Slopes to Test for Different Orders for $CO_2$ Gasification Data

| Exp. Num. | Temp. (°C) | $CO_2$ Conc., (%) | Gas Flow | Carrier Gas | Prebt. Proc. | $R^2$ n=0 | $R^2$ n=.5 | $R^2$ n=1 | $R^2$ n=1.5 | $R^2$ n=2 | slope n=0 | slope n=.5 | slope n=1 | slope n=1.5 | slope n=2 |
|---|---|---|---|---|---|---|---|---|---|---|---|---|---|---|---|
| 4909 | 601 | 4.3 | 5.3 | $N_2$ | RTPP | 0.88 | 0.88 | 0.88 | 0.87 | 0.87 | 0.66 | 0.68 | 0.7 | 0.72 | 0.74 |
| 4910 | 600 | 4.3 | 5.3 | $N_2$ | RTPP | 0.87 | 0.87 | 0.87 | 0.87 | 0.87 | 0.95 | 0.97 | 0.99 | 1.02 | 1.05 |
| 4911 | 604 | 4.4 | 5.3 | $N_2$ | RTPP | 0.78 | 0.78 | 0.77 | 0.77 | 0.77 | 1.01 | 1.04 | 1.07 | 1.1 | 1.14 |
| 4902 | 702 | 4.3 | 5.3 | $N_2$ | RTPP | 0.81 | 0.86 | 0.9 | 0.92 | 0.92 | 0.58 | 0.65 | 0.73 | 0.81 | 0.91 |
| 4903 | 700 | 4.4 | 5.3 | $N_2$ | RTPP | 0.96 | 0.96 | 0.96 | 0.95 | 0.95 | 0.76 | 0.85 | 0.95 | 1.05 | 1.16 |
| 4904 | 701 | 4.3 | 5.3 | $N_2$ | RTPP | 0.89 | 0.89 | 0.89 | 0.89 | 0.89 | 0.85 | 0.95 | 1.05 | 1.16 | 1.29 |
| 4905 | 801 | 4.4 | 5.3 | $N_2$ | RTPP | 0.95 | 0.95 | 0.95 | 0.95 | 0.95 | 0.34 | 0.45 | 0.57 | 0.71 | 0.88 |
| 4906 | 800 | 4.4 | 5.4 | $N_2$ | RTPP | 0.97 | 0.97 | 0.96 | 0.96 | 0.96 | 0.35 | 0.46 | 0.6 | 0.77 | 0.97 |
| 4907 | 799 | 4.3 | 5.3 | $N_2$ | RTPP | 0.58 | 0.68 | 0.73 | 0.75 | 0.75 | 0.15 | 0.22 | 0.3 | 0.4 | 0.52 |
| 4979 | 604 | 4.8 | 5.4 | $N_2$ | MTPP | 0.5 | 0.5 | 0.5 | 0.51 | 0.51 | 0.95 | 0.96 | 0.97 | 0.98 | 1 |
| 4982 | 602 | 4.7 | 5.5 | $N_2$ | MTPP | 0.84 | 0.84 | 0.84 | 0.84 | 0.84 | 1.42 | 1.43 | 1.43 | 1.44 | 1.44 |
| 4972 | 712 | 4.8 | 5.5 | $N_2$ | MTPP | 0.83 | 0.84 | 0.85 | 0.85 | 0.85 | 0.91 | 0.95 | 0.99 | 1.04 | 1.08 |
| 4973 | 712 | 4.8 | 5.5 | $N_2$ | MTPP | 0.71 | 0.71 | 0.71 | 0.7 | 0.7 | 0.83 | 0.89 | 0.94 | 0.99 | 1.05 |
| 4975 | 699 | 4.8 | 5.4 | $N_2$ | MTPP | 0.86 | 0.86 | 0.86 | 0.87 | 0.87 | 0.93 | 0.98 | 1.03 | 1.08 | 1.13 |
| 4976 | 799 | 4.8 | 5.5 | $N_2$ | MTPP | 0.82 | 0.81 | 0.78 | 0.76 | 0.74 | 0.27 | 0.49 | 0.82 | 1.25 | 1.79 |
| 4977 | 795 | 4.8 | 5.5 | $N_2$ | MTPP | 0.91 | 0.96 | 0.96 | 0.96 | 0.95 | 0.6 | 0.89 | 1.27 | 1.77 | 2.3 |
| 4989 | 801 | 5.1 | 5.2 | $N_2$ | MTPP | 0.97 | 0.99 | 0.99 | 0.99 | 0.98 | 0.4 | 0.6 | 0.88 | 1.23 | 1.65 |

Next, the slope was forced equal to 1.0 and the regression of the experimental data about this slope was determined (using eqns. 15 and 16). Table 12 summarizes the $R^2$ values for the respective orders. From this analysis, it is also difficult to conclude that one value of n adequately represents all of the data.

**Table 12:** Summary of $R^2$ Values to Test for Different Orders for $CO_2$ Gasification Data

| Exp. Num. | Temp. (°C) | $CO_2$ Conc., (%) | Gas Flow | Carrier Gas | Preht. Proc. | $R^2$ n=0 | $R^2$ n=.5 | $R^2$ n=1 | $R^2$ n=1.5 | $R^2$ n=2 |
|---|---|---|---|---|---|---|---|---|---|---|
| 4909 | 601 | 4.3 | 5.3 | $N_2$ | RTPP | 0.88 | 0.88 | 0.88 | 0.87 | 0.87 |
| 4910 | 600 | 4.3 | 5.3 | $N_2$ | RTPP | 0.87 | 0.87 | 0.87 | 0.87 | 0.87 |
| 4911 | 604 | 4.4 | 5.3 | $N_2$ | RTPP | 0.78 | 0.78 | 0.77 | 0.77 | 0.77 |
| 4902 | 702 | 4.3 | 5.3 | $N_2$ | RTPP | 0.81 | 0.86 | 0.9 | 0.92 | 0.93 |
| 4903 | 700 | 4.4 | 5.3 | $N_2$ | RTPP | 0.96 | 0.96 | 0.96 | 0.95 | 0.95 |
| 4904 | 701 | 4.3 | 5.3 | $N_2$ | RTPP | 0.89 | 0.89 | 0.89 | 0.89 | 0.88 |
| 4905 | 801 | 4.4 | 5.3 | $N_2$ | RTPP | 0.95 | 0.95 | 0.95 | 0.95 | 0.94 |
| 4906 | 800 | 4.4 | 5.4 | $N_2$ | RTPP | 0.97 | 0.96 | 0.96 | 0.95 | 0.95 |
| 4907 | 799 | 4.3 | 5.3 | $N_2$ | RTPP | 0.58 | 0.68 | 0.73 | 0.75 | 0.75 |
| 4979 | 604 | 4.8 | 5.4 | $N_2$ | MTPP | 0.5 | 0.5 | 0.5 | 0.51 | 0.52 |
| 4982 | 602 | 4.7 | 5.5 | $N_2$ | MTPP | 0.84 | 0.84 | 0.84 | 0.84 | 0.84 |
| 4972 | 712 | 4.8 | 5.5 | $N_2$ | MTPP | 0.8 | 0.81 | 0.82 | 0.83 | 0.84 |
| 4973 | 712 | 4.8 | 5.5 | $N_2$ | MTPP | 0.71 | 0.71 | 0.71 | 0.71 | 0.71 |
| 4975 | 699 | 4.8 | 5.4 | $N_2$ | MTPP | 0.87 | 0.86 | 0.86 | 0.87 | 0.87 |
| 4976 | 799 | 4.8 | 5.5 | $N_2$ | MTPP | 0.79 | 0.75 | 0.71 | 0.68 | 0.66 |
| 4977 | 795 | 4.8 | 5.5 | $N_2$ | MTPP | 0.91 | 0.95 | 0.96 | 0.95 | 0.95 |
| 4989 | 801 | 5.1 | 5.2 | $N_2$ | MTPP | 0.97 | 0.99 | 0.99 | 0.99 | 0.98 |

Fractional Conversion Profile

Initially, the rate constant was expected to remain independent of fractional conversion and the analyses were based on that assumption. However, some of the data do not remain independent of conversion (e.g. Figs. 8 and 9). Several researchers[50, 69, 78, 88, 91] studying the alkali catalyzed gasification of carbon with $CO_2$ have experienced similar results. In addition, the results of Li and van Heiningen[38, 41] and Frederick *et al.*[44] also show some results where the rate is dependent on fractional conversion.

Meijer[50] completed a comparative study on the kinetics of the alkali-catalyzed gasification reactivity in $CO_2$ of bituminous coal char at elevated pressures in a fixed-bed reactor (FBR) and a

thermobalance (TGA). It is interesting that their burn-off profiles, shown in Figs. 11 and 12, show the same distinguishable regions found in some of the results of this study. At the beginning, a high gasification rate is observed, which decreases at higher burn-off and passes through a minimum between 30 to 50 % burn-off. Depending on the experimental conditions and apparatus, from 50% up to 70 or 80% burn-off, either a constant or a continuously increasing rate is observed. At burn-offs greater than 80%, a strong rate decrease is observed for all experimental conditions.

In describing the burn-off profile, Meijer[50] assumed that the rate of gasification is directly proportional (first order) to the amount of potassium involved in gasification and independent of burn-off (zero order in carbon). Meijer[50] suggests that the gasification of alkali impregnated coal char particles is based on a model where the particle consists of very small (non-porous) grains which only react at its external surface. Therefore, only the alkali metal catalyst (potassium in this case) present at the external surface of the char grains is involved in gasification. At the initiation of a gasification experiment (0-10% fractional conversion), all of the potassium is preferentially present at the outer surface of the char grains, resulting in a high gasification rate. As gasification proceeds (10-30% fractional conversion), the potassium interface migrates into the grains and the amount of catalyst accessible for $CO_2$ decreases, resulting in a decrease in the gasification rate. Between 30-50% fractional conversion, the highest state of potassium homogeneity in the grains is reached; this is represented as the lowest potassium concentration at the external surface of the grains. Therefore, the rates are lowest in this regime. With increasing fractional conversion (up to 80%), the concentration of potassium catalyst in the grains homogeneously increases due to shrinking of the outer boundary of the char grains, resulting in an observed rate increase. Finally, at even higher fractional conversion (> 80%), Meijer[50] observed a strong rate decrease which was explained by the collapse of the particle structure, pore plugging, and catalyst loss by evaporation. Meijer[50] noted that because the rates of gasification are dependent on burn-off, a standard condition must be chosen for determining the kinetic parameters. Because the

highest state of potassium homogeneity occurs at the minimum, the kinetic parameters were determined there.

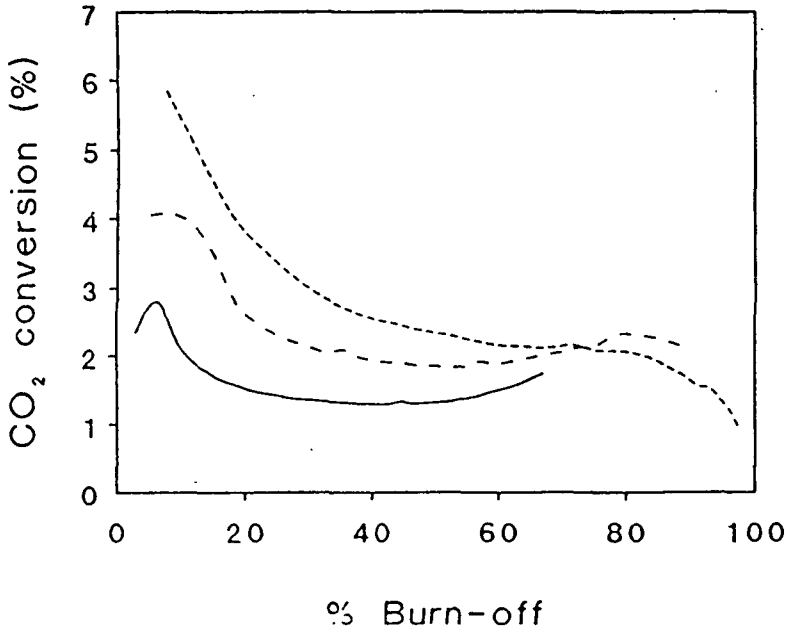


**Figure 11.** Typical burn-off profiles obtained in the fixed-bed reactor at different $pCO_2$ (4 wt% $K_2CO_3$/char Westerholt, T = 1073K)[50].
(_____ = 1.5 bar; __ __ __ = 5 bar; --------- = 20 bar)

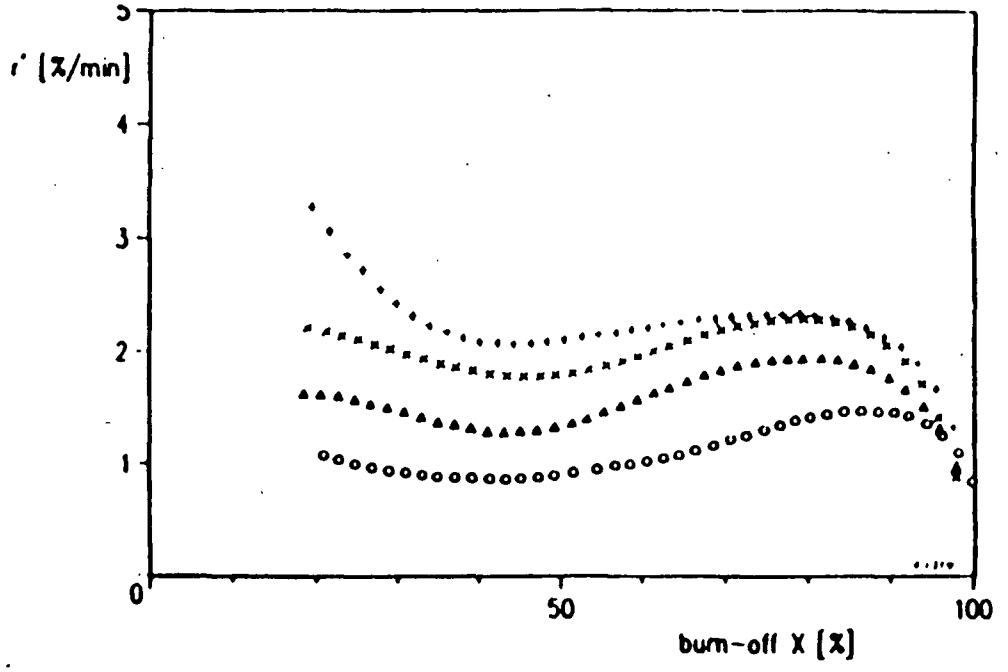


**Figure 12.** Typical burn-off profiles obtained in the thermobalance at different $pCO_2$ (4 wt% $K_2CO_3$/char Westerholt, T = 1073K)[50].
(o = 2 bar, ▲ = 5 bar, x = 10 bar, + = 20 bar)

Sams and Shadman[78] also investigated gasification kinetics in alkali impregnated coal char. They also found that the reaction rate changes as the sample is consumed. The rates were a function of carbon conversion for four catalyst concentrations as shown in Figure 13. Sams and Shadman[78] suggested that the change of rate with conversion is initially slow and the rate may increase or decrease depending on the initial catalyst concentration. However, in all cases the rate drops dramatically after a certain level of conversion is achieved. They suggested that a constant reaction rate seems unlikely because the rate is a complex function of catalyst concentration and internal surface area, both of which vary with conversion. Moreover, they expected that the rate would also change due to catalyst loss by various mechanisms such as irreversible reactions with char ash and escape to the gas phase.

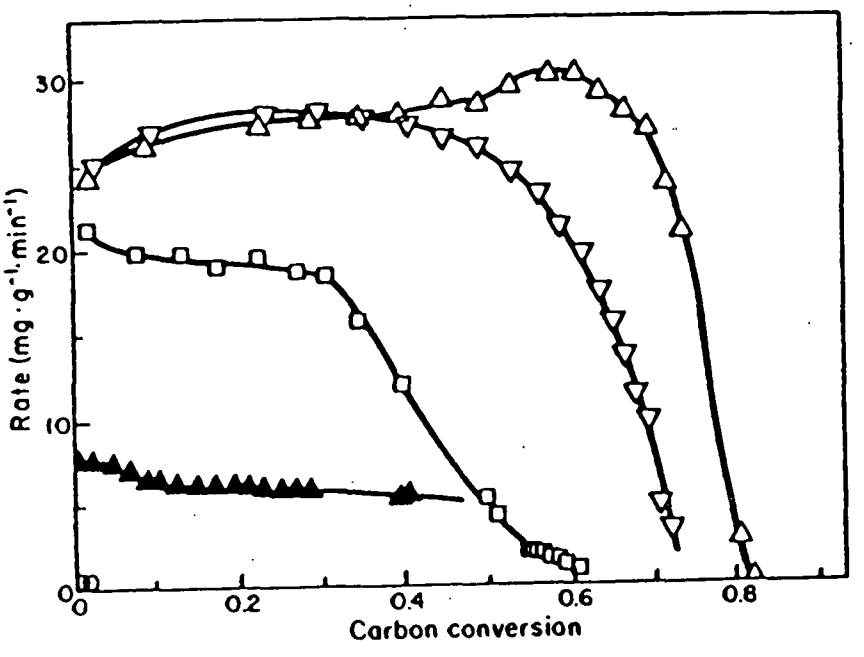


**Figure 13.** Variation of Gasification rate with Carbon Conversion[78]. K/C Atomic Ratio: Δ, 0.019; ▲, 0.040; ∇, 0.043; ■, 0.123.

Li and van Heiningen[38, 41] and Frederick *et al.*[44] have also reported rate changes with carbon conversion as a result of their gasification experiments with black liquor char. Figure 14 illustrates the gasification rate for black liquor chars as reported by Li and van Heiningen.[38] Figure 15 illustrates the gasification rate for black liquor char as reported by Frederick *et al.*[44] Both groups of researchers suggest that the very high alkali catalyst loading found in BLC results in high gasification rates at mid-levels of conversion since the catalyst is finely dispersed in the carbon. The rate increase as carbon was depleted (up to 60% conversion) was explained by the proportional increase in the catalyst/carbon ratio. Frederick and Hupa suggested that the decrease in rate at higher conversion may be due to the loss of catalyst activity through $Na_2CO_3$ formation, loss of free carbon sites, and /or pore plugging. It is curious that the curve reported by Frederick *et al.* goes to a rate of 0 at 75% conversion of organic carbon and no explanation was provided. Frederick *et al.* speculated that a part of the inorganic fraction is molten at the experimental temperature and would coalesce as carbon is depleted. The coalesced smelt could plug pores, further reducing the rate of gasification and leading to the significant carbon levels found in the residue following gasification. In addition, Frederick *et al.* suggested that sodium was not lost from the chars by volatilization, so this would not account for the reduction in rate. Our visual observations from this study support the idea that smelt coalescence does occur at the higher temperatures (800°C), and it therefore may contribute to the observed kinetics.

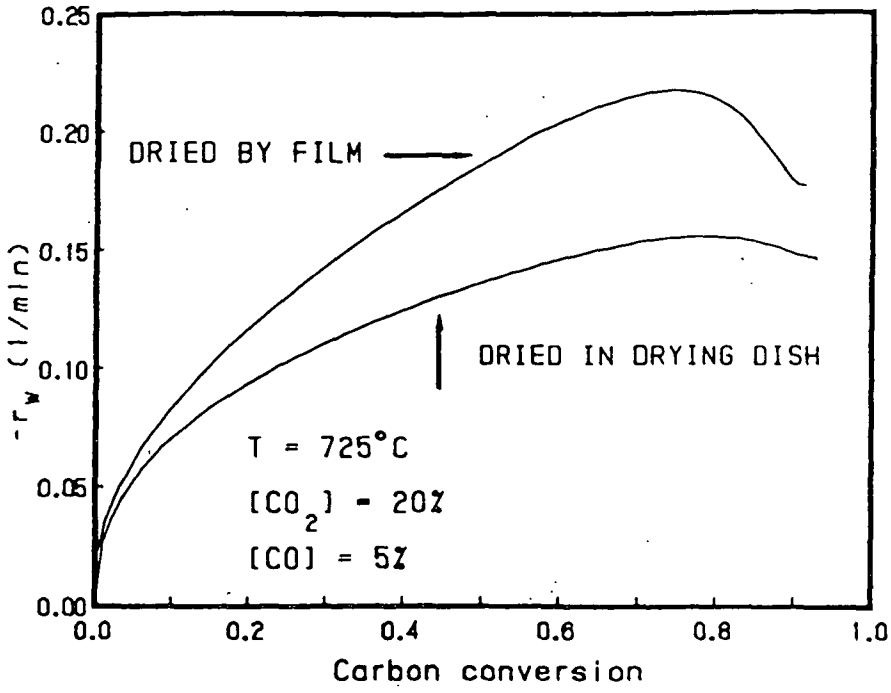


**Figure 14.** Typical Profile of Black Liquor Char Gasification Rate as a Function of Conversion Reported by Li and van Heiningen[38]. (725°C, 20% $CO_2$, 5%CO).

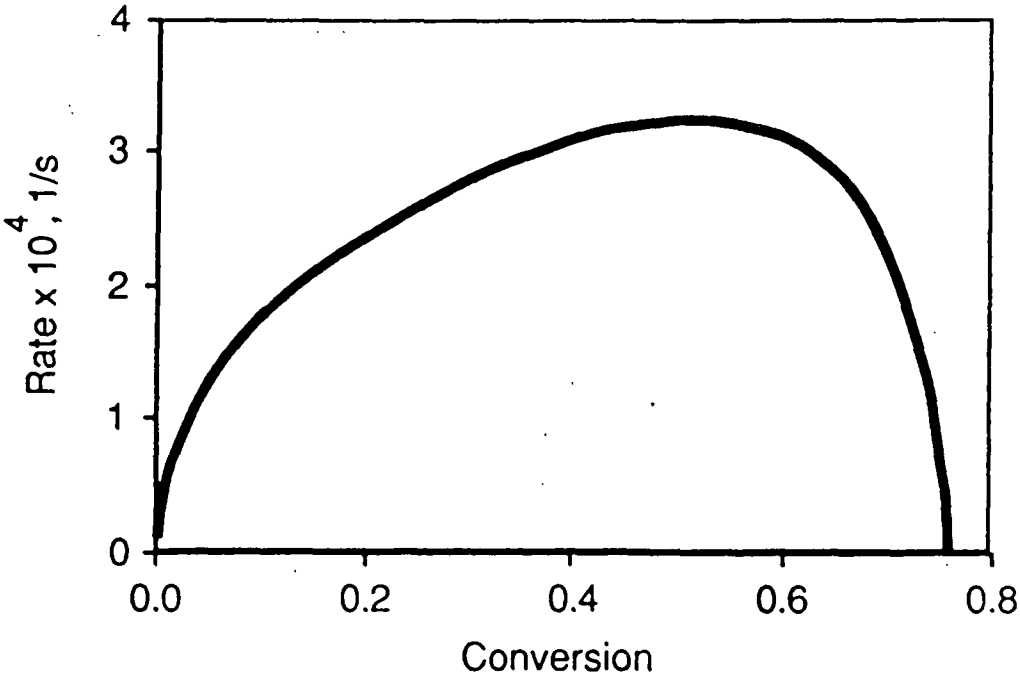


**Figure 15.** Typical Profile of Black Liquor Char Gasification Rate as a Function of Conversion Reported by Frederick *et al.*[44]. (700°C, 4.0 bar $CO_2$, $N_2$ carrier gas).

Assuming a rate expression which is first order in $CO_2$ concentration, the experimental rate constants in this study (and therefore the rates) show a dependence on fractional conversion as shown previously in Figs. 8 and 9. In the 800°C case, Fig. 9, the rate increases slighly from 30% to 75% conversion, with a minimum at about 20%. In contrast, the rate at 700°C, shown in Fig. 10, is independent of conversion from 10% to 75% conversion. The rate from 0-10% shows a decrease for chars gasified at 600°C, 700°C, and 800°C for char prepared according to the RTPP and MTPP. The slight differences in rate behavior for chars prepared according to the RTPP experienced between 10%-75% conversion may be due to the differences in chars due to the different preheat tempertures.

The behavior experienced in this study is very similar to the behavior reported by Meijer.[50] Meijer selected the minimum gasification rate as the standard condition for determining the kinetic parameters of alkali catalyzed coal gasification reaction because the highest state of potassium homogeneity occurs at the minimum. Therefore, the minimum value of the rate constant was also used to determine activation energies and frequency factors for this study. In fact, most of the data in this study show minimums which are constant over a large region of conversion, although it does vary.

It is logical that the gasification of kraft black liquor char particles can be described according to the same model proposed by Meijer[50] for alkali-impregnated coal char. While the details of the two chars are undoubtedly different, the similarities, with respect to the catalysis reactions involving alkalis, make a strong case for the same general mechanisms which yield similar plots of the reaction rate versus conversion. In support of this logical connection, Table 13 summarizes the sodium mass in the initial and residual chars for each of the $CO_2$ gasification experiments for black liquor chars prepared according to MTPP. The residual sodium mass is less than the initial sodium mass indicating that the sodium mass is not independent of fractional conversion of organic carbon. In fact, the sodium loss encountered during the 600°C experiments is as great as that encountered during the 700°C or 800°C indicating that

the greatest sodium loss occurs in the regime where fractional conversion of organic carbon is less than 10%. This observation explains the large drop in rate as the fractional conversion of organic carbon approaches 10%. Since the sodium losses experienced during the 700°C and 800°C gasification experiments are approximately equal to the losses encountered during the 600°C gasification experiments, the levelling of the rate above 20% fractional conversion of organic carbon would be expected.

Consequently, the model of Meijer[50] is believed to be operative here and therefore can be used to explain the BLC gasification experiments of this study. The same procedures for determining and reporting the kinetic parameters were utilized in the following sections.

**Table 13:** Summary of Sodium Losses Observed During $CO_2$ Gasification of Kraft Black Liquor Char Prepared According to the Maximum Temperature Preheat Procedure.

| Exp. Num. | Temp. (°C) | $CO_2$ Conc., (%) | Gas Flow | Carrier Gas | Reaction Time | Initial Sodium (g) | Residual Sodium (g) | Ratio (Residual Sodium :Initial Sodium) |
|---|---|---|---|---|---|---|---|---|
| 4979 | 604 | 4.8 | 5.4 | $N_2$ | 30 | 0.85 | 0.4 | 0.47 |
| 4982 | 602 | 4.7 | 5.5 | $N_2$ | 30 | 0.85 | 0.28 | 0.33 |
| 4972 | 712 | 4.8 | 5.5 | $N_2$ | 30 | 0.85 | 0.44 | 0.52 |
| 4973 | 712 | 4.8 | 5.5 | $N_2$ | 30 | 0.85 | 0.44 | 0.52 |
| 4975 | 699 | 4.8 | 5.4 | $N_2$ | 30 | 0.85 | 0.45 | 0.53 |
| 4976 | 799 | 4.8 | 5.5 | $N_2$ | 20 | 0.85 | 0.42 | 0.49 |
| 4977 | 795 | 4.8 | 5.5 | $N_2$ | 20 | 0.85 | 0.51 | 0.6 |
| 4989 | 801 | 5.1 | 5.2 | $N_2$ | 20 | 0.85 | 0.49 | 0.58 |
| 4985 | 696 | 4.8 | 2.7 | $N_2$ | 30 | 0.85 | 0.47 | 0.55 |
| 4990 | 699 | 5.1 | 2.6 | $N_2$ | 30 | 0.85 | 0.4 | 0.47 |
| 4991 | 693 | 5.1 | 2.7 | $N_2$ | 30 | 0.85 | 0.43 | 0.51 |
| 4974 | 697 | 5 | 5.3 | He | 30 | 0.85 | 0.61 | 0.72 |
| 4983 | 698 | 4.8 | 5.5 | He | 30 | 0.85 | 0.58 | 0.68 |

$CO_2$ Gasification Kinetics for Char Prepared According to the Reaction Temperature Preheat Procedure

An Arrhenius plot for the 600°C, 700°C, and 800°C data for BLC prepared according to the reaction temperature preheat procedure is shown in Fig. 16. The low rate constant values at 800°C were initially thought to indicate the presence of mass transfer limitations at this temperature. However, tests were performed to evaluate mass transfer effects and these showed that the observed rate was not limited by mass transfer. To test for film mass transfer effects, experiments were performed using different gas velocities. Experiments were also completed using He as the carrier gas and compared to the results where $N_2$ was the carrier gas to test for pore diffusion effects. For meaningful interpretation of data, it is necessary to know the degree of certainty that a piece of data is accurate. Directly-measured data inherently contain some degree of error, and the extent to which the accuracy of information calculated from these data are affected by propagation of measurement errors must be quantified. In Appendix XIV, uncertainty analysis for the experimental data of this thesis is performed to account for the effects of both bias and precision errors on accuracy. As shown in Table 14, the resulting average rate constants were approximately the same indicating that neither film nor pore diffusion effects were appreciable. This was supported by statistical analysis at the 95% confidence interval. Uncertainty analysis reveals an uncertainty of 0.24% for the rate constant.

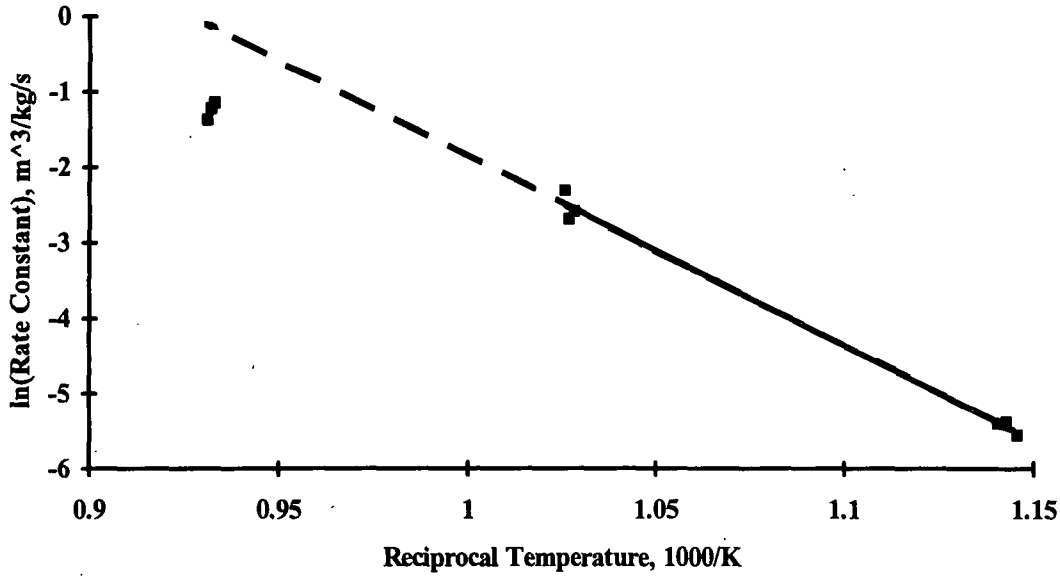


**Figure 16.** Arrhenius Plot for $CO_2$ Gasification of Kraft Black Liquor Char at 600°C, 700°C, and 800°C for Char Prepared According to the Reaction Temperature Preheat Procedure.

**Table 14.** Comparison of Rate Constants for Varying Mass Transfer Conditions at 800°C for Char Prepared According to the Reaction Temperature Preheat Procedure.

| Carrier Gas | Superficial Gas Velocity, (m/s) | Rate Constant, ($m^3$/kg/s) | Calculated Mass Transfer Coefficient, ($m^3$/kg/s) |
|---|---|---|---|
| $N_2$ | 0.08 | 0.29(+/-)0.033 | 9.68 |
| He | 0.08 | 0.39(+/-)0.086 | 14.3 |
| $N_2$ | 0.17 | 0.22(+/-)0.040 | 14.6 |

The pore diffusion effects can be estimated theoretically by comparing the rate of reaction with the rate of diffusion in the form of the Thiele modulus,[92] $M_{TM}$, based on simple first order kinetics in $CO_2$:

$$M_{TM}=\frac{d_p}{6}\sqrt{\frac{k\rho_{bed}}{D_{eff}}} \qquad \text{eqn. 17}$$

where $d_p$ = average diameter of the char particles, (m)

$k$ = reaction rate constant, ($m^3/kg/s$)

$\rho_{bed}$ = density of char bed, (kg organic $C/m^3$ char)

$D_{eff}$ = $\frac{D_C\varepsilon_{bed}}{\tau'}$, ($m^2/s$)

$D_c$ = combined diffusivity, $\frac{1}{\frac{1}{D_k}+\frac{1}{D_{AB}}}$, ($m^2/s$)

$D_{AB}$ = Diffusivity of gas A ($CO_2$) through gas B ($N_2$ or He), ($m^2/s$)

$D_k$ = Knudsen diffusivity, $0.97\bullet\bar{r}\bullet\sqrt{\frac{T}{M}}$, ($m^2/s$)

$\tau'$ = tortuosity factor, $\left(\frac{1}{\varepsilon_p}\right)$

$\varepsilon_p$ = porosity of the char particle, (0.91), $\left[\frac{\text{void volume of char particle}}{\text{total volume of char particle}}\right]$

$\bar{r}$ = pore radius, $\frac{2V_g}{S_g}$, (m)

$T$ = temperature, K

$M$ = molecular weight

$V_g$ = void volume per weight of char, $\frac{\varepsilon_p}{\rho_p}$, ($m^3/kg$)

$S_g$ = surface area per weight of char, ($m^2/kg$)

$\rho_p$ = density of the char particle, ($kg/m^3$)

The effective diffusivity, $D_{eff}$, was determined according to a method outlined by Hill.[93] The approximation for the tortuosity factor is taken from Froment and Bishoff.[94] According to Levenspiel,[92] no resistance to pore diffusion exists when $M_{TM} < 0.40$ for first order kinetics . Calculated values of $M_{TM}$ for char exposed in $N_2$-$CO_2$ and He-$CO_2$ were 0.12 and 0.14, respectively; therefore, the diffusivity of $CO_2$ inside the char particles had no effect on the gasification rate. Uncertainty analysis reveals an uncertainty of 0.061% for the Thiele Modulus.

In addition, the average film mass transfer coefficient was calculated using a correlation for packed beds as[89, 95]

$$k_m a_m = \left(\frac{0.455}{\varepsilon_{bed}}\right)\left(\frac{u d_p \rho}{\mu}\right)^{-0.407}\left(\frac{\mu}{\rho D_{AB}}\right)^{-2/3} a_m u \qquad \text{eqn. 18}$$

where $a_m$ = external surface area per unit mass, ($m^2/kg$)
$\varepsilon_{bed}$ = void fraction of char bed, (0.40)
$u$ = superficial velocity in the direction of flow, (m/s)
$d_p$ = average diameter of the char particles, (0.005 m)
$\mu$ = viscosity of the fluid, (kg/m/s)
$\rho$ = density of the fluid, ($kg/m^3$)
$D_{AB}$ = molecular diffusivity of component being transferred, ($m^2/s$)

The other quantities are as defined for eqn. 10. The average film mass transfer coefficient, $k_m a_m$, predicted at 800°C was 9.68 $m^3/kg/s$ (see Table 14), which is more than an order of magnitude greater than the observed global first order rate constant. This argument, based on global first order kinetics, is justified since first order fits the data as well as any other value of n. Uncertainty analysis reveals an uncertainty of 0.014% for the average film mass transfer coefficient. Consequently, film mass transfer and pore diffusion limitations in the fixed bed reactor were considered negligible at 800°C.

To determine the temperature where the rate of $CO_2$ gasification is completely controlled by film mass transfer, the mass transfer controlled rate and the kinetically controlled rate were determined using the following equations.

$$Rate_{mass\ transfer} = k_m a_m C_{CO_2} \qquad \text{eqn. 19}$$

$$Rate_{kinetic} = \eta k_r C_{CO_2}^n \qquad \text{eqn. 20}$$

where $k_m$ = film mass transfer coefficient (eqn. 18), (m/s)
$a_m$ = external surface area per unit mass, ($m^2/kg$)
$C_{CO_2}$ = carbon dioxide concentration, ($kg/m^3$)
$\eta$ = Thiele modulus-based effectiveness factor (see eqn. 21),
$k_r$ = kinetic rate constant (eqns. 11 and 12), and
$n$ = reaction order.

The rate limiting effect of pore diffusion was accounted for with a Thiele modulus-based effectiveness factor as defined by Levenspiel[92].

$$\eta = \frac{1}{M_T}\left(\frac{1}{\tanh(3M_T)} - \frac{1}{3M_T}\right) \qquad \text{eqn. 21}$$

where $M_{TM} = \frac{d_p}{6}\sqrt{\frac{k\rho_{bed}}{D_{eff}}}$ for first order kinetics eqn. 22

$$M_{TM} = \frac{d_p}{6}\sqrt{\frac{(n+1)k\rho_{bed}C_{CO_2}^{(n-1)}}{2D_{eff}}} \text{ for n order kinetics except n= 1.} \qquad \text{eqn. 23}$$

The ratio of the kinetically controlled rate to the film mass transfer controlled rate $\left(\frac{Rate_{kinetic}}{Rate_{mass\ transfer}}\right)$ was determined for reaction orders of 0, 0.5, 1, and 2. The transition temperature where the rate of $CO_2$ gasification is completely controlled by film mass transfer is shown in Figs. 17-20. For first order kinetics, the mass transfer transition temperature for char prepared according to the RTPP was 1240K(970°C) for the fixed bed reactor conditions. Levenspiel[92] notes that pore diffusion effects become important when the $M_{TM}$>0.40. For first order kinetics, pore diffusion effects begin at approximately 830°C. It is important to note that data above 1070K(800°C) has been extrapolated. As shown in Figs. 17-20, the film mass transfer transition temperature for 0, 0.5, and 2 order was 1180K(905°C), 1210K(935°C), and 1280K(1010°C); respectively. This indicates that the reaction order does influence the transition temperature. The pore diffusion effects begin at approximately 1100K(830°C) for all kinetic orders.

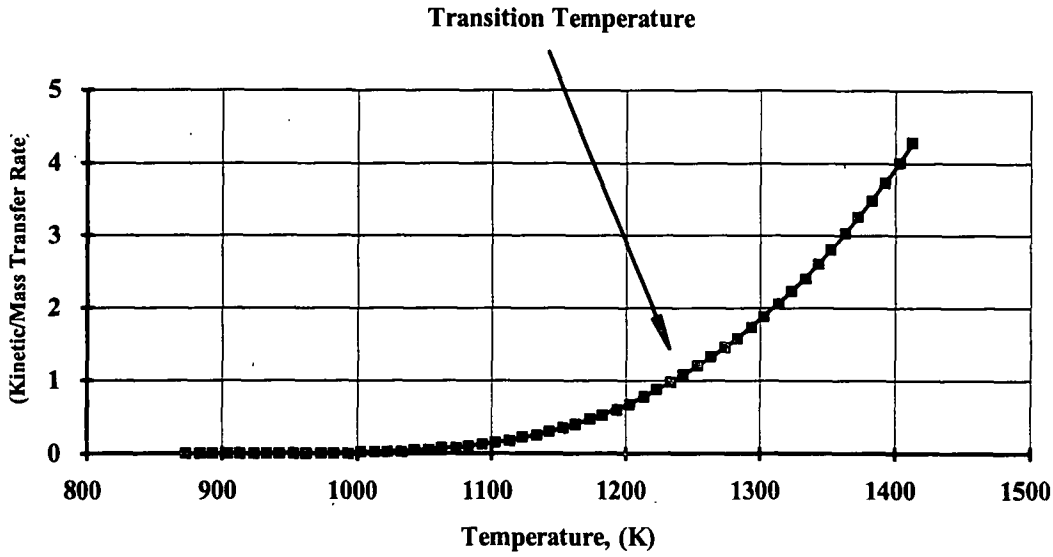


**Figure 17.** Mass Transfer Transition Temperature for Kraft Black Liquor Char Prepared According to the Reaction Temperature Preheat Procedure for the Fixed Bed Reactor Conditions and First Order Kinetics.

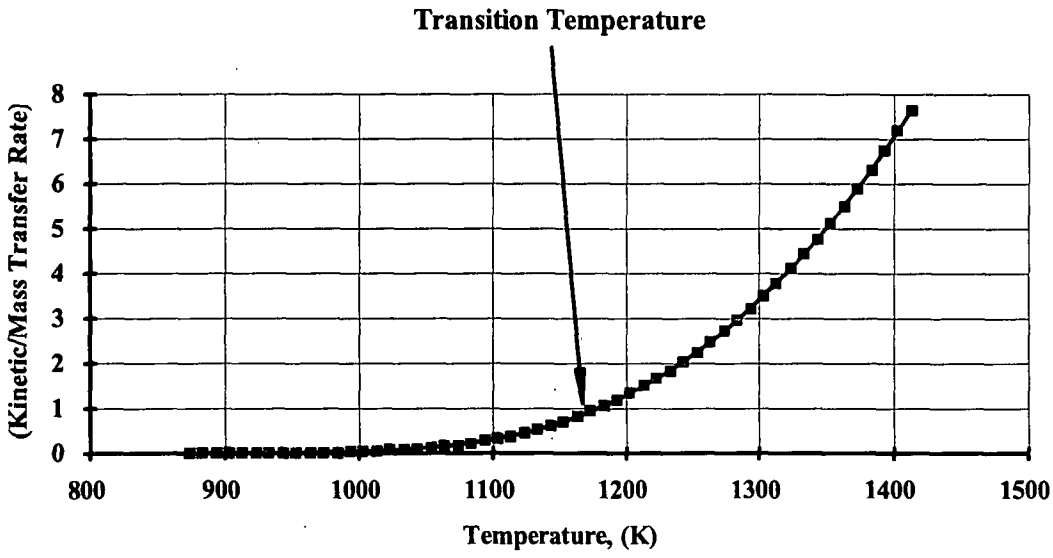


**Figure 18.** Mass Transfer Transition Temperature for Kraft Black Liquor Char Prepared According to the Reaction Temperature Preheat Procedure for the Fixed Bed Reactor Conditions and Zero Order Kinetics.

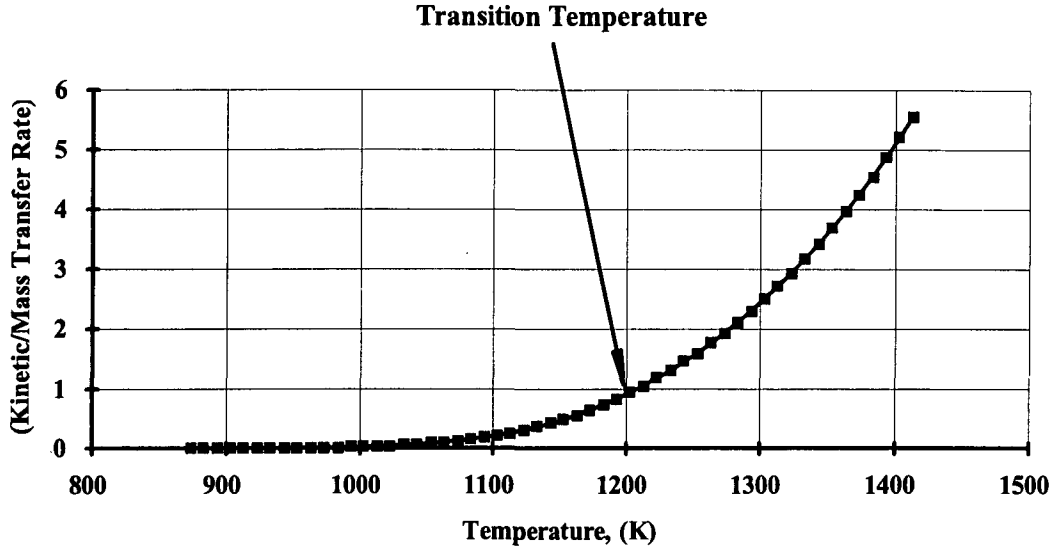


**Figure 19.** Mass Transfer Transition Temperature for Kraft Black Liquor Char Prepared According to the Reaction Temperature Preheat Procedure for the Fixed Bed Reactor Conditions and 0.5 Order Kinetics.

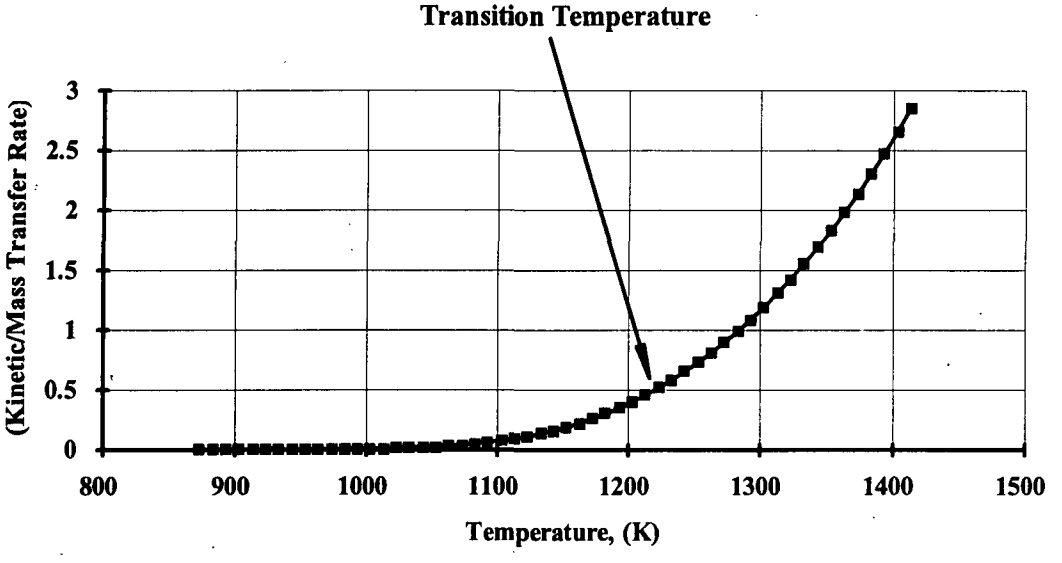


**Figure 20.** Mass Transfer Transition Temperature for Kraft Black Liquor Char Prepared According to the Reaction Temperature Preheat Procedure for the Fixed Bed Reactor Conditions and Second Order Kinetics.

Li[39] also observed a low rate at 800°C. As in this study, Li[39] reported data that was free of film mass transfer and pore diffusion limitations. Li[39] explained the lower-than-expected rate at 800°C. The deviation can be caused by a change from a gas-solid reaction to a three-phase reaction because the melting point of the sodium salt mixture is lower than 800°C. Therefore, Li[39] used data at the lower temperatures to determine the kinetic parameters. In addition, Frederick *et al.*[44] suggested that the coalescence of smelt could plug pores resulting in a reduction in the gasification. Since the melting point of the inorganics is below 800°C, this is a feasible explanation for the lower rate constants.

Oxygen mass balances show that take-up of oxygen by the char bed may be an explanation for the lower than expected rate constants at 800°C. Assuming that the only reaction occurring was char-C + $CO_2$--->2CO, the mass flow rate of oxygen entering as $CO_2$ should equal the mass flow rate of oxygen leaving as CO and $CO_2$. The ratio of oxygen out to oxygen in at 600°C and 700°C was very close to unity ( 0.98± 0.03); while the average value of the ratio for the 800°C experiments was significantly less than unity (0.85± 0.02). This suggests that oxygen was consumed by competing reactions during the high temperature experiments.

Two addtional observations, i.e., the formation of smelt and corrosion of the reactor walls, support oxygen consumption as an explanation for the lower-than-expected rate constants obtained at 800°C. First, two distinct residual solids were observed following each 800°C experiment. One solid was similar to the friable starting material, and the other solid consisted of beads of frozen smelt that were attached to nearby stainless steel. In the 800°C experiments, the fractional conversion of organic carbon ranged from 70%-99% depending on experimental conditions such as $CO_2$ concentration and gas flow rate. Grace *et al.*[4] have noted that as the organic carbon in char is decreased, the inorganics in the char will coalesce to form smelt. As the organic carbon is depleted, the oxidizer ($CO_2$) will react with

the inorganics. For example, the $Na_2S$ in the char would react with the $CO_2$ to form $Na_2CO_3$ ($Na_2S + 2\ CO_2 <---> Na_2CO_3 + COS$). Li and van Heiningen[96] have discussed the importance of this reaction during $CO_2$ gasification. Although the COS concentration in the product gas and the $Na_2CO_3$ concentration in the residual smelt were not determined, the mass of $Na_2CO_3$ which could be formed from oxygen not consumed through gasification or corrosion reactions was less than the mass of residual smelt. Therefore, the oxygen consumption at 800°C could be due to the inorganic reactions.

The second observation, corrosion of the stainless steel reactor walls, was observed by weight loss of the reactor walls during the 800°C experiments. Before and after each experiment the reactor tube that held the char was weighed to determine the weight loss encountered during each experiment. In addition, the reactor tube was cleaned with soap and water following each experiment to remove the corrosion scale and frozen smelt from the reactor walls. Assuming that the weight loss was primarily $Cr_2O_3$, through mass balances it was determined that 38-100% of the unaccountable oxygen appeared in the $Cr_2O_3$.

Thus, smelt reactions and corrosion reactions could account for the discrepancies in oxygen mass balances for the 800°C tests and are likely responsible for the lower-than-expected rate constant values by consuming part of the $CO_2$. For first order kinetics, the activation energy calculated by using data from 600°C ,700°C, and 800°C is 39,800 cal/mol. However, the activation energy using just the 600°C and 700°C data is 50,000 cal/mol, and is considered a more reliable value.

$CO_2$ Gasification Kinetics for Char Prepared According to the Maximum Temperature Preheat Procedure

An Arrhenius plot for the 600°C, 700°C, and 800°C data for char prepared according to the maximum temperature preheat procedure is shown in Fig. 21. Tests were performed to evaluate mass transfer effects and showed the observed rate at 700°C was not limited by mass transfer. To test for film mass transfer effects, experiments were performed using different gas velocities. Experiments were completed using He as the carrier gas and compared to the results where $N_2$ was the carrier gas to test for pore diffusion effects. As shown in Table 15, the resulting average rate constants were approximately the same indicating that neither film nor pore diffusion effects were appreciable. This was supported by statistical analysis at the 95% confidence interval. As noted earlier, the pore diffusion effects can be estimated theoretically by comparing the rate of reaction with the rate of diffusion in the form of the Thiele modulus according to eqn. 17. According to Levenspiel,[92] no resistance to pore diffusion exists when $M_{TM} < 0.40$ for first order kinetics. Calculated values of $M_{TM}$ for char exposed in $N_2$-$CO_2$ and He-$CO_2$ were 0.084 and 0.087, respectively; therefore, the diffusivity of $CO_2$ inside the char particles had no effect on the gasification rate. In addition, the average film mass transfer coefficient was calculated using the correlation for packed beds as defined in eqn. 18. The average film mass transfer coefficient, $k_m a_m$, predicted at 700°C was 5.44 $m^3/kg/s$, which is more than an order of magnitude greater than the observed global first order rate constant. Therefore, film mass transfer and pore diffusion limitations in the fixed bed reactor were considered negligible at 700°C.

To determine the temperature where the rate of $CO_2$ gasification is completely controlled by film mass transfer, the mass transfer controlled rate and the kinetically controlled rate were determined using eqns. 19 and 20. The rate limiting effect of pore diffusion was accounted for with a Thiele modulus-based effectiveness factor (eqn. 21) as defined by Levenspiel[92]. The ratio of the kinetically controlled rate to the film mass transfer controlled rate $\left(\frac{\text{Rate}_{\text{kinetic}}}{\text{Rate}_{\text{mass transfer}}}\right)$ was determined for reaction

orders of 0, 0.5, 1, and 2. The transition temperature where the rate of $CO_2$ gasification is completely controlled by film mass transfer is shown in Figs. 22-25. For first order kinetics, the mass transfer transition temperature for char prepared according to the MTPP is 1260K(990°C) for the fixed bed reactor conditions. Levenspiel[92] notes that pore diffusion effects become important when the $M_{TM}>0.40$. For first order kinetics, pore diffusion effects begin at approximately 1130K(860°C). It is important to note that data above 1070K(800°C) has been extrapolated. As shown in Figs. 22-25, the film mass transfer transition temperature for 0, 0.5, and 2 order was 1220K(950°C), 1240K(970°C), and 1280K(1010°C); respectively. This indicates that the reaction order does influence the transition temperature. The pore diffusion effects begin at approximately 1130K(860°C) for all kinetic orders.

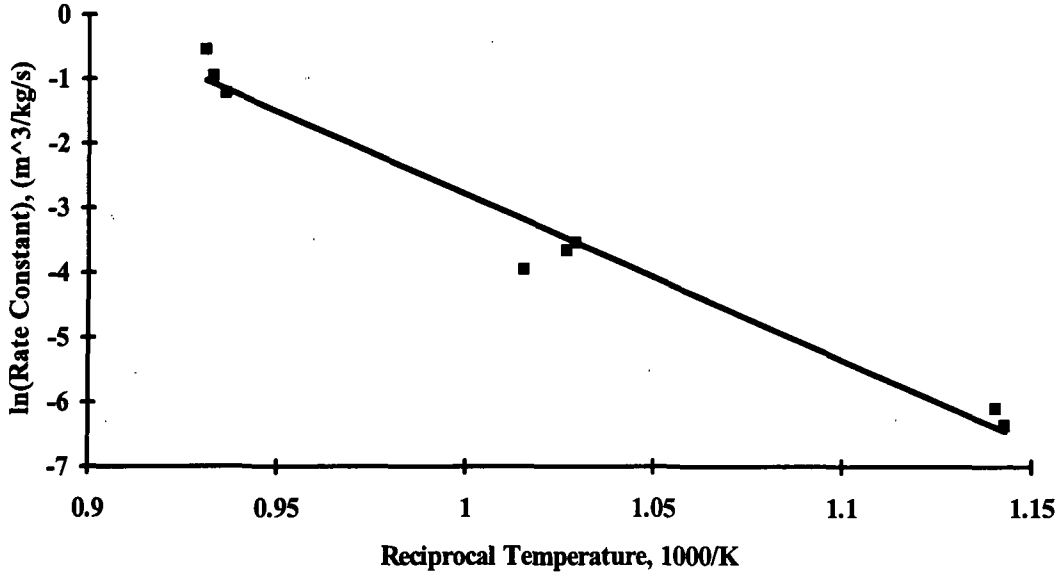


**Figure 21.** Arrhenius Plot for $CO_2$ Gasification of Kraft Black Liquor Char at 600°C, 700°C, and 800°C for Char Prepared According to the Maximum Temperature Preheat Procedure.

**Table 15.** Comparison of Rate Constants for Varying Mass Transfer Conditions at 700°C for Char Prepared According to the Maximum Temperature Preheat Procedure.

| Carrier Gas | Superficial Gas Velocity, (m/s) | Rate Constant, ($m^3$/kg/s) | Calculated MassTransfer Coefficient, ($m^3$/kg/s) |
|---|---|---|---|
| $N_2$ | 0.08 | .025(+/-).0049 | 5.44 |
| He | 0.08 | .023(+/-).0033 | 8.06 |
| $N_2$ | 0.04 | .032(+/-).0021 | 3.59 |

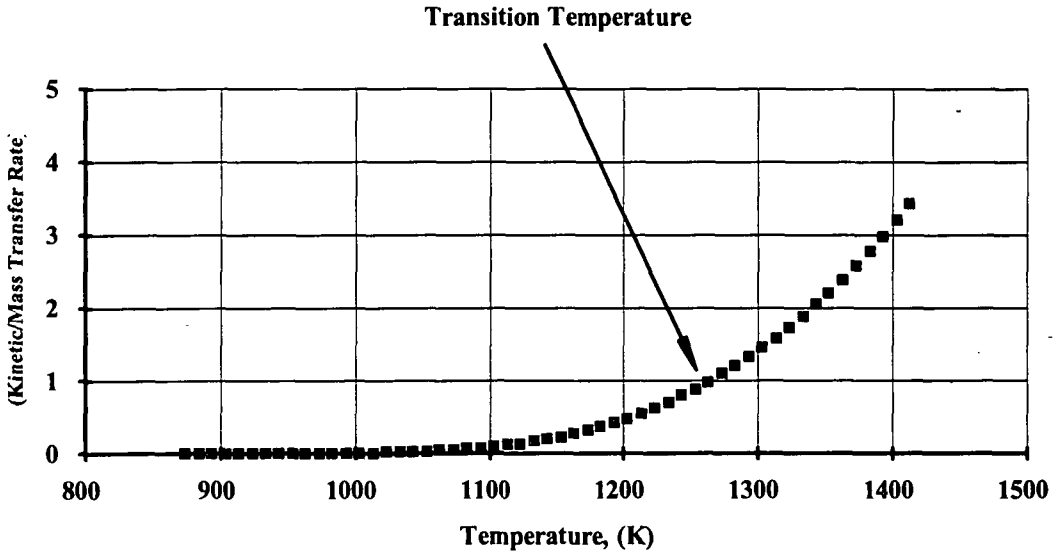


**Figure 22.** Mass Transfer Transition Temperature for Kraft Black Liquor Char Prepared According to the Maximum Temperature Preheat Procedure for the Fixed Bed Reactor Conditions and First Order Kinetics.

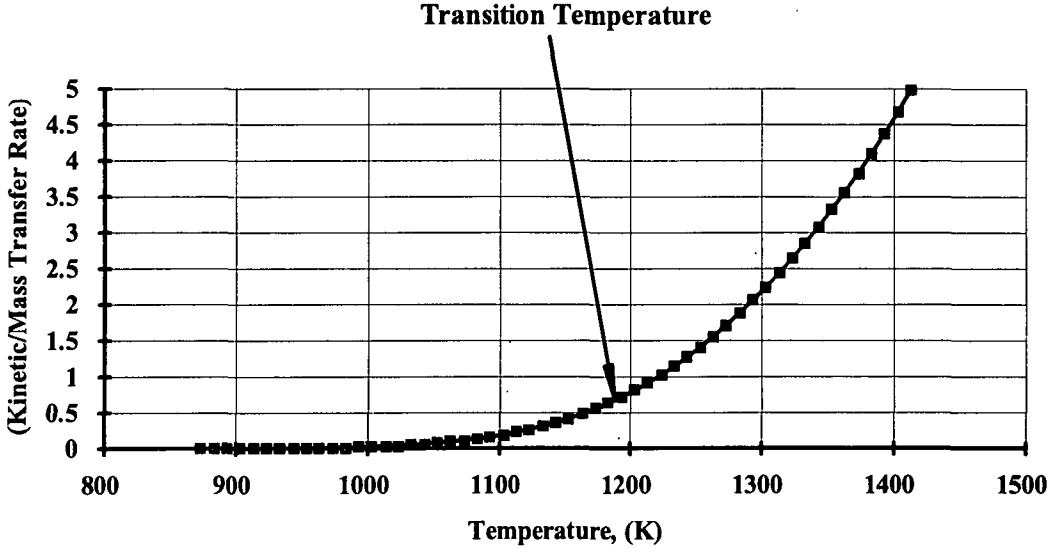


**Figure 23.** Mass Transfer Transition Temperature for Kraft Black Liquor Char Prepared According to the Maximum Temperature Preheat Procedure for the Fixed Bed Reactor Conditions and Zero Order Kinetics.

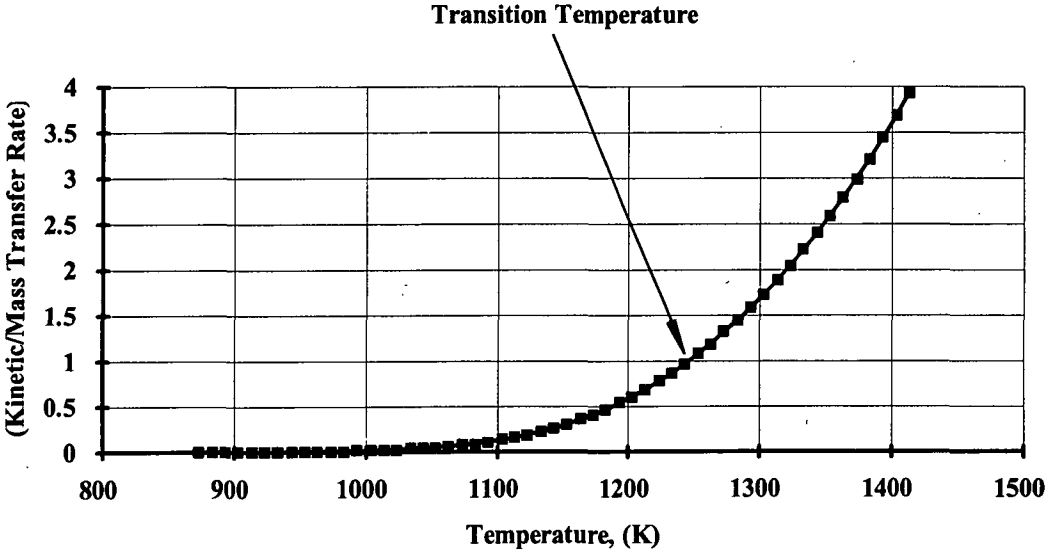


**Figure 24.** Mass Transfer Transition Temperature for Kraft Black Liquor Char Prepared According to the Maximum Temperature Preheat Procedure for the Fixed Bed Reactor Conditions and 0.5 Order Kinetics.

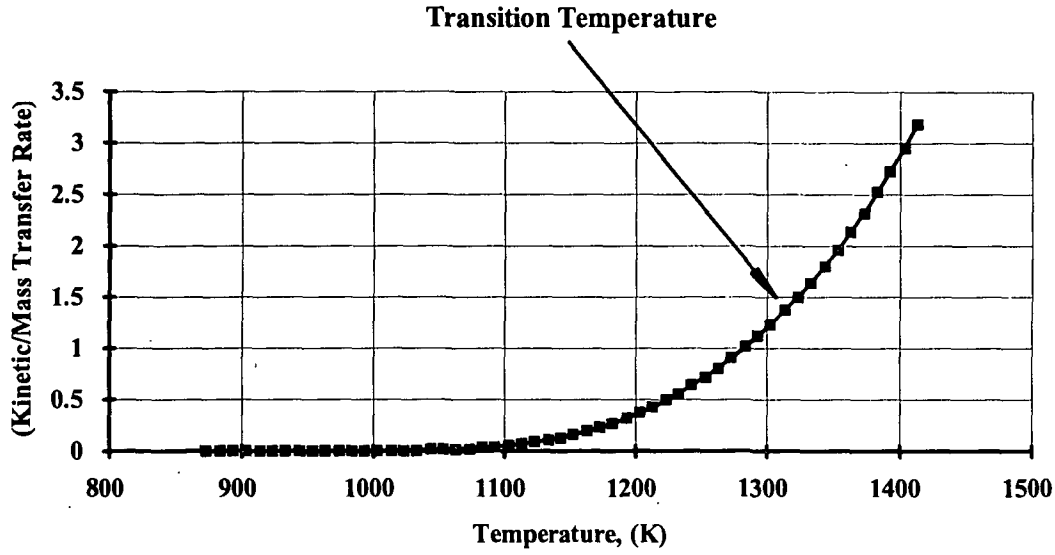


**Figure 25.** Mass Transfer Transition Temperature for Kraft Black Liquor Char Prepared According to the Maximum Temperature Preheat Procedure for the Fixed Bed Reactor Conditions and Second Order Kinetics.

As noted in the previous section, the mass flow rate of oxygen entering as $CO_2$ should equal the mass flow rate of oxygen leaving as CO and $CO_2$. The ratio of oxygen out to oxygen in at 600°C and 700°C was very close to unity (0.95±0.02); while the average value of the ratio for the 800°C experiments was significantly less than unity (0.79±0.08). This again suggests that oxygen was consumed by competing reactions during the high temperature experiments.

The same two reactions discussed earlier, smelt reactions and corrosion reactions, could account for all the discrepancies in oxygen mass balances for the 800°C tests. Corrosion of the reactor walls, Haynes Alloy HR160 (36%Ni, 29%Co, 28%Cr, 2.75%Si, 2%Fe), was observed by weight loss of the reactor walls during the 800°C experiments. Before and after each experiment, the reactor tube that held the char was weighed to determine the mass loss/gain encountered during each experiment. In addition, the reactor tube was cleaned with a wire brush, steel wool, soap, and water following each experiment to remove the corrosion scale and frozen smelt from the reactor walls. Assuming that the weight loss was

primarily $Cr_2O_3$, the oxygen appearing as $Cr_2O_3$ represented 65-77% of the unaccountable oxygen for the range of experiments at 800°C.

The remaining portion of the unaccountable oxygen could be consumed in the smelt reaction discussed earlier ($Na_2S + 2CO_2 <=> Na_2CO_3 + COS$). As noted earlier, the COS concentration in the product gas and the $Na_2CO_3$ concentration in the residual smelt were not determined. However, the mass of $Na_2CO_3$ which could be formed from oxygen not consumed through gasification or corrosion reactions was less than the mass of residual smelt. Therefore, the oxygen consumption at 800°C could be due to the inorganic reactions.

The activation energy for 600°C, 700°C, and 800°C data for char prepared according to the MTPP is 50,700 cal/mole.

Comparison of $CO_2$ Gasification Kinetics for Chars Prepared According to the RTPP and the MTPP

Fig. 26 shows the Arrhenius plots of the 600°C, 700°C and 800°C gasification data for chars prepared according to the reaction temperature preheat procedure (RTPP) and the maximum temperature preheat procedure (MTPP). The two preheat methods are reviewed briefly. The RTPP involved heating partially devolatlized char particles in an atmosphere of 95% $N_2$/5%CO to various temperatures (600°C, 700°C, or 800°C), achieving complete devolatilization at the given temperature, and, upon complete devolatilization, retaining the char at the given temperature for one hour. The MTPP involved heating partially devolatilized char particles in an atmosphere of 95% $N_2$/5%CO to a temperature of 950°C, and then, upon complete devolatilization, maintaining the char at 950°C for one additional hour, and then cooling down to the predetermined reaction temperature (600°C, 700°C, or 800°C) to begin the gasification experiment.

Table 16 summarizes the rate constants and preheat parameters for the range of experimental temperatures. Analysis of the two groups of data at 600°C, 700°C, and 800°C suggests that rate constants of the char prepared according to the two preheat methods are statistically different. The rate constants for char prepared according to the RTPP are higher than the rate constants for char prepared according to the MTPP at 600-800°C. Considering that the different preheat procedures result in chars with different composition (especially the inorganic composition), the difference in rate constants is not surprising. In addition, the lower rates for char prepared according to the MTPP could be due to a greater number of plugged pores and lower concentration of sodium in the initial char as a result of the higher preparation temperature (950°C). Finally, some contribution to the difference may be due to slight differences in initial black liquors.

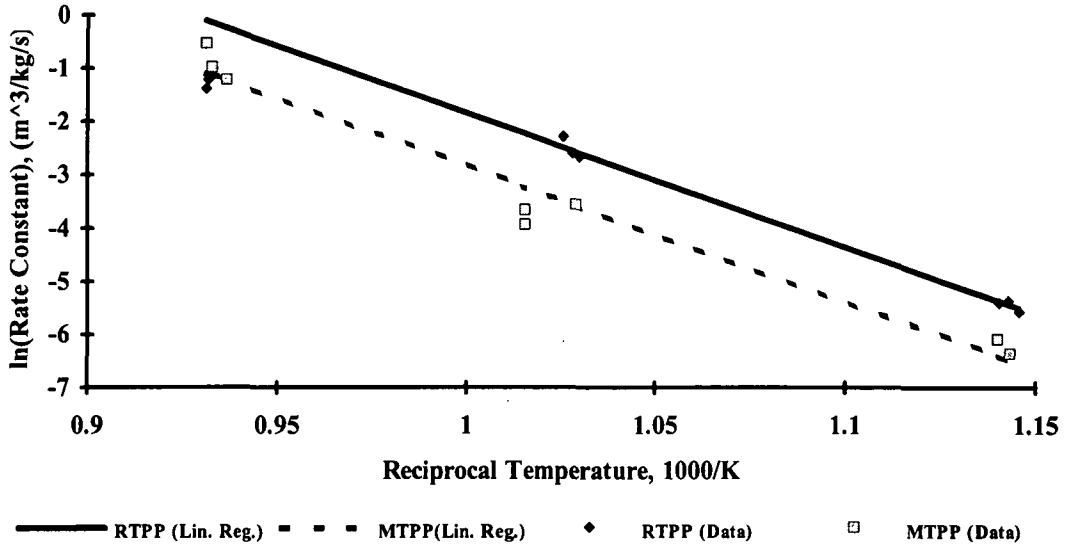


**Figure 26.** Arrhenius Plots for $CO_2$ Gasification of Kraft Black Liquor Char at 600°C, 700°C, and 800°C for Char Prepared According to the Reaction Temperature Preheat Procedure (Top Line) and the Maximum Temperature Preheat Procedure (Bottom Line).

**Table 16.** Comparison of $CO_2$ Gasification Rate Constants for Chars Prepared According to the Reaction Temperature Preheat Procedure and the Maximum Temperature Preheat Procedure.

| Average Temperature °C | Average Rate Constant ($m^3/kg/s$) | Preheat Method | Liquor Classification |
|---|---|---|---|
| 603 (+/- 3) | 0.00434(+/-)0.000431 | RTPP | I |
| 603 (+/- 1) | 0.00201(+/-)0.000367 | MTPP | II |
| 701 (+/- 1) | 0.0824(+/-)0.0168 | RTPP | I |
| 704 (+/- 7) | 0.0247(+/-)0.00486 | MTPP | II |
| 800 (+/- 1)* | 0.880(+/-)0.0192 | RTPP | I |
| 798 (+/- 3) | 0.421(+/-)0.146 | MTPP | II |

* extrapolated from 600°C and 700°C data

Comparison to Previously Reported Results

Li and van Heiningen,[38-41] Frederick and Hupa,[42,43] and Frederick *et al.*[44] employed BLC gasification using small quantities of char and thermo-gravimetric analysis. Goerg and Cameron[14,46] used a kraft char and $Na_2CO_3$ mixture and fixed bed purge reactor. A primary objective of this study was to provide independent $CO_2$ gasification rate data using 10-15 grams of BLC in a fixed bed reactor. An additional goal was to apply the results of this work toward a better understanding of the rate controlling processes for $CO_2$ gasification in recovery furnaces.

Table 17 summarizes the rates, activation energies, and conditions of the available BLC gasification experiments. Considering that different chars will yield somewhat different rates, there is fair agreement in rates among the various investigations excepting the Goerg and Cameron[14,46] data. Goerg and Cameron used a mixture of char and $Na_2CO_3$ as the starting material; whereas, char was the only solid reactant used in other studies. Goerg and Cameron[14,46] heated the char-$Na_2CO_3$ mixture to reaction temperature in an atmosphere of $N_2$ gas. Li[39] has suggested that when a char-$Na_2CO_3$ mixture is heated to reaction temperature, $Na_2CO_3$ will react with organic carbon yielding products such as gaseous Na, CO, and some $CO_2$. Therefore, it is likely that the initial organic carbon concentration for the Goerg and Cameron experiments was low if not negligible. Since the rate of gasification is a function of the organic carbon concentration, low organic concentration at the beginning of gasification would have resulted in much slower observed gasification rates than the observed rates of the other studies. In addition, the inherent kinetic rate may not have been accurately reflected by the observed rate since the $CO_2$ may not have reached the surface of the char because of poor mixing or because of pore plugging due to molten salt and smelt. The large concentration of $Na_2CO_3$ at the experimental temperatures (927-1010°C) resulted in a decrease in reaction rate probably because of pore pluggage by the molten salt.

The rates of this study are somewhat faster than the rates reported in the other studies when the differences in $CO_2$ concentrations are considered. The $CO_2$ concentration of this study (4.4% and 4.8%) was lower than the $CO_2$ concentration of Frederick and Hupa[42,43] and Li and van Heiningen[38-41] (20%). For example, if 20% $CO_2$ and a first order global rate for $CO_2$ gasification is assumed, the projected rate would be 10.0 $hr^{-1}$ for char preheated according to the RTPP which is approximately 2.0-10.0 times faster than the rates reported by others. The rates of the other studies are inhibited by CO in the reactant gas. In contrast, no CO was present in the reactant gas in this study. The activation energy of this study compares well to the activation energies reported by others. The similarities in rates and activation energies are remarkable considering the differences in char quantity, liquors used to produce the chars, the char production process, and the differences in the experimental reactors. This work confirms that a fixed bed reactor can be utilized to adequately study the kinetics of the $CO_2$ gasification of kraft BLC.

**Table 17.** Comparison of $CO_2$ Gasification Rates of Kraft BLC.

| Rate @ 700°C ($hr^{-1}$) | $E_A$ (kcal/mol) | Temp. Range (°C) | Gas Pressure. (atm.) | Gas Composition, % $CO_2$/CO/$N_2$ | Exp. Method | Char Mass, (g) | Investigator |
|---|---|---|---|---|---|---|---|
| 1.9 | 44.4 | 700-900 | 1 | 20/4/76 | PTG* | ~0.1 | Frederick& Hupa[42] |
| 0.9 | 49 | 650-800 | 20 | 20/4/76 | PTG | ~0.1 | Frederick & Hupa[43] |
| 3.0-4.8 | 60 | 675-775 | 1 | 20/10/70 | TGA** | ~0.005 | Li & van Heiningen[40] |
| 1.1 | 44.7 | 700-775 | 1 | 20/10/70 | TGA | ~0.005 | Li & van Heiningen[41] |
| 2.52E-3 | 46.8 | 927-1010 | 1 | 5/5/90 | Purged Bed | 1 | Goerg & Cameron[14,47] |
| 2.1 | 50 | 600-800 | 1 | 4.4/0/95.6 | Fixed Bed | 10-15 | Present Study RTPP@ |
| 0.78 | 50.7 | 600-800 | 1 | 4.8/0/95.2 | Fixed Bed | 20 | Present Study MTPP@@ |

*PTG = Pressurized Thermogravimetric
**TGA = Thermogravimetric Analysis
@RTPP = Reaction Temperature Preheat Procedure
@@MTPP = Maximum Temperature Preheat Procedure

Available in Table 18 are kinetic data for some selected carbonaceous materials. The reactivity of kraft BLC is at least one and four orders of magnitude larger than coal char impregnated with 10% $Na_2CO_3$ and electrode carbon, respectively. The activation energy determined for kraft BLC compares well to the activation energies reported for the various carbonaceous materials. Li[38] showed that the gasification rate of $Na_2CO_3$ impregnated activated carbon is one order of magnitude lower than black liquor char over almost the entire range of carbon conversion.

**Table 18.** Comparison of $CO_2$ Gasification Rates of Carbonaceous Materials.

| Rate @ 700°C ($hr^{-1}$) | $E_A$ (kcal/mol) | Temp. Range (°C) | Gas Pressure (atm.) | Gas Composition, % $CO_2/CO/N_2$ | Material | Catalyst | Investigator |
|---|---|---|---|---|---|---|---|
| 9.0E-4 | 54 | 727-977 | 1 | 20/0/80 | Electrode Carbon | None | Austin and Walker[97] |
| 8.2E-2 | 44.9 | 700-800 | 1 | 5/0/95 | German, High-Volatile Coal | 3.5-4..0 % $K_2CO_3$ | Meijer[50] |
| 6.0E-4 | 70 | 750-950 | 1 | 100/0/0 | Graphite | 5% $K_2CO_3$ | McKee[53] |
| 5.4E-4 | NA | 750-950 | 1 | 100/0/0 | Graphite | 5% $Na_2CO_3$ | McKee[53] |
| 7.9E-2 | 57.4 | 727 | 1 | 15/0/85 | Norit Rx extra, acid-washed steam activated peat char | 5% $Na_2CO_3$ | Kapteijn *et al.*[58] |
| 2.6E-2 | NA | 800-900 | 1 | 100/0/0 | Coal Char | 5% $Na_2CO_3$ | Spiro *et al*[59] |
| 0.12 | NA | 800-900 | 1 | 100/0/0 | Coal Char | 10% $Na_2CO_3$ | Spiro *et al.*[59] |
| 2.1 | 50 | 600-800 | 1 | 4.4/0/95.6 | Kraft Black Liquor Char | $Na_2CO_3$ | Present Study RTPP@ |
| 0.78 | 50.7 | 600-800 | 1 | 4.8/0/95.2 | Kraft Black Liquor Char | $Na_2CO_3$ | Present Study MTPP@@ |

@RTPP = Reaction Temperature Preheat Procedure
@@MTPP = Maximum Temperature Preheat Procedure

## 2. MASS TRANSFER TRANSITION TEMPERATURE FOR $CO_2$ GASIFICATION OF BLC

Having established a rate constant for the gasification of black liquor char by $CO_2$, the implication of these results for typical kraft recovery furnace conditions was examined. The mass transfer coefficient for the burning rate of black liquor char in $CO_2$ can be developed using eqn. 18.

$$k_m a_m = \left(\frac{0.455}{\varepsilon_{bed}}\right)\left(\frac{u d_p \rho}{\mu}\right)^{-0.407}\left(\frac{\mu}{\rho D_{AB}}\right)^{-2/3} a_m u \qquad \text{eqn. 18}$$

where $k_m$ = mass transfer coefficient, (m/s)
$a_m$ = external surface area per unit mass, ($m^2$/kg)
$\varepsilon_{bed}$ = void fraction of char bed,
$u$ = superficial velocity in the direction of flow, (m/s)
$d_p$ = average diameter of the char particles, (m)
$\mu$ = viscosity of the fluid, (kg/m/s)
$\rho$ = density of the fluid, (kg/$m^3$)
$D_{AB}$ = molecular diffusivity of component being transferred, ($m^2$/s)

The rate limiting effect of pore diffusion was accounted for with a Thiele modulus-based effectiveness factor using eqn. 21.

$$\eta = \frac{1}{M_{TM}}\left(\frac{1}{\tanh(3M_{TM})} - \frac{1}{3M_{TM}}\right) \qquad \text{eqn. 21}$$

where $\eta$ = dimensionless effectiveness factor
$M_{TM}$ = Thiele modulus

$$M_{TM} = \frac{d_p}{6}\sqrt{\frac{k\rho_{bed}}{D_{eff}}} \text{ for first order kinetics} \qquad \text{eqn. 22}$$

$$M_{TM} = \frac{d_p}{6}\sqrt{\frac{(n+1)k\rho_{bed}C_{CO_2}^{(n-1)}}{2D_{eff}}} \text{ for n order kinetics except n = 1.} \qquad \text{eqn. 23}$$

The global first order rate constant for chemical kinetic control conditions, eqn. 24, was calculated from the data for char prepared according to the RTPP. The frequency factor, activation energy, and units for $k_r$ vary for the different values of n.

$$k_r = Ae^{-E/RT} \qquad \text{eqn. 24}$$

where $k_r$ = global first order rate constant, ($m^3/kg/s$)
$A$ = preexponential factor or frequency factor = 1.35E10 $m^3/kg/s$
$E$ = activation energy = 50,000 cal/mol
$R$ = gas constant = 1.987 cal/mol/K
$T$ = absolute temperature, (K)

To determine the temperature where the rate of $CO_2$ gasification is completely controlled by film mass transfer, the mass transfer controlled rate and the kinetically controlled rate were determined using the following equations.

$$Rate_{mass\ transfer} = k_m a_m C_{CO_2} \qquad \text{eqn. 19}$$

$$Rate_{kinetic} = \eta k_r C_{CO_2}^n \qquad \text{eqn. 20}$$

The ratio of the kinetically controlled rate to the film mass transfer controlled rate $\left(\frac{Rate_{kinetic}}{Rate_{mass\ transfer}}\right)$ was determined for a range of recovery boiler parameters. Table 19 summarizes the range of recovery boiler parameters which influence the kinetic rate coefficient, pore diffusion effectiveness factor, and the film mass transfer coefficient. The calculated ratio of the kinetic rate constant to mass transfer constant was plotted for varying conditions and first order kinetics in Figs. 27-29. As expected, higher temperatures, lower gas velocities, larger particle sizes, and increased char density promote film mass transfer control of the $CO_2$ gasification reaction. As noted from these comparisons, the lowest transition temperature where the rate of $CO_2$ gasification is completely controlled by film mass transfer is predicted to be approximately 1300K. Figs. 30-33 show the calculated ratio for recovery boiler conditions where film mass transfer control would be greatest for global kinetic orders of 1, 0, 0.5, and 2; respectively. The

transition temperature increases with the kinetic order. The absolute lowest transition temperature where the rate of $CO_2$ gasification is controlled by film mass transfer is predicted to be approximately 1125K.

**Table 19.** Typical Recovery Furnace Parameters Which Influence the Kinetic Rate Coefficient, Pore Diffusion Effectiveness Factor, and the Film Mass Transfer Coefficient.

| Parameter | Low | Typical | High |
|---|---|---|---|
| Velocity, (m/s) | 0.5 | 10 | 80 |
| Particle Diameter, (mm) | 3 | 10 | 20 |
| Char Density, ($kgC/m^3$) | 2 | 7.8 | 20 |
| Temperature, (K) | 1030 | 1250 | 1480 |

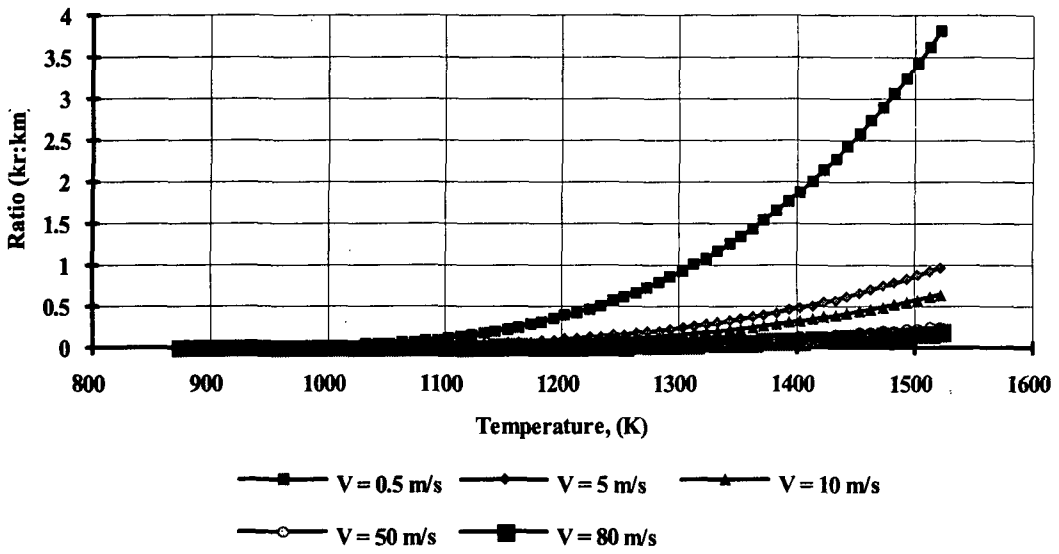


**Figure 27.** Calculated Ratio of Kinetic Rate Constant to Mass Transfer Constant for Kraft Black Liquor Char Prepared According to the Reaction Temperature Preheat Procedure for Typical Recovery Furnace Conditions, First Order Kinetics, and Varying Gas Velocities ($d_p = 0.01m$, $\rho_{bed} = 7.8\ kgC/m^3$, $\varepsilon_{bed} = 0.40$, $\varepsilon_p = 0.91$).

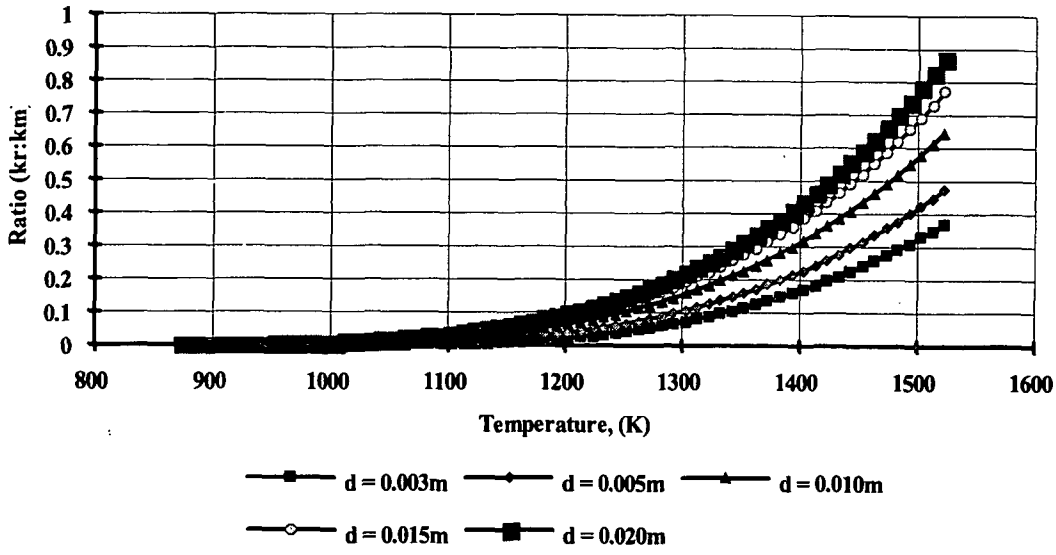


**Figure 28.** Calculated Ratio of Kinetic Rate Constant to Mass Transfer Constant for Kraft Black Liquor Char Prepared According to the Reaction Temperature Preheat Procedure for Typical Recovery Furnace Conditions, First Order Kinetics, and Varying Particle Sizes ($V = 10$ m/s, $\rho_{bed} = 7.8$ kgC/m$^3$, $\varepsilon_{bed} = 0.40$, $\varepsilon_p = 0.91$).

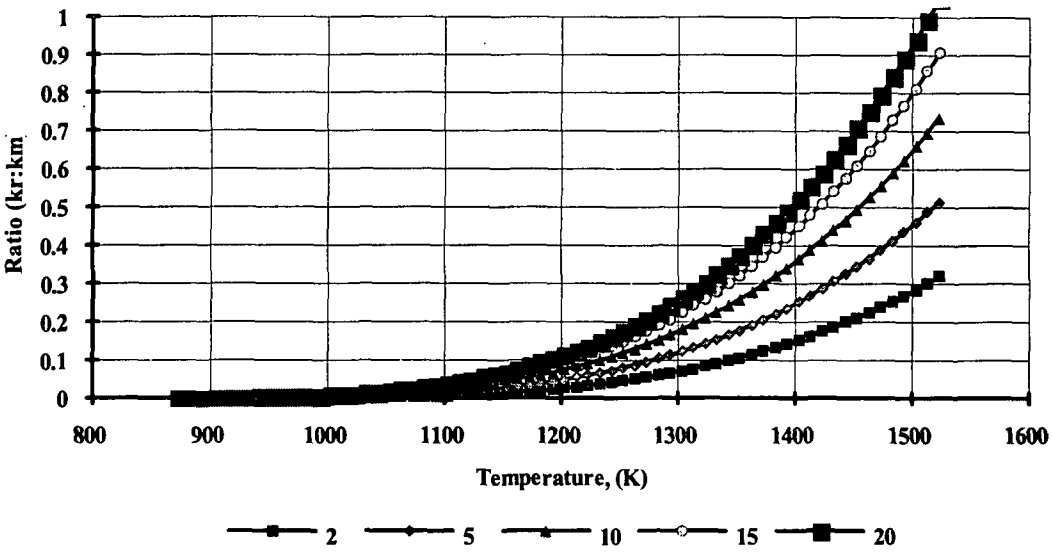


**Figure 29.** Calculated Ratio of Kinetic Rate Constant to Mass Transfer Constant for Kraft Black Liquor Char Prepared According to the Reaction Temperature Preheat Procedure for Typical Recovery Furnace Conditions, First Order Kinetics, and Varying Organic Carbon Concentrations (kgC/m$^3$) ($V = 10$ m/s, $d_p = 0.010$ m, $\varepsilon_{bed} = 0.40$, $\varepsilon_p = 0.91$).

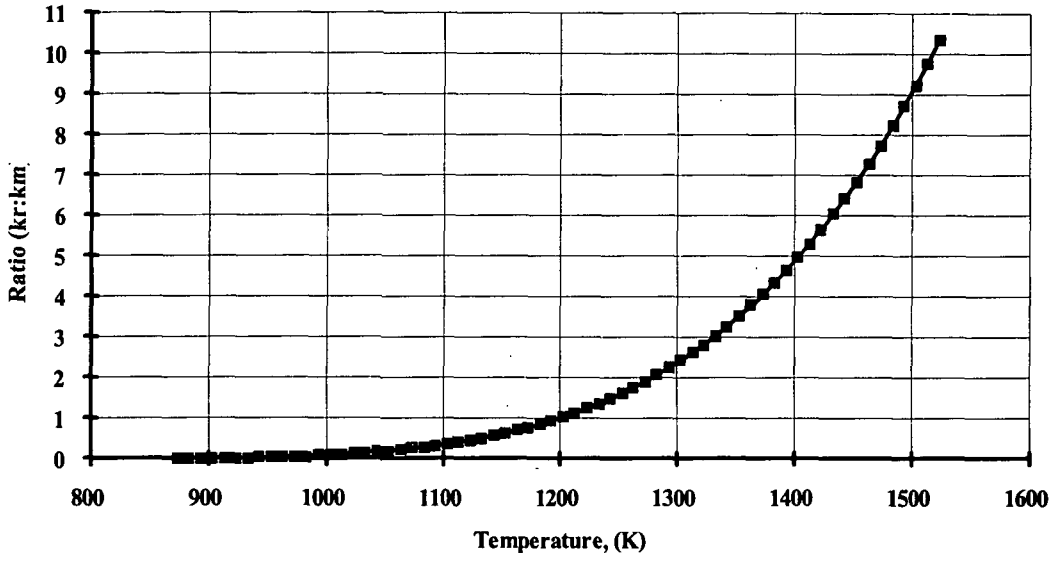


**Figure 30.** Calculated Ratio of Kinetic Rate Constant to Mass Transfer Constant for Kraft Black Liquor Char Prepared According to the Reaction Temperature Preheat Procedure for Extreme Recovery Furnace Conditions and First Order Kinetics (V = 0.5 m/s, $d_p$ = 0.020 m, $\rho_{bed}$ = 20 kgC/m$^3$, $\varepsilon_{bed}$ = 0.40, $\varepsilon_p$ = 0.91).

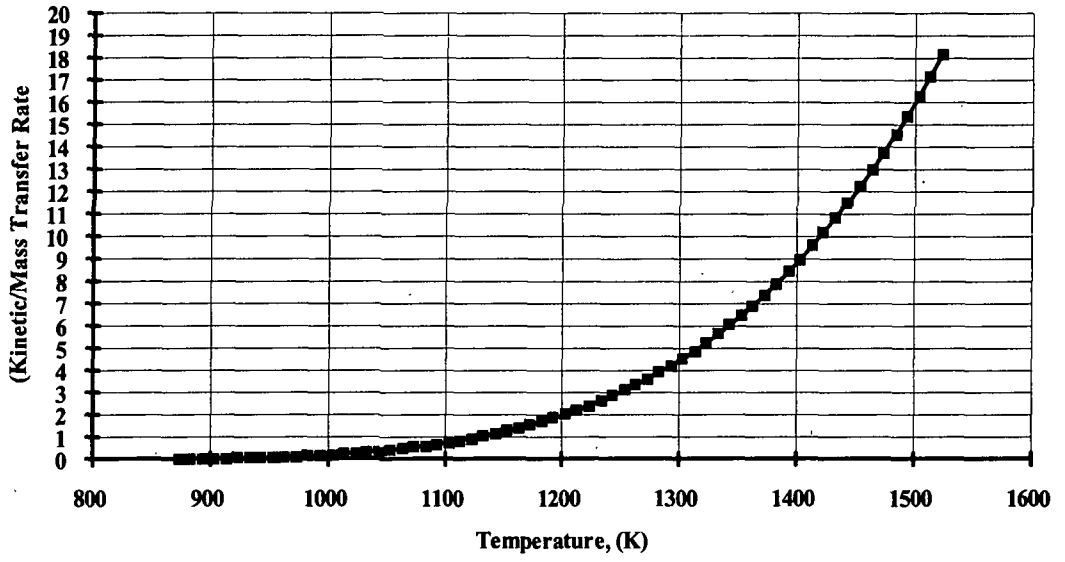


**Figure 31.** Calculated Ratio of Kinetic Rate to Mass Transfer Rate for Kraft Black Liquor Char Prepared According to the Reaction Temperature Preheat Procedure for Extreme Recovery Furnace Conditions and Zero Order Kinetics (V = 0.5 m/s, $d_p$ = 0.020 m, $\rho_{bed}$ = 20 kgC/m$^3$, $\varepsilon_{bed}$ = 0.40, $\varepsilon_p$ = 0.91).

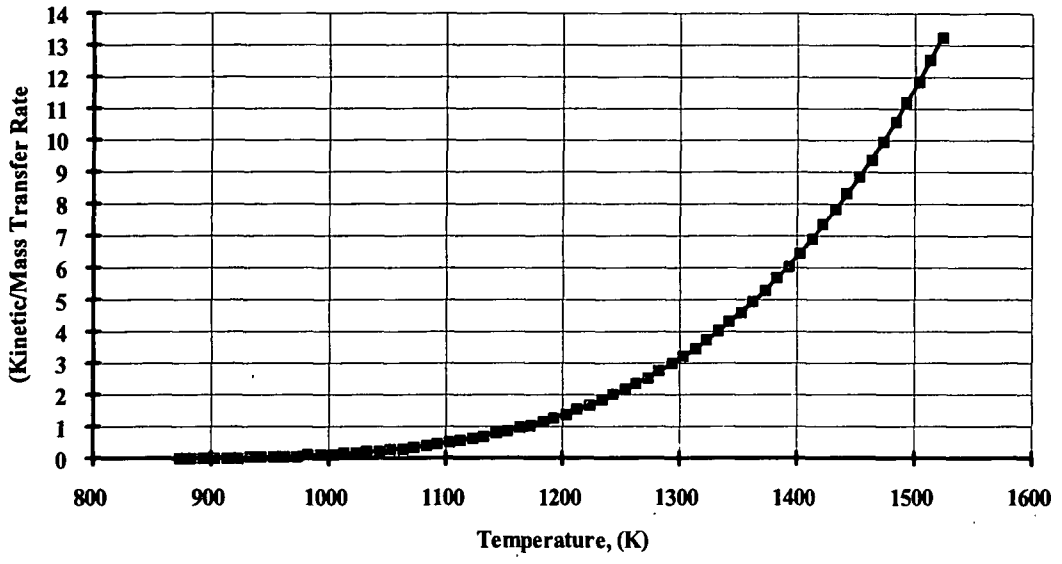


**Figure 32.** Calculated Ratio of Kinetic Rate to Mass Transfer Rate for Kraft Black Liquor Char Prepared According to the Reaction Temperature Preheat Procedure for Extreme Recovery Furnace Conditions and 0.5 Order Kinetics (V = 0.5 m/s, $d_p$ = 0.020 m, $\rho_{bed}$ = 20 kgC/m$^3$, $\varepsilon_{bed}$ = 0.40, $\varepsilon_p$ = 0.91).

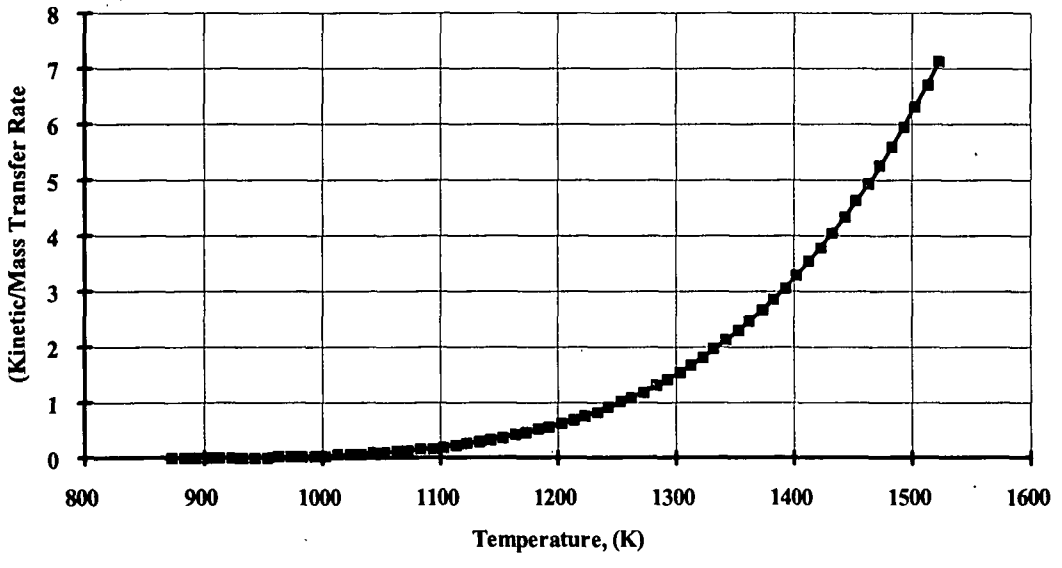


**Figure 33.** Calculated Ratio of Kinetic Rate to Mass Transfer Rate for Kraft Black Liquor Char Prepared According to the Reaction Temperature Preheat Procedure for Extreme Recovery Furnace Conditions and Second Order Kinetics (V = 0.5 m/s, $d_p$ = 0.020 m, $\rho_{bed}$ = 20 kgC/m$^3$, $\varepsilon_{bed}$ = 0.40, $\varepsilon_p$ = 0.91).

## 3. $O_2$ OXIDATION OF KRAFT BLACK LIQUOR CHAR IN A FIXED BED REACTOR

The $O_2$ oxidation rate of kraft BLC prepared according to the maximum temperature preheat procedure was studied using the fixed bed reactor at 700°C. This study provides baseline information on the rate of oxidation of BLC with $O_2$ which will be utilized for the combined oxidation/gasification study in the next section. This section determines whether $O_2$ oxidation of kraft BLC is controlled by mass transfer or reaction kinetics utilizing the Phase III experiments.

A typical set of CO, $CO_2$, and $O_2$ concentration profiles obtained at the reactor outlet are shown in Figs. 34 and 35, for chars exposed to approximately 2% and 5% $O_2$, respectively. Complete sets of CO, $CO_2$, and $O_2$ product stream concentration profiles for char oxidized in 2% and 5% $O_2$ are provided in Appendix XV.

The product stream concentration profiles suggest that $O_2$ is readily consumed within the fixed bed reactor. The absence of CO, $CO_2$, and $O_2$ in the product stream during $O_2$ oxidation of char was also observed by Grace *et al.*,[101] but no explanation was proposed. Assuming that char-C reacts with $O_2$ through the sulfate-sulfide cycle to yield CO and $CO_2$, the mass flow rate of oxygen entering as $O_2$ should equal the mass flow rate of oxygen leaving as CO, $CO_2$, and $O_2$. The ratio of oxygen out to oxygen in at 2% $O_2$ ranged from 6.79-20.7%. The ratio of oxygen out to oxygen in at 5% $O_2$ ranged from 0.904-26.9%. Therefore, the oxygen mass balances suggest that oxygen was also consumed by other reactions.

To determine where oxygen was consumed in the fixed bed reactor, the reactor was divided into two distinct regions for mass balance purposes as shown in Fig. 36. Region one includes the char bed (initial and residual char bed), the inlet and outlet gas streams, and the char retort. Region two includes the exhaust line downstream from the char bed, since inorganic aerosol condenses on the cooler surfaces.

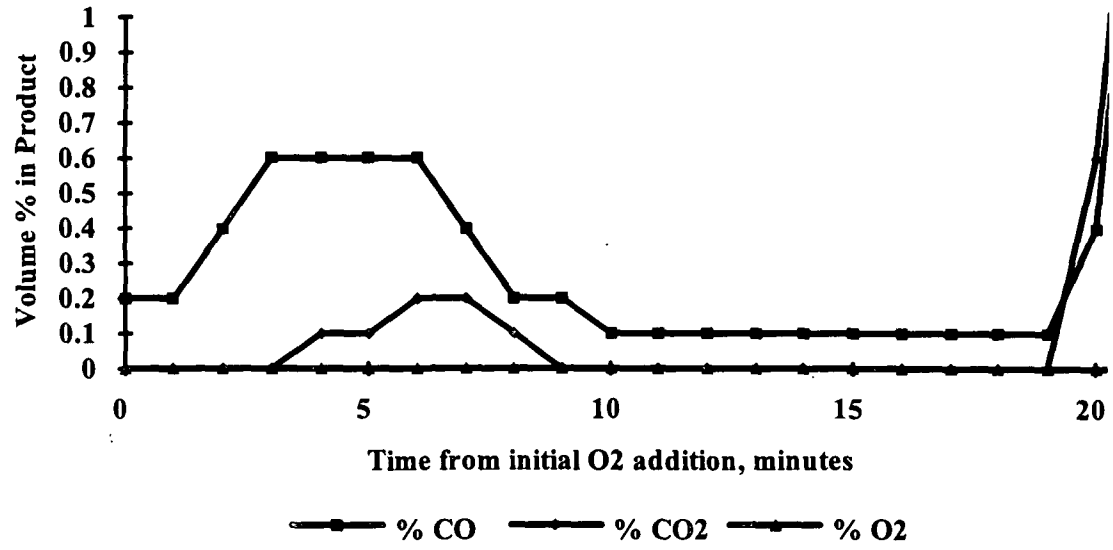


**Figure 34.** %CO, $\%CO_2$, and $\%O_2$ in Product Gas as a Function of Time for a Typical Gasification Experiment for Char Prepared According to the Maximum Temperature Preheat Procedure (702°C, 2.2%$O_2$, 5.4 slpm, $N_2$ Carrier Gas).

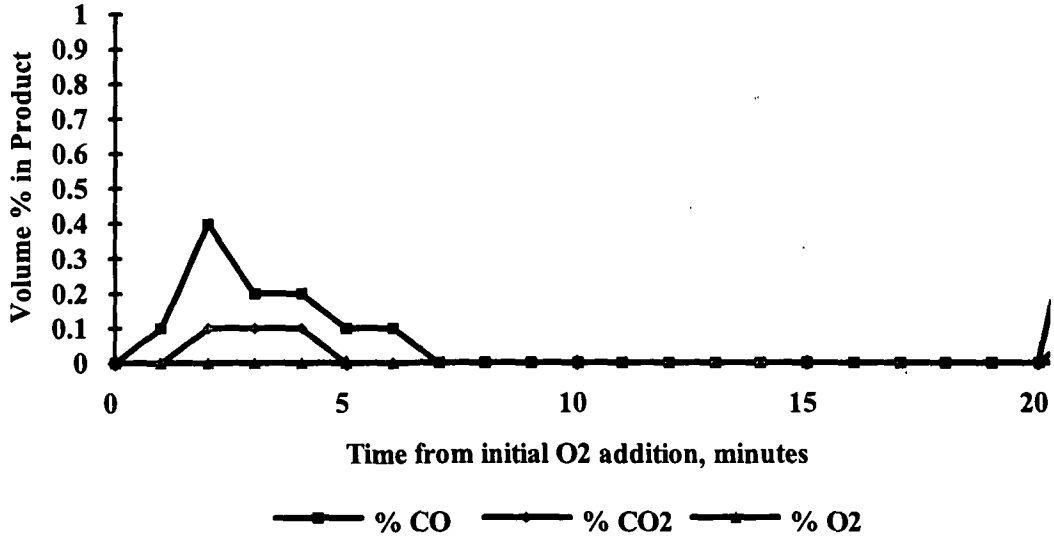


**Figure 35.** %CO, $\%CO_2$, and $\%O_2$ in Product Gas as a Function of Time for a Typical Gasification Experiment for Char Prepared According to the Maximum Temperature Preheat Procedure (697°C, 4.5%$O_2$, 5.4 slpm, $N_2$ Carrier Gas).

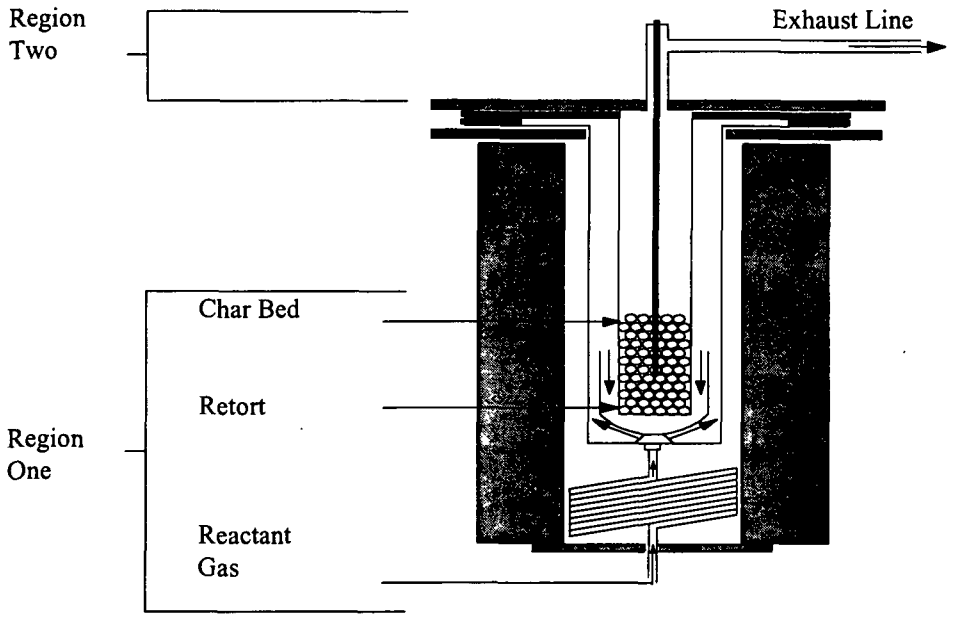


**Figure 36.** Schematic of Fixed Bed Reactor Showing Regions One and Two for Mass Balances.

Before mass balances on these two regions or the entire reactor are discussed, the Maximum Temperature Preheat Procedure (MTPP), the preheat procedure employed for $O_2$ experiments, will be briefly reviewed. In addition, a few experimental observations will be discussed. The MTPP involved heating partially pyrolyzed char particles in an atmosphere of 95% $N_2$/5% CO to a maximum temperature of 950°C, achieving complete pyrolysis at 950°C, upon complete pyrolysis retaining char at 950°C for one hour, and cooling down to 700°C. As noted in Fig. 4, approximately 60% of the Na (3.4 g) that is in the partially devolatilized char is devolatilized during the preheat procedure. In addition, experimental observations following a series of preheat experiments include the presence of a white powder residue in the exhaust line that flashed when exposed to $H_2O$ during experimental clean up. This white powder residue is likely the Na lost during the preheat process.

Table 20 summarizes the mass balances around region one of the fixed bed reactor for the respective $O_2$ combustion experiments. These mass balances suggest that oxygen and carbon are consumed between region one and the gas analyzers; the unaccountable oxygen and carbon are consumed in region two. Hydrogen depletion during the reaction is negligible suggesting that the oxygen did not exit as $H_2O$ and carbon did not exit as $CH_4$. In other words, very little hydrogen left the system in the gas phase.

**Table 20.** A Summary of Mass Balances Around Region One of the Fixed Bed Reactor for the Respective $O_2$ Oxidation Experiments.

| Experiment Number | Gas Composition $O_2/N_2$ | Exposure Time (minutes) | $C_i$-$C_f$ (gmoles) | $Na_i$-$Na_f$ (gmoles) | $S_i$-$S_f$ (gmoles) | $O_i$-$O_f$ (gmoles) | $H_i$-$H_f$ (gmoles) |
|---|---|---|---|---|---|---|---|
| 4993 | 2.0/98.0 | 15 | 0.006 | -0.012 | -0.007 | 0.019 | 0 |
| 4994 | 2.4/97.6 | 15 | 0.001 | -0.021 | -0.011 | 0.006 | 0.01 |
| 5002 | 2.2/97.8 | 20 | 0.012 | 0.005 | 0.005 | 0.062 | 0 |
| 5001 | 2.2/97.8 | 60 | 0.051 | 0.012 | 0.006 | 0.19 | 0.01 |
| 4996 | 2.0/98.0 | 65 | 0.041 | 0 | 0.004 | 0.15 | 0.01 |
| 4999 | 4.7/95.3 | 20 | 0.043 | -0.002 | -0.004 | 0.14 | 0.01 |
| 5000 | 4.5/95.5 | 20 | 0.041 | -0.012 | -0.005 | 0.13 | 0.01 |
| 4998 | 4.6/95.4 | 25 | 0.041 | 0.019 | 0.012 | 0.18 | 0.01 |
| 4997 | 4.6/95.4 | 31 | 0.038 | -0.008 | -0.001 | 0.12 | 0.01 |

i = refers to element amount at point of $O_2$ addition (determined from preheat experiments)
f = refers to element amount of residual material

The following theory is proposed for the combustion of oxygen and carbon in region two. Char-C reacts with $O_2$ through the sulfate-sulfide cycle or direct oxidation to yield CO and $CO_2$ in region one. Since very little CO is observed in the exhaust stream and carbon is consumed, the CO reacts with $O_2$ to form $CO_2$. According to the rate expressions by Gardiner *et al.*[102] and Rawlins *et al.*, [103] this homogeneous reaction is feasible at 700°C. Therefore, the main product of the char-C reaction with $O_2$ is

$CO_2$. Any excess $O_2$ that enters the exhaust line (region two) will readily react with Na to form $Na_2O$ through the following thermodynamically feasible reaction (at 700°C):

$$2Na + (\tfrac{1}{2})O_2(g) \Leftrightarrow Na_2O \qquad \text{rxn. 18}$$

In turn, the $CO_2$ product of the char-C reaction reacts with the $Na_2O$ to form $Na_2CO_3$ through the following thermodynamically feasible reaction (at 700°C):

$$Na_2O + CO_2(g) \Leftrightarrow Na_2CO_3 \qquad \text{rxn. 19}$$

In addition, any $SO_2$ leaving the char bed reacts with $Na_2O$ to form $Na_2SO_4$ through the following thermodynamically feasible reaction (at 700°C):

$$Na_2O + SO_2 + (\tfrac{1}{2})O_2 \Leftrightarrow Na_2SO_4 \qquad \text{rxn. 20}$$

To verify the theory, the following assumptions were made:

1. The Na lost during the char preheat period for each experiment condenses on the exhaust line surfaces.
2. The Na reacts with $O_2$ (rxn. 18) to form $Na_2O$.
3. Unaccountable C, ($C_i$-$C_f$) in Table 20, leaves the char boundary layer as $CO_2$.
4. The $CO_2$ reacts with $Na_2O$ (rxn. 19) to form $Na_2CO_3$ in the exhaust line.
5. Unaccountable S, ($S_i$-$S_f$) in Table 20, leaves the char surfaces as $SO_2$.
6. The $SO_2$ reacts with $Na_2O$ and $(\tfrac{1}{2})O_2$ to form $Na_2SO_4$ (rxn. 20) in the exhaust line.

Table 21 summarizes the oxygen trapped in region 2 (the exhaust line) as $Na_2CO_3$ and $Na_2SO_4$. The total oxygen trapped in region 2, oxygen existing in $Na_2SO_4$ and $Na_2CO_3$, is approximately equal to the unaccountable oxygen from region one (Table 20). In addition, the amount of Na that must be present in region 2 is less than or equal to the Na (3.4 g) that evolves during devolatilization. Therefore, the hypothesized theory of oxygen and carbon consumption is substantiated.

**Table 21.** Oxygen Trapped in the Fixed Bed Reactor Exhaust Line.

| Exper. Num. | Gas Comp. $O_2/N_2$ | Exp. Time (min.) | Oxygen in evolved $Na_2CO_3$ (gmole)* | Oxygen in evolved $Na_2SO_4$ (gmole)** | Oxygen in exhaust line (gmole) | $O_i$-$O_f$ (gmole) from Table 15 | Oxygen Balance (gmole) | Na in exhaust line (g) |
|---|---|---|---|---|---|---|---|---|
| 4993 | 2.0/98.0 | 15 | 0.018 | - | 0.018 | 0.019 | 0.001 | 0.56 |
| 4994 | 2.4/97.6 | 15 | 0.004 | - | 0.004 | 0.006 | 0.002 | 0.54 |
| 5002 | 2.2/97.8 | 20 | 0.036 | 0.021 | 0.057 | 0.062 | 0.005 | 0.68 |
| 5001 | 2.2/97.8 | 60 | 0.15 | 0.022 | 0.17 | 0.19 | 0.02 | 2.4 |
| 4996 | 2.0/98.0 | 65 | 0.12 | 0.016 | 0.14 | 0.15 | 0.01 | 2.1 |
| 4999 | 4.7/95.3 | 20 | 0.13 | - | 0.13 | 0.14 | 0.01 | 2.1 |
| 5000 | 4.5/95.5 | 20 | 0.12 | - | 0.12 | 0.13 | 0.01 | 2.2 |
| 4998 | 4.6/95.4 | 25 | 0.12 | 0.047 | 0.17 | 0.18 | 0.01 | 2.1 |
| 4997 | 4.6/95.4 | 31 | 0.11 | - | 0.11 | 0.12 | 0.01 | 1.9 |

*Determine from $C_i$-$C_f$ from Table 20
**Determined from $S_i$-$S_f$ from Table 20

Mass Transfer Coefficient for Oxidation of Kraft Black Liquor Char

Average oxygen mass transfer coefficients, $k_{avg.}$, were calculated from the experimental burning rates as follows:

$$k_{avg.} = \frac{R'_{O_2}}{C_{O_2}} \qquad \text{eqn. 21}$$

where $R'_{O_2}$ = calculated oxygen flux to the char bed surface, (gmole/m$^2$/s)
$C_{O_2}$ = average oxygen concentration over the char bed, (gmole/m$^3$).

An oxygen material balance is used to determine an outlet $O_2$ concentration for use in the average by subtracting the oxygen consumed by carbon reactions from the inlet oxygen flow. The actual measured outlet $O_2$ concentration could not be used directly because of added $O_2$ consumption by the Na in the exhaust line. The oxygen flux to the char bed, $R'_{O_2}$, is determined as follows:

$$R'_{O_2} = \left(\frac{\text{Oxygen Consumed by C}}{(A_{ext.} \bullet t)}\right) \qquad \text{eqn. 22}$$

Oxygen Consumed by C = $\left(O_{input} - O_{Na_2O} - O_{out}\right)$

$A_{ext.}$ = external surface area, ($m^2$)

t = reaction time, (seconds)

Table 22 summarizes the average oxygen mass transfer coefficient, $k_{avg.}$, calculated for the respective char burning experiments.

The average film mass transfer coefficient was calculated using a correlation for packed beds[81,85] as

$$k_m = \left(\frac{0.455}{\varepsilon_{bed}}\right)\left(\frac{u\rho d_p}{\mu}\right)^{-0.407}\left(\frac{\mu}{\rho D_{AB}}\right)^{-\frac{2}{3}} u \qquad \text{eqn. 23}$$

The quantities have been defined in eqn. 18. The average film mass transfer coefficient, km, predicted at 700°C was 0.041 m/s. The theoretical mass transfer coefficient is slightly greater than the experimental mass transfer coefficient (ranging from 0.037-0.047). However, the values are of the same order of magnitude. The correlation between the experimental values and the theoretical values indicate that the oxidation of kraft BLC at 700°C is mass transfer controlled.

**Table 22.** Average Oxygen Mass Transfer Coefficient for Char Exposed to $O_2$ in the Fixed Bed Reactor at 700°C.

| Experiment Number | Gas Composition ($O_2/N_2$) | Exposure Time (minutes) | kavg. (m/s) |
|---|---|---|---|
| 4993 | 2.0/98.0 | 15 | 0.046 |
| 4994 | 2.4/97.6 | 15 | 0.041 |
| 5002 | 2.2/97.8 | 20 | 0.038 |
| 5001 | 2.2/97.8 | 60 | 0.037 |
| 4996 | 2.0/98.0 | 65 | 0.039 |
| 4999 | 4.7/95.3 | 20 | 0.039 |
| 5000 | 4.5/95.5 | 20 | 0.039 |
| 4998 | 4.6/95.4 | 25 | 0.039 |
| 4997 | 4.6/95.4 | 31 | 0.047 |

## 4. COMBINED OXIDATION/COMBUSTION OF KRAFT BLACK LIQUOR CHAR IN A FIXED BED REACTOR

The combination oxidation/gasification rate of kraft BLC prepared according to the maximum tempeature preheat procedure was studied using the fixed bed reactor at 700°C. The interaction between $O_2$ and $CO_2$ was investigated utilizing the $CO_2$ gasification and $O_2$ oxidation results and the results of the Phase IV experiments.

A typical set of CO, $CO_2$, and $O_2$ concentration profiles obtained at the reactor outlet are shown in Figs. 37 and 38, for chars exposed to approximately $2\%O_2/5\%CO_2/93\%N_2$ and $5\%O_2/5\%CO_2/90\%N_2$, respectively. Complete sets of CO, $CO_2$, and $O_2$ product stream concentration profiles for these conditions are provided in Appendix XVI. The product stream concentration profiles are similar in shape to those for $CO_2$ gasification (note Fig. 6). However, the $CO_2$ concentration is slightly higher for the $O_2/CO_2$ combination experiments versus the $CO_2$ gasification experiments. In addition, the CO exit concentration is slightly lower for the $O_2/CO_2$ combination experiments versus the $CO_2$ gasification experiments. Assuming that char-C reacts with $O_2$ through the Boudouard reaction and the sulfate-sulfide cycle, the mass flow rate of oxygen entering as $O_2$ and $CO_2$ should equal the mass flow rate of oxygen leaving as CO, $CO_2$, and $O_2$. The ratio of oxygen out to oxygen in at $2\%O_2/5\%CO_2/95\%N_2$ and $5\%O_2/5\%CO_2/90\%N_2$ was less than unity ($0.65\pm 0.026$ and $0.52\pm0.030$, respectively). Therefore, the oxygen mass balances and the produtct gas concentration profiles suggest that oxygen was also consumed by other reactions.

As outlined in the previous section, the reactor was divided into two distinct regions to determine where oxygen was consumed in the fixed bed reactor Region one includes the char bed (initial and residual char bed, the inlet and outlet gas streams, and the char retort). The second region includes the exhaust line downstream from the char bed, since inorganic aerosol condenses on the cooler surfaces.

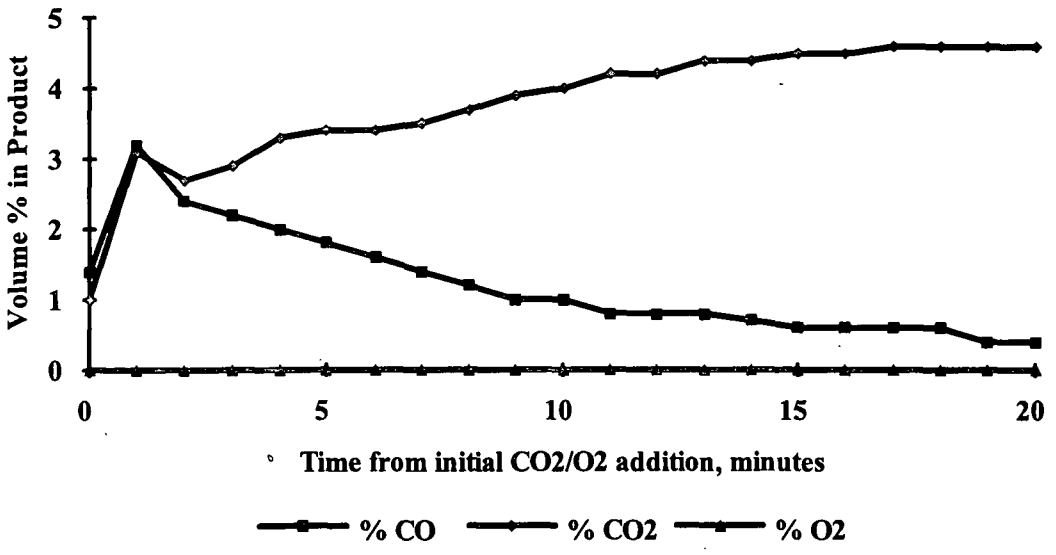


**Figure 37.** %CO, $\%CO_2$, and $\%O_2$ in Product Gas as a Function of Time for a Typical Gasification Experiment for Char Prepared According to the Maximum Temperature Preheat Procedure (701°C, 2.0%$O_2$, 5.0%$CO_2$, 5.4 slpm, $N_2$ Carrier Gas)

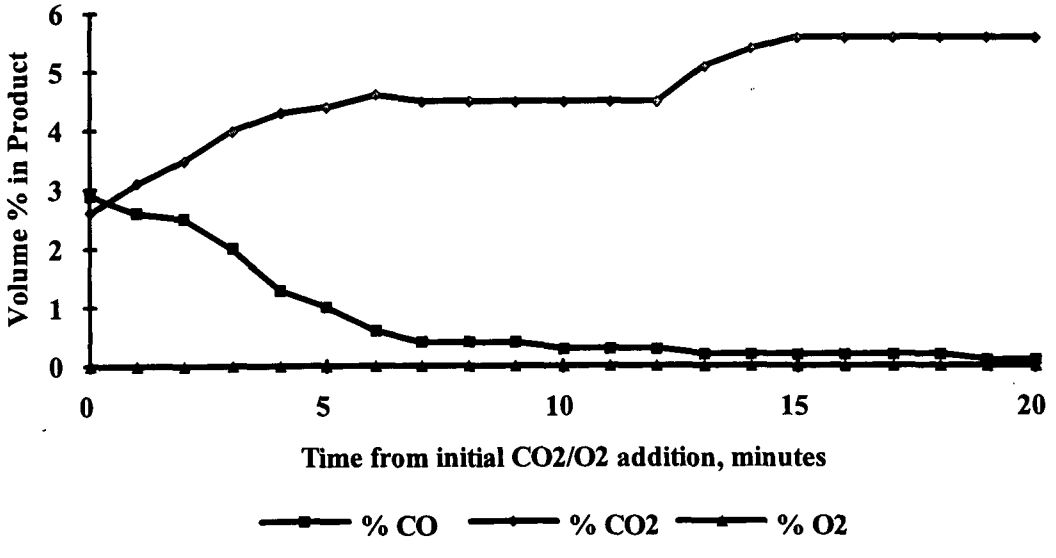


**Figure 38.** %CO, $\%CO_2$, and $\%O_2$ in Product Gas as a Function of Time for a Typical Gasification Experiment for Char Prepared According to the Maximum Temperature Preheat Procedure (708°C, 4.8%$O_2$, 4.8%$CO_2$, 5.4 slpm, $N_2$ Carrier Gas).

In addition, it is important to recall that approximately 60% of the Na that is in the partially devolatilized char at the beginning of every experiment is devolatilized during the preheat procedure.

Before mass balances on these two regions or the entire reactor are discussed, the Maximum Temperature Preheat Procedure (MTPP), the preheat procedure employed for $O_2$ experiments, will be briefly reviewed. In addition, a few experimental observations will be discussed. The MTPP involved heating partially pyrolyzed char particles in an atmosphere of 95% $N_2$/5% CO to a maximum temperature of 950°C, achieving complete pyrolysis at 950°C, upon complete pyrolysis retaining char at 950°C for one hour, and cooling down to 700°C. As noted in Fig. 4, approximately 60% of the Na (3.4 g) that is in the partially devolatilized char is devolatilized during the preheat procedure. In addition, experimental observations following a series of preheat experiments include the presence of a white powder residue in the exhaust line that flashed when exposed to $H_2O$ during experimental clean up. This white powder residue is likely the Na lost during the preheat process.

Table 23 summarizes the mass balances around region one of the fixed bed reactor for the respective oxidation/gasification experiments. These mass balances suggest that oxygen and carbon are consumed between region one and the gas analyzers; the unaccountable oxygen and carbon are consumed in region two. Hydrogen depletion during the reaction is negligible suggesting that the oxygen did not exit as $H_2O$ and carbon did not exit as $CH_4$. In other words, very little hydrogen left the system in the gas phase.

**Table 23.** A Summary of Mass Balances Around Region One of the Fixed Bed Reactor for the Respective Oxidation/Gasification Experiments.

| Experiment Number | Gas Composition $O_2/CO_2/N_2$ | Exposure Time (minutes) | $C_i$-$C_f$ (gmoles) | $Na_i$-$Na_f$ (gmoles) | $S_i$-$S_f$ (gmoles) | $O_i$-$O_f$ (gmoles) | $H_i$-$H_f$ (gmoles) |
|---|---|---|---|---|---|---|---|
| 5006 | 2.0/5.0/93.0 | 20 | 0.019 | 0.028 | 0.017 | 0.13 | 0.01 |
| 5008 | 2.2/4.9/92.9 | 20 | 0.017 | 0.018 | 0.014 | 0.12 | 0.01 |
| 5003 | 4.9/4.9/90.2 | 20 | 0.037 | 0.016 | 0.01 | 0.16 | 0.02 |
| 5004 | 4.8/4.8/90.4 | 20 | 0.039 | 0.031 | 0.012 | 0.18 | 0 |
| 5005 | 4.9/4.7/90.3 | 20 | 0.039 | 0.039 | 0.021 | 0.21 | 0 |

i = refers to element amount at point of $O_2/CO_2$ addition (determined from preheat experiments)
f = refers to element amount of residual material

The following theory is proposed for the combustion of oxygen and carbon in region two. Char-C reacts with $O_2$ through the sulfate-sulfide cycle or direct oxidation to yield CO and $CO_2$ in region one. As noted in the previous section, the main product of the char-C reaction with $O_2$ is probably $CO_2$. Simultaneously, char-C reacts with $CO_2$ through the Boudouard reaction to yield CO. Any excess $O_2$ that enters the exhaust line (region two) will readily react with Na to form $Na_2O$ through the rxn. 18. In turn, a stoichiometric equivalent amount of product $CO_2$ reacts with the $Na_2O$ to form $Na_2CO_3$ through rxn. 19. In addition, any $SO_2$ leaving the char bed reacts with $Na_2O$ to form $Na_2SO_4$ through rxn. 20.

To verify the theory, the following assumptions were made:

1. The Na lost during the char preheat period for each experiment condenses on the exhaust line surfaces.
2. The Na reacts with $O_2$ (rxn. 18) to form $Na_2O$.
3. Unaccountable C, ($C_i$-$C_f$) in Table 23, leaves the char boundary layer as $CO_2$.
4. The $CO_2$ reacts with a stoichiometric proportion of $Na_2O$ (rxn. 19) to form $Na_2CO_3$ in the exhaust line.
5. Unaccountable S, ($S_i$-$S_f$) in Table 23, leaves the char bed as $SO_2$.
6. The $SO_2$ reacts with a stoichiometric proportion of $Na_2O$ and $(\frac{1}{2})O_2$ to form $Na_2SO_4$ (rxn. 20) in the exhaust line.

7. The conversion of a fraction of the CO from the $CO_2$ gasification reaction to $CO_2$ is accounted for in the observed exit gas concentration.

Table 24 summarizes the oxygen trapped in region 2 (the exhaust line) as $Na_2CO_3$ and $Na_2SO_4$. The total oxygen trapped in region 2, oxygen existing in $Na_2SO_4$ and $Na_2CO_3$, is approximately equal to the unaccountable oxygen from region one (Table 23). In addition, the amount of Na that must be present in region 2 is less than the Na (3.4 g) that evolves during devolatilization. Therefore, the hypothesized theory of oxygen and carbon consumption is possible.

**Table 24.** Oxygen Trapped in the Fixed Bed Reactor Exhaust Line.

| Exper. Num. | Gas Comp. $O_2/CO_2/N_2$ | Exp. Time (min.) | Oxygen in evolved $Na_2CO_3$ (gmole)* | Oxygen in evolved $Na_2SO_4$ (gmole)** | Oxygen in exhaust line (gmole) | $O_i$-$O_f$ (gmole) from Table 15 | Oxygen Balance (gmole) | Na in exhaust line (g) |
|---|---|---|---|---|---|---|---|---|
| 5006 | 2.0/5.0/93.0 | 20 | 0.056 | 0.068 | 0.12 | 0.13 | 0.01 | 0.99 |
| 5008 | 2.2/4.9/92.9 | 20 | 0.051 | 0.058 | 0.11 | 0.12 | 0.01 | 1.1 |
| 5003 | 4.9/4.9/90.2 | 20 | 0.11 | 0.041 | 0.15 | 0.16 | 0.01 | 1.8 |
| 5004 | 4.8/4.8/90.4 | 20 | 0.12 | 0.048 | 0.17 | 0.18 | 0.01 | 1.6 |
| 5005 | 4.9/4.7/90.3 | 20 | 0.11 | 0.083 | 0.19 | 0.21 | 0.01 | 1.6 |

*Determine from $C_i$-$C_f$ from Table 23
**Determined from $S_i$-$S_f$ from Table 23

Rate Expression for Combined Oxidation/Gasification

As noted earlier, Grace *et al.*[13] evaluated combined oxidation/gasification mathematically. Their expression is slightly modified for this study. No $H_2O$ was used during the combined oxidation/gasification experiments in this study, therefore, $R_{H_2O} = 0$. The value of $f$ is 0 since the product of rxn. 17 is $CO_2$. This is supported by the mass balances and low concentration of CO in the exhaust stream for the oxidation experiments. Therefore, $R'_{O_2}$ and $R_C$ reduce to the following expressions:

$$R'_{O_2} = R_{O_2} - \chi(R_{CO_2}) \text{ and} \qquad \text{eqn. 24}$$

$$R_C = R_{O_2} + (1 - \chi)R_{CO_2}. \qquad \text{eqn. 25}$$

For this study, the parameter $\chi$ is redefined as follows:

$$\chi = \frac{\text{CO product from } CO_2 \text{ gasification and } O_2 \text{ oxidation that reacts with } O_2 \text{ to form } CO_2}{\text{CO product from } CO_2 \text{ gasification and } O_2 \text{ oxidation}} \qquad \text{eqn. 26}$$

The CO that is available from the $CO_2$ gasification and $O_2$ oxidation reactions was determined from the $CO_2$ gasification and $O_2$ oxidation data at 700°C. The CO that reacts was determined by subtracting the CO product of the respective oxidation/gasification experiment from the average sum of CO products of the $CO_2$ gasification and $O_2$ oxidation experiments at 700°C. An example calculation for $\chi$ for experiment 5003 is as follows:

$$\chi = \frac{A + B - C}{A + B} = 0.31$$

| | | | | | |
|---|---|---|---|---|---|
| where | A | = | CO evolved during $CO_2$ gasification | = | 0.025 gmole |
| | B | = | CO evolved during $O_2$ oxidation | = | 0.0036 gmole |
| | C | = | CO evolved during combination $CO_2/O_2$ | = | 0.0198 gmole |

Although the combination oxidation/gasification experiments were conducted only at 700°C, the

temperature dependency of the parameter $\chi$ would be expected to be the same as the temperature dependency of the reaction $CO + (\frac{1}{2})O_2 \Leftrightarrow CO_2$. Gardiner *et al.*[102] provided the following Arrhenius expression for the reaction.

$$k = 3.1\times10^8 \exp\left(\frac{-38{,}000}{RT}\right), \left(\frac{liter}{mol \bullet s}\right) \qquad \text{eqn. 27}$$

Table 25 summarizes the calculated rates for gasification, oxidation, and gasification/oxidation. In addition, these calculated values are compared to the experimental values for gasification/oxidation. The calculated values compare well to the experimental values with the percent difference between the two varying between 2-15%.

**Table 25.** Comparison of Calculated Rates and Experimental Rates for Combined Oxidation/Gasification.

| Experiment Number | Gas Composition ($O_2/CO_2/N_2$) | Exp. conv. param. | Calc. $R_{CO2}$, ($hr^{-1}$) | Calc. $R_{O2}$, ($hr^{-1}$) | Calc. $R_C$, ($hr^{-1}$) | Exp. $R_C$, ($hr^{-1}$) | % Difference |
|---|---|---|---|---|---|---|---|
| 5006 | 2.0/5.0/93.0 | 0.31 | 1.28 | 0.933 | 1.82 | 2.01 | -10.2 |
| 5008 | 2.2/4.9/92.9 | 0.35 | 1.24 | 0.981 | 1.79 | 1.82 | -2.26 |
| 5003 | 4.9/4.9/90.2 | 0.31 | 1.23 | 2.26 | 3.12 | 2.65 | 15.1 |
| 5004 | 4.8/4.8/90.4 | 0.54 | 1.21 | 2.28 | 2.84 | 2.59 | 9.11 |
| 5005 | 4.9/4.7/90.3 | 0.59 | 1.25 | 2.21 | 2.72 | 2.66 | 2.25 |

## 5. EFFECT OF $CO_2$ GASIFICATION ON CHAR DENSITY

Density Results for Char Prepared According to the Reaction Temperature Preheat Procedure (RTPP)

The data shown in Fig. 39 indicate that organic carbon concentration decreased upon the initiation of gasification and leveled off as gasification proceeded for char prepared according to the RTPP. Averages and standard deviations of groupings of the data represented in Fig. 39 are as follows: 10.8±1.36 kg carbon/$m^3$ at 0% fractional conversion of organic carbon, 7.33±0.508 kg carbon/$m^3$ at 10% fractional conversion of organic carbon, 5.52±1.79 kg carbon/$m^3$ at 40-56% fractional conversion of organic carbon, and 6.87±2.59 kg carbon/$m^3$ at 54-95% fractional conversion of organic carbon. These last three groupings are results at gasification temperatures at 600°C, 700°C, and 800°C, respectively. The average carbon concentration was 7.8 kg/$m^3$ for the range of fractional conversion from 0-97%. Initial organic carbon concentration was statistically higher (at the 99% confidence level) than the organic carbon concentration of char after 10% conversion. The organic carbon concentration in kraft char was statistically independent of fractional conversion at burnout levels greater than 10%.

Of necessity, the organic carbon concentration will approach zero as the conversion of organic carbon approaches 100%. Organic carbon concentration did not decrease linearly as a function of the fractional conversion of organic carbon. At 95% conversion of organic carbon, the concentration of organic carbon was approximately 6 kg carbon/$m^3$; therefore the organic carbon concentration is greatly reduced between conversions of 95% and 100%.

A review of the bulk density provides insight into the char behavior. As shown in Fig. 40, the char density reaches a minimum value of 25 kg/$m^3$ at a fractional organic carbon burnout of organic carbon of approximately 10%. Char bulk density calculated from data reported by Miller[9] is of the same order of magnitude as the bulk density reported in this study. Char density gradually increases as the organic carbon is depleted. This increase is statistically valid at the 99% confidence limit. The low char

density values at organic carbon conversions of approximately 10% resulted from particle volumes remaining constant while the char mass was only slightly decreasing. In contrast, at higher conversions of organic carbon, the particle volume decreased steadily as the organic carbon was depleted. The char density increases at higher fractional conversion because the inorganic salts coalesce as the organic carbon is depleted.

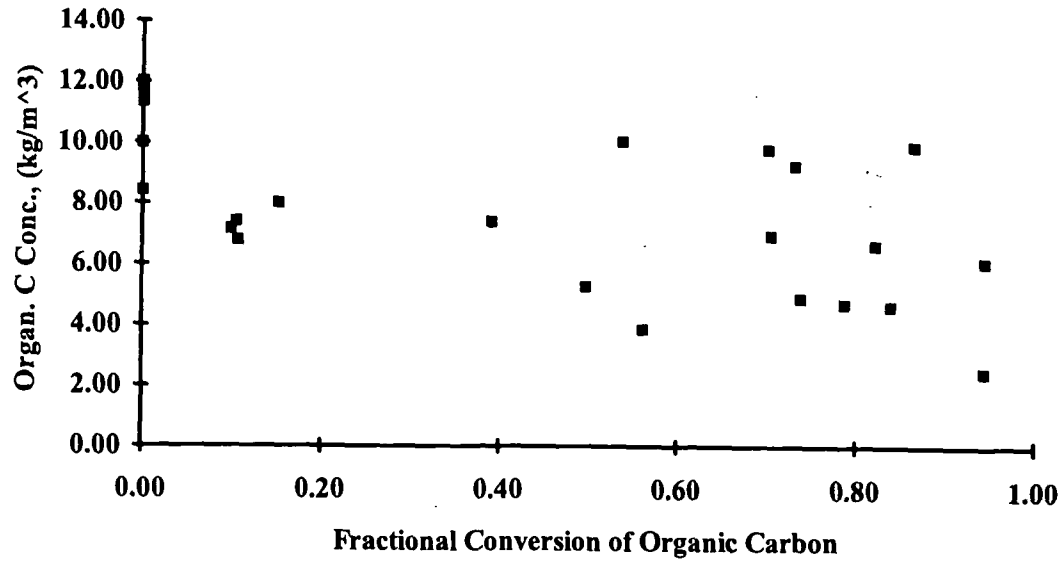


**Figure 39.** Concentration of Organic Carbon as a Function of Fractional Conversion of Organic Carbon for Char Prepared According to the Reaction Temperature Preheat Procedure.

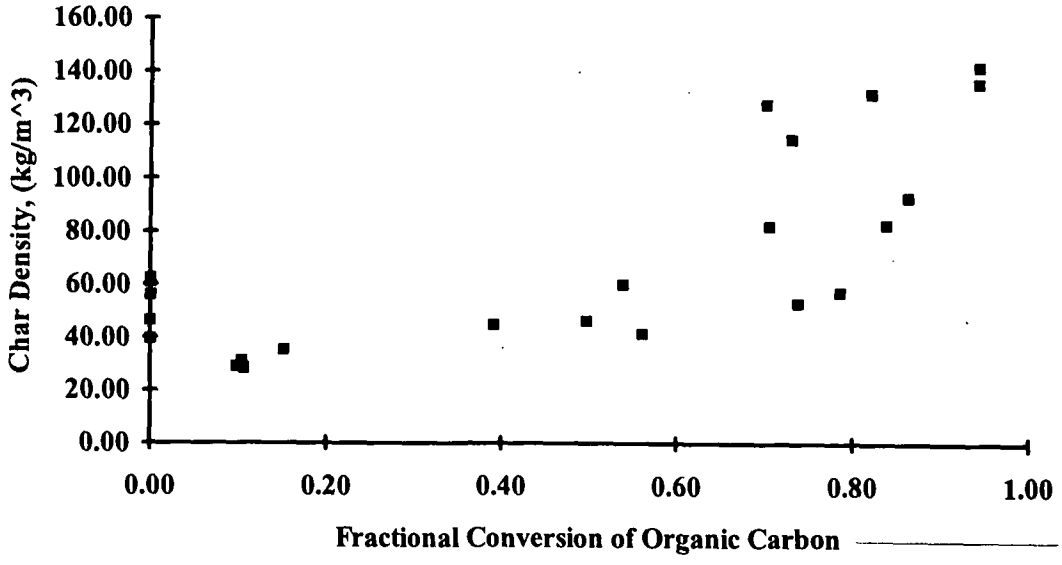


**Figure 40.** Bulk Density of Char as a Function of Fractional Conversion of Organic Carbon for Char Prepared According to the Reaction Temperature Preheat Procedure.

Density Results for Char Prepared According to the Maximum Temperature Preheat Procedure (MTPP)

The data shown in Fig. 41 indicate that organic carbon concentration in kraft char was statistically independent of fractional conversion at levels up to approximately 80% conversion of organic carbon for char prepared according to the MTPP. Averages and standard deviations of groupings of data represented in Fig. 41 are as follows: 13.0±2.57 kg carbon/$m^3$ at 0% fractional conversion of organic carbon, 7.27±0.788 kg carbon/$m^3$ at 12% fractional conversion of organic carbon, 13.4±5.05 kg carbon/$m^3$ at 17-46 fractional conversion of organic carbon, and 5.41±4.01 kg carbon/$m^3$ at 77-97% fractional conversion of organic carbon. These last three groupings are results at gasification temperatures of 600°C, 700°C, and 800°C. The average carbon concentration 12.46±4.68 for the range of fractional conversion from 0-97%. The organic carbon concentration was statistically lower (at the 95% confidence level) at levels of fraction conversion greater than 80%.

Again, a review of the bulk density provides insight into the char behavior. As shown in Fig. 42, the char density reaches a maximum value of 20 kg/$m^3$ at a fractional organic carbon burnout of approximately 12%. Char density gradually increases as the organic carbon is depleted. This increase is statistically valid at the 99% confidence interval. These bulk density observations are similar to the observations made from char preheated according to the RTPP.

Richardson and Merriam[104] have provided the only other char density measurements directly applicable to the char burning stage of black liquor combustion. Char density values of Richardson and Merriam (465-1320 kg/$m^3$) are at least an order of magnitude greater than the density values reported in this study. Char samples for this study were taken from a uniform bed of previously pyrolyzed char particles, in contrast to the nonuniform recovery furnace bed from which Richardson and Merriam collected their char samples. The high char density values reported by Richardson and Merriam are probably the result of sampling a mixture of smelt and char rather than pure char. This hypothesis is

supported by considering that the char density measured by Richardson and Merriam (465-1320 $kg/m^3$) is less than the smelt density measured by Richardson and Merriam (2083 $kg/m^3$) and much greater than the density of fully devolatilized char measured in this study (55 $kg/m^3$).

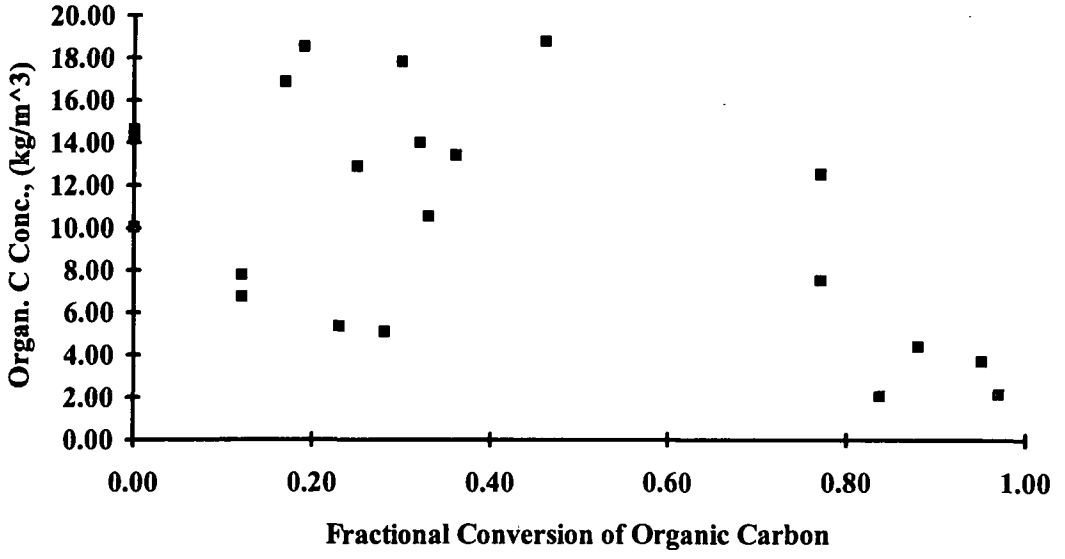


**Figure 41.** Concentration of Organic Carbon as a Function of Fractional Conversion of Organic Carbon for Char Prepared According to the Maximum Temperature Preheat Procedure.

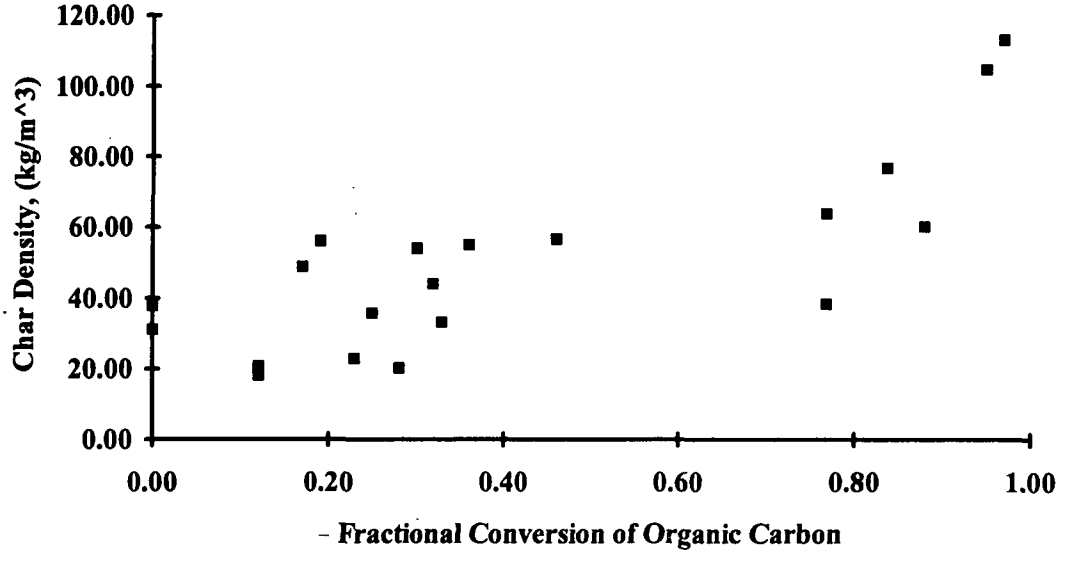


**Figure 42.** Bulk Density of Char as a Function of Fractional Conversion of Organic Carbon for Char Prepared According to the Maximum Temperature Preheat Procedure.

Specific Volume of Single Particles

The specific volume of single particles exposed in gas atmospheres of 5%CO/95%$N_2$, 5%$O_2$/95%$N_2$, and 20%$CO_2$/5%CO/75%$N_2$ was determined at various temperatures, gas velocities, and exposure times. The effects of these process variables on specific volume was determined from these experiments.

The effect of temperature on specific volume, in an environment of 5%CO/95%$N_2$, was studied over a temperature range of 600-900°C under otherwise identical conditions. The results are plotted in Figs. 43 and 44 as averages of 10-15 observations; error bars indicate one standard deviation in the mean. As shown in Figs. 43 and 44, specific volume increased with temperature at exposure times of 10 seconds and 30 seconds, respectively. Statistical analysis at the 99% confidence interval verified that the specific volume increased with temperature. In contrast, Frederick *et al.*[31] report that the swollen volume of droplets burnt in air swell less at higher temperatures for the temperature range encountered in real furnaces.

Gas composition influences the swelling of black liquor droplets. Under otherwise identical conditions, the data in Figs. 45 and 46 show that the droplet swelling was the same in gas environments of 20%$CO_2$/5%CO and 5%CO when the furnace temperature was 600°C and the gas velocity was 0.61 m/s. Despite the difference in furnace temperature for particles exposed in 5%$O_2$/95%$N_2$ (500°C), 5%CO/95%$N_2$ (600°C), and 20%$CO_2$/5%CO/75%$N_2$ (600°C), the particle swelling was much greater at reduced oxygen concentrations as shown in Fig. 47. The particles exposed in low $O_2$ concentrations had much greater volumes than particles exposed in CO or $CO_2$, yet the particle mass remained approximately constant. The reaction of $O_2$ with the char is exothermic and would cause the particle to be hotter than 500°C. For example, the maximum adiabatic flame temperature was calculated to be approximately 565°C based on the total exposure time. Therefore, the true particle temperature may have

been much greater than 500°C. As noted earlier, the specific swollen volume in an atmosphere of 5%CO/95%$N_2$ increased as the temperature increased. A similar trend may occur in an atmosphere of 5%$O_2$/95%$N_2$.

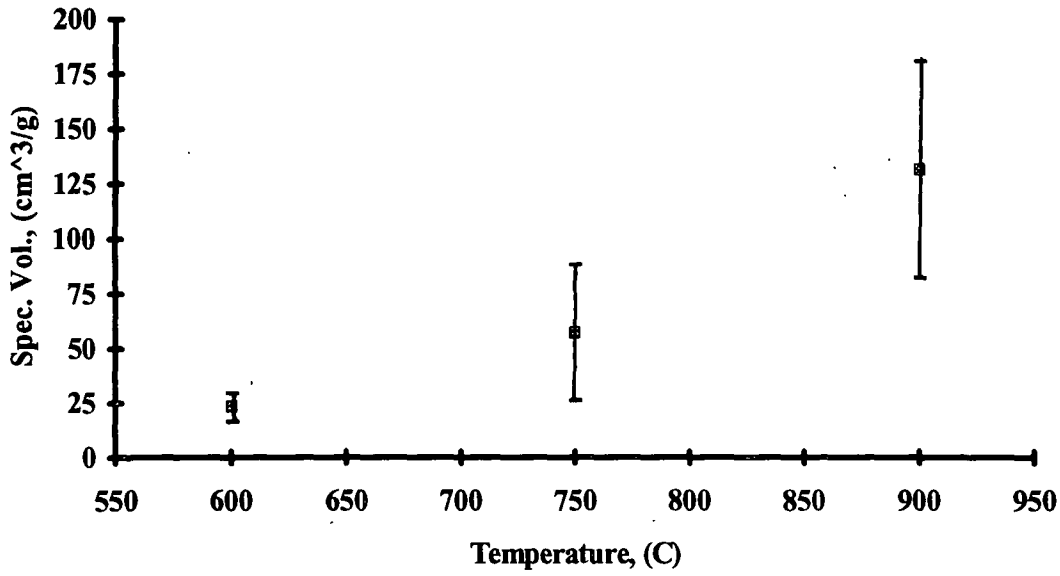


**Figure 43.** Specific Volume of Kraft Black Liquor Char as a Function of Temperature in 5%CO/95%$N_2$ at Exposure Time of 10 Seconds and Gas Velocity of 0.61 m/s.

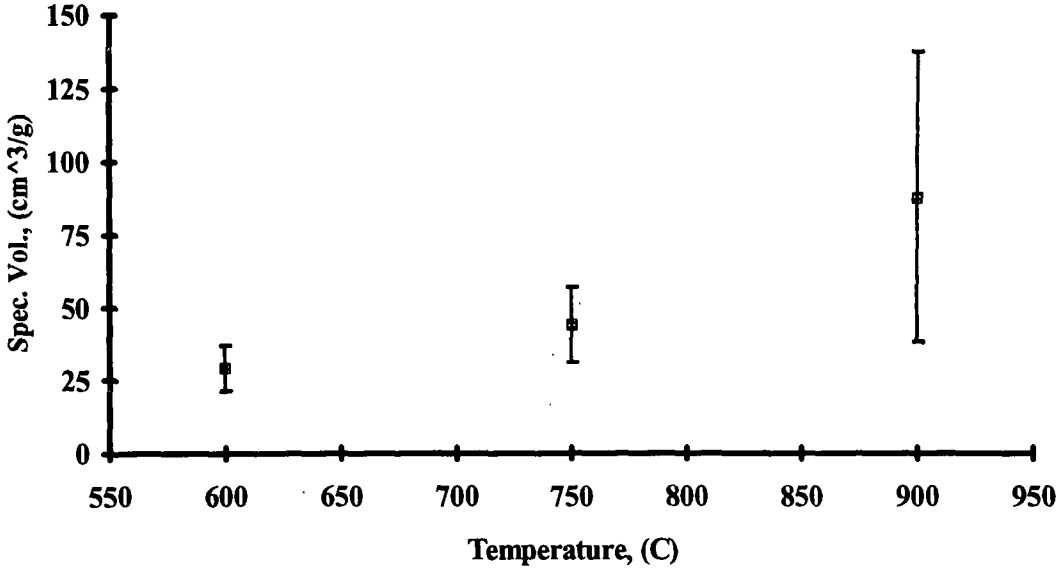


**Figure 44.** Specific Volume of Kraft Black Liquor Char as a Function of Temperature in 5%CO/95%$N_2$ at Exposure Time of 30 Seconds and Gas Velocity of 0.61 m/s.

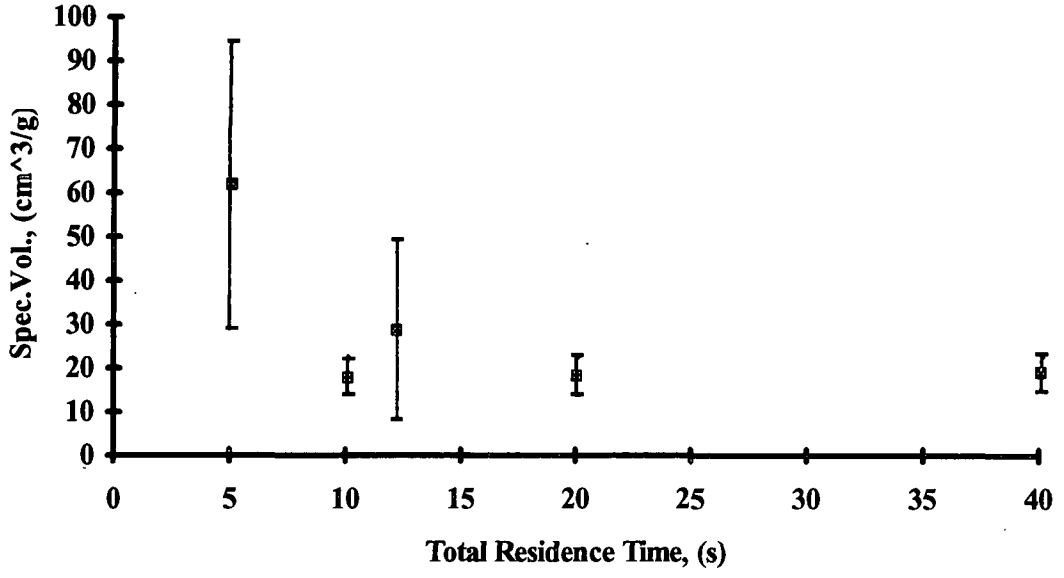


**Figure 45.** Specific Volume of Kraft Black Liquor Char as a Function of Total Residence Time in 20%$CO_2$/5%CO/75%$N_2$ at 600°C and 0.61 m/s.

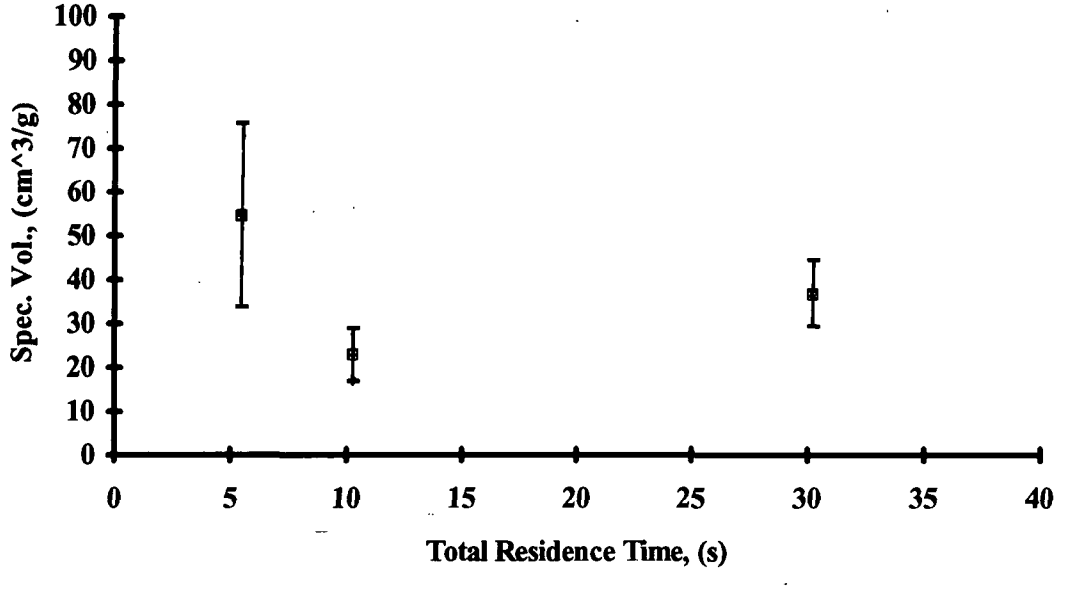


**Figure 46.** Specific Volume of Kraft Black Liquor Char as a Function of Total Residence Time in 5%CO/95%$N_2$ at 600°C and 0.61 m/s.

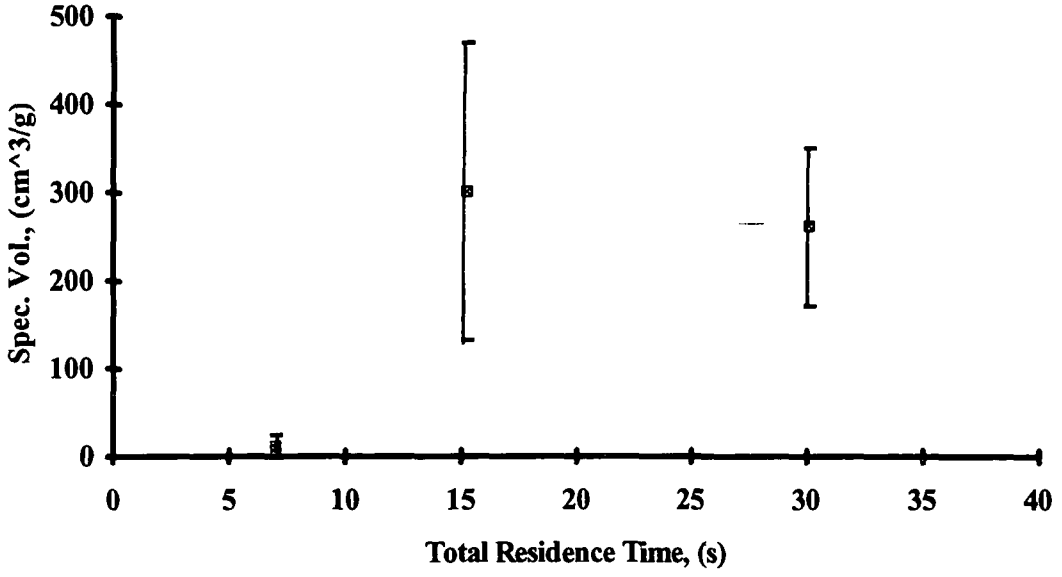


**Figure 47.** Specific Volume of Kraft Black Liquor Char as a Function of Total Residence Time in 5%$O_2$/95%$N_2$ at 500°C and 0.61 m/s.

Specific char volume as a function of exposure time was largely dependent on the furnace conditions. As shown in Figs. 45 and 46, for temperatures of 600°C and gas velocities of 0.61 m/s the specific volume was greatest at low exposure times (<10 seconds) and decreased for times greater than 10 seconds in gas atmospheres of 5%CO/95%$N_2$ and 20%$CO_2$/5%CO/75%$N_2$. Statistical analysis at the 99% confidence interval confirmed that the specific volume at 5 seconds residence time was significantly greater than the specific volume at higher residence times. Videotape observations revealed that the high specific volume at the low exposure time was associated with the point of maximum volume that occurred at 3-7 seconds exposure time in an atmosphere of 5%CO/95%$N_2$ and 20%$CO_2$/5%CO/75%$N_2$. In contrast, Fig. 47 shows that in an atmosphere of $O_2$ at 500°C and 0.61 m/s the specific volume increased from a minimum at 7 seconds exposure time, leveled off after 15 seconds, and remained constant up to exposure times of 30 seconds. This was also supported by an analysis of variance test at the 99% confidence interval. Video observations revealed that the maximum volume in low concentrations of $O_2$ did not occur until approximately 10-12 seconds exposure time, therefore, the data reported at low exposure times in Fig. 47 were from before the time of maximum swelling. Specific volume data was not obtained at the point of maximum volume for any of the gas environments.

At higher temperatures of 750°C and 900°C in 5%CO/95%$N_2$, the specific volume reached a maximum at the lowest exposure times and remained constant over the range of exposure times as shown in Figs. 48 and 49. This was supported by statistical analysis at the 99% confidence interval. A review of video images showed the point of maximum volume for pyrolysis at 750°C occurred after approximately 3 seconds had elapsed; this corresponds to data reported at the lowest exposure time. In addition, the point of maximum volume for 900°C occurred after 1 second exposure time; therefore, all the data reported in Fig. 49 were after maximum swelling had occurred. As noted from these results, the time of maximum volume decreases as the temperature increases. The specific volume versus exposure time trends from pyrolysis in an atmosphere of 5%CO/95%$N_2$ at 600°C, 750°C, and 900°C agree with the

swollen volume versus exposure time trends reported by Miller[9] for char exposed in an atmosphere of $N_2$ over a temperature range of 500-900°C.

The influence of gas velocity on swelling behavior was investigated by comparing the data at 0.61 m/s in Fig. 48 to those at 1.83 m/s in Fig. 50. There was no apparent effect of gas velocity on the specific volume of char devolatilized in an atmosphere of 5%CO/95%$N_2$. These data suggest that the conditions employed for devolatilization in 5%CO/95%$N_2$ were kinetically controlled rather than film mass transfer controlled. The change in gas flowrate (at constant gas temperature) was used to change the mass flux of gas to the particle. Since the char particle was heated predominantly by radiative heat transfer with convective heat transfer increasing with increased gas velocity, these results show that convection did not have a significant effect on the final swollen volume This finding agrees with Miller's[9] conclusion that swelling is independent of convective heat transfer.

Assuming that char particles are spherical and packed together with a bed void fraction of 0.40, the specific volume results for an atmosphere of 20%$CO_2$/5%CO/95%$N_2$ at 40 seconds exposure time, shown in Fig. 45, correspond to an average bulk density of $30.8 \pm 8.21$ kg/m$^3$ . These single particle results are in agreement with the density measured for char, gasified to a fractional conversion of 10% organic carbon in 5%$CO_2$/95%$N_2$, ($\rho$=25 kg/m$^3$) which was discussed earlier. The density results from this single particle study are approximately twice as high as the swollen volume results reported by Frederick *et al.*[31] for particles exposed to a gas environment of 20%$CO_2$/80%$N_2$ at 800°C. These differences may be due to differences in swollen volume versus specific volume or variations between liquors and experimental temperatures.

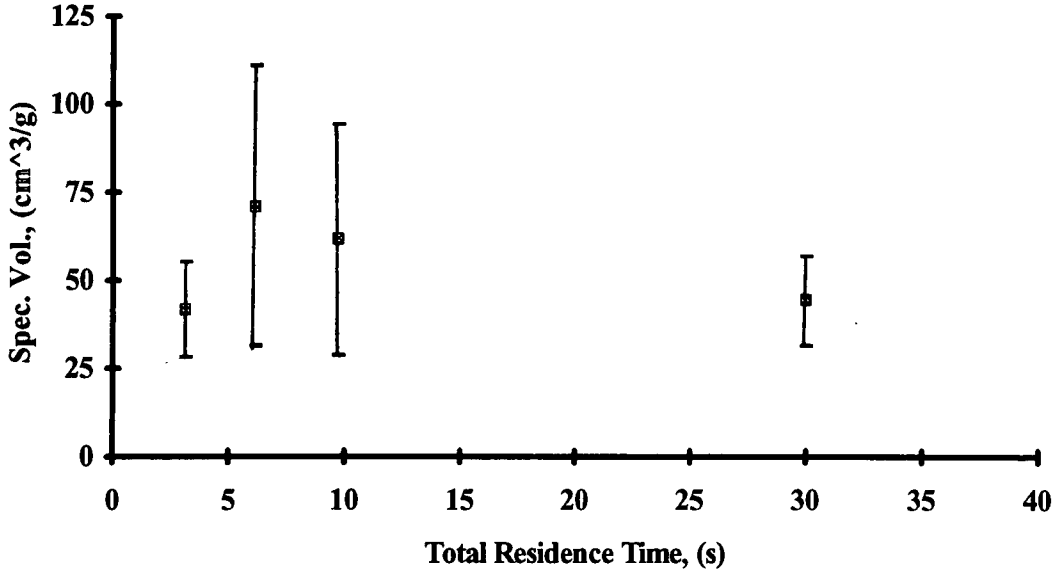


**Figure 48.** Specific Volume of Kraft Black Liquor as a Function of Total Residence Time in 5%CO/95%$N_2$ at 750°C and 0.61 m/s.

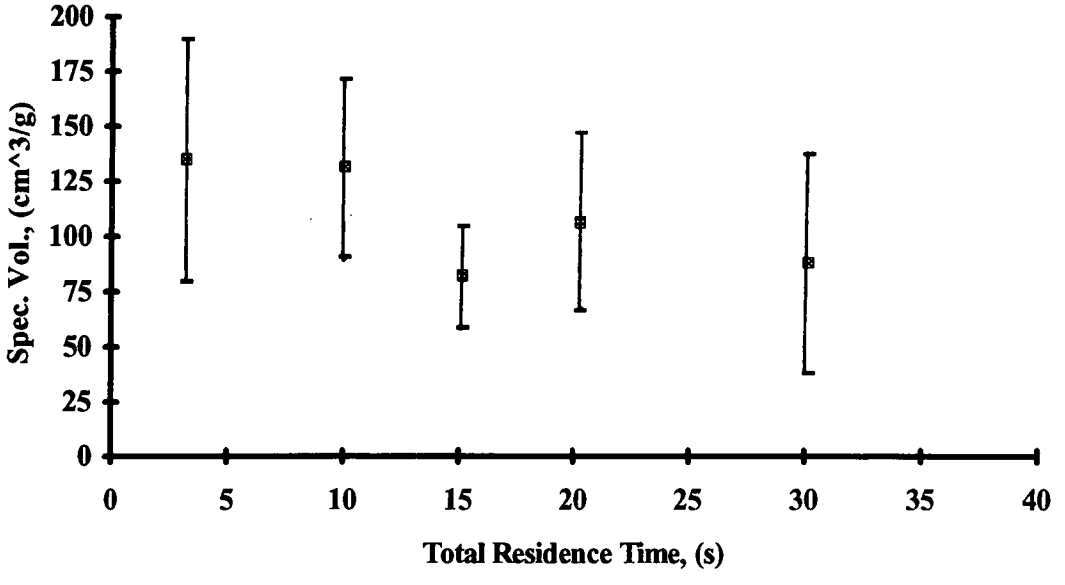


**Figure 49.** Specific Volume of Kraft Black Liquor as a Function of Total Residence Time in 5%CO/95%$N_2$ at 900°C and 0.61 m/s.

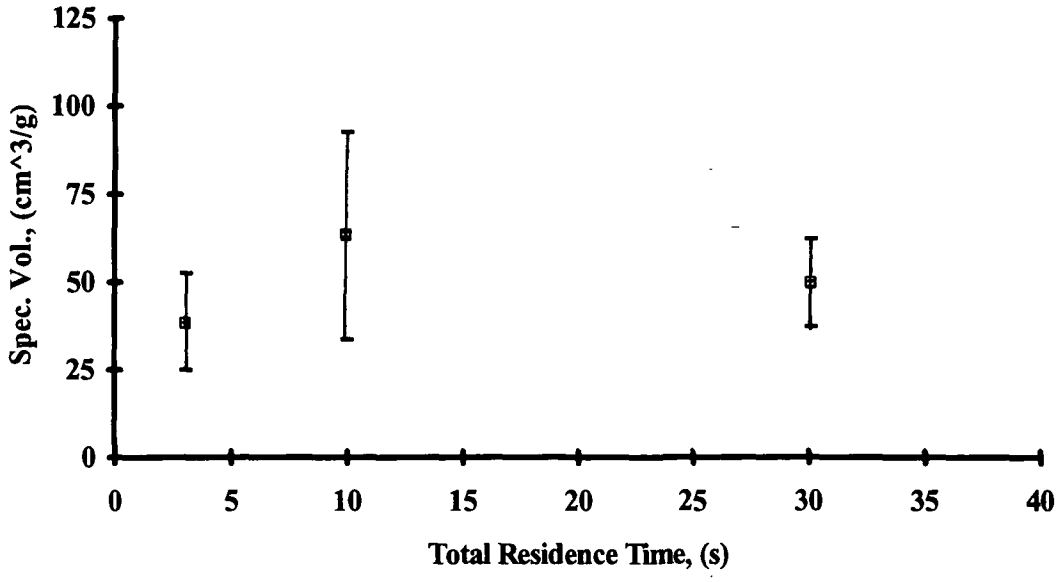


**Figure 50.** Specific Volume of Kraft Black Liquor Char as a Function of Total Residence Time in 5%CO/95%$N_2$ at 750°C and 1.83 m/s.

Observations of Drop Pyrolysis and Comparison of Char Photomicrographs

For the various experimental conditions, all drops exhibited the same behavior during drying. However, there were substantial differences in devolatilization observed at the different conditions. Particles produced in 5%CO/95% $N_2$ were porous and brittle. Swelling of these particles was uniform and spherical. Char formed during all experiments at 600°C shrank substantially after reaching maximum swollen volume; much less collapse was noted at 750°C and 900°C. Chars produced in 20%$CO_2$/5%CO/75% $N_2$ at 600°C were identical in appearance to the samples from pyrolysis at 600°C. As noted earlier, particles exposed to the oxygen-containing atmosphere at 500°C had higher specific volumes than particles exposed in other gas atmospheres. These drops underwent serpentine expansion and formed hollow char particles with delicate but resilient external films. The increased extent of swelling at low oxygen concentrations has been observed by others.[31]

The char surface structure was investigated under a Scanning Electron Microscope (SEM). Results are presented in micrographic form in Figs. 51- 56. Figs. 51-53 are example SEM photomicrographs of the residual char from liquor pyrolysis in 5%CO/95%$N_2$ at 600°C for gas velocity of 0.61 m/s at 600°C, 750°C, and 900°C, respectively. The concentration of "whiskers" or dendritic structures appeared to decrease as the temperature increased. The "whiskers" at 600°C evolved into "agglomerated platelets and whiskers" at 750°C and became "isolated agglomerates of whiskers and platelets" at 900°C.

Fig. 54 shows the char surface from liquor exposed in 5%CO/95%$N_2$ with gas velocity of 1.83 m/s at 750°C. In comparison to Fig. 52, the "whiskers" are minimized and replaced predominantly by platelets at the higher gas velocity. The specific volume remained unchanged as the mass flux of CO to the particle was increased.

Fig. 55 is an example SEM photomicrograph of the residual char from liquor exposed in 5%CO/20%$CO_2$/75%$N_2$ with gas velocity of 0.61 m/s at 600°C. The char in Fig. 56 was produced from liquor exposed in 5%$O_2$/95%$N_2$ for gas velocity of 0.61 m/s at 500°C. Exposure in low concentrations of $O_2$ resulted in the greatest concentration of "whiskers." As the organic carbon is depleted from the surface of the char, the residual inorganics may appear in the form of these "whiskers." As the temperature is raised above the melting point of the inorganic salts (for example 750°C or 900°C), these "whiskers" may transform into platelets. In an atmosphere of $CO_2$ and CO, the "whiskering" effect is not as pronounced as observed in an atmosphere of CO; however, the formation of "platelets" is not as evident as that observed at higher temperatures in CO.

Li and van Heiningen[41] suggest that drying rate affects the distribution of inorganics in the char; lower drying rates result in crystallization and precipitation of the inorganics. Li and van Heiningen employed two methods for drying liquor: thin films dried on watch glasses at 120°C, and large (but unspecified) quantities dried in dishes under IR lamps. Chars were made from both types of dried solids by an identical procedure (pyrolysis in 90%$N_2$/10%CO at 580°C for 20 minutes). The chars made from dish-dried solids exhibited 20-30% lower gasification rates than the film-dried liquor chars; the authors attributed this to nonuniformities in sodium distribution.

Li and van Heiningen[41] found that the surface layer of the dish-dried solids contained substantially less $SO_4^=$ and slightly less sodium than did the lower layer, presumably the slow drying rate resulted in concentration and precipitation of the inorganic salts in the lower layer of liquor. An SEM photomicrograph of char, made from dish-dried solids, showed dendritic crystals which were not apparent on the surface of chars made from film-dried liquor. These structures resemble those shown in the photomicrographs of our study. The dendritic crystals observed by Li and van Heiningen were identified as sodium salt crystals.

From the appearance of the "whiskers" and tabulated properties of inorganic materials, it can be deduced that the dendrites must be composed of a crystalline material with a melting point of about 750°C. Furthermore, because these char samples were exposed to ambient conditions for several months before the SEM work was done, the crystalline substance must not be deliquescent. Sodium sulfate and sodium carbonate are two species which fit these criteria. Due to the $SO_4^=$ enrichment in the bottom layer of Li and van Heiningen's dish-dried solids, the dendrites are therefore expected to be primarily $Na_2SO_4$.

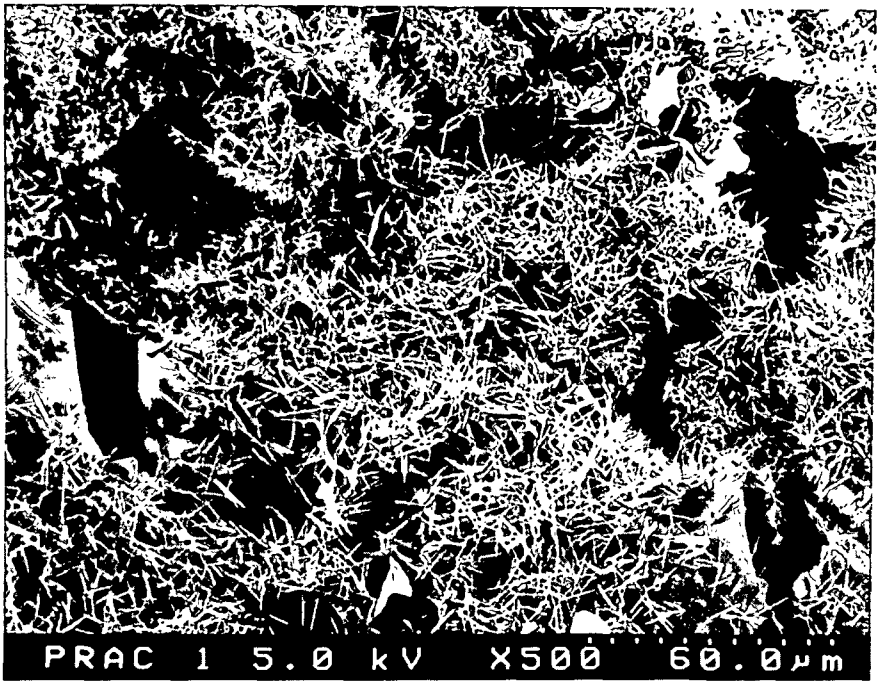


**Figure 51.** Scanning Electron Micrograph of Kraft Black Liquor Char Exposed in 5%CO/95%$N_2$ at 600°C and 0.61 m/s.

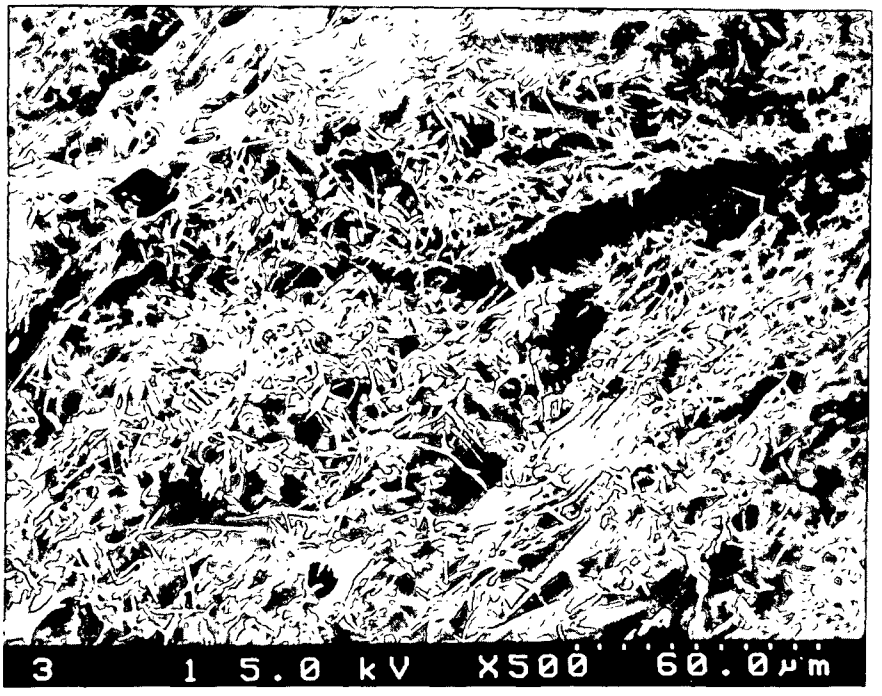


**Figure 52.** Scanning Electron Micrograph of Kraft Black Liquor Char Exposed in 5%CO/95%$N_2$ at 750°C and 0.61 m/s.

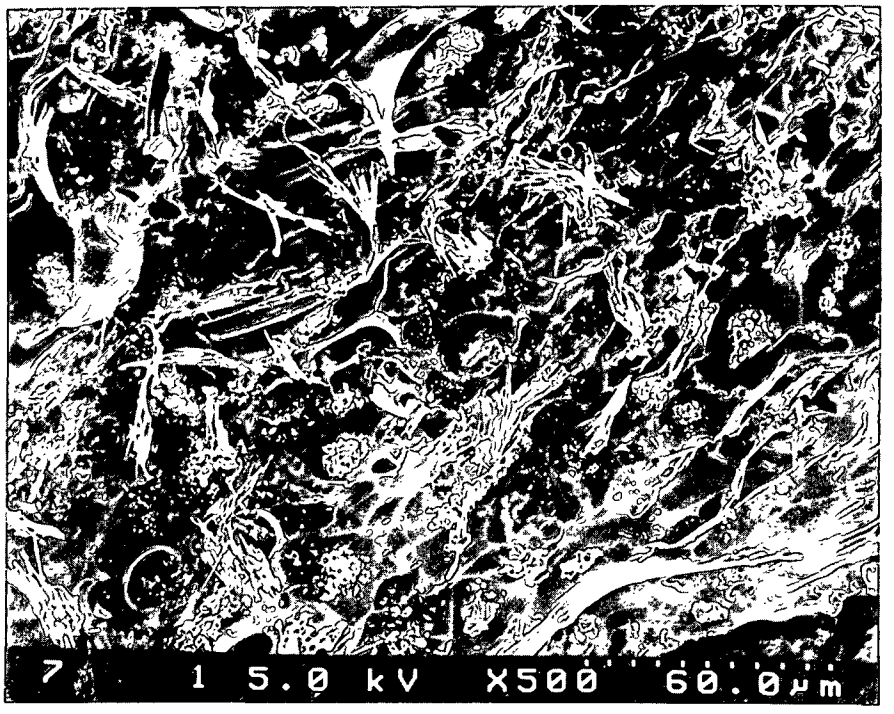


**Figure 53.** Scanning Electron Micrograph of Kraft Black Liquor Char Exposed in 5%CO/95%$N_2$ at 900°C and 0.61 m/s.

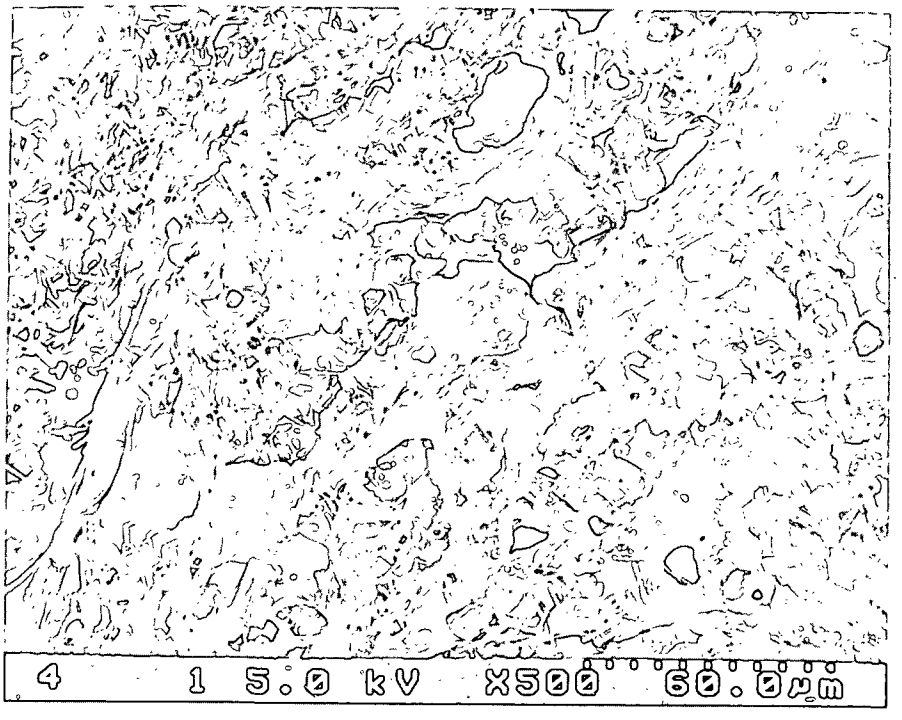


**Figure 54.** Scanning Electron Micrograph of Kraft Black Liquor Char Exposed in 5%CO/95%$N_2$ at 750°C and 1.83 m/s.

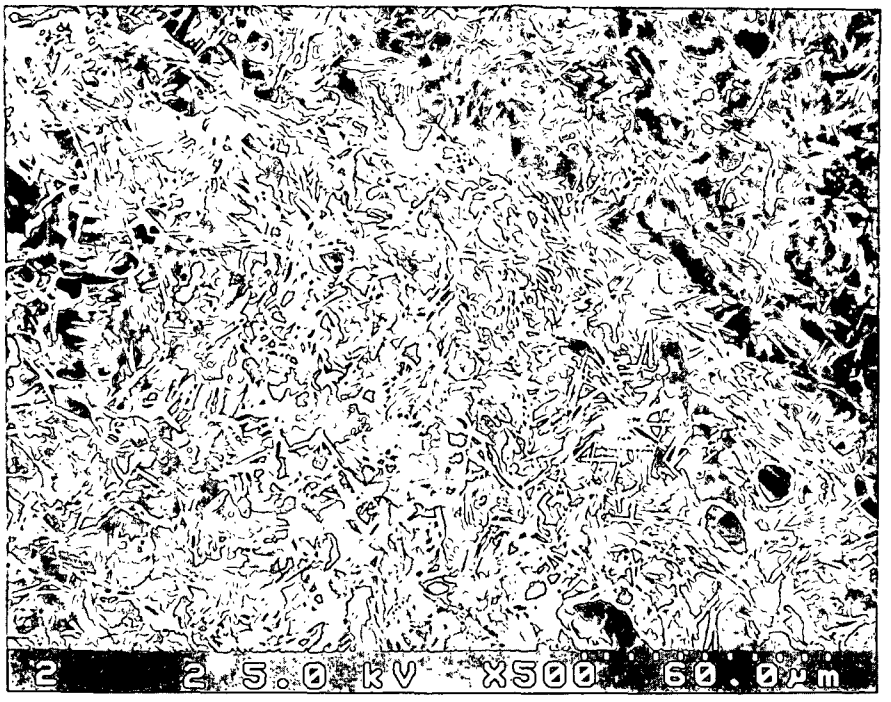


**Figure 55.** Scanning Electron Micrograph of Kraft Black Liquor Char Exposed in 5%CO/20%$CO_2$/75%$N_2$ at 600°C and 0.61 m/s.

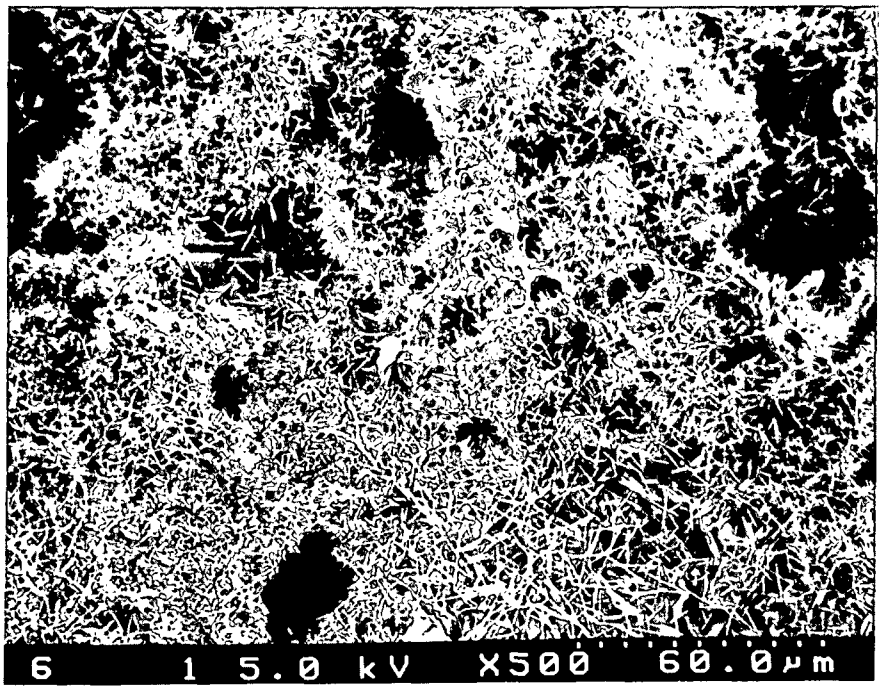


**Figure 56.** Scanning Electron Micrograph of Kraft Black Liquor Char Exposed in 5%$O_2$/95%$N_2$ at 500°C and 0.61 m/s.

# CONCLUSIONS

1. Two different procedures used to preheat kraft black liquor char prior to heterogeneous combustion were compared to determine the effect of the procedures on char composition. The elemental composition of chars prepared according to the reaction temperature preheat procedure were significantly affected by the pyrolysis temperature. More specifically, the C, H, O and S compositions were affected by the pyrolysis temperature. The Na, Carbonate C, Sulfate S, and Thiosulfate S concentrations were not affected by pyrolysis temperature. In contrast, the elemental composition of the resulting chars from the maximum temperature preheat procedure were not affected by the cool down temperatures. Therefore, prior to heterogeneous reaction the char composition will be uniform regardless of temperature when the Maximum Temperature Preheat procedure is employed.

2. The $CO_2$ gasification rate of kraft black liquor char prepared according to the reaction temperature preheat procedure was studied using a fixed bed reactor at temperatures of 600°C, 700°C, and 800°C. A first order global rate was shown to fit the data as well as any other value of n. The behavior experienced in this study is very similar to the behavior observed during $CO_2$ gasification of alkali-catalyzed coal. The burn-off profile can be explained by the behavior of the alkali catalyst (sodium in this study) during char burning. The observed rate was not affected by film mass transfer or pore diffusion.

3. The $CO_2$ gasification rate of kraft black liquor char prepared according to the maximum temperature preheat procedure was studied using a fixed bed reactor at temperatures of 600°C, 700°C, and 800°C. Assuming a global rate which is first order in $CO_2$ concentration, experiments using different gas velocities and different carrier gases ($N_2$ or He) showed that the observed rate was not affected by film mass transfer or pore diffusion.

4. The rate constants of $CO_2$ gasification for the chars according to the two preheat procedures are statistically different. The rate constants for char prepared according to the reaction temperature preheat procedure are (1.4-2.4 times) higher than the rate constants for char prepared according to the maximum temperature preheat procedure. The lower rates for char prepared according to the MTPP may be due to a greater number of plugged pores and lower concentration of sodium in the initial char as a result of the higher preparation temperature (950°C).

5. The rate of $CO_2$ gasification and the activation energy derived from the data compare well to rates and activation energies reported for previous thermogravimetric investigations. These similarities in rates and activation energies are significant considering the differences in char quantity, liquors used to produce the chars, the char production processes, and the experimental reactors. Therefore, the fixed bed reactor can be used to determine the gasification kinetics of kraft black liquor char.

6. Using the measured $CO_2$ gasification rates, the implications for kraft recovery furnaces were examined. Application of the $CO_2$ gasification rate to typical recovery furnace operating conditions shows that $CO_2$ gasification becomes completely mass transfer controlled at

temperatures as low as 1125K. However, below this temperature the reaction would be kinetically controlled or heavily influenced by pore diffusion effects.

7. The $O_2$ oxidation rate of kraft black liquor char was studied using a fixed bed reactor at 700°C. The observed rate was affected by film mass transfer diffusion. The concentration of CO, $CO_2$, and $O_2$ in the product gas were lower than expected. This was shown by material balances on oxygen, carbon, sulfur, and sodium to be due to $O_2$ and $CO_2$ consuming reactions in the exhaust line.

8. The combination oxidation/gasification rate of kraft black liquor char was studied using a fixed bed reactor at 700°C. The combination $CO_2$ gasification and $O_2$ oxidation results suggest that the rate is not equivalent to the sum of the individual rates. Product stream concentration profiles for CO and $CO_2$ indicated that a portion of the CO from $CO_2$ gasification reacted with oxygen to form $CO_2$. Oxygen, carbon, sulfur, and sodium balances suggested that $O_2$ and $CO_2$ were consumed in the exhaust line.

9. Combination oxidation/gasification can be expressed with the following rate expression: $R_C = R_{O_2} + (1-\chi)R_{CO_2}$ where $R_C$ = total carbon depletion rate, $R_{O_2}$ = reaction rate for oxidation, $R_{CO_2}$ = reaction rate for gasification, and $\chi$ = conversion parameter. The experimentally determined values of $\chi$ ranged from 0.31-0.59 depending on experimental conditions. Experimental results compare well to the calculated values.

10. The bulk density of kraft black liquor char was determined by measuring the volume and mass of the residual char following the completion of devolatilization and gasification experiments. This study provides the first indication of organic carbon concentration and char bulk density as a function of organic carbon depletion during the char burning stage of black liquor combustion for char prepared according to the reaction temperature preheat procedure. The organic carbon concentration in the kraft char averages 7.8 $kg/m^3$ and is independent of fractional carbon conversion at burnout levels greater than 10%. For char prepared according to the maximum temperature preheat procedure, the organic carbon concentration in kraft char averages 12.5 $kg/m^3$ and is independent of fractional conversion at burnout levels greater than 12%.

11. Char bulk density went through a minimum of approximately 20-25 $kg/m^3$ at 10% carbon conversion and gradually increased as the organic carbon was depleted. The char density increased at higher fractional conversion due to inorganic salt coalescence as the organic carbon was depleted. The bulk density from this study is more representative of the actual furnace char density than the high smelt containing values reported earlier.

12. Char specific volume was determined from single particle swelling experiments in gas atmospheres of 5%CO/95%$N_2$, 5%$O_2$/95%$N_2$, and 20%$CO_2$/5%CO/75%$N_2$. Char specific volume was found to be independent of the mass flux of gas to the char particle. In addition, char specific volume decreased with increasing temperature when exposed in 5%CO/95%$N_2$. Particles exposed for longer than 10-15 seconds to an atmosphere containing low concentrations of $O_2$ had higher specific volumes than the particles reacted in CO or $CO_2$. The effect of particle exposure time on specific volume was strongly dependent on the gas atmosphere. For particles exposed in high concentrations of $CO_2$ or low concentrations of CO, the particle specific volume

was greatest at lower exposure times. In contrast, in low concentrations of $O_2$ the swelling was lowest at the lower exposure times. However, in all gas environments the swelling leveled off at exposure times greater than 15 seconds.

13. Scanning Electron Microscope images of residual char revealed differences in surface morphology for the various furnace conditions. As the organic carbon was depleted from the surface of the char, the residual inorganic appeared in the form of dendrite structures or "whiskers." As the temperature is raised above the melting point of the inorganic salts (for example 750°C or 900°C), these "whiskers" transformed into platelets.

# SUGGESTIONS FOR FUTURE WORK

Although a better understanding of the role of $CO_2$ in the combustion of kraft black liquor char has been established in this thesis, there is ample opportunity to supplement the current understanding of black liquor combustion through future experimental studies. Recommendations for future research efforts are summarized as follows:

1. Efforts to understand the mechanism of $CO_2$ gasification of kraft black liquor char should be continued. The mechanism of $CO_2$ gasification is expected to be similar to the mechanism for alkali-catalyzed carbon, but a few detailed mechanistic experiments could confirm this for BLC. Further study of the reaction mechanism should include isotope labeled gases for identification of reaction intermediates and products. The fixed bed reactor developed during this study is well suited for this type of experimentation with one exception. Detection equipment for radioactive isotopes would be necessary versus the NDIR analyzers currently employed.

2. Efforts to understand the influence of alkali metals on the rate and mechanism should be continued. The effect of catalyst concentration (Na/C and K/C) and the internal porous structure of the solid on the rate of char-$CO_2$ gasification should be investigated.

3. The fixed bed reactor should be modified to allow for char oxidation and char oxidation/gasification rates to be determined free of competing downstream reactions. Fourier transform infrared spectroscopy can be used to determine the gas temperatures and concentrations (CO and $CO_2$) above a burning, laboratory scale black liquor char bed. The fixed bed reactor designed for this study should be modified to allow for the implementation of the FT-IR equipment.

4. The oxidation/gasification reaction ($O_2/H_2O$) of kraft black liquor char should be studied since a significant concentration of $H_2O$ could be present above a furnace char bed. This would require a fundamental understanding of the $H_2O$ gasification reaction. An experimental design similar to the one completed during this thesis for the $CO_2/O_2$ system could be incorporated.

5. The next logical step would include a study of oxidation/gasification with $O_2$, $CO_2$, and $H_2O$. This would require a fundamental understanding of the reaction of each of the heterogeneous reactions and the homogeneous reactions in the gas phase.

6. As discussed throughout this thesis, char bed combustion in a black liquor recovery boiler is a complicated process. An understanding of char bed combustion is important for stable furnace operation and improved furnace design. Current efforts at the Institute of Paper Science and Technology include the application of computational fluid dynamics methods in recovery furnace simulations to produce valuable information about the complicated transport and reaction processes which occur on the char bed. The char reaction information and char density data presented here can be incorporated in these char modeling efforts.

# NOMENCLATURE

SYMBOLS

| | |
|---|---|
| $a_m$ | external surface area per unit mass, ($m^2$/kg) |
| $A_{ext.}$ | external surface area, ($m^2$) |
| $C_{O_2}$ | average oxygen concentration over the char bed, (gmole/$m^3$) |
| $C_p$ | heat capacity, (J/K) |
| $d_p$ | average diameter of the char particle, (m) |
| $D_{AB}$ | diffusivity of gas A through gas B, ($m^2$/s) |
| $D_c$ | combined diffusivity, ($m^2$/s) |
| $D_{eff}$ | effective diffusivity, ($m^2$/s) |
| $D_k$ | Knudsen diffusivity, ($m^2$/s) |
| $E_A$ | activation energy, (kcal/mol) |
| f | final elemental composition |
| *f* | dimensionless fanning friction factor |
| *f* | stoichiometric factor for direct carbon oxidation defined by the reaction $\left[1-\frac{f}{2}\right]O_2 + C \Leftrightarrow fCO + (1-f)CO_2$ |
| $F_t$ | molal feed flow rate |
| $G_T$ | total free energy of the system |
| $h_o$ | overall heat transfer coefficient |
| i | initial elemental composition |
| k | thermal conductivity, (W/m/K) |
| k | reaction rate constant, ($m^3$/kg/s) |
| $k_{avg.}$ | average oxygen mass transfer coefficient, (m/s) |
| $k_m$ | average film mass transfer coefficient, (m/s) |
| K | equilibrium constant |
| L | char bed height, (m) |
| L | length of coils in fixed bed reactor preheater zone, (m) |
| m | mass of organic carbon in the fixed bed reactor, (kg) |
| m | mass flow rate, (kg/s) |
| M | molecular weight |
| $M_{TM}$ | Thiele modulus |
| N | number of coils in fixed bed reactor preheater zone |
| $N_{nu}$ | Nusselt number |
| $N_{pr}$ | Prandtl number |
| $N_{Re}$ | Reynolds number |
| n | reaction order |
| $\bar{r}$ | pore radius, (m) |
| Q | reaction quotient |
| R | gas constant |
| $R_c$ | total carbon depletion rate |
| $R_{CO_2}$ | reaction rate for $CO_2$ gasification |
| $R_{H_2O}$ | reaction rate for $H_2O$ gasification |
| $R_{O_2}$ | reaction rate for oxidation |
| $R'_{O_2}$ | the net oxygen flux to the surface |
| $S_g$ | surface area per gram of char, ($m^2$/kg) |

| | |
|---|---|
| $t$ | time, (s) |
| $t$ | reaction time, (s) |
| $T$ | temperature, (K) |
| $u$ | superficial velocity in the direction of flow, (m/s) |
| $V_g$ | void volume per gram of char, ($m^3$/kg) |
| $z$ | axial position in the char bed, (m) |

GREEK SYMBOLS

| | |
|---|---|
| $\varepsilon_{bed}$ | void fraction of char bed |
| $\varepsilon_p$ | porosity of the char particle |
| $\eta$ | effectiveness factor |
| $\rho$ | density of the fluid, (kg/$m^3$) |
| $\rho_{bed}$ | density of char bed, (kg organic C/$m^3$ char) |
| $\rho_p$ | density of the char particle, (kg/$m^3$) |
| $\tau'$ | tortuosity factor |
| $\mu$ | viscosity of the fluid, (kg/m/s) |
| $\chi$ | conversion parameter |

ABBREVIATIONS

| | |
|---|---|
| BLC | black liquor char |
| DOE | Department of Energy |
| IPST | Institute of Paper Science and Technology |
| IR | Infrared |
| MTPP | maximum temperature preheat procedure |
| RTPP | reaction temperature preheat procedure |
| SEM | Scanning Electron Microscope |

ACKNOWLEDGMENTS

The success of this thesis has been largely due to the assistance, advice, and expectations of several people. First, I thank the Institute of Paper Science and Technology and the member companies for supporting my education. I am grateful to Dr. Jeff Colwell for his motivation throughout this thesis, his insight in solving life's problems, and his friendship over the past few years. I express my gratitude to Dr. Ken Nichols for his encouragement throughout graduate school, his intuition regarding the thesis subject, and his comradery on and off the court. I appreciate the support and guidance of my advisory committee, Dr. Jeff Empie, Dr. James Frederick, and Dr. Robert Horton. I also acknowledge Dr. Richard Ellis' contributions as a former committee member.

The faculty, staff, and students of IPST are recognized as prominent contributors to my education. To the faculty who have taught or advised me, I express my sincere appreciation. The staff at IPST are among the finest group of folks with whom I have ever worked. I am much obliged to Don Sachs, Doug Samuels, Steve Lien, and Wen Rui Wang for their assistance. The students at IPST have challenged and stretched me beyond all expectations. I have enjoyed the opportunity to work and socialize with such a diverse group of young professionals. I especially recognize my fellow Recovery Group peers and those Ph.D. candidates who started at IPST with me.

Finally, I am grateful to my family. My brothers, Douglas Lee and Charles Lee, have been advocates of my continued education, and I hope that I have inspired them as much as they have inspired me. I am forever indebted to my parents, Linda and Nelson Lee, for instilling in me a drive and ambition to do my best, serving as excellent role models, and being my friends. I am most thankful for my wife and daughter, Kim and Jenna, for providing the love, patience, inspiration, and support that was essential for completion of this thesis. Finally, I thank my Lord and Savior, Jesus Christ, for through him all things are possible.

## LITERATURE CITED


1. Hupa, M.; Solin, P.; Hyoty, P. Combustion Behavior of Black Liquor Droplets. Proceedings of the TAPPI/CPPA International Chemical Recovery Conference. New Orleans, LA, April, 1985:335-344.

2. Grace, T.M.; Cameron, J.H.; Clay, D.T. Role of the Sulfate-Sulfide Cycle in Char Burning: Experimental Results and Implications. Tappi 69(10):108-113(1986).

3. Adams, T.N.; Frederick, W.J. Kraft Recovery Boiler Physical and Chemical Processes. The American Paper Institute, New York, New York, 1988.

4. Grace, T.M.; Cameron, J.H.; Clay, D.T. Char Burning, Project 3473-6 Summary Technical Report. Appleton, WI, The Institute of Paper Chemistry, 1985.

5. Cameron, J.H.; Grace, T.M. Kinetic Study of Sulfate Reduction with Carbon. Industrial and Engineering Chemistry Fundamentals. 22(4):486-494(1983).

6. Blackwell, B.; King, T. Chemical Reactions in Kraft Recovery Boilers. Vancouver, B.C., Sandwell and Company Limited, 1985.

7. Grace, T.M.; Walsh, A.; Jones, A.; Sumnicht, D.; Farrington, T. A Three-Dimensional Mathematical Model of the Kraft Recovery Furnace. Proceedings of the International Chemical Recovery Conference. Ottawa, Canada, April 3-6, 1989:1-8.

8. Kulas, K.A. An Overall Model of the Combustion of a Single Droplet of Kraft Black Liquor. Doctoral Dissertation. Appleton, WI, The Institute of Paper Chemistry, 1990.

9. Miller, P.T. Swelling of Kraft Black Liquor. An Understanding of the Associated Phenomena During Pyrolysis. Doctoral Dissertation. Appleton, WI, The Institute of Paper Chemistry, 1986.

10. Aiken, G.W. The Use of a Char Pile Reactor to Study Char Bed Processes. Doctoral Dissertation. Appleton, WI, The Institute of Paper Chemistry, 1988.

11. Brown, C.A.; Grace, T.M.; Lien, S.J.; Clay, D.T. Char Bed Burning Rates-Experimental Results. Proceedings of the International Chemical Recovery Conference. Ottawa, Canada, April 3-6, 1989:65-73.

12. Clay, D.T.; Grace, T.M.; Kapheim, R.J.; Semerjan, H.G.; Macek, A.; Charagundla, S.R. Fundamental Studies of Black Liquor Combustion, Report No. 1-Phase 1, U.S. DOE Report No. DE85013773, January, 1985.

13. Grace, T.M.; Lien, S.J.; Brown, C.A. Char Bed Burning-Laboratories Studies. Proceedings of the International Chemical Recovery Conference. Seattle, WA, June 7-11, 1992:539-549.

14. Goerg, K.A. The Gasification of Kraft Char with Carbon Dioxide. M.S. Dissertation. Appleton, WI, The Institute of Paper Chemistry, 1986.

15. Lee, S.R. Kraft Char Gasification-Determination of the Gasification Rate of Char-Carbon with $CO_2$. M.S. Dissertation. Atlanta, GA, The Institute of Paper Science and Technology, 1990.

16. Lee, S.R.; Nichols, K.M. $CO_2$ Gasification of Kraft Black Liquor Char in a Fixed Bed Reactor. Accepted for Publication. Journal of Pulp and Paper Science. Fall, 1993.

17. Harper, F.D. Sulfur Release During the Pyrolysis of Kraft Black Liquor. Doctoral Dissertation. Appleton, WI, The Institute of Paper Chemistry, 1989.

18. Goerg, K.A. A Study of Fume Particle Deposition. Doctoral Dissertation. Appleton, WI, The Institute of Paper Chemistry, 1989.

19. Verrill, C.L. Inorganic Aerosol Formation During Black Liquor Drop Combustion. Doctoral Dissertation. Atlanta, GA, The Institute of Paper Science and Technology, 1992.

20. Spielbauer, T. The Stability and Disintergration of Radially Thinning Liquid Sheets. Doctoral Dissertation. Atlanta, GA, The Institute of Paper Science and Technology, 1992.

21. Empie, J.J.; Lien, S.J.; Yang, W.R.; and Adams, T.N. Spraying Characteristics of Commercial Black Liquor Nozzles. Proceedings of the International Chemical Recovery Conference. Seattle, WA, June 7-11, 1992:429-440.

22. Medvecz, P.J. Spectroscopic Evaluation of the Gas Phase Above a Burning Black Liquor Char Bed. Doctoral Dissertation. Atlanta, GA, The Institute of Paper Science and Technology, 1991.

23. Martin, D. M.; Medvecz, P.J.; Nichols, K.M. Application of FT-IR Absorption Spectroscopy for In Situ Gas Concentration and Temperature Measurements in Laboratory and Pilot-Scale Combustion Environments. Submitted for Publication. Applied Spectroscopy. (1993).

24. Nichols, K.M.; Thompson, L.M.; Empie, H.J. A Review of $NO_x$ Formation Mechanisms in Recovery Furnaces.

25. Nichols, K.M.; Lien, S.J. Relative Importance of Fuel-$NO_x$ in Black Liquor Combustion. Submitted for Publication. TAPPI Journal. (1992).

26. Frederick , W.J. Combustion Processes in Black Liquor Recovery: Analysis and Interpretation of Combustion Rate Data and an Engineering Design Model. Report No. 1 for U.S. DOE, DOE/CE/40637-T8 (DE9001272), March, 1990.

27. Noopila, T.; Hupa, M. Measuring the Combustion Properties of Black Liquors by Different Techniques. Combustion Chemistry Research Group Report 88-5. Turku, Finland, Abo Akademi, 1988.

28. Crane, K.A. An Empirical Equation of the Volatilization of Kraft Black Liquor Droplets During Burning. Presented at the 1987 AIChE Annual Meeting. Minneapolis, MN, August 16-20, 1987.

29. Krause, H.H.; Simon, R.; Levy, A. Final Report on Smelt-Water Explosions to the Fourdrinier Kraft Board Institute, Inc., Battelle Columbus Laboratories, January, 1973.

30. Magnusson, H.; Warnqvist, B. Properties of Sodium Sulfide-Sodium Carbonate Melt. Svensk Paperstidning 78(18):614-616(1975).

31. Frederick, W.J.; Noopila, T.; Hupa, M. Swelling of Spent Pulping Liquor During Combustion. Journal of Pulp and Paper Science 17(5):164-170(1991).

32. Milanova, E.; Kubes, G.J. The Combustion of Kraft Liquor Chars. Journal of Pulp and Paper Science 12(6):187-192(1986).

33. Borg, A.; Teder, A.; Warnqvist, B. Inside a Kraft Recovery Furnace-Studies on the Origins of Sulfur and Sodium Emissions. Tappi 57(1):126-129(1974).

34. Li, J.; van Heiningen, A.R.P. Kinetics of Gasification of Black Liquor Char by Steam. Industrial and Engineering Chemistry Research 30(7):1594-1601(1991).

35. Li, J.; van Heiningen, A.R.P. Kinetics of Gasification of Black Liquor Char by Steam. Nineteenth Biennial Conference on Carbon, Pennsylvania State University, June 25-30, 1989.

36. van Heiningen, A.R.P.; Arpiainen, V.T.; Alen, R. Effects of Liquor Type and Pyrolysis Rate on the Steam Gasification Reactivities of Black Liquors. Proceedings of the International Chemical Recovery Conference. Seattle, WA, June 7-11, 1992:641-649.

37. Whitty, K.; Frederick, W.J.; Hupa, M. Gasification of Black Liquor Char with $H_2O$ at Elevated Pressures. Proceedings of the International Chemical Recovery Conference. Seattle, WA, June 7-11, 1992:627-639.

38. Li, J. Rate Processes During Gasification and Reduction of Black Liquor Char. Doctoral Dissertation. Montreal, Canada, McGill University, 1989.

39. Li, J. Pyrolysis and $CO_2$ Gasification of Black Liquor Char, M. Eng. Dissertation, Montreal, Canada, McGill University, 1986.

40. Li, J.; van Heiningen, A.R.P. Reaction Kinetics of Gasification of Black Liquor Char. The Canadian Journal of Chemical Engineering 67(8):693-697(1989).

41. Li, J.; van Heiningen, A.R.P. Kinetics of $CO_2$ Gasification of Fast Pyrolysis Black Liquor Char. Industrial and Engineering Chemistry Research 29(9):1776-1785(1990).

42. Frederick, W.J.; Hupa, M. Gasification of Black Liquor Char with $CO_2$ at Elevated Pressures. Tappi 74(7):177-184(1991).

43. Frederick, W.J.; Hupa, M. Gasification of Black Liquor at Elevated Pressures Part 2. Rate Data with $CO_2$ and Water Vapor. Combustion Chemistry Research Group Report 90-12. Turku, Finland, Abo Akademi University, 1990.

44. Frederick, W.J.; Wag, K.; Hupa, M. Pressurized $CO_2$ Gasification of a High Sodium Content Char from Spent Pulping Liquor. Twenty-Fourth International Symposium on Combustion. Sydney, Australia, July 5-10, 1992.

45. Kapteijn, F.; Moulijn, J.A. Kinetics of the Potassium Carbonate-Catalyzed $CO_2$ Gasification of Activated Carbon. Fuel 62:221-225(1983).

46. Goerg, K.A.; Cameron, J.H. A Kinetic Study of Kraft Char Gasification with $CO_2$. AIChE Meeting, Boston, Preprint No. 67g:(Aug. 24-27, 1986).

47. Laurendaeu, N.M. Heterogenous Kinetics of Coal Char Gasification and Combustion. Progress in Energy Combustion Science. 4:221-268(1978).

48. Harris, D.J.; Smith, I.W. Intrinsic Reactivity of Petroleum Coke and Brown Coal Char to Carbon Dioxide, Steam and Oxygen. CSIRO Division of Coal Technology. North Ryde, Australia.

49. Smoot, D.L.; Smith, P.J. Coal Combustion and Gasification. Plenum Press, New York, NY, 1985.

50. Meijer, R. Kinetics and Mechanisms of the Alkali-Catalysed Gasification of Carbon. Doctoral Dissertation. Amsterdam, The Netherlands, University of Amsterdam, 1992.

51. Rao, Y.K.; Adjorlolo, A.; Haberman, J.H. On the Mechanism of Catalysis of the Boudouard Reaction by Alkali-Metal Compounds. Carbon 20(3):207-212(1982).

52. McKee, D.W.; Chatterji, D. The Catalytic Behavior of Alkali Metal Carbonate and Oxides in Graphite Oxidation Reactions. Carbon 13:381-390(1975).

53. McKee, D.W. Gasification of Graphite in Carbon Dioxide and Water Vapor-The Catalytic Effects of Alkali Metal Salts. Carbon 20(1):59-66(1982).

54. McKee, D.W.; Spiro, C.L.; Kosky, P.G.; Lamby, E.J. Catalysis of Coal Char Gasification by Alkali Metal Salts. Fuel 62:217-220(1983).

55. McKee, D.W. Mechanisms of the Alkali Metal Catalyzed Gasification of Carbon. Fuel 62:170-175(1983).

56. McKee, D.W. Metal Oxides as Catalysts for the Oxidation of Graphite. Carbon 8:623-635(1970).

57. Saber, J.M.; Falconer, J.L.; Brown, L.F. Interaction of Potassium Carbonate with Surface Oxides of Carbon. Fuel 65:1356-1359(1986).

58. Kapteijn, F.; Abbel, G.; Moulijn, J.A. $CO_2$ Gasification of Carbon Catalyzed by Alkali Metals-Reactivity and Mechanism. Fuel 63:1036-1042(1984).

59. Spiro, C.L.; McKee, D.W.; Kosty, P.G.; Lamby, E.J. Catalytic $CO_2$-Gasification of Graphite Versus Coal Char. Fuel 62:180-184(1983).

60. Mims, C.A.; Pabst, J.K. Alkali-Catalyzed Carbon Gasification Kinetics: Unification of $H_2O$, $D_2O$, and $CO_2$ Reactivities. Journal of Catalysis 107:209-220(1987).

61. Mims, C.A.; Pabst, J.K. Rate of Surface Salt Complexes in Alkali-Catalyzed Carbon Gasification. Fuel 62:176-179(1983).

62. Wigmans, T.; Elfring, R.; Moulijn, J.A. On the Mechanism of the Potassium Carbonate Catalyzed Gasification of Activated Carbon: The Influence of the Catalyst Concentration on the Reactivity and Selectivity at Low Steam Pressures. Carbon 21(1):1-12(1983).

63. Wigmans, T.; Doorn, J.V.; Moulijn, J.A. Temperature Programmed Desorption Study of $Na_2CO_3$-Containing Activated Carbon. Fuel 62:190-195(1983).

64. Tromp, P.J.J.; Cordfunke, E.H.P. A Thermochemical Study of the Reactive Intermediate in the Alkali-Catalyzed Carbon Gasification. II. Alkali Metal Vapour Pressures. Thermochimica Acta 81:113-123(1984).

65. Moulijn, J.A.; Cerfontain, M.B.; Kapteijn, F. Mechanism of the Potassium Carbonate Gasification of Carbon in $CO_2$. Fuel 63:1043-1047(1984).

66. Sams, D.A.; Shadman, F. Mechanism of Potassium-Catalyzed Carbon/$CO_2$ Reaction. AIChE Journal 32(7):1132-1137(1986).

67. Cerfontain, M.B.; Moulijn, J.A. Alkali-Catalyzed Gasification Reactions Studied by *in-situ* FTIR Spectroscopy. Fuel 62:256-258(1983).

68. Cerfontain, M.B.; Moulijn, J.A. The Interaction of $CO_2$ and CO with an Alkali Carbonate Carbon System Studied by *in-situ* Fourier Transform Infrared Spectroscopy. Fuel 65:1349-1355(1986).

69. Koenig, P.C.; Squires, R.G.; Laurendeau, N.M. Effect of Potassium Carbonate on Char Gasification by Carbon Dioxide. Journal of Catalysis 100:228-229 (1986).

70. Kelemen, S.R.; Freund, H. Model $CO_2$ Gasification Reactions on Uncatalyzed and Potassium Catalyzed Glassy Carbon Surfaces. Journal of Catalysis 102:80-91(1986).

71. Saber, J.M.; Kester, K.B.; Falconer, J.L.; Brown, L.F. A Mechanism for Sodium Oxide Catalyzed $CO_2$ Gasification of Carbon. Journal of Catalysis 109:329-346(1988).

72. Kapteijn, F.; Peer, O.; Moulijn, J.A. Kinetics of the Alkali Carbonate Catalyzed Gasification of Carbon. Fuel 65: 1371-1376 (1986).

73. Freund, H. Kinetics of Carbon Gasification by $CO_2$. Fuel 64:657-660(1985).

74. Freund, H. Gasification of Carbon by $CO_2$: A Transient Kinetics Experiment. Fuel 64:63-66(1986).

75. Cerfontain, M.B.; Meijer, R.; Kapteijn, F.; Moulijn, J.A. Alkali-Catalyzed Carbon Gasification in CO/$CO_2$ Mixtures: An Extended Model for the Oxygen Exchange and Gasification Reaction. Journal of Catalysis 107:173-180(1987).

76. Cerfontain, M.B.; Kapteijn, F.; Moulijn, J.A. Characterization of Alkali Carbonate Catalyst for Carbon Gasification with $^{18}O$ Labeled $CO_2$. Carbon 26:41-48(1988).

77. Meijer, R.; Weeda, M.; Kapteijn, F.; Moulijn, J.A. Catalyst Loss and Retention During Alkali-Catalyzed Carbon Gasification in $CO_2$. Carbon 29(7):929-941(1991).

78. Sams, D.A.; Shadman, F. Catalytic Effect of Potassium on the Rate of Char-$CO_2$ Gasification. Fuel 62:880-882(1983).

79. Kapteijn, F., Meijer, R.; Moulijn, J.A. Kinetics and Mechanism of the Alkali Catalyzed Gasification of Carbon. 1991 International Conference on Coal Proceedings. University of Newcastle-upon Tyne, United Kingdom, September 16-20, 1991, 295-299.

80. Empie, H.J.; Frederick, J.W.; Grace, T.M.; Horton, R.R.; Nichols, K.M.; Medvecz, P.J.; Verrill, C.L. Black Liquor Combustion-Validated Recovery Boiler Modeling Capability, Project 3605-2, Atlanta, GA, The Institute of Paper Science and Technology, December, 1991.

81. Wendlandt, W. W. Thermal Analysis, New York, NY, John Wiley & Sons, pp. 9-86, 1986.

82. Newkirk, A.E. Analytical Chemistry 32:1558(1960).

83. Lukaszewski, G.M. Nature, 194:959(1962).

84. Weekman, V.W. Laboratory Reactors and Their Limitations. AIChE Journal 20(5):833-840(1974).

85. Shadman, F.; Sams, D.A.; Punjak, W.A. Significance of the Reduction of Alkali Carbonates in Catalytic Carbon Gasification. Fuel 66:1658-1663(1987).

86. Chitsora, C.T.; Muhlen, H.J.; van Heek, K.H.; Juntgen, H. The Influence of Pyrolysis Conditions on the Reactivity of Char in $H_2O$. Bergbau-Forschung GmbH, P.O. Box 13 01 40, 4300 Essen 13 (Fed. Rep. of Germany).

87. Hamilton, R.T.; Sams, D.A.; Shadman, F. Variation of Rate During Potassium-Catalyzed $CO_2$ Gasification of Coal Char. Fuel 63:1008-1012(1984).

88. Meijer, R.; Weeda, M.; Kapteijn, F.; Moulijn, J.A. Catalyst Loss and Retention During Alkali-Catalysed Carbon Gasification in $CO_2$. Carbon 29(7):929-941(1991).

89. Smith, J.M. Chemical Engineering Kinetics, New York, NY, McGraw-Hill Book Company, pp. 394-397 and 655-658, 1981.

90. Levenspiel, O. Chemical Reaction Engineering, Second Edition. New York, NY, John Wiley & Sons, pp. 253-283, 1972.

91. Hamilton, R.T.; Sams, D.A.; Shadman, F. Variation of Rate During Potassium-Catalysed $CO_2$ Gasification of Coal Char. Fuel 63:1008-1012 (1984).

92. Levenspiel, O. The Chemical Reactor Ominibook, First Edition. Corvallis,OR, OSO Book Stores, Inc., p. 22.3, 1979.

93. Hill, C.G. An Introduction to Chemical Engineering Kinetics & Reactor Design. New York, NY, John Wiley & Sons, pp. 431-437, 1977.

94. Froment, G.F.; Bischoff, K.B. Chemical Reactor Analysis and Design, New York, NY, John Wiley & Sons, p. 171, 1979.

95. Geankopolis, C.J. Transport Processes and Unit Operations, London, England, Allyn and Bacon, Inc., pp. 436-437, 1983.

96. Li, J.; van Heiningen, A.R.P. Sulfur Emission During Gasification of Black Liquor Char. Proceedings of the International Chemical Recovery Conference. Ottawa, Canada, April 3-6, 1989:209-216.

97. Austin, L.G.; Walker, P.L. Effect of Carbon Monoxide in Causing Nonuniform Gasification of Graphite by Carbon Dioxide. A.I.Ch.E. Journal 9(3):303-306(1963).

98. McCann, D. A Review of Recovery Boilers Process Design. 77th Annual Meeting of the Technical Section of the Canadian Pulp and Paper Association. January 29-30, 1991:A49-A58.

99. Hough, G. Chemical Recovery in the Alkaline Pulping Process, Atlanta, GA, TAPPI Press, 1985.

100. Lee, S.R.; Verrill, C.L.; Nichols, K.M. Kraft Black Liquor Char Density. Proceedings of the 1992 AIChE Annual Meeting. Miami Beach, FL, November 6, 1992.

101. Grace, T.M.; Lien, S.J.; Brown, C.A. Char Bed Burning Report. The Institute of Paper Chemistry.

102. Gardiner, W.C.; McFarland, M.; Morinaga, K.; Takeyama, T.; Walker, B.F. Initiation Rate for Shock-Heated Hydrogen-Oxygen-Carbon Monoxide-Argon Mixtures as Determined by OH Induction Time Measurements. The Journal of Physical Chemistry 75(10):1504-1509(1971).

103. Rawlins, W.T.; Gardiner, W.C. Rate Constant for $CO + O_2 = CO_2 + O$ from 1500 to 2500K. A Reevaluation of Induction Times in the Shock-Initiated Combustion of Hydrogen-Oxygen-Carbon Monoxide-Argon Mixtures. The Journal of Physical Chemistry 78(5):497-500(1974).

104. Richardson, D.L.; Merriam, R.L. Study of Cooling and Smelt Solidification in Black Liquor Recovery Boiler. Phase I Report. Prepared for the American Paper Institute. Arthur D. Little, Inc., Cambridge, MA, February, 1977.

APPENDICES

# APPENDIX I. GLOSSARY

**Black Liquor** The spent liquor obtained from the pulp-washing system. It contains almost all of the inorganic cooking chemicals along with the lignin and other organics separated from the wood during pulping in the digester. It is distinctly alkaline, but not caustic. It has an intense black color.[3,105]

**Black Liquor Solids** The material left after drop drying.

**Char** Char is the solid product of the devolatilization stage. A black, porous, and friable material consisting primarily of organic carbon and the inorganic salts $Na_2CO_3$, $Na_2SO_4$, and $Na_2S$. Approximately one-half of the carbon and most of the sodium contained in the incoming black liquor are found in the char.[4]

**Char Burning** Hupa *et al.*[1] identified the char burning stage as the longest stage of black liquor combustion which extends from extinction of the volatile flame to the sudden collapse of the residue into a molten smelt bead. The char burning occurs as heterogeneous reactions in which the residual carbon is oxidized and inorganics are reduced and coalesced. Char burning can occur either in-flight or on the char bed.

**Combustion** The process of burning fuel. When sufficient oxygen is present for complete combustion, the reaction products are $H_2O$, $CO_2$, and inorganic residue or ash.

**Devolatilization** This stage of burning occurs as the black liquor is heated in an inert or oxidizing environment. The black liquor devolatilization stage is a complex process which is characterized by rapid particle swelling, the appearance and disappearance of a surrounding yellow diffusion flame, volatiles yield, and a continuously increasing particle temperature.

**Drying** This stage of burning occurs as the water in the black liquor is evaporated.

**Gasification** The thermal conversion of a solid or liquid fuel to a gaseous fuel of relatively high heating value. Gasification is commonly thought of as incomplete combustion with $O_2$, $H_2O$, $CO_2$, or $H_2$ as the oxidizer.

**Global Modeling of Char Oxidation** If the particle is porous, then diffusion of the product into the porous volume and reaction on the larger internal surface area will influence the overall reaction rate. Because the details of this complex internal structure are not always known, it has been common to relate the char reaction rate to the external surface area. This type of char model is refered to as a global model.[49]

**Maximum Temperature Preheat Procedure** Procedure used to heat partially pyrolyzed black liquor char prior to heterogeneous combustion. This procedure involves heating partially pyrolyzed char particles in an atmosphere of 95%$N_2$/5%CO to a maximum temperature of 950°C, achieving complete pyrolysis at 950°C for one hour, and cooling down to a predetermined temperature (600°C, 700°C, or 800°C).

**Pyrolysis** The thermal decomposition of organic material conducted in an oxidizer-free environment that yields volatile substances and a carbonaceous solid residue.[49]

**Reaction Temperature Preheat Procedure** Procedure used to heat partially pyrolyzed black liquor char prior to heterogeneous combustion. This procedure involves heating partially pyrolyzed char particles in an atmosphere of 95% $N_2$/5%CO to various temperatures (600°C, 700°C, and

800°C), achieving complete pyrolysis at the given temperature, and upon complete pyrolysis retaining the char at the given temperature for one hour.

**Smelt** The reduced molten salt residue left at the end of char burning.

**Specific Volume** Defined as the particle volume divided by the particle mass at the time of measurement. Knowledge of the specific volume of char allows the data to be converted to density as a function of time.

**Specific Swollen Volume** The maximum volume attained by the droplet during swelling divided by the initial dry solids mass of the droplet. This term is commonly used when referrring to swelling during devolatilization.

**Stage** Black liquor drop combustion is characterized by four distinct stages: drying, devolatilization, char burning, and inorganic reactions (smelt oxidation).[1]

**Sulfate-Sulfide Cycle** Grace *et al.*[2,4] have noted that kraft char burns via a sulfate-sulfide cycle. Oxygen comes in from the combustion air and oxidizes $Na_2SO_4$. The $Na_2SO_4$ carries the oxygen over to the carbon, where it reacts to form $CO_2$ and CO. The $Na_2SO_4$, in turn, is reduced back to sulfide, completing the cycle.

**Swelling Factor** Defined as the ratio of the diameter of a swollen particle to its initial diameter. This term is commonly used when referring to swelling during drying.

## APPENDIX II. LIST OF EXPERIMENTAL EQUIPMENT

| COMPONENT | DESCRIPTION | VENDOR |
|---|---|---|
| Temperature controlled tube furnace | ATS Series 3110 tube furnace | Applied Test Systems, Inc., Butler, PA |
| Mass flowmeter: CO, $CO_2$, $N_2$, $O_2$ flow (3) | Hastings Mass Flowmeter: model ST-10K flow transducer, model PR-4 four channel flow monitor, 0-10 L/min air capacity. | Teledyne-Hastings-Raydist, Hampton, VA |
| Temperature control thermocouples | Type K | Omega Engineering, Inc., Stamford, CT |
| Gas-preheat coil | 1/4-in. ID 304 stainless steel tube, length 12.2 m | IPST Machine Shop, Atlanta, GA |
| Exterior retort | 304 stainless steel, 16 gage | IPST Machine Shop, Atlanta, GA |
| Char containing retort 1 | 304 stainless steel, 16 gage, 3 " OD, length 38 cm | IPST Macine Shop, Atlanta, GA |
| Char containing retort 2 | Haynes HR-160 alloy, 3 in. OD, length 38 cm, 2.5" sch. 40x15", (36% Ni, 29% Co, 28% Cr, 2.75% Si, 2% Fe) | Haynes International, Inc., Kokomo, IN |
| Char containing screen | Nichrome mesh | IPST Machine Shop, Atlanta, GA |
| Ceramic crucible | Aluminum Oxide, 4" tube body with one hemispherical closed end | McDanel Refractory Co. |
| Steam gasket | Generic steam gaskets used to maintain seal of furnace cap | IPST Machine Shop, Atlanta, GA |
| $CO/CO_2$ Infrared Analyzer | Nondispersive infrared gas analyzer, Model IR702, duel channel | Altamon Technologies, Inc., Livermore, CA |
| $O_2$ Analyzer | Microfuel cell detector, Model 326A | Teledyne Analytical Inst., City of Industry, CA |
| External Insulation | Thermo-12 calcium silicate block insulation: 2.5 in. thickness | Industrial Insulation Corp., Appleton, WI |
| Temperature limit controller | Watlow Service 140 open board limit control | Watlow Controls, Winona, MN |
| Furnace cap | Custom fabricated stainless steel cap, 1" thickness, 10" diameter. Machined by IPST machine shop | IPST Machine Shop, Atlanta, GA |
| Gas filtering device | Custom fabricated plastic tube with capped ends packed with glass wool, 2.5" ID, 12" length | IPST Machine Shop, Atlanta, GA |
| U-shaped preheat reactor | Custom fabricated stainless steel tubing connected with stainless steel elbows and tees, longest leg 3.0', shortest leg 2.5' | IPST Machine Shop, Atlanta, GA |
| Char containing basket | Nichrome wire mesh basket | IPST Machine Shop, Atlanta, GA |

APPENDIX III: ELEMENTAL ANALYSIS DATA FOR INITIAL CHARS AND CHARS PREPARED ACCORDING TO THE REACTION TEMPERATURE PREHEAT PROCEDURE (RTPP) AND MAXIMUM TEMPERATURE PREHEAT PROCEDURE (MTPP)

Table A3-1 contains the elemental analysis data for the partially devolatilized char particles which were formed using the drop tube furnace and the fully devolatilized particles which were prepared according to the RTPP. Table A3-2 contains the elemental analysis data for the partially devolatilized char particles which were formed using the drop tube furnace and the fully devolatilized particles which were prepared according to the MTPP.

**Table A3-1:** Elemental Analysis of Partially Devolatilized Char Particles Formed Using the Drop Tube Furnace and Fully Devolatilized Particles Prepared According to the RTPP.

| Exp. Num. | Preheat Temp. (°C) | Carbon, (wt. %) | Carbonate C, (wt. %) | Sulfur, (wt. %) | Sulfate S, (wt. %) | Thiosulfate S, (wt. %) | Sodium, (wt. %) | Oxygen-Merz, (wt. %) | Hydrogen, (wt. %) |
|---|---|---|---|---|---|---|---|---|---|
| Initial Char | NA | 34.5 | NA | 3.66 | NA | NA | 25.67 | 34.27 | 3.19 |
| 4938 | 600 | 34.1 | 5.1 | 3.72 | 1.74 | 0.23 | 25.15 | 30.53 | 1.27 |
| 4931 | 700 | 28.18 | 6.63 | 4.23 | 1.32 | 0.63 | 27.43 | 28.62 | 0.83 |
| 4933 | 800 | 25.27 | 6.62 | 5.54 | 2.2 | 0.22 | 26.12 | 31.85 | 0.39 |

**Table A3-2:** Elemental Analysis of Partially Devolatilized Char Particles Formed Using the Drop Tube Furnace and Fully Devolatized Particles Prepared According to the MTPP.

| Exp. Num. | Preheat Temp. (°C) | Carbon, (wt. %) | Carbonate C, (wt. %) | Sulfur, (wt. %) | Sulfate S, (wt. %) | Thiosulfate S, (wt. %) | Sodium, (wt. %) | Oxygen-Merz, (wt. %) | Hydrogen, (wt. %) |
|---|---|---|---|---|---|---|---|---|---|
| Initial Char | NA | 33.9 | 3.45 | 4.38 | NA | NA | 28.55 | 32.1 | 1.37 |
| 4959 | 600 | 29.95 | 5.5 | 5.26 | 0.29 | 1.92 | 26.91 | 34.23 | 1.42 |
| 4961 | 600 | 29.14 | 5.11 | NA | NA | NA | NA | NA | NA |
| 4963 | 600 | 34.15 | 4.92 | NA | NA | NA | NA | NA | NA |
| 4964 | 700 | 30.57 | 5.51 | 5.05 | 0.85 | 1.45 | 25.59 | 35.59 | 0.87 |
| 4965 | 700 | 33.33 | 5.08 | NA | NA | NA | NA | NA | NA |
| 4966 | 700 | 23.3 | 5.77 | NA | NA | NA | NA | NA | NA |
| 4968 | 800 | 32.84 | 5.14 | 5.67 | 0.9 | 1.31 | 27.8 | 32.21 | 1.02 |
| 4969 | 800 | 31.66 | 5.71 | NA | NA | NA | NA | NA | NA |
| 4955 | 950 | 26.54 | 5.21 | 5.55 | 0.39 | 2.68 | 27.53 | 33.33 | 1.62 |
| 4956 | 950 | 27.07 | 5.35 | NA | NA | NA | NA | NA | NA |
| 4957 | 950 | 30.1 | 5.37 | NA | NA | NA | NA | NA | NA |

## APPENDIX IV: CONTROL EXPERIMENTS FOR THE FIXED BED REACTOR

The gasification reaction of interest for this thesis is Char C + $CO_2 \Leftrightarrow 2CO$. The retorts, Nichrome screen, and heating coils used in these experiments are manufactured from 304 stainless steel. To determine the effect of $CO_2$ on these materials, a series of experiments were conducted. The object of the experiments was to observe how much $CO_2$ was converted to CO when the $CO_2$ flowed through the experimental reactor in the absence of black liquor char at 600°C, 700°C, and 800°C. These control experiments were performed at $CO_2$ concentrations ranging from approximately 4.0-8.3 volume percent with total gas flows ranging from 5.5-10.3 slpm. Table A4.1 shows the $CO_2$ conversion data for the different experimental conditions tested. As suggested by the results shown in Table A4-1, the $CO_2$ was not depleted significantly by the reactor walls.

**TABLE A4-1:** Control Experiments to Determine the Conversion of $CO_2$ at 600°C, 700°C, and 800°C for the Fixed Bed Reactor.

| Temperature, (°C) | $N_2$ Flow, (slpm) | $CO_2$ Flow, (slpm) | Inlet $CO_2$ Concentration, (Vol. %) | Outlet $CO_2$ Concentration, (Vol. %) | Ratio (Outlet:Inlet) |
|---|---|---|---|---|---|
| 600 | 5.42 | 0.26 | 4.6 | 4.6 | 1 |
| 618 | 5.03 | 0.26 | 5 | 5 | 1 |
| 608 | 4.81 | 0.25 | 4.9 | 4.9 | 1 |
| 701 | 4.85 | 0.23 | 4.5 | 4.4 | 0.98 |
| 701 | 4.85 | 0.23 | 4.5 | 4.4 | 0.98 |
| 703 | 4.82 | 0.23 | 4.5 | 4.4 | 0.98 |
| 709 | 8.63 | 0.49 | 5.4 | 5.3 | 0.98 |
| 709 | 8.28 | 0.48 | 5.5 | 5.6 | 1.02 |
| 711 | 8.3 | 0.48 | 5.5 | 5.4 | 0.98 |
| 713 | 9.55 | 0.75 | 7.3 | 7.2 | 0.99 |
| 806 | 5.02 | 0.2 | 3.9 | 3.9 | 1 |
| 806 | 5.07 | 0.28 | 5.3 | 5.3 | 1 |
| 806 | 4.91 | 0.44 | 8.3 | 8.3 | 1 |
| 812 | 8.83 | 0.6 | 6.3 | 6.4 | 1.01 |
| 813 | 8.47 | 0.55 | 6.2 | 6.1 | 0.99 |
| 813 | 9.08 | 0.69 | 7.1 | 7.2 | 1.01 |

## APPENDIX V: DETERMINATION OF TUBE LENGTH FOR GAS PREHEAT COIL

The minimum length heating coil tubing required to heat the gas to the maximum temperature will be determined. The simplified geometry of the system is shown in Figure A5-1.

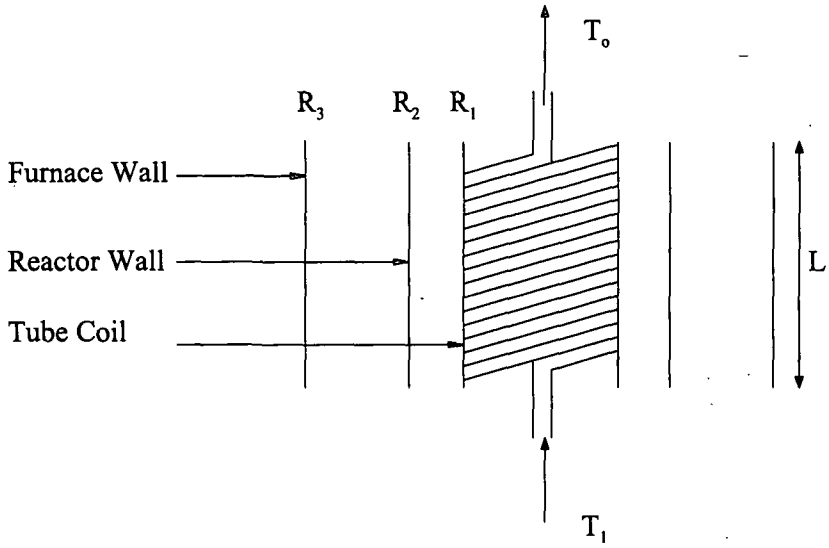


**Figure A5-1.** Simplified Geometry of the Preheat System of the Experimental Reactor.

For the dimensions in Figure A3-1 ($R_1$ = 0.13 m, $R_2$ = 0.15 m, and $R_3$ = 0.20 m), the length of a 0.013 m OD tube is calculated as follows:

$$N = \text{Number of Coils} = \left[\frac{0.2\text{ m}}{0.013\text{ m}}\right]\bullet 0.60 = 9.23$$

$$C_L = \text{Length of Coils} = 2\bullet N\bullet\pi\bullet 0.13 = 7.54$$

The method for determining if 3.8m of tubing (one-half of the tube length) is adequate is as follows:

Assumptions:

The coil (surface 1) is treated as a cylinder.
Natural convection is negligible on the outside of the tube.
The tube surface is at a constant temperature.

| | | | | |
|---|---|---|---|---|
| $T_3$ | = | furnace wall temperature | = | 1600K |
| $T_i$ | = | inlet gas temperature | = | 298K |
| $T_o$ | = | maximum required gas temperature | = | 1473K |
| $A_1$ | = | cross sectional area of region one | = | $0.053m^2$ |
| $A_2$ | = | cross sectional area of region two | = | $0.071m^2$ |

| | | | | | |
|---|---|---|---|---|---|
| $A_3$ | = | cross sectional area of region three | = | $0.13m^2$ | |
| $E_3$ | = | power to furnace | = | 9200W | |
| $A_T$ | = | total cross-sectional area of furnace | = | $0.33m^2$ | |
| $q_{r,3-2}$ | = | $\left(\frac{9200W}{0.33m^2}\right) \bullet \pi \bullet 0.02m \bullet 0.02m$ | = | 3500W | |
| $q_{r,3-2}$ | = | $q_{r,2-1}$ = q | = | $U_i \bullet A_i \bullet \Delta T_{lm}$ | |

The following equations are used:

$$q_{r,3-2} = \sigma \bullet \varepsilon_{3-2} \bullet A_3 \bullet \left(T_3^4 - T_2^4\right)$$

$$q_{r,2-1} = \sigma \bullet \varepsilon_{2-1} \bullet A_2 \bullet \left(T_2^4 - T_1^4\right)$$

$$q_{r,2-1} = A_1 \bullet h_1 \bullet \left[\frac{[(T_i - T_o) - (T_1 - T_i)]}{\ln\left(\frac{T_1 - T_o}{T_1 - T_i}\right)}\right]$$

$$q_{r,2-1} = m \bullet C_p \bullet (T_o - T_i)$$

$$q_{r,3-2} = q_{r,2-1}$$

These equations provide five equations and five unknowns. The gas through the tube is $N_2$. The gas properties at the average temperature (865K) and 1 atm. are:

| | | | | | | |
|---|---|---|---|---|---|---|
| $\mu$ | = | viscosity of the fluid | = | 3.8E5 kg/m/s | | |
| $\rho$ | = | density of the fluid | = | $0.165\ kg/m^3$ | | |
| $C_p$ | = | heat capacity | = | 1084 J/K | | |
| k | = | thermal conductivity | = | 0.0665 W/m/K | | |
| $N_{Pr}$ | = | Prandtl number | = | 0.68 | | |
| m | = | mass flow rate | = | 6.88E-5 kg/s | | |
| $\sigma$ | = | constant | = | $5.67E\text{-}8\ W/m^2/K^4$ | | |
| $\varepsilon$ | = | emissivity | = | 0.65 | | |
| $D_{tube}$ | = | tube diameter | = | 0.011m | | |
| $N_{Re}$ | = | Reynolds number | = | $\frac{4 \bullet m}{D_{tube} \bullet \pi \bullet \mu}$ | = | 209 |
| $N_{Nu}$ | = | Nusselt number | = | 1.33 | | |
| $h_1$ | = | heat transfer coeff. | = | $\frac{k \bullet N_{Nu}}{D_{tube}}$ | = | $8.04\ W/m^2/K$ |

Three working equations can be formed from eqns. 5-1 - 5-3 as follows:

$$T_2 = \left[\left(\frac{4}{7} \bullet T_3^4\right) + \left(\frac{3}{7} \bullet T_1^4\right)\right]^{0.25} \qquad \text{eqn. 5-1}$$

$$T_1 = \left[\frac{(T_o \bullet exp(14.02)) - T_i}{\exp(14.02) - 1}\right] \qquad \text{eqn. 5-2}$$

$$T_o = 4.45E\text{-}8 \bullet \left(T_2^4 - T_1^4\right) + T_i \qquad \text{eqn. 5-3}$$

Using trial and error with these three equations can allow the prediciton of $T_o$. First, $T_o$ should be guessed. Use eqn. 5-2 to solve for $T_1$. Use eqn. 5-1 to solve for $T_2$. Finally, use eqn. 5-3 to solve for $T_o$. Compare the $T_o$ values and repeat if necessary.

For a coil that is 3.8 meters in length, the maximum outlet gas temperature would be approximately 3K less than the furnace temperature. To ensure that the gas is heated to the temperature of the char bed, 12 meters of coil will be installed.

## APPENDIX VI: FREE ENERGY CALCULATIONS FOR $CO_2$ GASIFICATION OF KRAFT BLACK LIQUOR CHAR

The following discussion is based on chemical equilibrium summaries of Swalin[106] and Snoeyink and Jenkins.[107] For a closed system at constant pressure and constant temperature, the criterion for equilibrium is that the total free energy of the system ($G_T$) is a minimum. Consider the $CO_2$ gasification reaction,

$$C+CO_2 \leftrightarrow 2CO. \qquad \text{rxn. 6-1}$$

When $CO_2$ passes through the char and $G_T$ is calculated as a function of the extent of reaction as the reaction proceeded, the result would be a decrease in $G_T$ to some minimum. $G_T$ is the sum of the partial free energies of each of the reaction components times the molar contribution for each.

$$G_T = n_C G_C + n_{CO2} G_{CO2} + n_{CO} G_{CO} \qquad \text{rxn. 6-2}$$

where $n_C$, $n_{CO2}$, $n_{CO}$ represent the number of moles of C, $CO_2$, and CO and $G_C$, $G_{CO2}$, and $G_{CO}$ represent the free energy/mole of each substance. The reaction in the direction that decreases $G_T$ is spontaneous while reaction in the direction that increase $G_T$ is not spontaneous.

As the gasification reaction increases an incremental amount, the change in $G_T$ is proportional to $\Delta G$ where

$$\Delta G=(\Sigma \gamma_i G_i)_{prod}-(\Sigma \gamma_i G_i)_{reac} \qquad \text{rxn. 6-3}$$

where $\gamma_i$ is the stoichiometric coefficient and
$G_i$ is the free energy per mole.

Therefore, if

1. $\Delta G<0$ - the reaction may proceed spontaneously to form CO.
2. $\Delta G>0$ - the reaction cannot proceed spontaneously as written.
3. $\Delta G=0$ - the reaction is at equilibrium.

To calculate $\Delta G$ for the gasification reaction, the following relationship can be used

$$\Delta G = \Delta G^o + RT\frac{\{CO\}^2}{\{C\}\{CO_2\}} \qquad \text{rxn. 6-4}$$

{ } is the activity, or active concentration
$\Delta G^o$ refers to a reaction for which all reactants and products are in their standard states at the given temperature and 1 atm. pressure.

The sign of $\Delta G^o$ for a particular reaction can be used only as a criterion of spontaneity if all substances are in their standard states. The real significance of $\Delta G^o$ lies not in connection with the predictability of spontaneity but in connection with equilibrium constant calculations. For rxn. 6-1, the change in free energy when all the reactants and products are at standard state is determined from the following:

$$\Delta G^o = 2\Delta G^o_{f,CO} - \left(\Delta G^o_{f,C} + \Delta G^o_{f,CO2}\right) \qquad \text{rxn. 6-5}$$

Using the HSC thermodynamic package,[108] $\Delta G^o$ for rxn. 6-1 is positive at temperatures less than 705°C. The free energy change can now be determined from rxn. 6-4. In examining this equation, it is noted that the logarithmic term has a form that is reminiscent of the equilibrium constant for the reaction as written in rxn. 6-1. However, because the magnitude of the logarithmic term is not equal to the equilibrium constant except at equilibrium, this term will be called the reaction quotient, Q, where

$$Q = \frac{\{CO\}^2}{\{CO_2\}\bullet 1} \qquad \text{rxn. 6-6}$$

When the value of Q is identical to that of the equilibrium constant K (the system is at equilibrium and $\Delta G = 0$), $\Delta G^o$ can be expressed as

$$\Delta G^o = -RT\ln K \qquad \text{rxn. 6-7}$$

The free energy, $\Delta G$, was calculated for gas concentrations of 3-5% $CO_2$ and 0.1-4% CO for RTPP experiments at 600°C. The calculations were based on the assumption that the activity of carbon is 1, and suggest that the gasification reaction is thermodynamically possible at 600°C since the free energy, $\Delta G$, was approximately -30 KJ/gmole.

APPENDIX VII: EXPERIMENTAL DATA FOR $CO_2$ GASIFICATION OF KRAFT BLACK LIQUOR CHAR PREPARED ACCORDING TO THE REACTION TEMPERATURE PREHEAT PROCEDURE.

Figs. A7-1-A7-16 are the complete sets of CO and $CO_2$ concentration profiles recorded at the various experimental conditions outlined in Table 6.

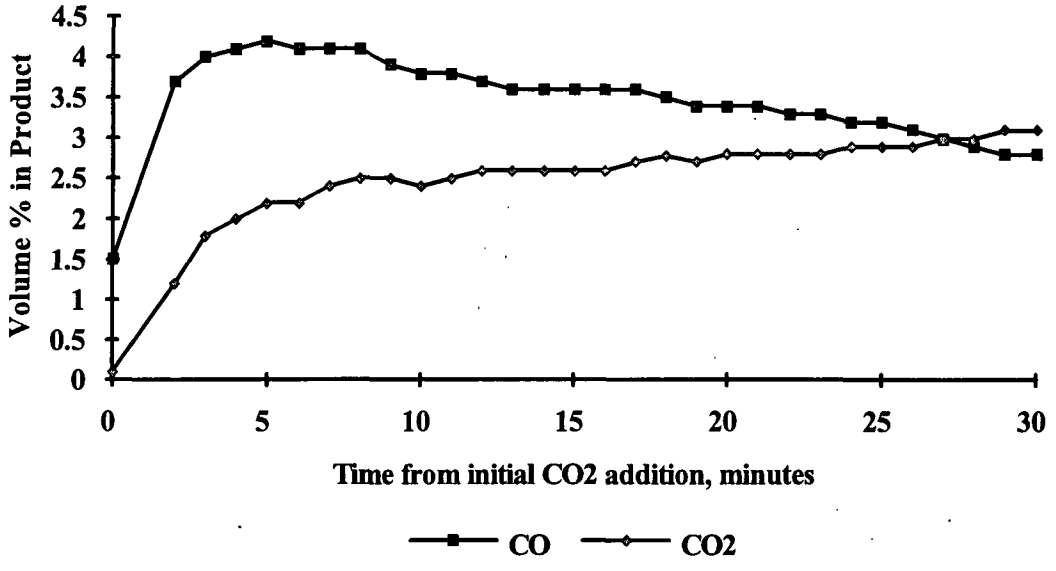


**Figure A7-1.** %CO and $\%CO_2$ in Product Gas as a Function of Time for Gasification Experiment 4902 (702°C, 4.3%$CO_2$, 5.3 slpm, $N_2$ Carrier Gas).

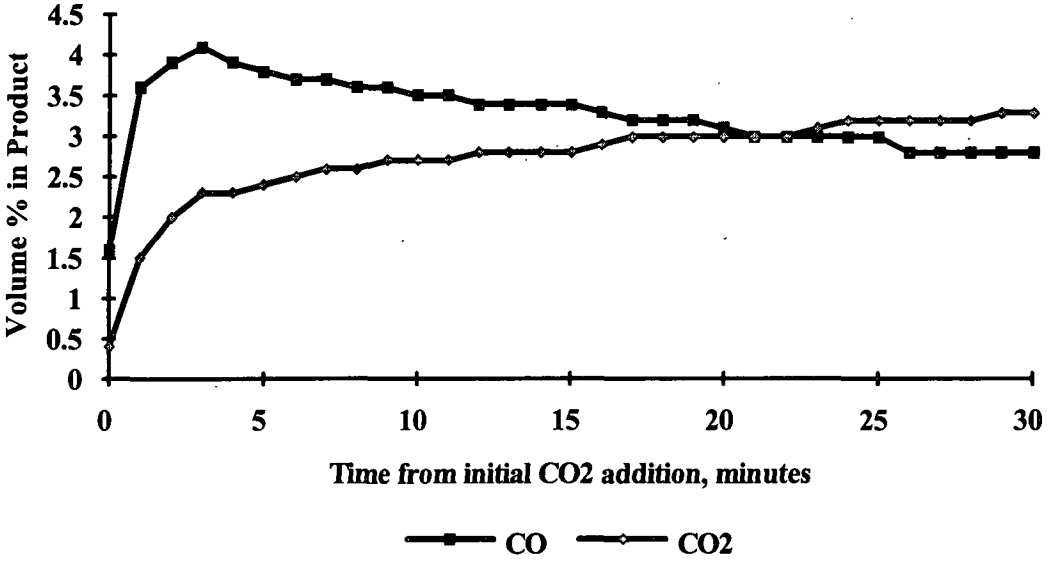


**Figure A7-2.** %CO and $\%CO_2$ in Product Gas as a Function of Time for Gasification Experiment 4903 (700°C, 4.4%$CO_2$, 5.3 slpm, $N_2$ Carrier Gas).

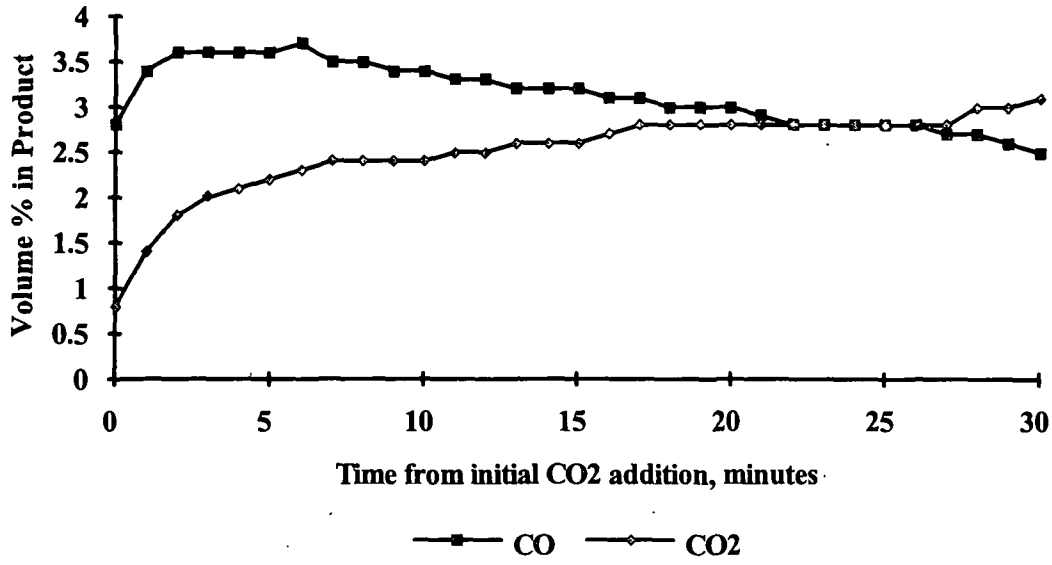


**Figure A7-3.** %CO and $\%CO_2$ in Product Gas as a Function of Time for Gasification Experiment 4904 (701°C, 4.3%$CO_2$, 5.3 slpm, $N_2$ Carrier Gas).

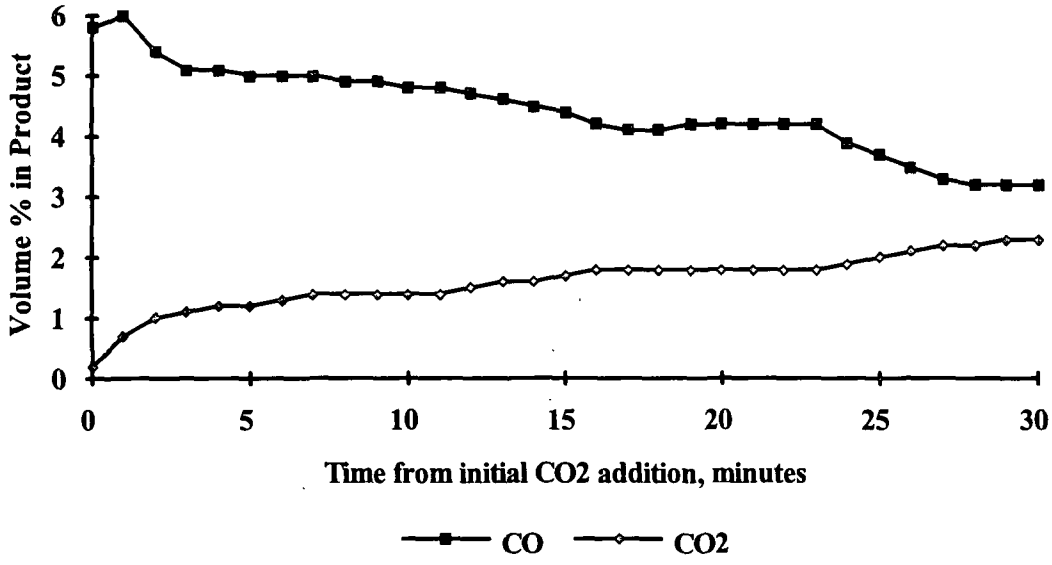


**Figure A7-4.** %CO and $\%CO_2$ in Product Gas as a Function of Time for Gasification Experiment 4905 (801°C, 4.4%$CO_2$, 5.3 slpm, $N_2$ Carrier Gas).

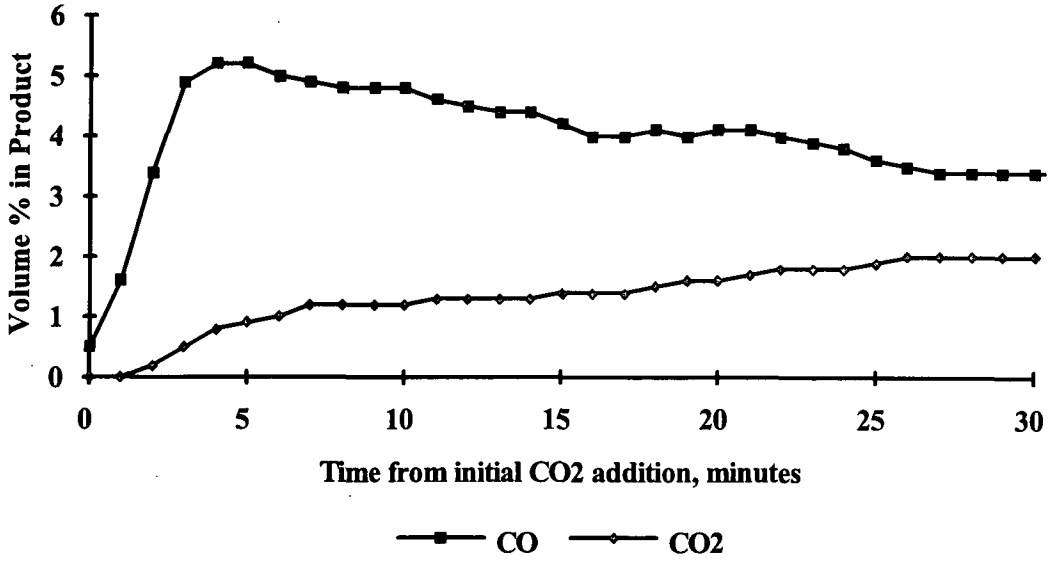


**Figure A7-5.** %CO and $\%CO_2$ in Product Gas as a Function of Time for Gasification Experiment 4906 (800°C, 4.4%$CO_2$, 5.4 slpm, $N_2$ Carrier Gas).

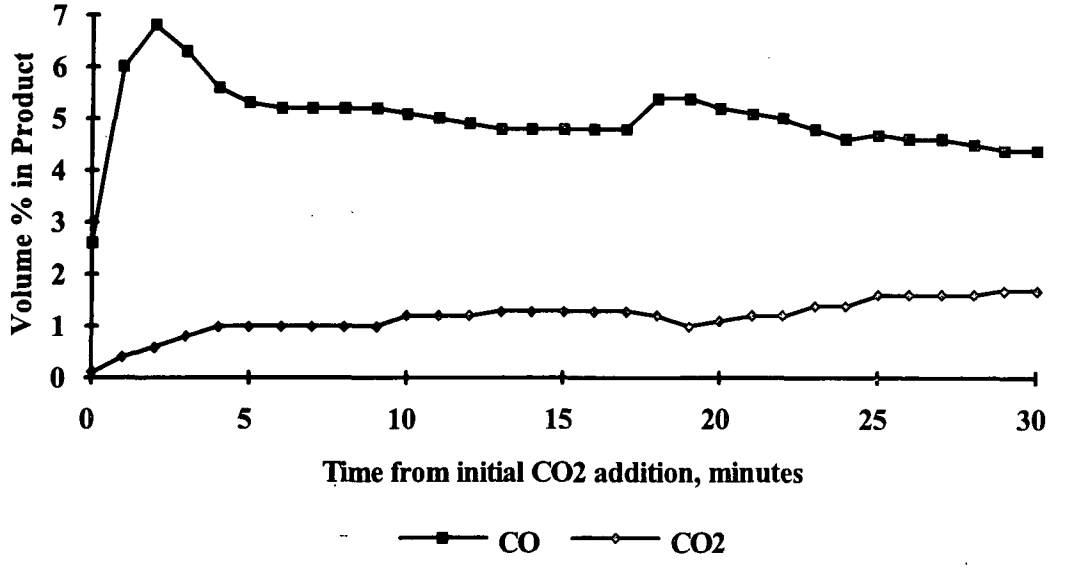


**Figure A7-6.** %CO and $\%CO_2$ in Product Gas as a Function of Time for Gasification Experiment 4907 (799°C, 4.3%$CO_2$, 5.3 slpm, $N_2$ Carrier Gas).

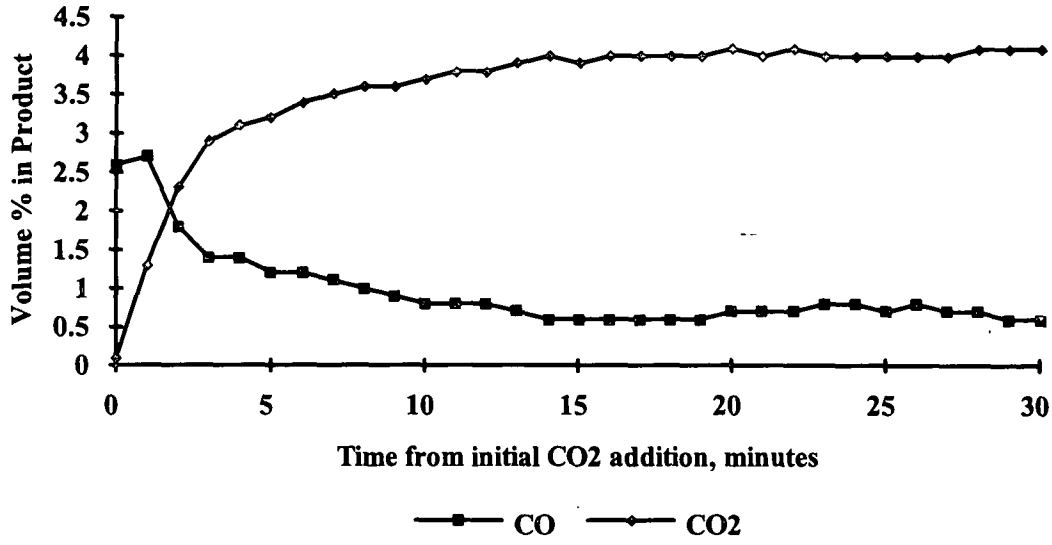


**Figure A7-7.** %CO and $\%CO_2$ in Product Gas as a Function of Time for Gasification Experiment 4908 (608°C, 4.3%$CO_2$, 5.3 slpm, $N_2$ Carrier Gas).

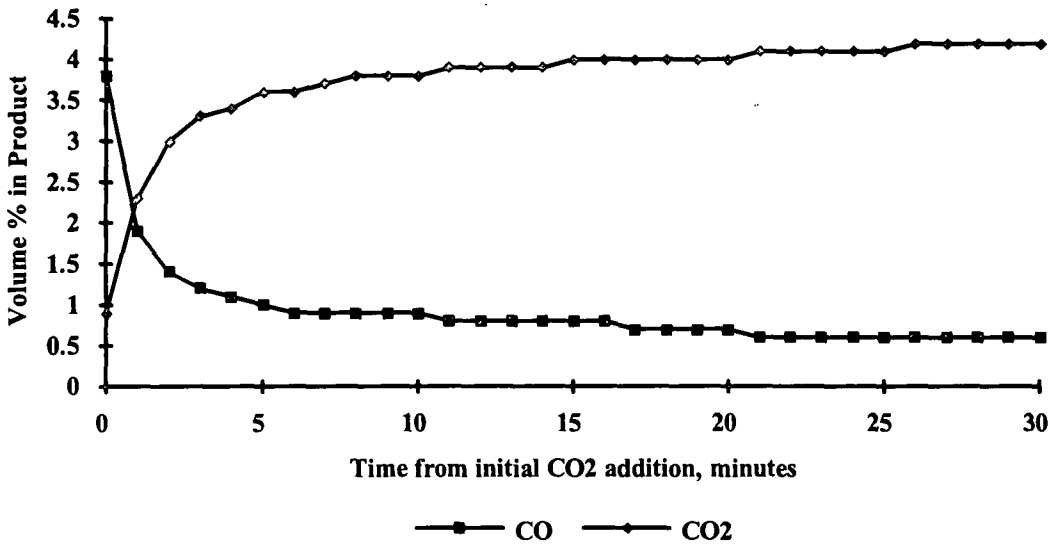


**Figure A7-8.** %CO and $\%CO_2$ in Product Gas as a Function of Time for Gasification Experiment 4909 (601°C, 4.3%$CO_2$, 5.3 slpm, $N_2$ Carrier Gas).

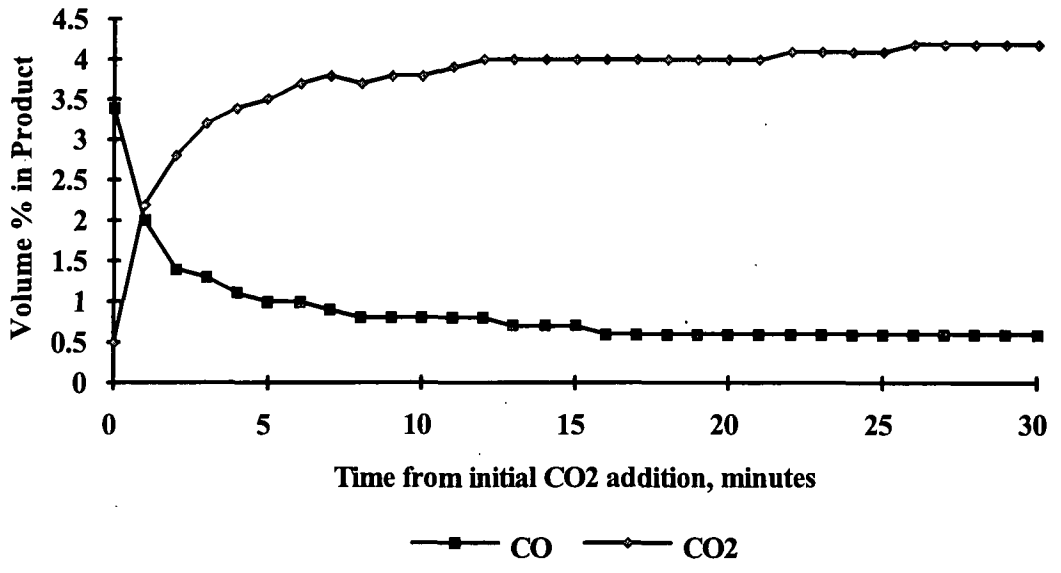


**Figure A7-9.** %CO and $\%CO_2$ in Product Gas as a Function of Time for Gasification Experiment 4910 (600°C, 4.3%$CO_2$, 5.3 slpm, $N_2$ Carrier Gas).

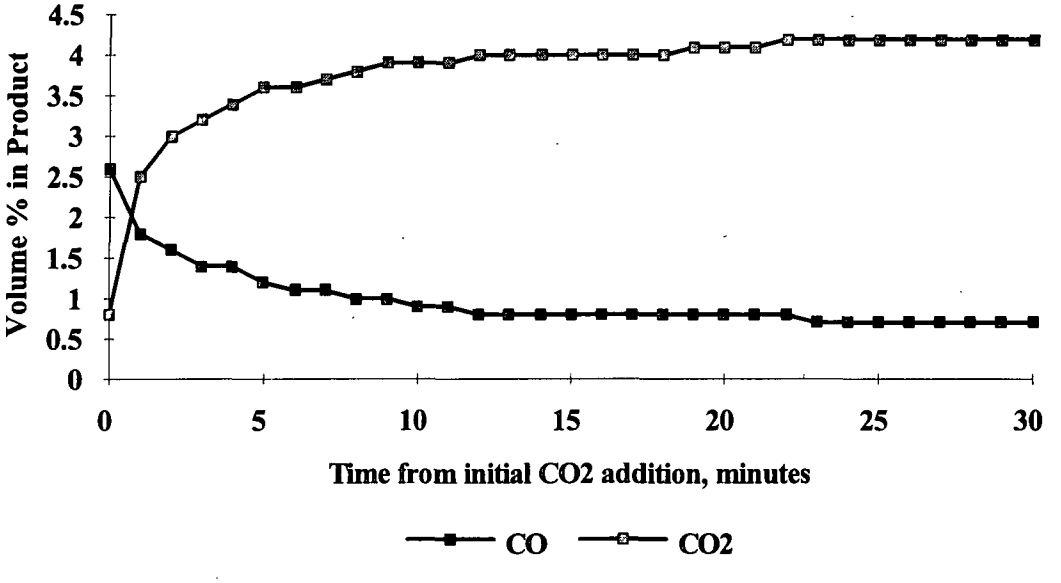


**Figure A7-10.** %CO and $\%CO_2$ in Product Gas as a Function of Time for Gasification Experiment 4911 (604°C, 4.4%$CO_2$, 5.3 slpm, $N_2$ Carrier Gas).

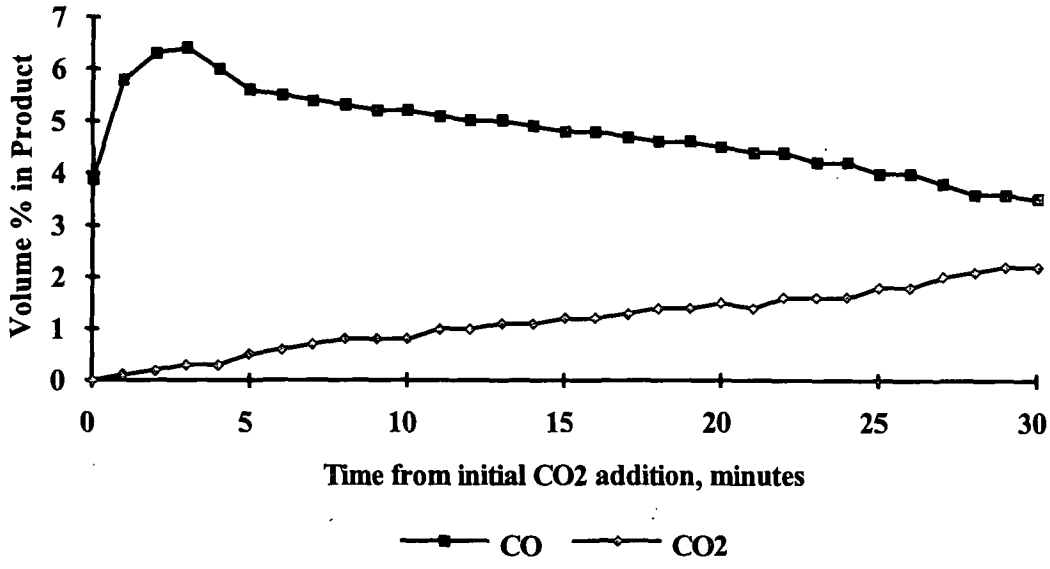


**Figure A7-11.** %CO and $\%CO_2$ in Product Gas as a Function of Time for Gasification Experiment 4913 (800°C, 4.9%$CO_2$, 5.4 slpm, He Carrier Gas).

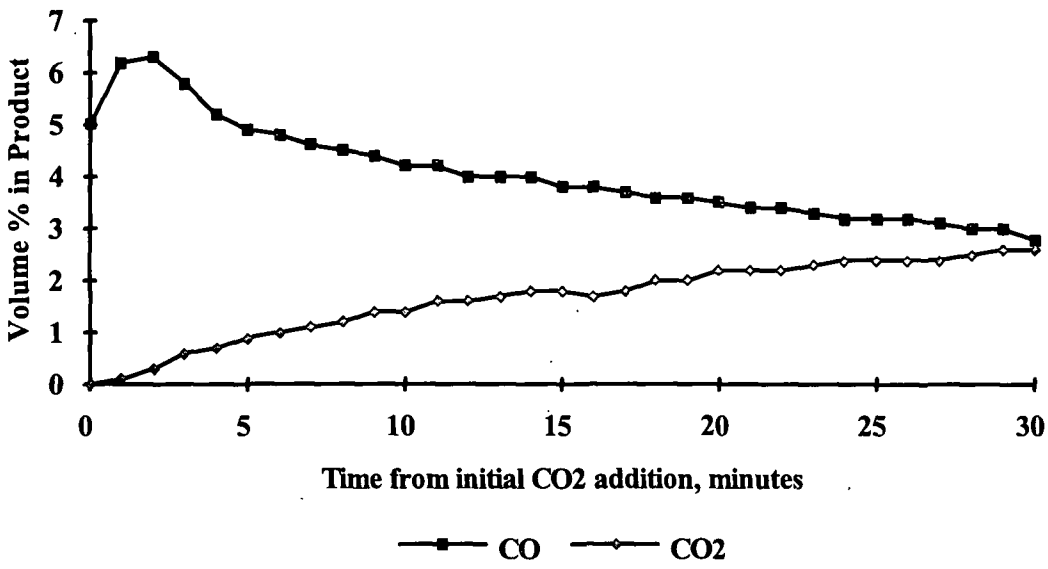


**Figure A7-12.** %CO and $\%CO_2$ in Product Gas as a Function of Time for Gasification Experiment 4914 (800°C, 4.8%$CO_2$, 5.4 slpm, He Carrier Gas).

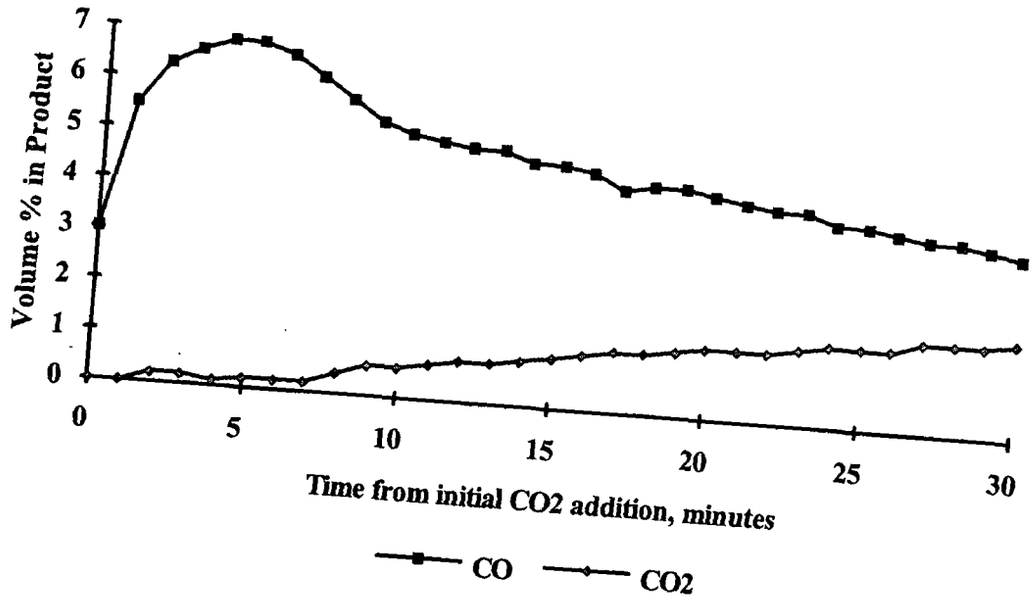


**Figure A7-13.** %CO and $\%CO_2$ in Product Gas as a Function of Time for Gasification Experiment 4915 (803°C, 4.9%$CO_2$, 5.4 slpm, He Carrier Gas).

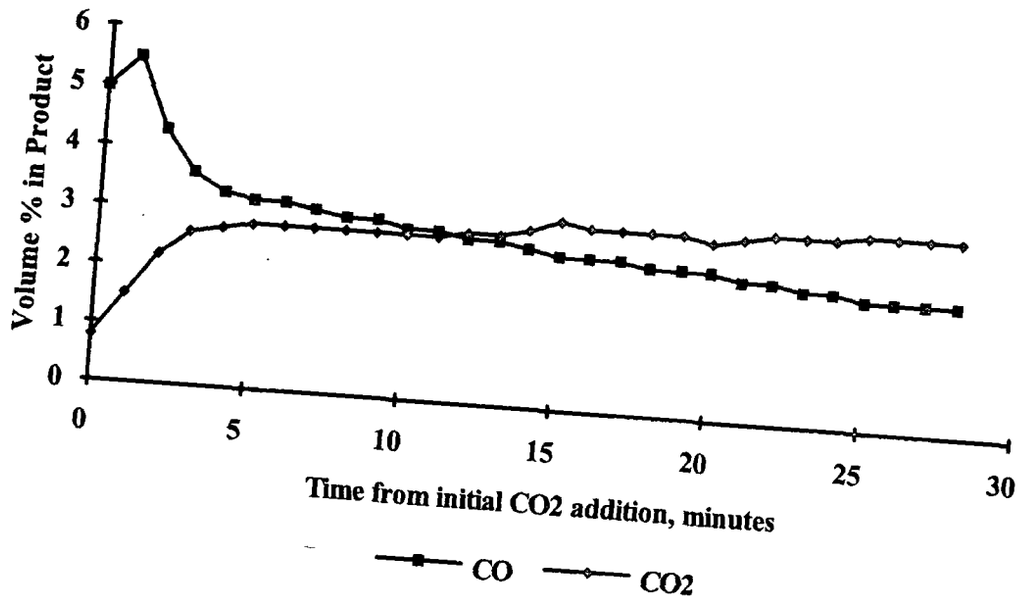


**Figure A7-14.** %CO and $\%CO_2$ in Product Gas as a Function of Time for Gasification Experiment 4916 (801°C, 4.7%$CO_2$, 10.6 slpm, $N_2$ Carrier Gas).

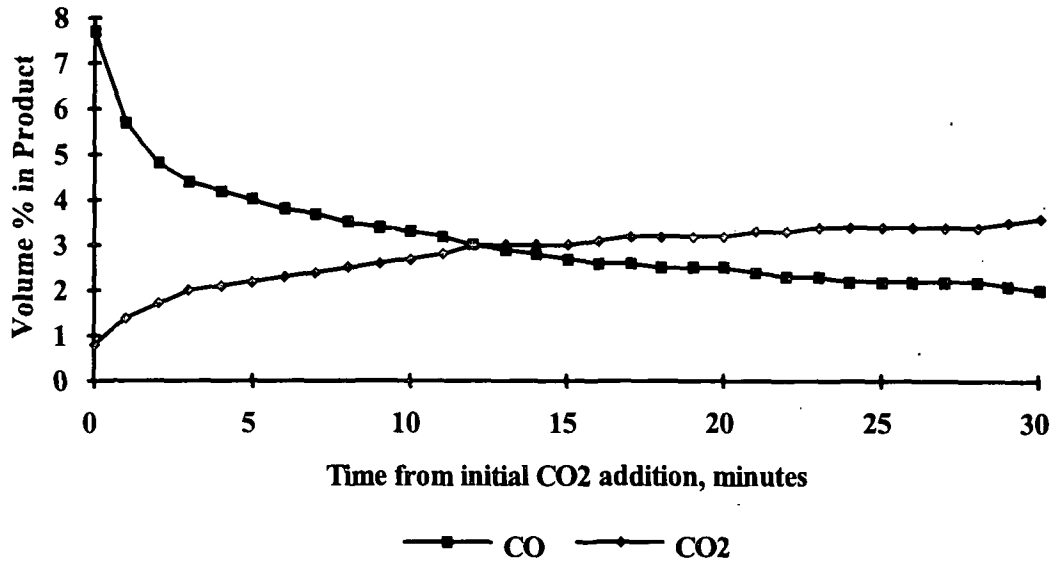


**Figure A7-15.** %CO and $\%CO_2$ in Product Gas as a Function of Time for Gasification Experiment 4917 (805°C, 4.8%$CO_2$, 10.6 slpm, $N_2$ Carrier Gas).

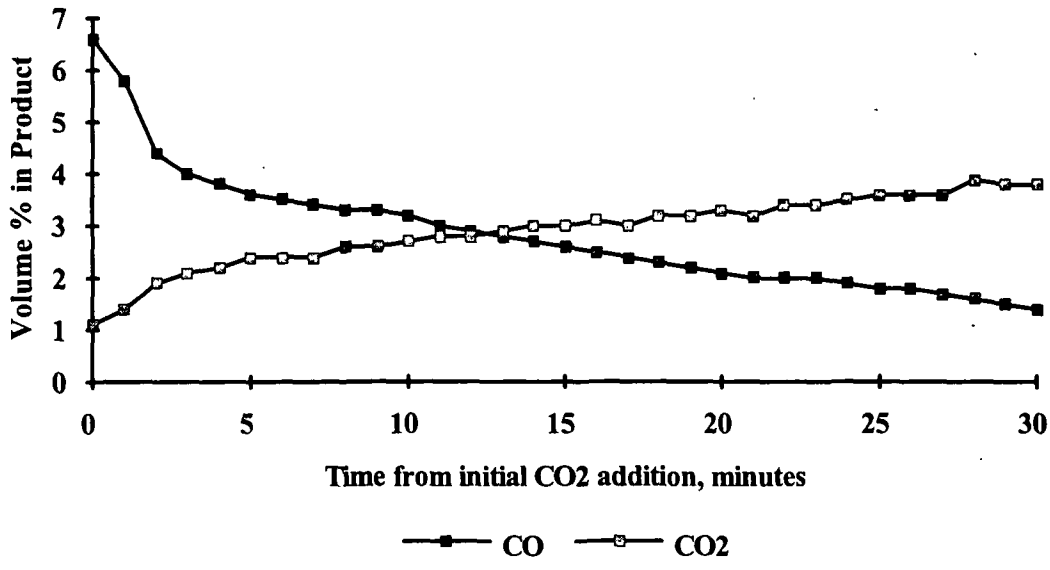


**Figure A7-16.** %CO and $\%CO_2$ in Product Gas as a Function of Time for Gasification Experiment 4918 (803°C, 4.7%$CO_2$, 10.6 slpm, $N_2$ Carrier Gas).

APPENDIX VIII. EXPERIMENTAL DATA FOR $CO_2$ GASIFICATION OF KRAFT BLACK LIQUOR CHAR PREPARED ACCORDING TO THE MAXIMUM TEMPERATURE PREHEAT PROCEDURE

Figs. A8-1-A8-14 are the complete sets of CO and $CO_2$ concentration profiles recorded at the various experimental conditions outlined in Table 7.

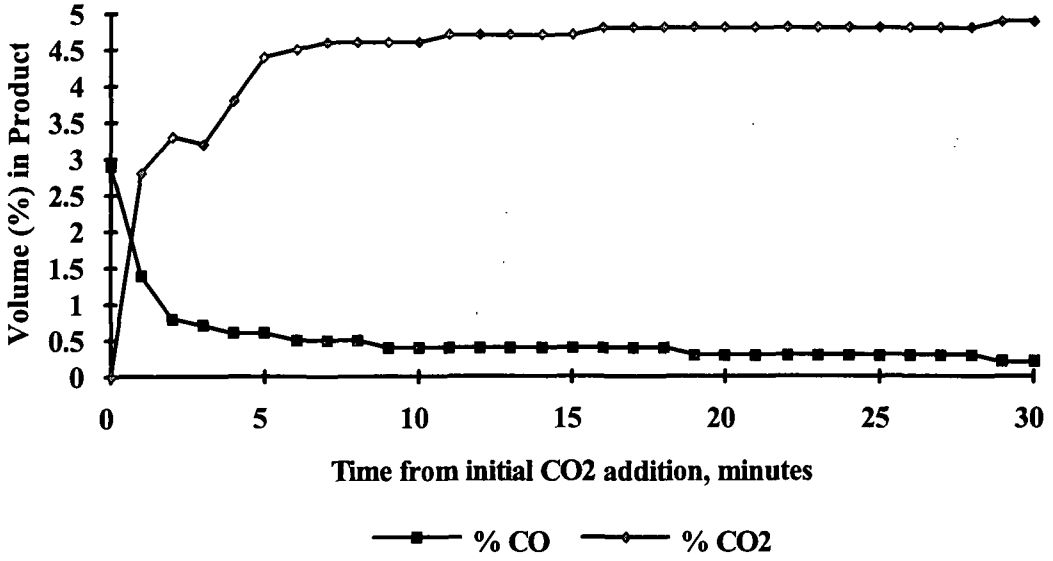


**Figure A8-1.** %CO and $\%CO_2$ in Product Gas as a Function of Time for Gasification Experiment 4979 (604°C, 4.8%$CO_2$, 5.4 slpm, $N_2$ Carrier Gas).

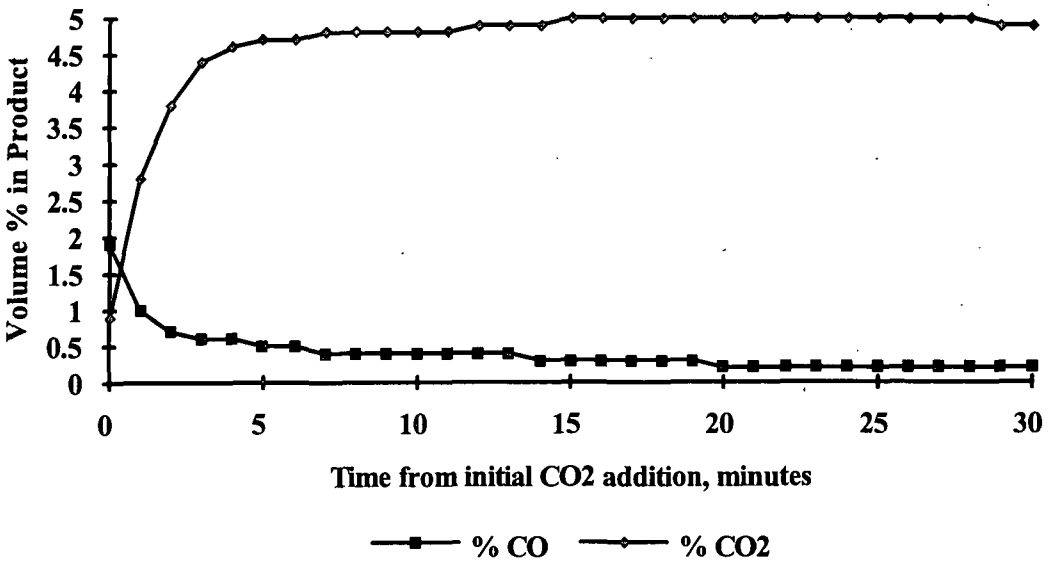


**Figure A8-2.** %CO and $\%CO_2$ in Product Gas as a Function of Time for Gasification Experiment 4982 (602°C, 4.7%$CO_2$, 5.5 slpm, $N_2$ Carrier Gas).

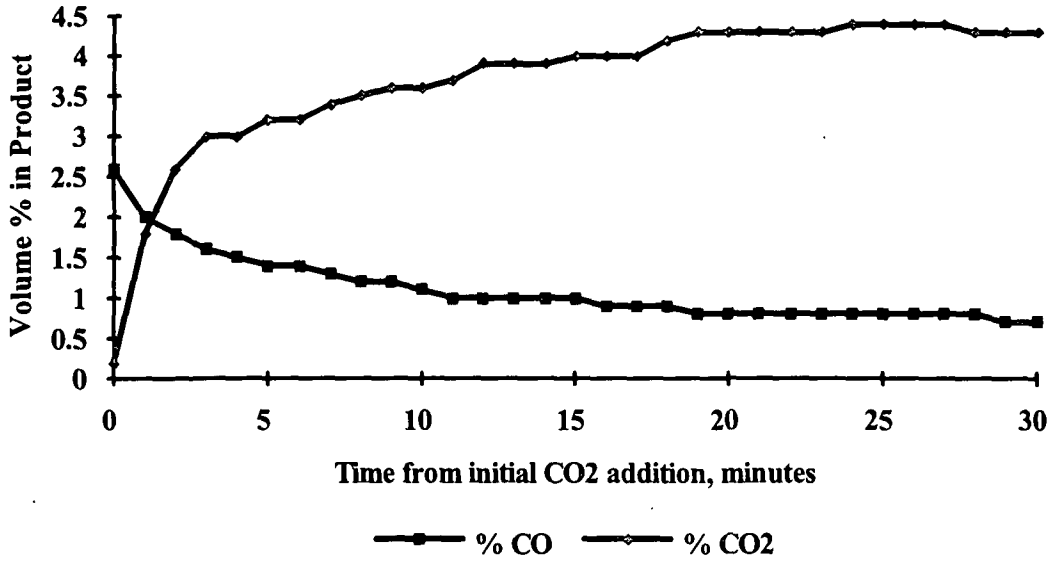


**Figure A8-3.** %CO and $\%CO_2$ in Product Gas as a Function of Time for Gasification Experiment 4972 (712°C, 4.8%$CO_2$, 5.5 slpm, $N_2$ Carrier Gas).

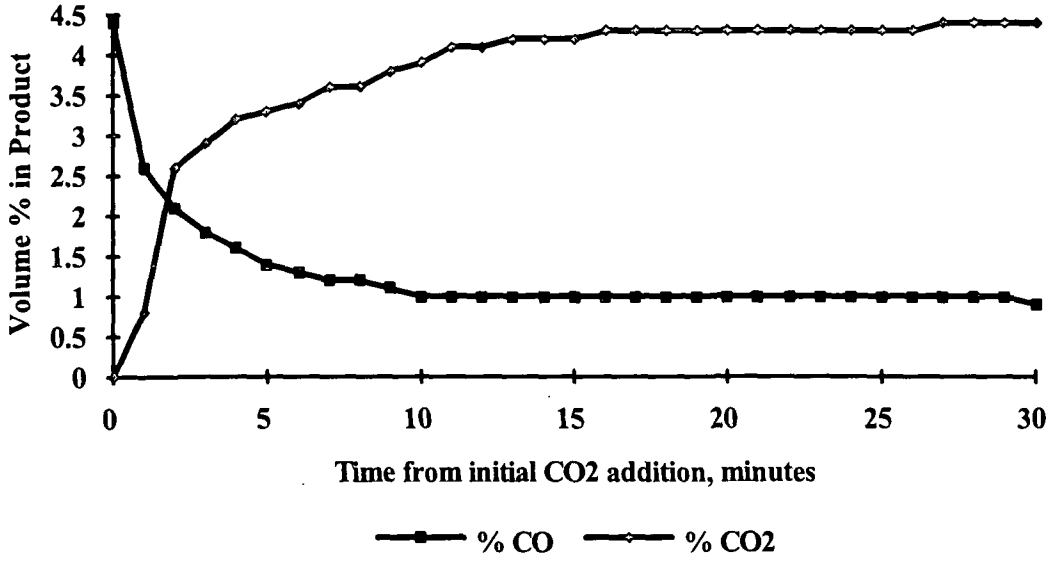


**Figure A8-4.** %CO and $\%CO_2$ in Product Gas as a Function of Time for Gasification Experiment 4973 (712°C, 4.8%$CO_2$, 5.5 slpm, $N_2$ Carrier Gas).

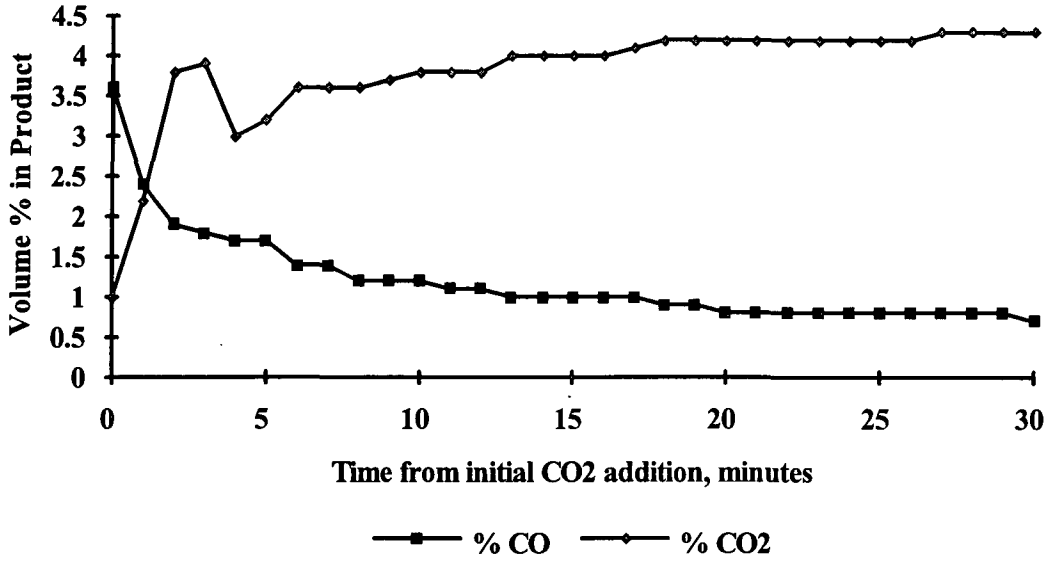


**Figure A8-5.** %CO and $\%CO_2$ in Product Gas as a Function of Time for Gasification Experiment 4975 (699°C, 4.8%$CO_2$, 5.4 slpm, $N_2$ Carrier Gas).

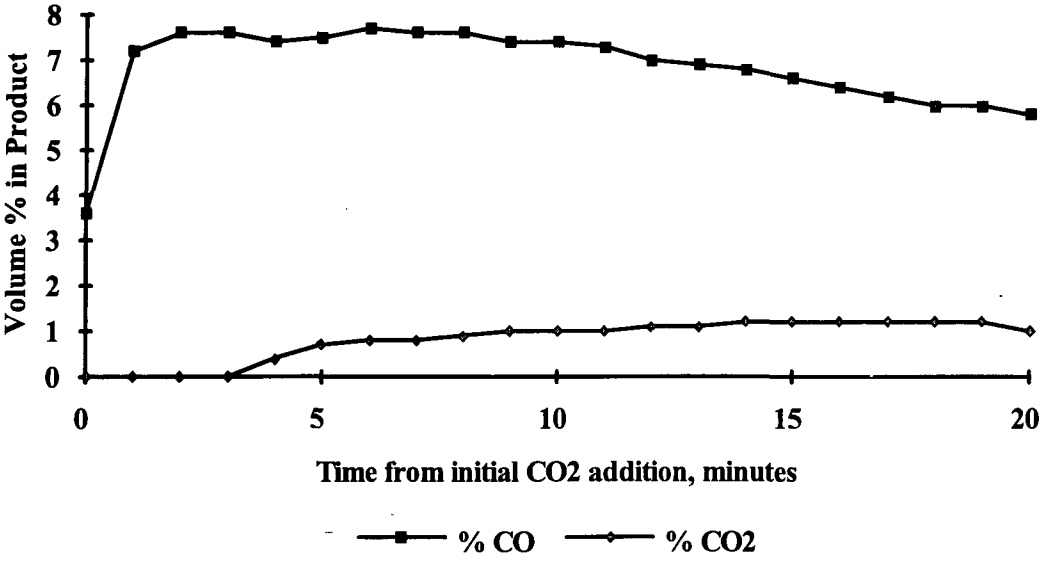


**Figure A8-6.** %CO and $\%CO_2$ in Product Gas as a Function of Time for Gasification Experiment 4976 (799°C, 4.8%$CO_2$, 5.5 slpm, $N_2$ Carrier Gas).

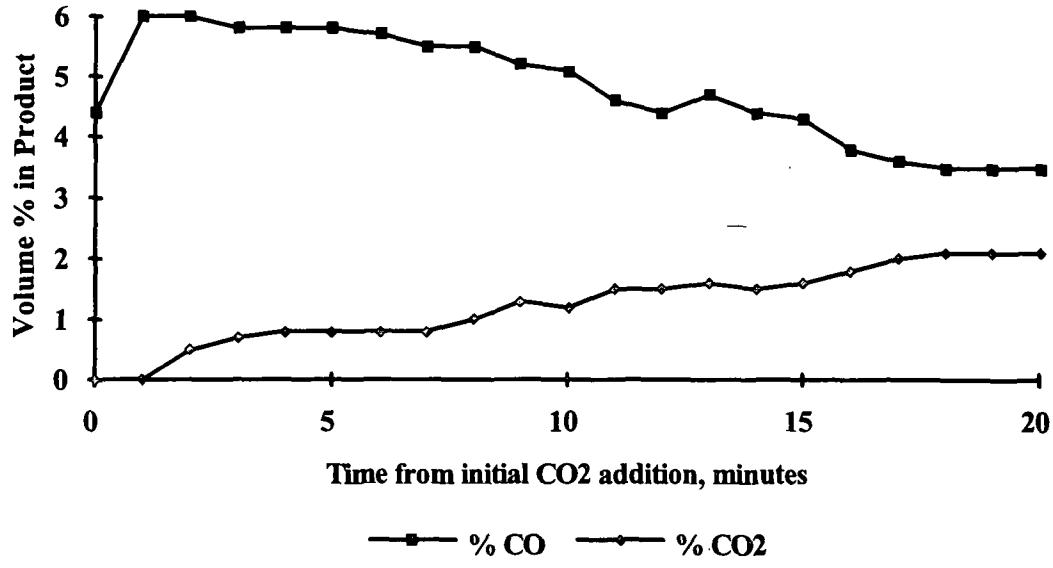


**Figure A8-7.** %CO and $\%CO_2$ in Product Gas as a Function of Time for Gasification Experiment 4977 (795°C, 4.8%$CO_2$, 5.5 slpm, $N_2$ Carrier Gas).

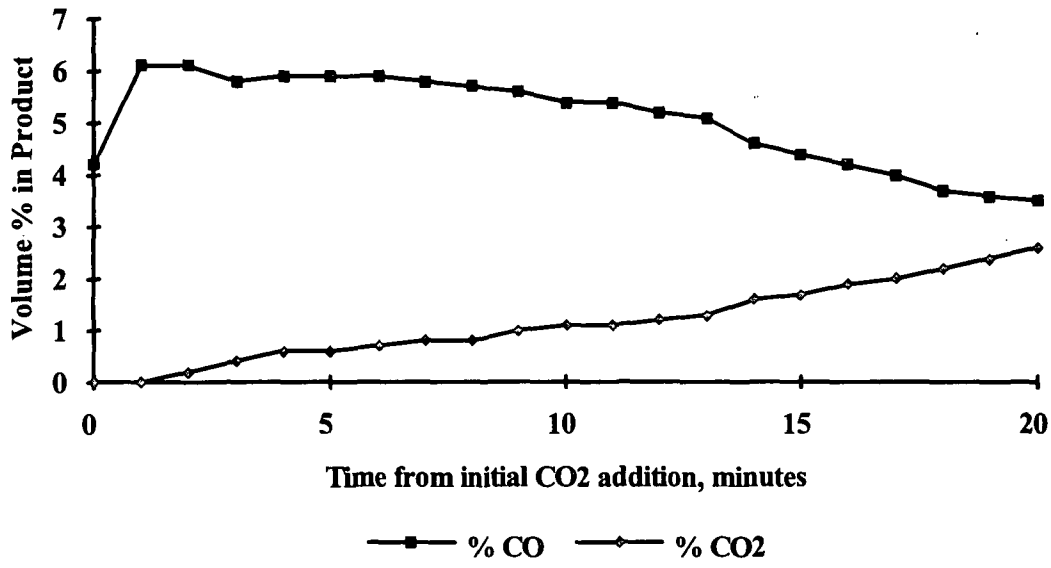


**Figure A8-8.** %CO and $\%CO_2$ in Product Gas as a Function of Time for Gasification Experiment 4989 (801°C, 5.1%$CO_2$, 5.2 slpm, $N_2$ Carrier Gas).

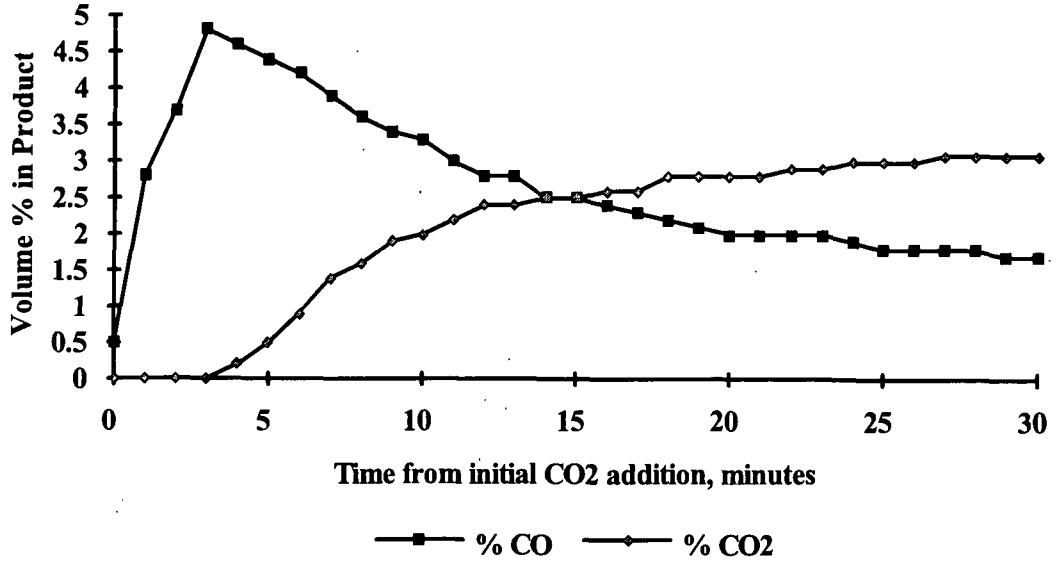


**Figure A8-9.** %CO and $\%CO_2$ in Product Gas as a Function of Time for Gasification Experiment 4985 (696°C, 4.8%$CO_2$, 2.7 slpm, $N_2$ Carrier Gas).

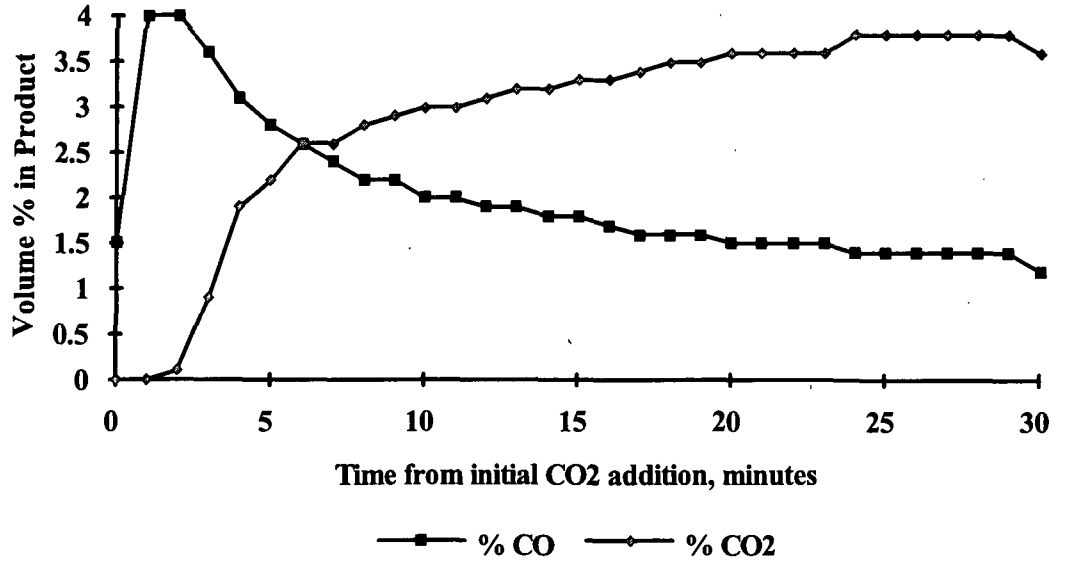


**Figure A8-10.** %CO and $\%CO_2$ in Product Gas as a Function of Time for Gasification Experiment 4990 (699°C, 5.1%$CO_2$, 2.6 slpm, $N_2$ Carrier Gas).

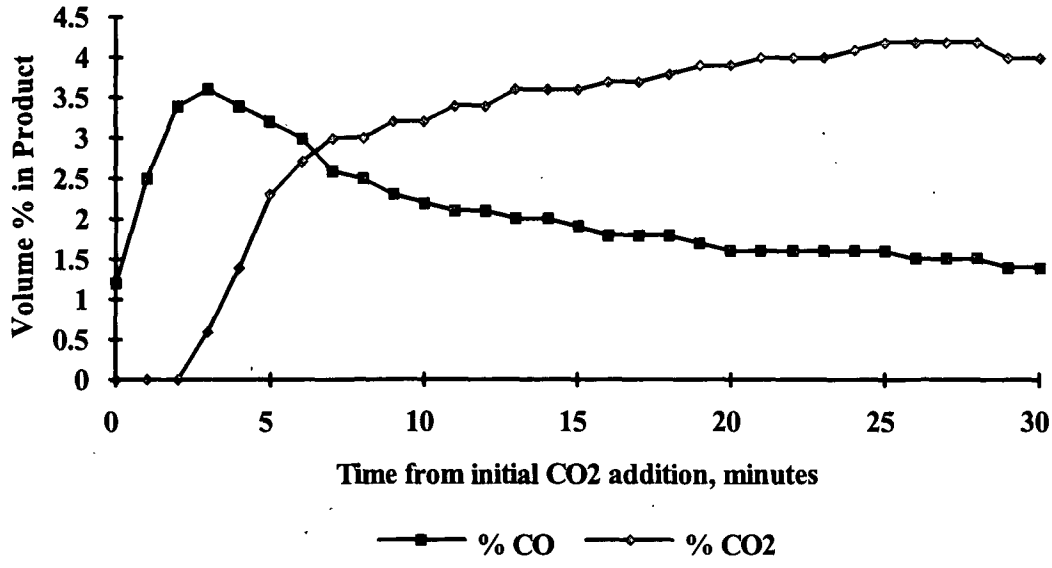


**Figure A8-11.** %CO and $\%CO_2$ in Product Gas as a Function of Time for Gasification Experiment 4991 (693°C, 5.1%$CO_2$, 2.7 slpm, $N_2$ Carrier Gas).

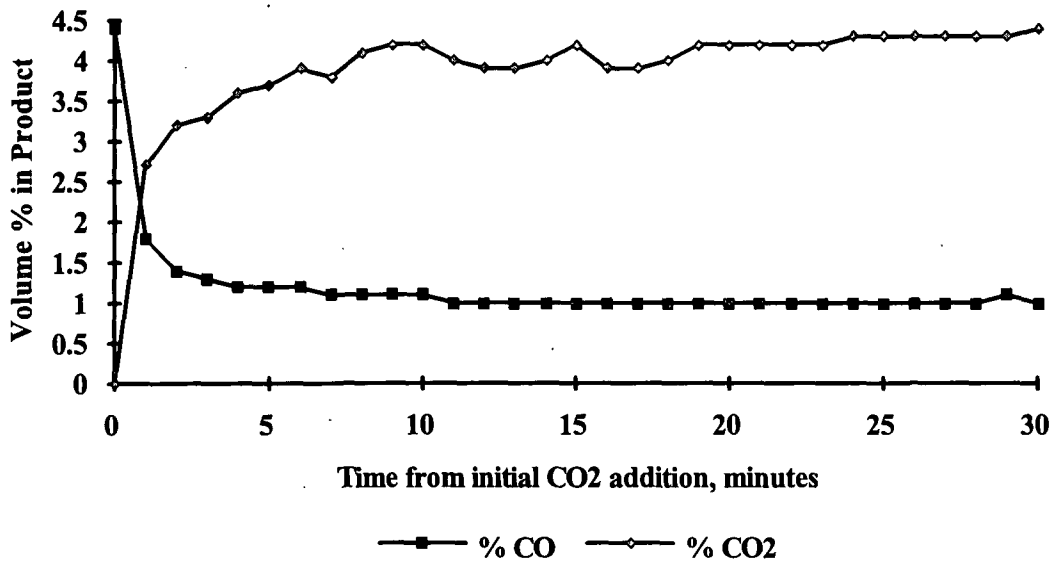


**Figure A8-12.** %CO and $\%CO_2$ in Product Gas as a Function of Time for Gasification Experiment 4974 (697°C, 5.0%$CO_2$, 5.3 slpm, He Carrier Gas).

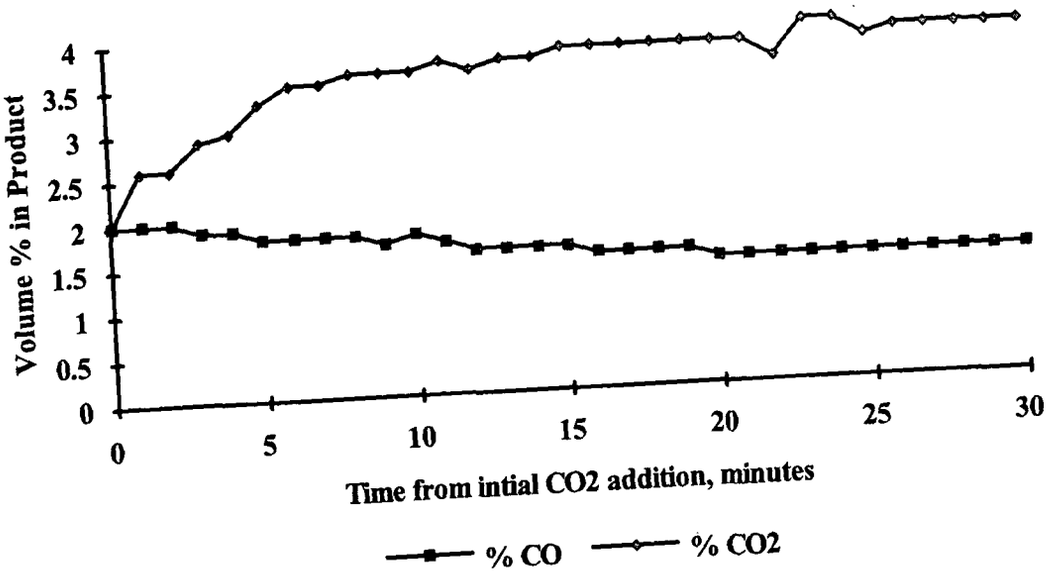


**Figure A8-13.** %CO and $\%CO_2$ in Product Gas as a Function of Time for Gasification Experiment 4983 (698°C, 4.8%$CO_2$, 5.5 slpm, He Carrier Gas).

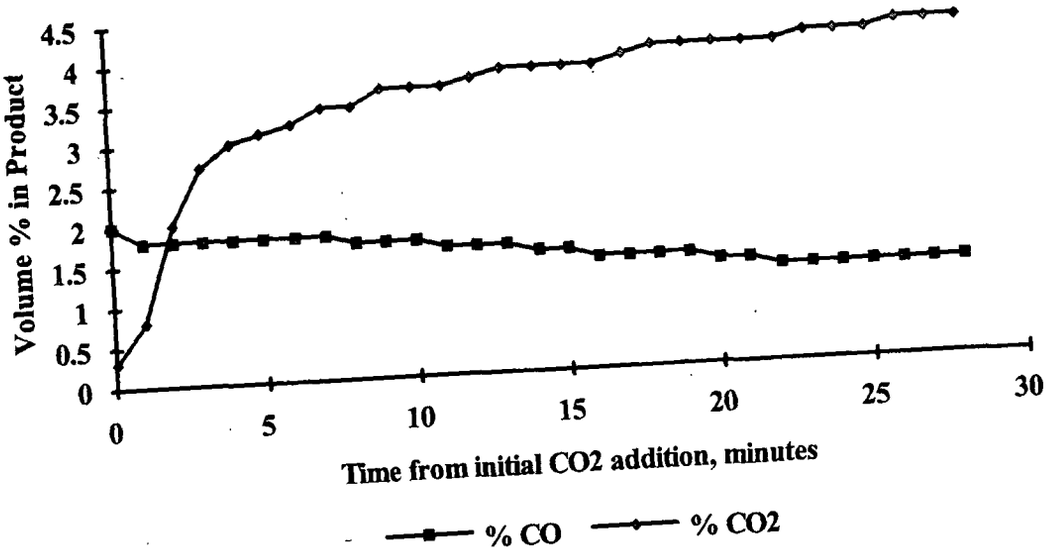


**Figure A8-14.** %CO and $\%CO_2$ in Product Gas as a Function of Time for Gasification Experiment 4984 (699°C, 4.9%$CO_2$, 5.4 slpm, He Carrier Gas).

# APPENDIX IX: ELEMENTAL ANALYSIS DATA

There were over 90 fixed bed experiments performed during the $CO_2$ gasification, $O_2$ oxidation, and $CO_2/O_2$ combustion studies. A few of the residual beds were lost or damaged during extraction from the furnace. Table A9-1 contains the elemental analysis data for the residual chars gasified by $CO_2$ and prepared according to the RTPP. Table A9-2 contains the elemental analysis data for the residual chars gasified by $CO_2$ and prepared according to the MTPP. Table A9-3 contains the elemental analysis data for the residual chars oxidized by $O_2$ and prepared according to the MTPP. Table A9-4 contains the elemental analysis data for the residual chars exposed to $CO_2/O_2$ and prepared according to the MTPP.

**Table A9-1.** Elemental Analysis of Residual Chars Gasified by $CO_2$ and Prepared According to the Reaction Temperature Preheat Procedure.

| Exp. Num. | Temp., (°C) | Intial $CO_2$ Conc., (vol. %) | Carrier Gas | Gas Flow Rate, (slpm) | Carbon, (wt. %) | Carbonate C, (wt. %) | Sulfur, (wt. %) | Sulfate S, (wt %) | Thiosulfate S, (wt. %) | Sulfide S, (wt. %) | Sulfite S, (wt. %) | Sodium, (wt. %) | Oxygen-Merz, (wt%) | Hydrogen, (wt. %) |
|---|---|---|---|---|---|---|---|---|---|---|---|---|---|---|
| 4,902 | 702 | 4.3 | $N_2$ | 5.3 | 16.5 | 7.22 | NA | 1.71 | 0.2 | NA | NA | NA | NA | 1.77 |
| 4,903 | 700 | 4.4 | $N_2$ | 5.3 | 18.32 | 6.93 | NA | 2.14 | 0.16 | NA | NA | NA | NA | 1.66 |
| 4,904 | 701 | 4.3 | $N_2$ | 5.3 | 22.73 | 6.3 | NA | 1.92 | 0.57 | NA | NA | NA | NA | 1.54 |
| 4,905 | 801 | 4.4 | $N_2$ | 5.3 | 14.48 | 6.02 | NA | 1.69 | 0.47 | NA | NA | NA | NA | 1.4 |
| 4,906 | 800 | 4.4 | $N_2$ | 5.4 | 15.35 | 7.13 | NA | NA | NA | NA | NA | NA | NA | 1.27 |
| 4,907 | 799 | 4.3 | $N_2$ | 5.3 | 29.75 | 5.67 | NA | 1.92 | 0.06 | NA | NA | NA | NA | 1.52 |
| 4,908 | 608 | 4.3 | $N_2$ | 5.3 | 29.55 | 5.78 | NA | 1.32 | 0.04 | NA | NA | NA | NA | 1.41 |
| 4,909 | 601 | 4.3 | $N_2$ | 5.3 | 30.31 | 6.02 | NA | 1.39 | 0.03 | NA | NA | NA | NA | 1.44 |
| 4,910 | 600 | 4.3 | $N_2$ | 5.3 | 28.97 | 6.41 | NA | 1.26 | 0.05 | NA | NA | NA | NA | 1.63 |
| 4,911 | 604 | 4.4 | $N_2$ | 5.3 | 22.52 | 5.81 | NA | 1.37 | 0.29 | NA | NA | NA | NA | 1.58 |
| 4,913 | 800 | 4.9 | He | 5.4 | 14.56 | 6.93 | NA | 1.6 | 0.7 | NA | NA | NA | NA | 1.42 |
| 4,914 | 800 | 4.8 | He | 5.4 | 14.9 | 6.83 | NA | 1.66 | 0.71 | NA | NA | NA | NA | 1.43 |
| 4,915 | 803 | 4.9 | He | 5.4 | 16.07 | 6.89 | NA | 1.88 | 0.34 | NA | NA | NA | NA | 1.34 |
| 4,916 | 801 | 4.7 | $N_2$ | 10.6 | 17.47 | 6.86 | NA | 0.23 | 0.49 | NA | NA | NA | NA | 1.44 |
| 4,917 | 805 | 4.8 | $N_2$ | 10.6 | 11.79 | 7.33 | NA | 1.66 | 0.82 | NA | NA | NA | NA | 1.45 |
| 4,918 | 803 | 4.7 | $N_2$ | 10.6 | 12.78 | 7.14 | NA | 1.4 | 0.66 | NA | NA | NA | NA | 1.49 |

**Table A9-2.** Elemental Analysis of Residual Chars Gasified by $CO_2$ and Prepared According to the Maximum Temperature Preheat Procedure.

| Exp. Num. | Temp., (°C) | Intial $CO_2$ Conc., (vol. %) | Carrier Gas | Gas Flow Rate, (slpm) | Carbon, (wt. %) | Carbonate C, (wt. %) | Sulfur, (wt. %) | Sulfate S, (wt %) | Thiosulfate S, (wt. %) | Sulfide S, (wt. %) | Sulfite S, (wt. %) | Sodium, (wt. %) | Oxygen-Merz, (wt%) | Hydrogen, (wt. %) |
|---|---|---|---|---|---|---|---|---|---|---|---|---|---|---|
| 4,979 | 604 | 4.8 | $N_2$ | 5.4 | 38.83 | 1.55 | 17.65 | 23.33 | 0.45 | 0.05 | 6.55 | 10.67 | 28.46 | 0.71 |
| 4,982 | 602 | 4.7 | $N_2$ | 5.5 | 39.6 | 2.3 | 18.88 | 12.94 | 2.37 | 2.25 | 3.52 | 9.28 | 27.86 | 0.57 |
| 4,972 | 712 | 4.8 | $N_2$ | 5.5 | 34.43 | 1.37 | 18.84 | 25.28 | 1.06 | 0.26 | 5.48 | 12.38 | 31.35 | 0.46 |
| 4,973 | 712 | 4.8 | $N_2$ | 5.5 | 35.43 | 1.27 | 18.87 | 26.37 | 0.86 | 0.29 | 3.4 | 12.8 | 30.59 | 0.58 |
| 4,975 | 699 | 4.8 | $N_2$ | 5.4 | 33.43 | 1.46 | 18.81 | 24.18 | 1.26 | 0.23 | 7.55 | 11.95 | 32.1 | 0.34 |
| 4,976 | 799 | 4.8 | $N_2$ | 5.5 | 21.43 | 1.86 | 20.26 | 26.34 | 0.05 | 0.83 | 13.08 | 14.78 | 38.22 | 1.08 |
| 4,977 | 795 | 4.8 | $N_2$ | 5.5 | 15.41 | 1.96 | 27.09 | 15.09 | 6.96 | 2.46 | 16.52 | 18.01 | 37.39 | 1.38 |
| 4,989 | 801 | 5.1 | $N_2$ | 5.2 | 9.38 | 2.06 | 33.91 | 3.83 | 13.86 | 4.09 | 19.96 | 21.24 | 36.55 | 1.67 |
| 4,985 | 696 | 4.8 | $N_2$ | 2.7 | 28.18 | 3.77 | 26.75 | 11.4 | 3.67 | 0.81 | 7.06 | 8.92 | 32.52 | 0.81 |
| 4,990 | 699 | 5.1 | $N_2$ | 2.6 | 29.2 | 3.62 | 27.83 | 12.32 | 0.84 | 0.32 | 14.11 | 10.51 | 30.41 | 0.44 |
| 4,991 | 693 | 5.1 | $N_2$ | 2.7 | 27.15 | 3.92 | 25.67 | 10.48 | 6.49 | 1.29 | NA | 7.33 | 34.63 | 1.17 |
| 4,974 | 697 | 5 | He | 5.3 | 37.46 | 2.92 | 18.35 | 15.64 | 3.61 | 0.92 | 3.89 | 9.64 | 32.97 | 0.7 |
| 4,983 | 698 | 4.8 | He | 5.5 | 37.95 | 2.03 | 16.42 | 15.23 | 4.85 | 0.05 | 7.77 | 10.95 | 34.81 | 0.75 |
| 4,984 | 699 | 4.9 | He | 5.4 | 36.96 | 3.81 | 20.27 | 16.05 | 2.37 | 1.78 | NA | 14.78 | 31.13 | 0.65 |

**Table A9-3.** Elemental Analysis of Residual Chars Oxidized by $O_2$ and Prepared According to the Maximum Temperature Preheat Procedure.

| Exp. Num. | Temp., (°C) | Intial $O_2$ Conc., (vol. %) | Carrier Gas | Gas Flow Rate, (slpm) | Carbon, (wt. %) | Carbonate C, (wt. %) | Sulfur, (wt. %) | Sulfate S, (wt %) | Thiosulfate S, (wt. %) | Sulfide S, (wt. %) | Sulfite S, (wt. %) | Sodium, (wt. %) | Oxygen-Merz, (wt%) | Hydrogen, (wt. %) |
|---|---|---|---|---|---|---|---|---|---|---|---|---|---|---|
| 4,996 | 704 | 1.97 | $N_2$ | 5.46 | 12.33 | 3.9 | 32.06 | 19.69 | 3.14 | 1.04 | 5.03 | 11.34 | 38.38 | 0.7 |
| 5,001 | 696 | 2.17 | $N_2$ | 5.46 | 10.15 | 3.6 | 31.57 | 19.61 | 6.27 | 1.08 | 2.76 | 12.23 | 41.09 | 0.85 |
| 4,993 | 694 | 1.98 | $N_2$ | 5.46 | 21.36 | 1.73 | 29.21 | 14 | 6.46 | 0.52 | 18.67 | 16.29 | 31.24 | 1.25 |
| 4,994 | 703 | 2.35 | $N_2$ | 5.46 | 20.56 | 2.2 | 29.87 | 12.35 | 7.21 | 1.02 | 18.64 | 16.66 | 41.96 | 0.56 |
| 5,002 | 702 | 2.2 | $N_2$ | 5.46 | 19.56 | 3.3 | 30.38 | 14.55 | 2.97 | 1.03 | 11.34 | 12.06 | 39.62 | 0.84 |
| 4,997 | 697 | 4.55 | $N_2$ | 5.46 | 4.54 | 2.98 | 33.55 | 27.16 | 2.79 | 0.46 | 7.12 | 13.86 | 46.36 | 0.69 |
| 4,998 | 709 | 4.64 | $N_2$ | 5.46 | 8.02 | 3.72 | 35.77 | 24.5 | 3.49 | 1.39 | 4.46 | 13.25 | 39.48 | 0.66 |
| 4,999 | 698 | 4.71 | $N_2$ | 5.46 | 12.42 | 2.85 | 27.34 | 25.02 | 3.33 | 2.42 | 8.74 | 16.07 | 38.35 | 0.6 |
| 5,000 | 697 | 4.48 | $N_2$ | 5.46 | 15.04 | 2.15 | 35.79 | 8.95 | 8.1 | 1.35 | 9.15 | 12.58 | 38.19 | 0.67 |

**Table A9-4.** Elemental Analysis of Residual Chars exposed to $CO_2/O_2$ and Prepared According to the Maximum Temperature Preheat Procedure.

| Exp. Num. | Temp., (°C) | Intial $O_2$ Conc., (vol. %) | Intial $CO_2$ Conc., (vol. %) | Carrier Gas | Gas Flow Rate, (slpm) | Carbon, (wt. %) | Carbonate C, (wt. %) | Sulfur, (wt. %) | Sulfate S, (wt %) | Thiosulfate S, (wt. %) | Sulfide S, (wt. %) | Sulfite S, (wt. %) | Sodium, (wt. %) | Oxygen-Merz, (wt%) | Hydrogen, (wt. %) |
|---|---|---|---|---|---|---|---|---|---|---|---|---|---|---|---|
| 5,006 | 701 | 1.95 | 5.03 | $N_2$ | 5.46 | 14.39 | 3.46 | 11.22 | 3.46 | 3.02 | 1.84 | 12.9 | 32.43 | 37.01 | 0.52 |
| 5,008 | 700 | 2.19 | 4.87 | $N_2$ | 5.46 | 14.39 | 3.46 | 11.22 | 3.46 | 3.02 | 1.84 | 12.9 | 32.43 | 37.01 | 0.52 |
| 5,003 | 711 | 4.85 | 4.88 | $N_2$ | 5.46 | 8.06 | 3.72 | 12.55 | 3.72 | 8.62 | 2.47 | 0.68 | 36.18 | 43.82 | 0.87 |
| 5,004 | 708 | 4.82 | 4.79 | $N_2$ | 5.46 | 8.18 | 3.37 | 12.7 | 3.37 | 9.62 | 2.65 | NA | 34.23 | 43.9 | 0.77 |
| 5,005 | 706 | 4.66 | 4.92 | $N_2$ | 5.46 | 7.93 | 4.07 | 12.39 | 4.07 | 7.61 | 2.29 | 1.35 | 38.12 | 43.74 | 0.97 |

## APPENDIX X: TEMPERATURE GRADIENTS IN THE CHAR BED

The following discussion is based on the review by Smith.[89] Conservation of energy in reactors can be written as follows:

{Energy in streams entering volume element}
\- {Energy in streams leaving volume element}
\+ {Energy transferred from surroundings into volume element}
= {Accumulation of energy within volume element}.

In flow reactors, the energy in the flowing streams includes kinetic and potential energy contributions in addition to the enthalpy. However, when reactions occur these two contributions are normally unimportant.

Tubular-Flow Reactors

Since a differential volume element is necessary for a tubular reactor, it is appropriate to write an energy balance assuming no accumulation as follows:

$$dQ' = dH' \qquad \text{eqn. 10-1}$$

where the differentials refer to a change over a volume element. That is, dH' is the change in energy rate between the streams entering and leaving the volume element and dQ' is the rate of energy transfer into the differential volume element. The enthalpy difference will be due to the temperature change dT and a composition change associated with the reaction. Hence, a procedure for deriving an expression for dH is applicable here. If $F_t$ is the total molal feed flow rate through the reactor, and $c_p$ is the molal heat capacity (assumed constant) of the reaction mixture,

$$dH' = F_t c_p dT + \Delta H_R (rdV) \qquad \text{eqn. 10-2}$$

where rdV is the moles of reactant disappearing per unit time in the reactor volume dV, and $\Delta H_R$ is the molal heat of reaction. If the heat transfer rate can be expressed in terms of an overall coefficient $h_o$ and the surrounding temperature, $T_s$.

$$dQ' = h_o(T_s\text{-}T)dA_h \qquad \text{eqn. 10-3}$$

Here $dA_h$ is the effective heat transfer area in the volume element.

Substituting eqns. 7-2 and 7-3 into the equation 1 yields

$$h_o(T_s\text{-}T)dA_h = \Delta H_R(rdV) + F_t c_p dT \qquad \text{eqn. 10-4}$$

Since there is heat transfer from the reactor wall to the char bed, the temperature in the reactor will depend on the length z. If z is the reactor length and d is its diameter,

$$dV = \frac{\pi d^2}{4}dz \qquad \text{eqn. 10-5}$$

$$dA_h = \pi ddz \qquad \text{eqn. 10-6}$$

Using these relations in eqn. 7-4 gives

$$(F_t c_p)dT = \pi d h_o(T_s\text{-}T)dz - (r\Delta H_R)\left(\frac{\pi d^2}{4}\right)dz \qquad \text{eqn. 10-7}$$

or

$$\frac{dT}{dz} = \frac{\pi d h_o(T_s - T) - (r\Delta H_R)\frac{\pi d^2}{4}}{F_t c_p} \qquad \text{eqn. 10-8}$$

Table A10-1 shows the results for the fixed bed reactor assuming that $(T_s\text{-}T)$ is 0. That is the temperature of the surroundings is approximately equal to the bed temperature. According to these results, dT is approximately -4.5°C from the bottom to the top of the fixed bed.

**TABLE A10-1.** Parameters used in Determining $\Delta T$.

| Parameter | Value |
|---|---|
| Rate (gmole/$m^3$) | 8.77 |
| Molal Feed Rate (gmole/hr) | 3.66 |
| Molal Heat Capacity (KJ/gmole/K) | 0.06 |
| Reactor Diameter (m) | 0.07 |
| Reactor Length (m) | 0.15 |
| Heat of Rxn. (KJ/gmole) | 172 |
| $T_s$-T | 0 |
| $T_f$ (Feed Temperature), (K) | 1,073 |
| Delta T | -4.5 |

## APPENDIX XI: DISPERSION IN THE FIXED BED REACTOR

The mass conservation equation (eqn. 10) used to predict the rate constant is written for isothermal plug-flow through the fixed bed. Experimental observations suggest that dispersion is neglible since the residual char beds are uniform in appearance and the product gas concentrations do not show any unusual peaks or dips. The degree of dispersion within the reactor was determined experimentally.

Levenspiel[90] explains that many types of models can be used to characterize nonideal flow within vessels. Dispersion models draw on the analogy between mixing in actual flow and a diffusional process. The model used in this study is useful in accounting for the deviation of real systems from plug flow. Levenspiel explains that the one parameter model used here adequately represents packed beds. The predictions of the dispersion model should range from plug flow at one extreme to mixed flow at the other. For molecular diffusion in the x direction the governing differential equation is given by Fick's second law

$$\frac{\partial C}{\partial t} = D\frac{\partial^2 C}{\partial x^2} \qquad \text{eqn. A11-1}$$

where the parameter $D$, the longitudinal or axial dispersion coefficient, uniquely characterizes the degree of backmixing during flow. Levenspiel uses the terms "longitudinal" and "axial" to distinguish mixing in the direction of flow from mixing in the lateral or radial direction. These two quantities may be quite different in magnitude. For example, Levenspiel notes that in streamline flow of fluids through pipes, axial mixing is mainly due to fluid velocity gradients whereas radial mixing is due to molecular diffusion alone.

In dimensionless form where $z = (ut + x)/L$ and $\theta = \frac{t}{\bar{t}} = \frac{tu}{L}$ the basic differential equation representing this dispersion model becomes

$$\frac{\partial C}{\partial \theta} = \left(\frac{D}{uL}\right)\frac{\partial^2 C}{\partial z^2} - \frac{\partial C}{\partial z} \qquad \text{eqn. A11-2}$$

Levenspiel defines the vessel dispersion number, $\left(\frac{D}{uL}\right)$, as the parameter which measures the extent of axial dispersion. Thus,

$\left(\frac{D}{uL}\right) \to 0$ negligible dispersion, hence plug flow

$\left(\frac{D}{uL}\right) \to \infty$ large dispersion, hence mixed flow

This model usually represents quite satisfactorily flow that deviates not too greatly from plug flow, thus simulating real packed beds and tubes.

Step Test

A step test was conducted on the fixed bed reactor at room temperature (25°C) to determine the vessel dispersion number. With no tracer ($CO_2$) initially present anywhere, a step input of $CO_2$ ($C_o$ = 5.5%) is imposed on the gas stream entering the vessel. Fig. A11-1 shows the input and output $CO_2$ concentration for a typical step experiment. It should be noted that the residence time is approximately 2 minutes. A time record of $CO_2$ in the exit stream from the vessel, measured as $C/C_o$, is called the F curve. Fig. A11-2 shows a sketch of this curve and it can be seen that it always rises from 0 to 1.

Levenspiel notes that elements of fluid taking different routes through the reactor may require different lengths of time to pass through the vessel. The distribution of these times for the stream of fluid leaving the vessel is called the exit age distributuon E, or the residence time distributuon RTD of fluid. Levenspiel conveniently represents the RTD in such a way that the area under the curve is unity, or

$$\int_0^\infty E dt = 1 \qquad \text{eqn. A11-3}$$

With this representation, the fraction of exit stream of age (Levenspiel defines the term "age" for an element of the exit stream as the time spent by that element in the vessel) between t and t + dt is

$$Edt \qquad \text{eqn. A11-4}$$

the fraction younger than age $t_1$ is

$$\int_0^{t_1} Edt. \qquad \text{eqn. A11-5}$$

The E curve, time versus E, is the distribution needed to account for nonideal flow. Levenspiel defines the area under a concentration-time curve as Q.

$$Q = \sum C\Delta t \qquad \text{eqn. A11-6}$$

To find E, the area under this curve must be unity; hence the concentration readings much each be divided by Q, giving

$$E = \frac{C}{Q}. \qquad \text{eqn. A11-7}$$

A typical E curve is shown in Fig. A11-3.

To relate E with F, imagine a steady flow of nitrogen through the fixed bed reactor. Then at time t = 0 switch to 5%$CO_2$/95%$N_2$ and record the rising concentration of $CO_2$ in the exit stream, the F curve. At any time t > 0, $CO_2$ and only $CO_2$ in the exit stream is younger than age t. Thus we have

(fraction of $CO_2$ in the exit stream) = (fraction of exit stream younger than age t)

But the first term is simply the F value, while the second is given by eqn. A11.5. So we have, at time t,

$$F = \int_0^t Edt. \qquad \text{eqn. A11-8}$$

It is desirable to characterize a distribution by a few numerical values. Levenspiel notes that the most important measure is the location of the distribution called the mean value or the centroid of the distribution. If the distribution curve is only known at a number of discrete time value $t_i$, then

$$\bar{t} = \sum t_i E_i \Delta t \qquad \text{eqn. A11-9}$$

The next most important descriptive quantity is the spread of the distribution. This is commonly measured by the variance $\sigma^2$.

$$\sigma^2 = \sum t_i^2 E_i \Delta t - \bar{t}^2 \qquad \text{eqn. A11-10}$$

Having defined the above mentioned parameters, the vessel dispersion number can be determined from the following relationships. The standard deviation is defined in dimensionless time units as follows:

$$\sigma_\theta = \frac{\sigma}{\bar{t}} \qquad \text{eqn. A11-11}$$

Hence the variance, $\sigma_\theta^2$ can be used to predict the vessel dispersion number for the system as follows:

$$\frac{D}{uL} = \frac{\sigma_\theta^2}{2} \qquad \text{eqn. A11-12}$$

The experimentally determined vessel dispersion number for three step experiments with the char bed and one without the char bed were 0.020, 0.019, 0.020, and 0.023, respectively. Levenspiel notes that when the vessel dispersion number is approximately 0.025, there exists only intermediate amounts of dispersion, so we conclude that there is an intermediate level of dispersion in our system. Levenspiel notes that dispersion is either negligible or large when the dispersion number is less 0.002 or greater than 0.2, respectively. Although the experimentally determined vessel dispersion number is considered to be of an intermediate level, the dispersion effects on our system can be considered negligible based on experimental observations that the residual char beds are uniform in appearance and the product gas concentrations do not show any unusual peaks or dips.

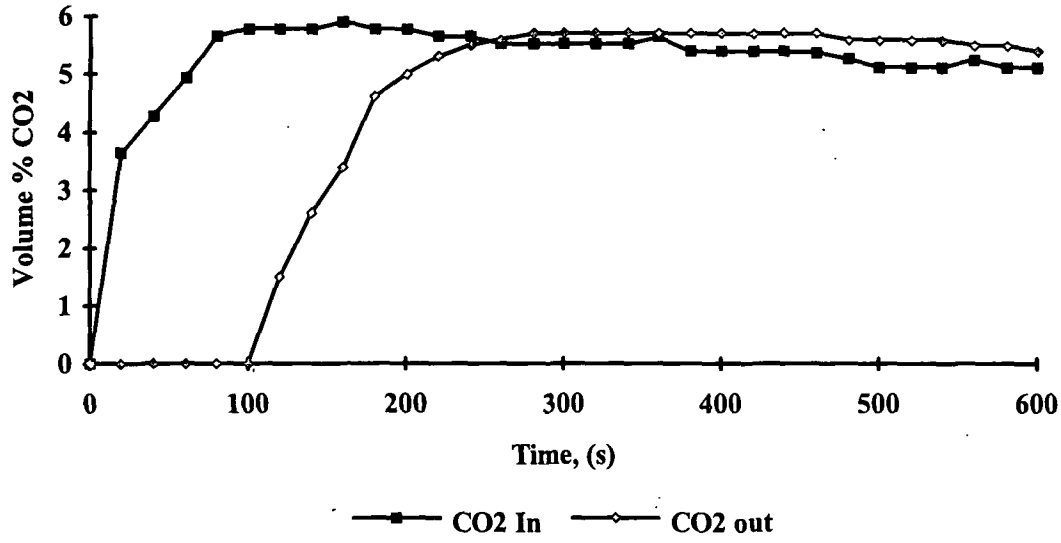


**Figure A11-1.** Typical $CO_2$ Input and Output Plot for Fixed Bed Reactor Step Test.

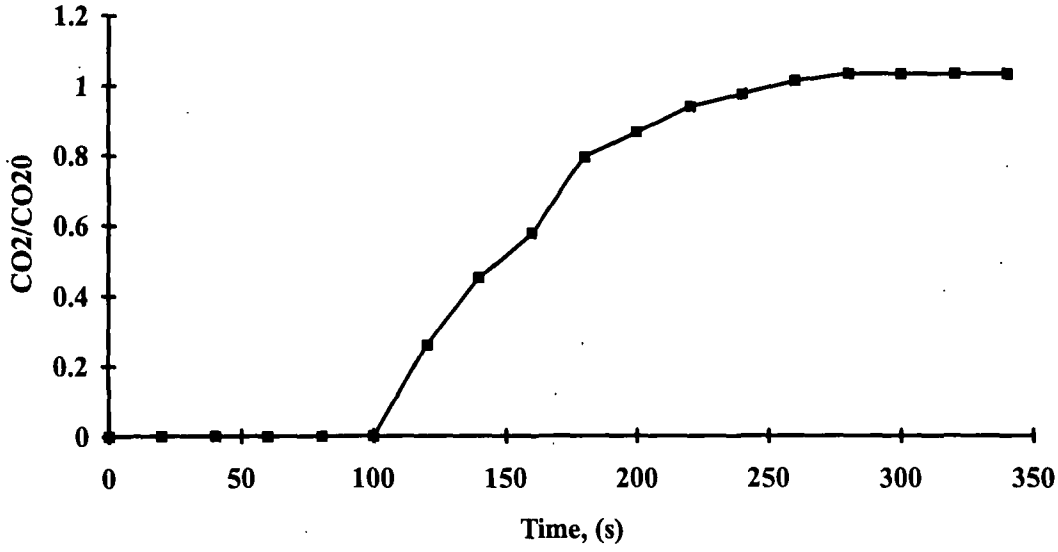


**Figure A11-2:** Typical F Curve for Fixed Bed Reactor Step Test.

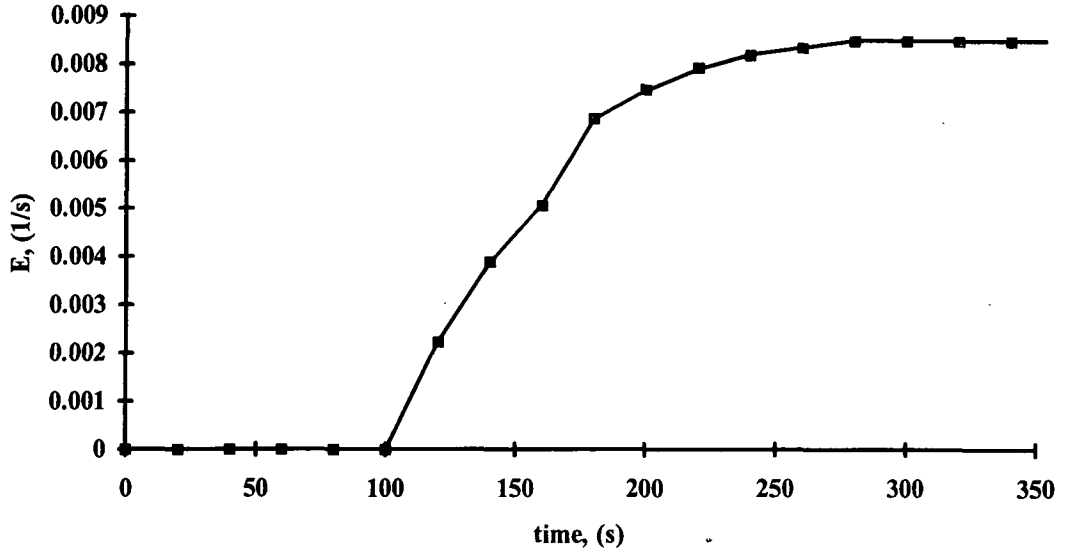


**Figure A11-3:** Typical E Curve for Fixed Bed Reactor Step Test.

APPENDIX XII. RATE CONSTANT PROFILES FOR $CO_2$ GASIFICATION OF KRAFT BLACK LIQUOR CHAR PREPARED ACCORDING TO THE REACTION TEMPERATURE PREHEAT PROCEDURE

Figs. A12-1-A12-16 are the complete sets of Rate Constant profiles recorded at the various experimental conditions outlined in Table 6.

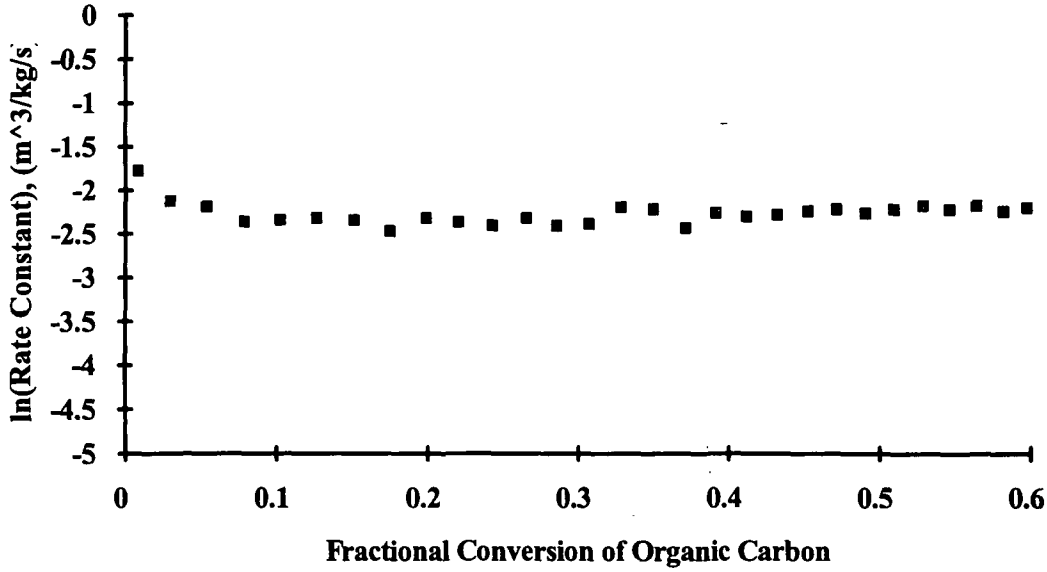


**Figure A12-1.** First Order Rate Constant vs. Fractional Burnout of Organic Carbon for Gasification Experiment 4902 (702°C, 4.3%$CO_2$, 5.3 slpm, $N_2$ Carrier Gas).

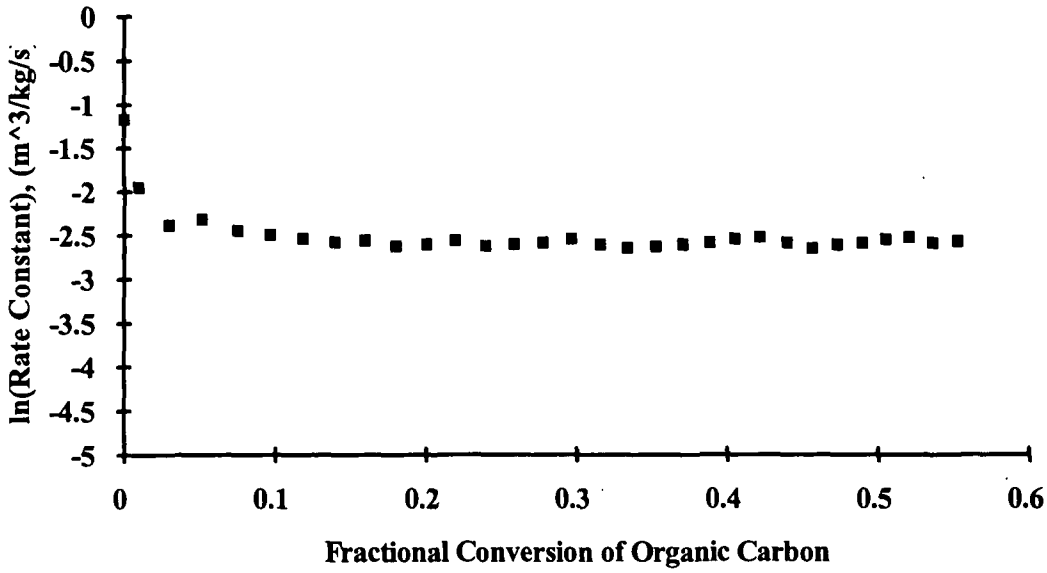


**Figure A12-2.** First Order Rate Constant vs. Fractional Burnout of Organic Carbon for Gasification Experiment 4903 (700°C, 4.4%$CO_2$, 5.3 slpm, $N_2$ Carrier Gas).

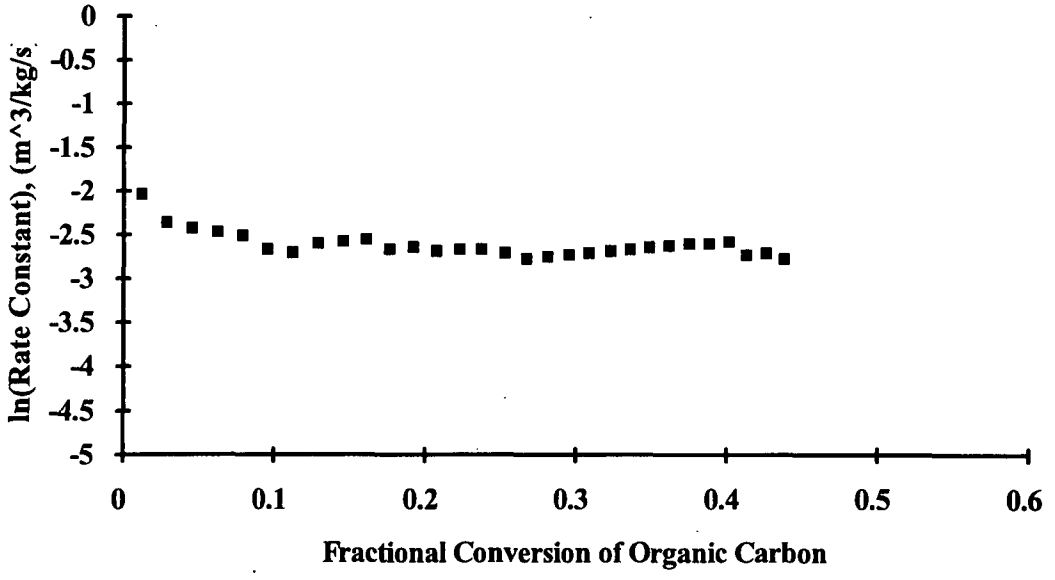


**Figure A12-3.** First Order Rate Constant vs. Fractional Burnout of Organic Carbon for Gasification Experiment 4904 (701°C, 4.3%$CO_2$, 5.3 slpm, $N_2$ Carrier Gas).

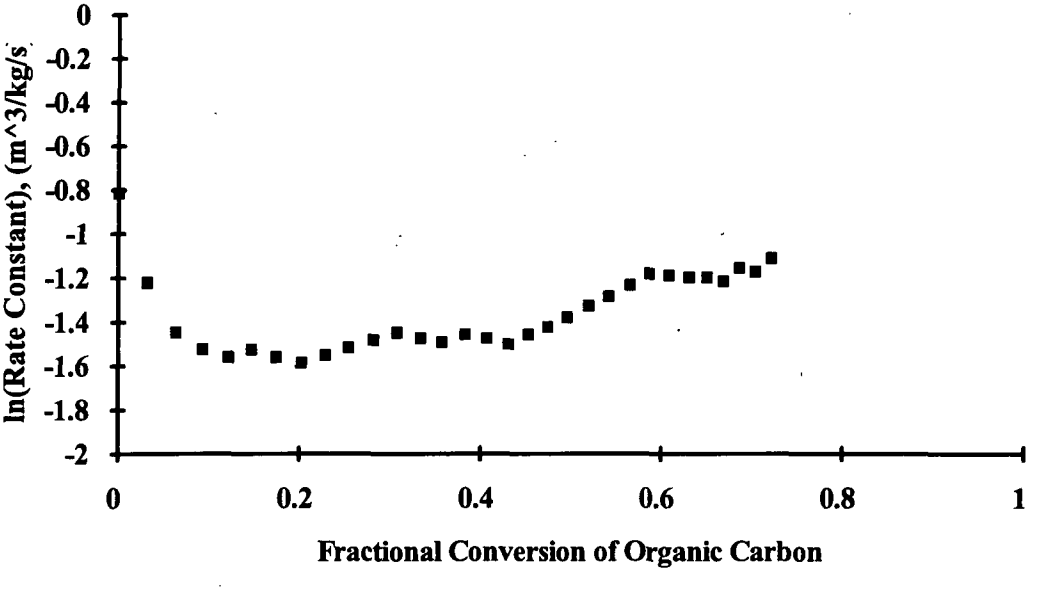


**Figure A12-4.** First Order Rate Constant vs. Fractional Burnout of Organic Carbon for Gasification Experiment 4905 (801°C, 4.4%$CO_2$, 5.3 slpm, $N_2$ Carrier Gas).

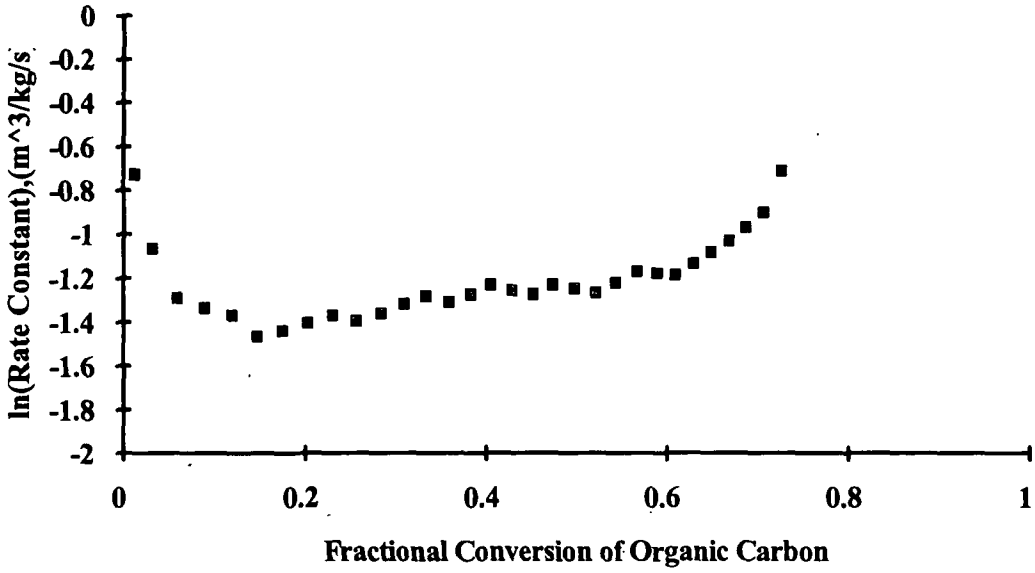


**Figure A12-5.** First Order Rate Constant vs. Fractional Burnout of Organic Carbon for Gasification Experiment 4906 (800°C, 4.4%$CO_2$, 5.4 slpm, $N_2$ Carrier Gas).

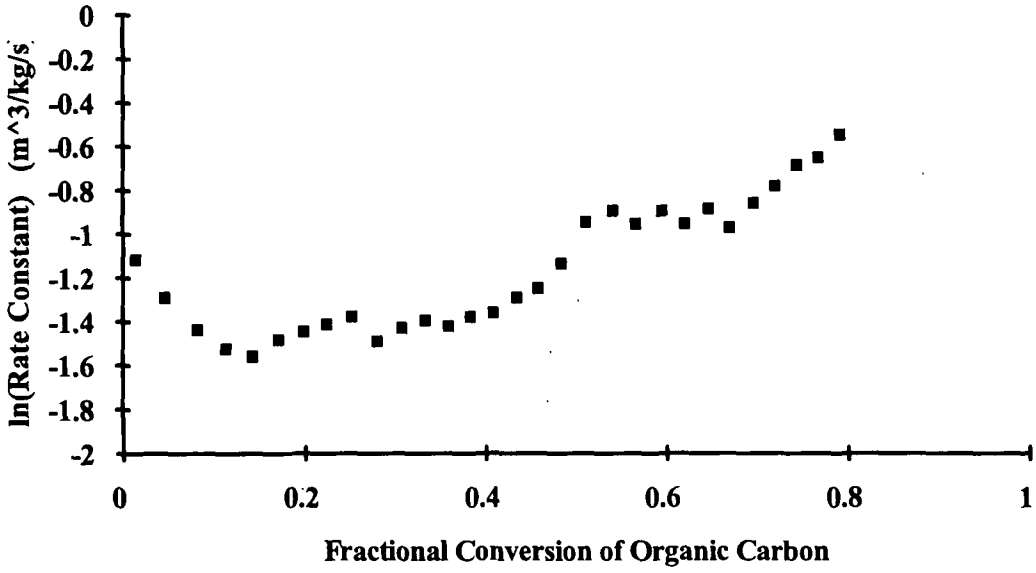


**Figure A12-6.** First Order Rate Constant vs. Fractional Burnout of Organic Carbon for Gasification Experiment 4907 (799°C, 4.3%$CO_2$, 5.3 slpm, $N_2$ Carrier Gas).

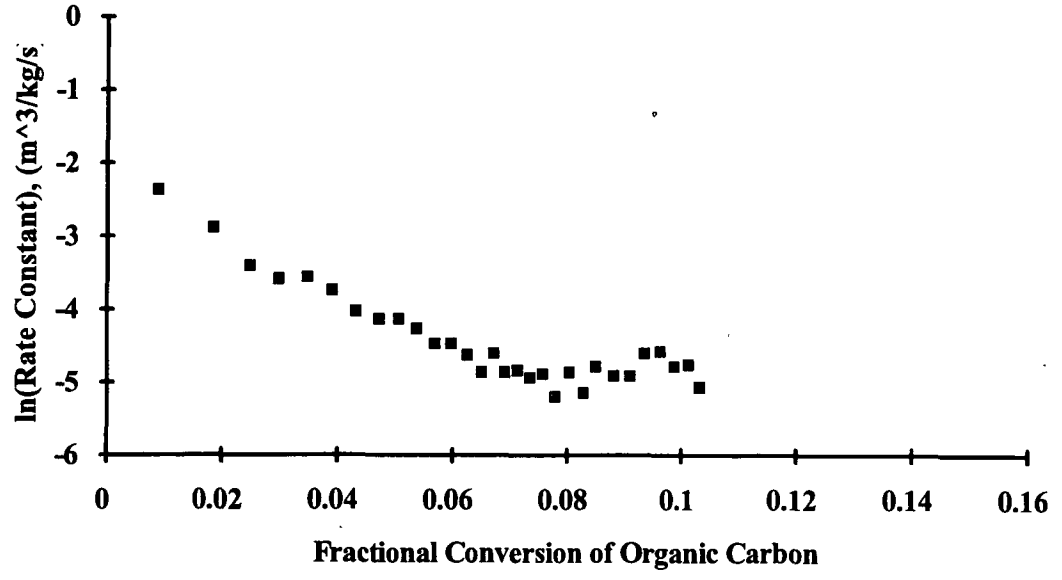


**Figure A12-7.** First Order Rate Constant vs. Fractional Burnout of Organic Carbon for Gasification Experiment 4908 (608°C, 4.3%$CO_2$, 5.3 slpm, $N_2$ Carrier Gas).

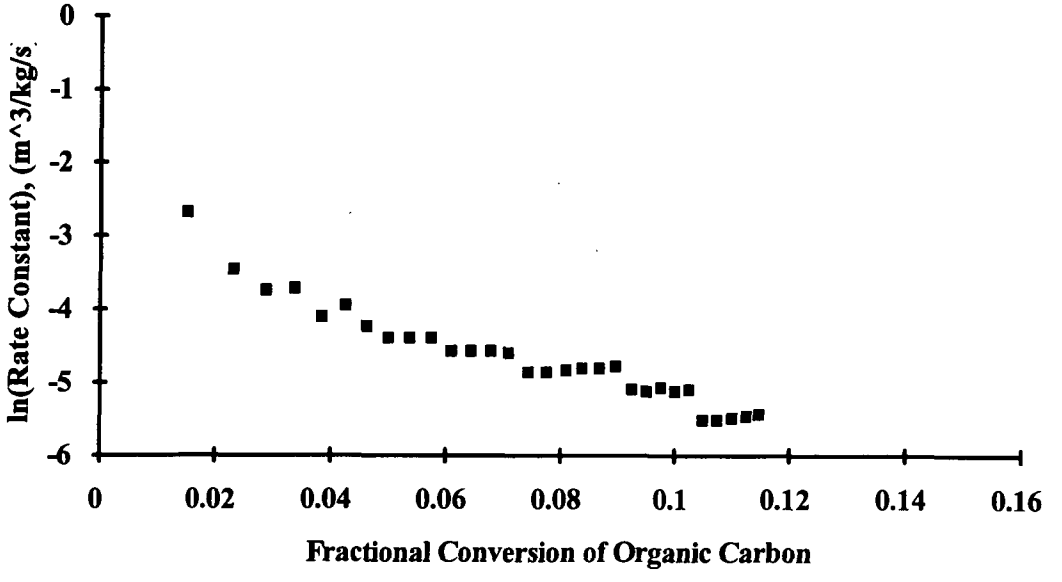


**Figure A12-8.** First Order Rate Constant vs. Fractional Burnout of Organic Carbon for Gasification Experiment 4909 (601°C, 4.3%$CO_2$, 5.3 slpm, $N_2$ Carrier Gas).

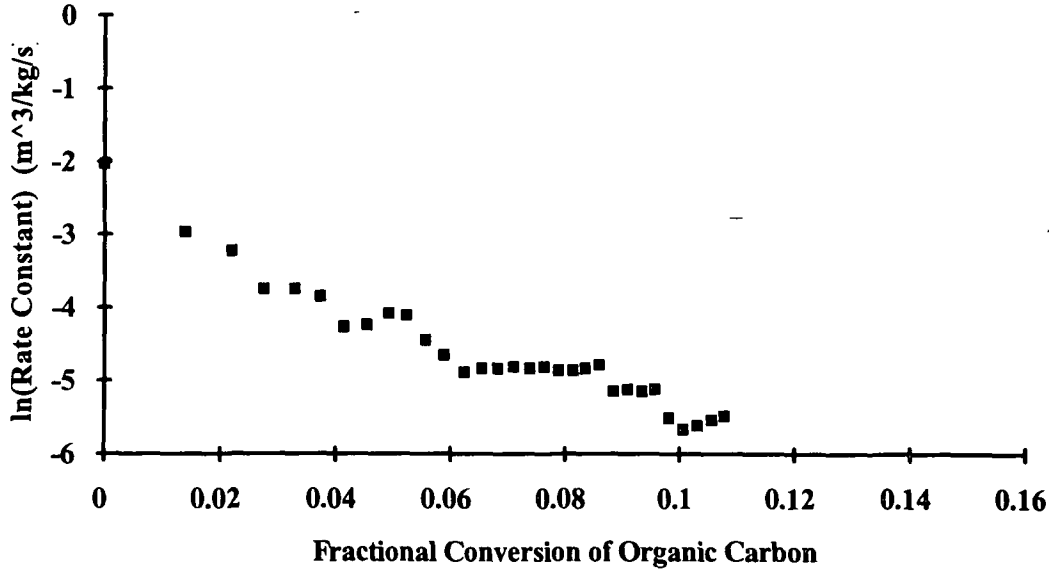


**Figure A12-9.** First Order Rate Constant vs. Fractional Burnout of Organic Carbon for Gasification Experiment 4910 (600°C, 4.3%$CO_2$, 5.3 slpm, $N_2$ Carrier Gas).

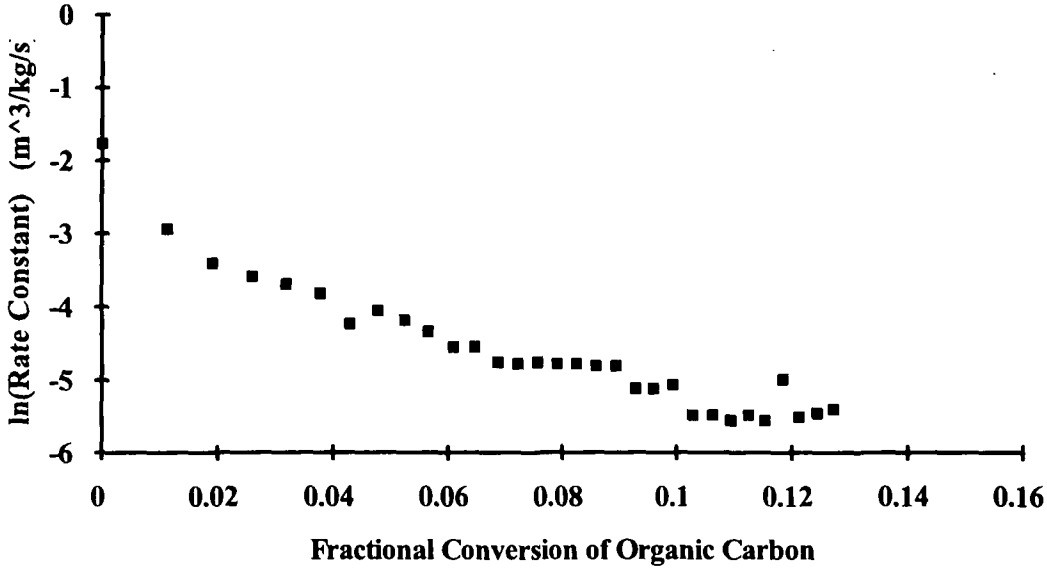


**Figure A12-10.** First Order Rate Constant vs. Fractional Burnout of Organic Carbon for Gasification Experiment 4911 (604°C, 4.4%$CO_2$, 5.3 slpm, $N_2$ Carrier Gas).

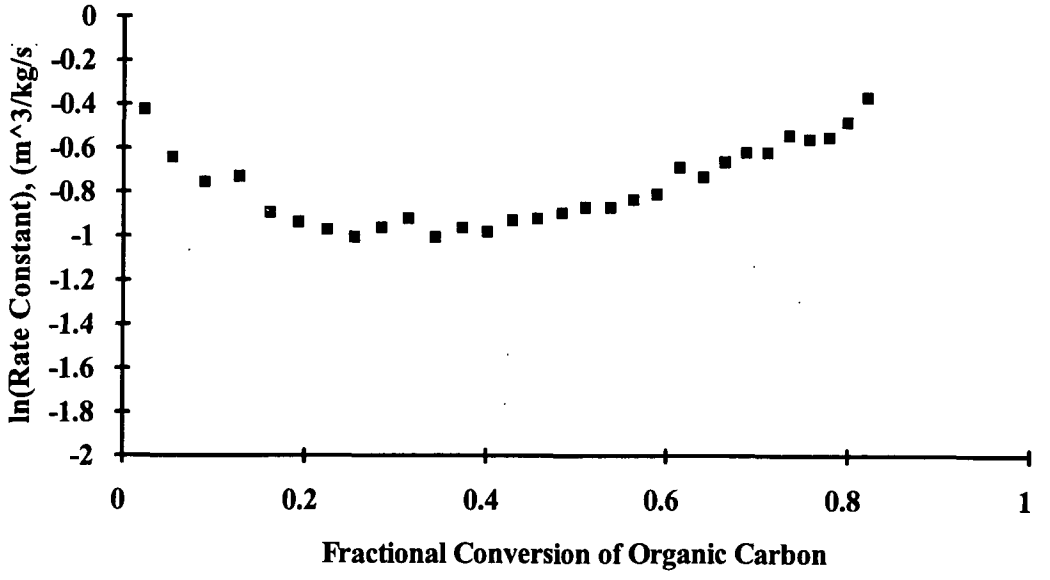


**Figure A12-11.** First Order Rate Constant vs. Fractional Burnout of Organic Carbon for Gasification Experiment 4913 (800°C, 4.9%$CO_2$, 5.4 slpm, He Carrier Gas).

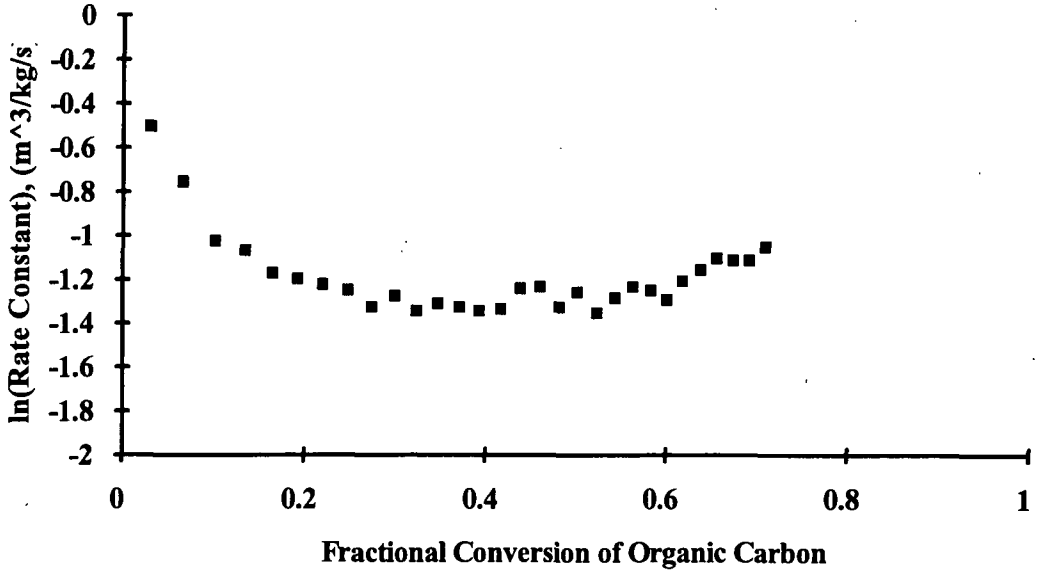


**Figure A12-12.** First Order Rate Constant vs. Fractional Burnout of Organic Carbon for Gasification Experiment 4914 (800°C, 4.8%$CO_2$, 5.4 slpm, He Carrier Gas).

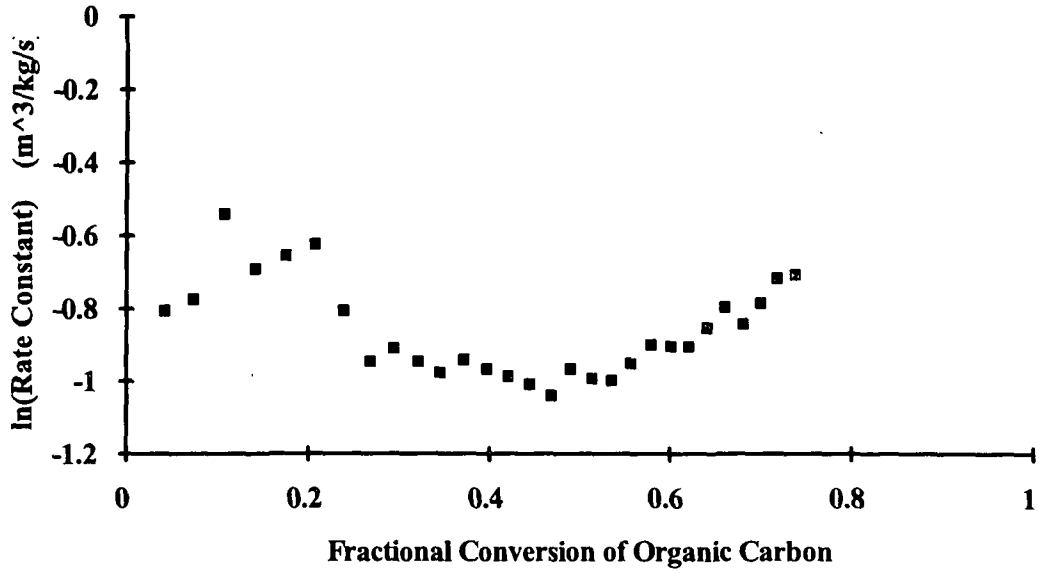


**Figure A12-13.** First Order Rate Constant vs. Fractional Burnout of Organic Carbon for Gasification Experiment 4915 (803°C, 4.9%$CO_2$, 5.4 slpm, He Carrier Gas).

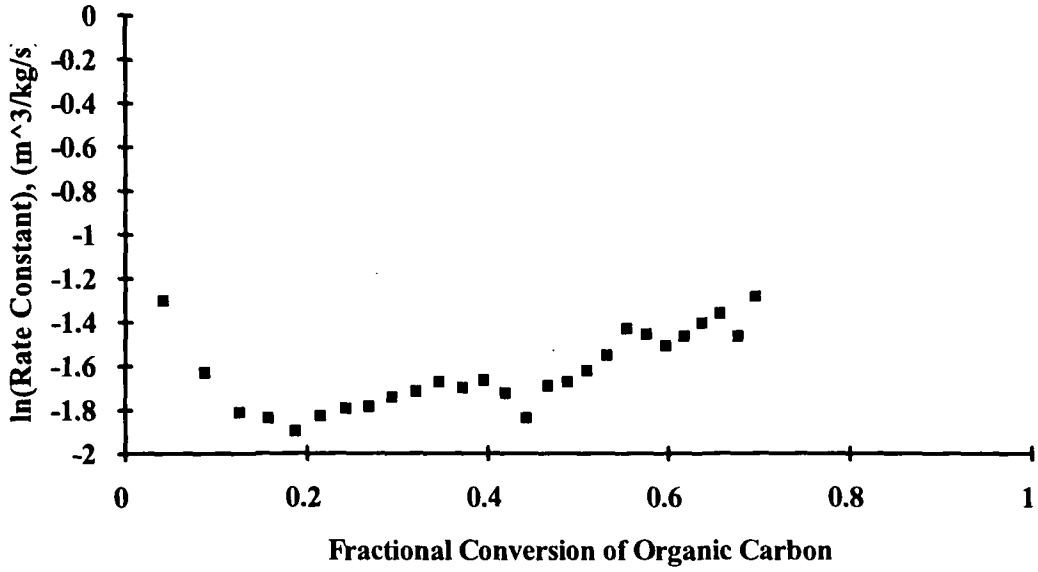


**Figure A12-14.** First Order Rate Constant vs. Fractional Burnout of Organic Carbon for Gasification Experiment 4916 (801°C, 4.7%$CO_2$, 10.6 slpm, $N_2$ Carrier Gas).

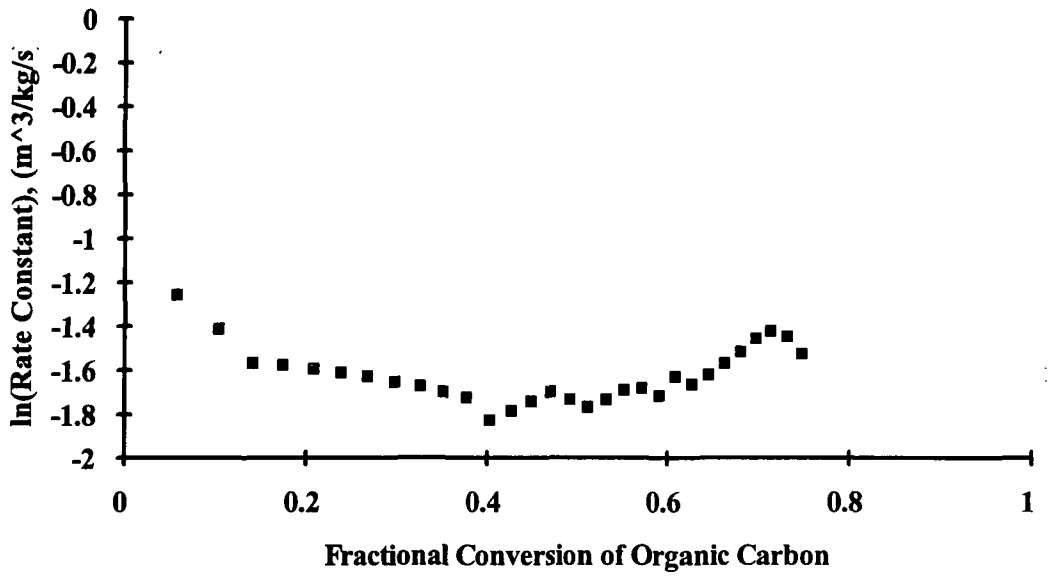


**Figure A12-15.** First Order Rate Constant vs. Fractional Burnout of Organic Carbon for Gasification Experiment 4917 (805°C, 4.8%$CO_2$, 10.6 slpm, $N_2$ Carrier Gas).

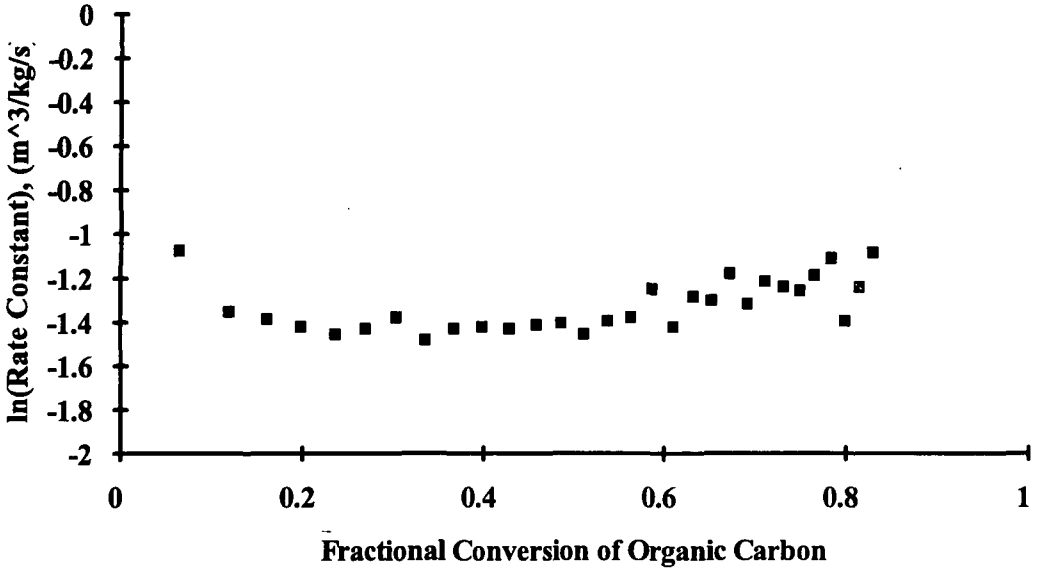


**Figure A12-16.** First Order Rate Constant vs. Fractional Burnout of Organic Carbon for Gasification Experiment 4918 (803°C, 4.7%$CO_2$, 10.6 slpm, $N_2$ Carrier Gas).

APPENDIX XIII. RATE CONSTANT PROFILES FOR $CO_2$ GASIFICATION OF KRAFT BLACK LIQUOR CHAR PREPARED ACCORDING TO THE MAXIMUM TEMPERATURE PREHEAT PROCEDURE

Figs. A13-1-A13-14are the complete sets Rate Constant profiles recorded at the various experimental conditions outlined in Table 7.

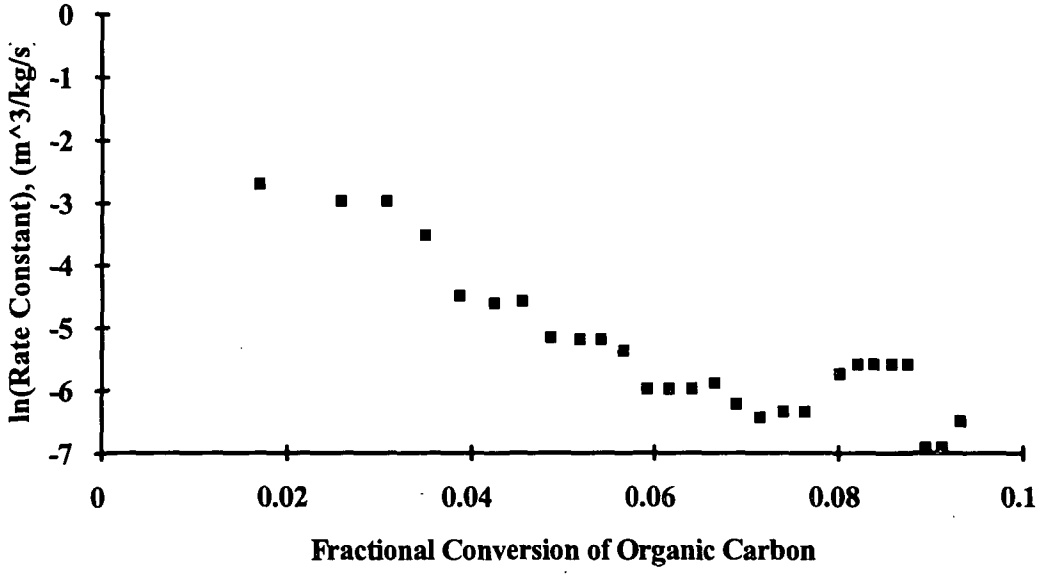


**Figure A13-1.** First Order Rate Constant vs. Fractional Burnout of Organic Carbon for Gasification Experiment 4979 (604°C, 4.8%$CO_2$, 5.4 slpm, $N_2$ Carrier Gas).

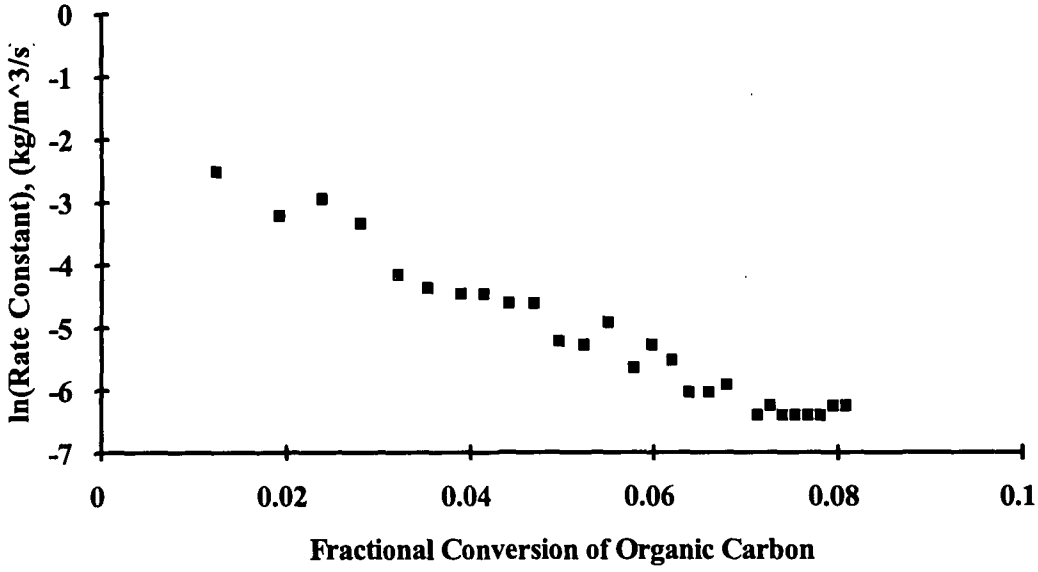


**Figure A13-2.** First Order Rate Constant vs. Fractional Burnout of Organic Carbon for Gasification Experiment 4982 (602°C, 4.7%$CO_2$, 5.5 slpm, $N_2$ Carrier Gas).

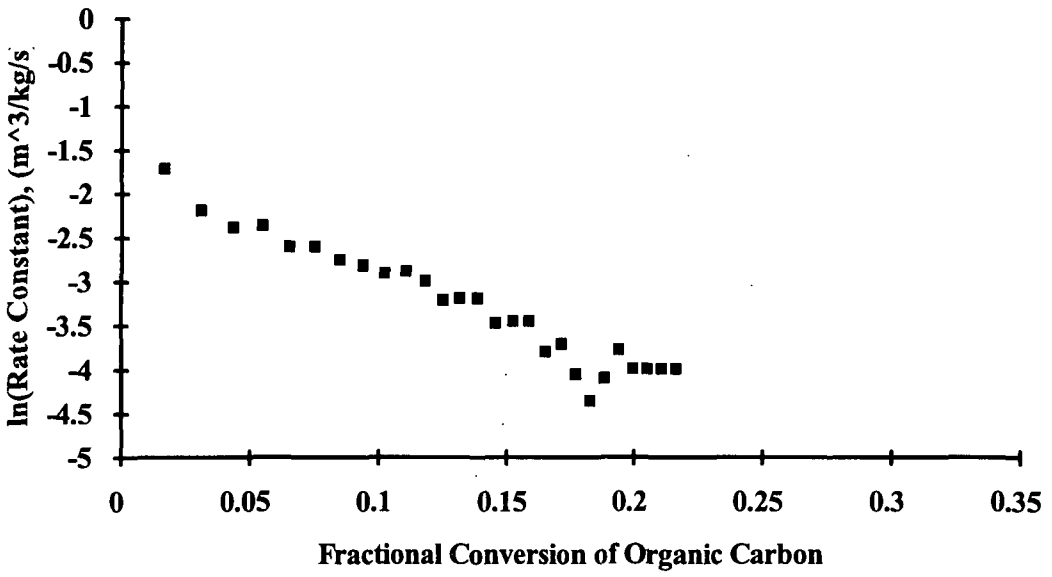


**Figure A13-3.** First Order Rate Constant vs. Fractional Burnout of Organic Carbon for Gasification Experiment 4972 (712°C, 4.8%$CO_2$, 5.5 slpm, $N_2$ Carrier Gas).

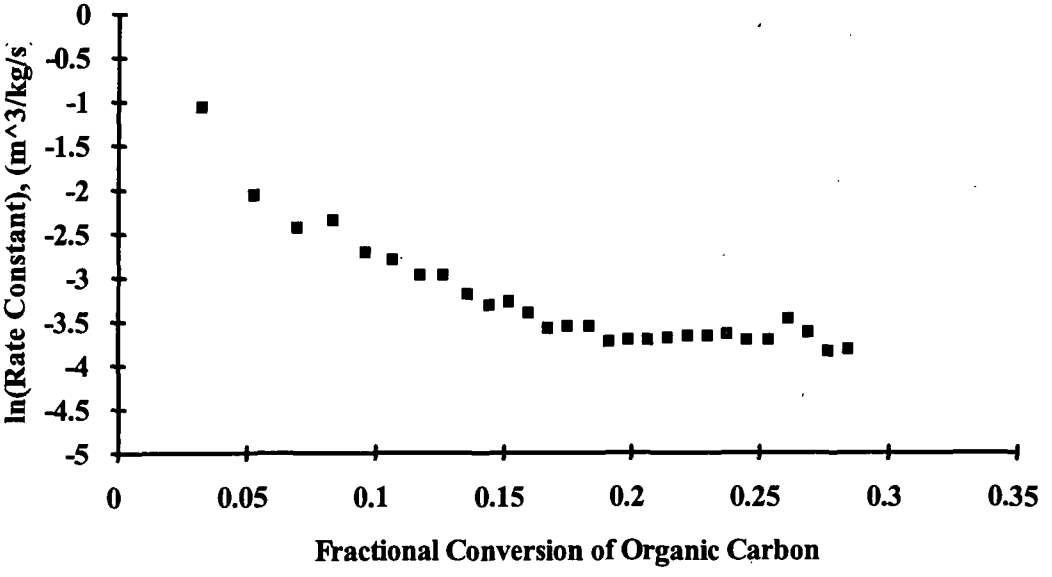


**Figure A13-4.** First Order Rate Constant vs. Fractional Burnout of Organic Carbon for Gasification Experiment 4973 (712°C, 4.8%$CO_2$, 5.5 slpm, $N_2$ Carrier Gas).

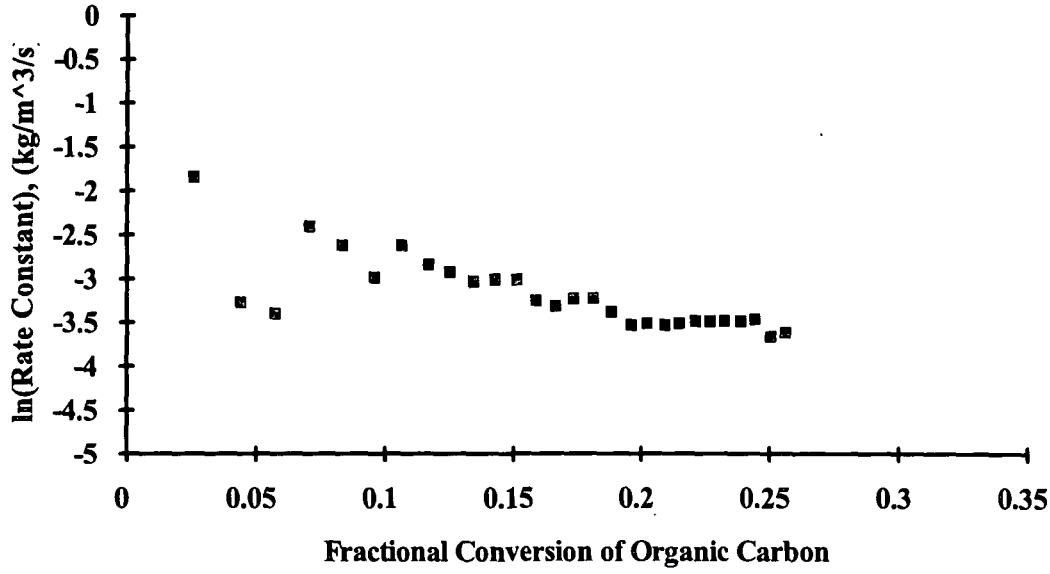


**Figure A13-5.** First Order Rate Constant vs. Fractional Burnout of Organic Carbon for Gasification Experiment 4975 (699°C, 4.8%$CO_2$, 5.4 slpm, $N_2$ Carrier Gas).

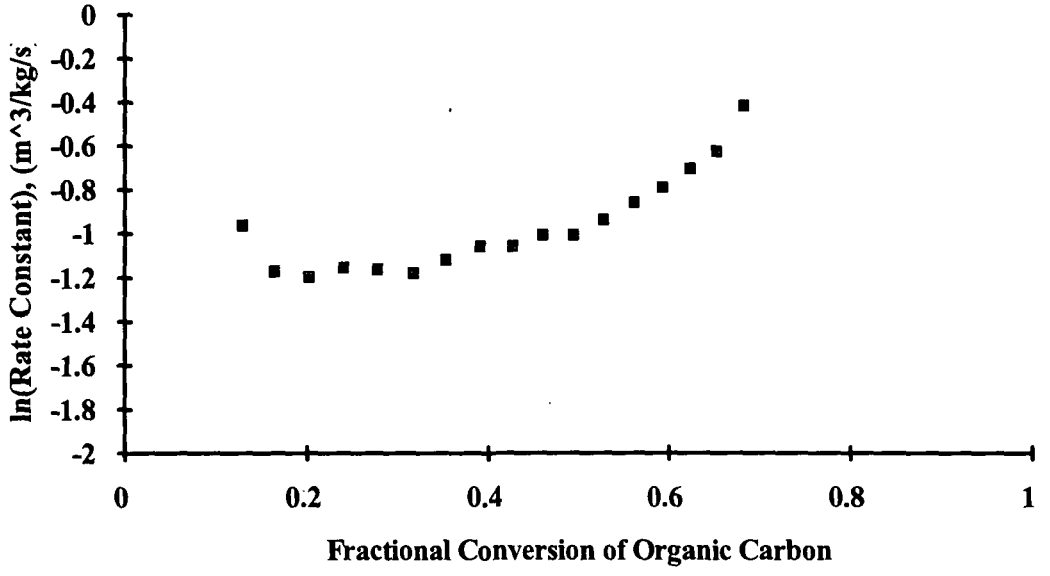


**Figure A13-6.** First Order Rate Constant vs. Fractional Burnout of Organic Carbon for Gasification Experiment 4976 (799°C, 4.8%$CO_2$, 5.5 slpm, $N_2$ Carrier Gas).

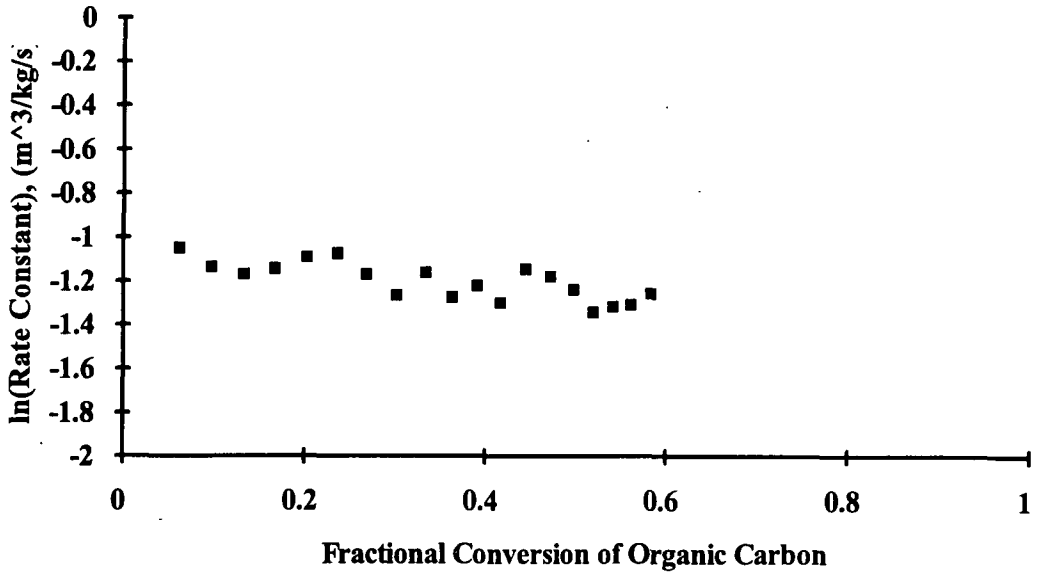


**Figure A13-7.** First Order Rate Constant vs. Fractional Burnout of Organic Carbon for Gasification Experiment 4977 (795°C, 4.8%$CO_2$, 5.5 slpm, $N_2$ Carrier Gas).

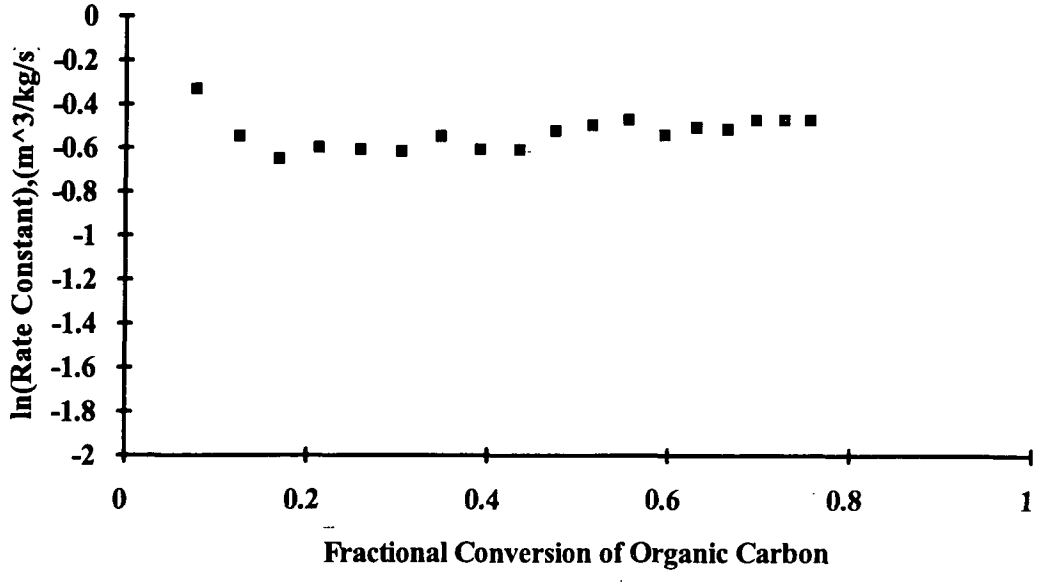


**Figure A13-8.** First Order Rate Constant vs. Fractional Burnout of Organic Carbon for Gasification Experiment 4989 (801°C, 5.1%$CO_2$, 5.2 slpm, $N_2$ Carrier Gas).

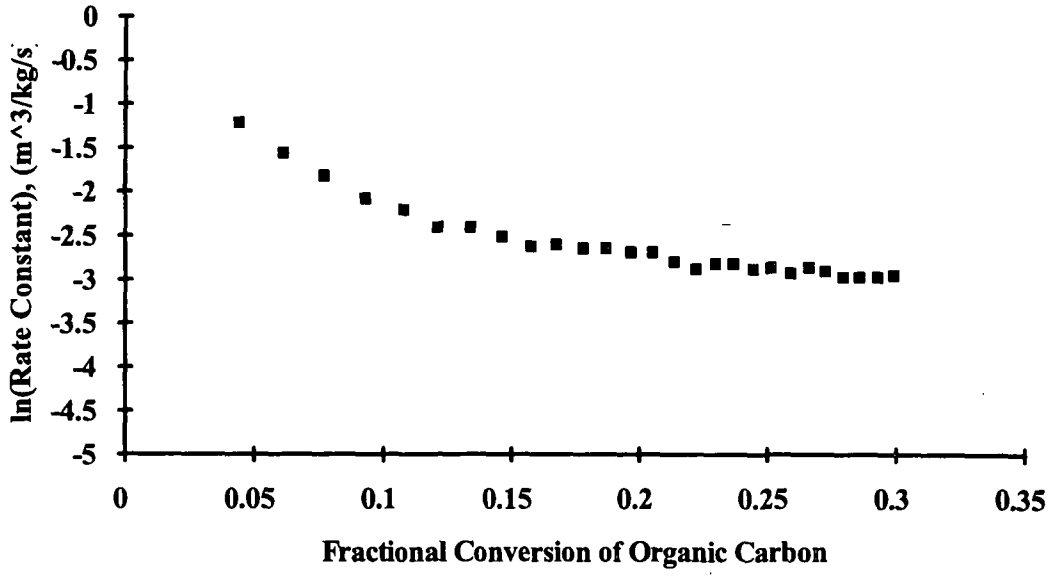


**Figure A13-9.** First Order Rate Constant vs. Fractional Burnout of Organic Carbon for Gasification Experiment 4985 (696°C, 4.8%$CO_2$, 2.7 slpm, $N_2$ Carrier Gas).

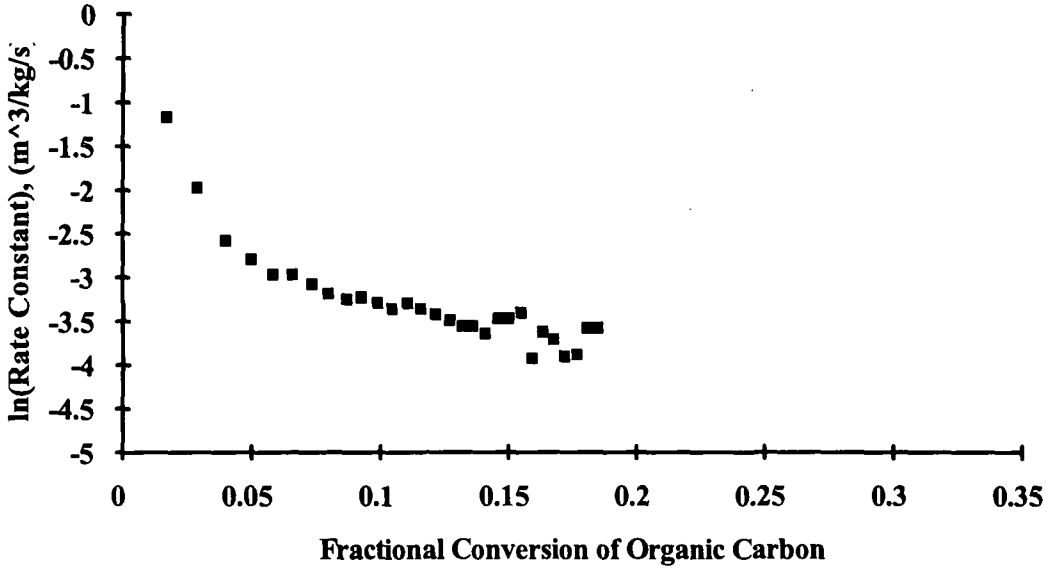


**Figure A13-10.** First Order Rate Constant vs. Fractional Burnout of Organic Carbon for Gasification Experiment 4990 (699°C, 5.1%$CO_2$, 2.6 slpm, $N_2$ Carrier Gas).

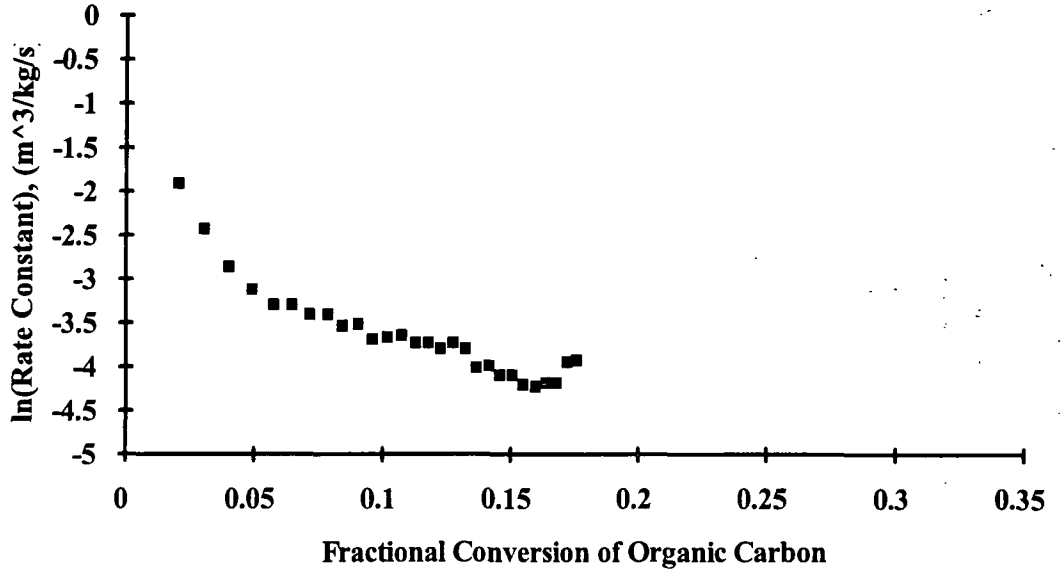


**Figure A13-11.** First Order Rate Constant vs. Fractional Burnout of Organic Carbon for Gasification Experiment 4991 (693°C, 5.1%$CO_2$, 2.7 slpm, $N_2$ Carrier Gas).

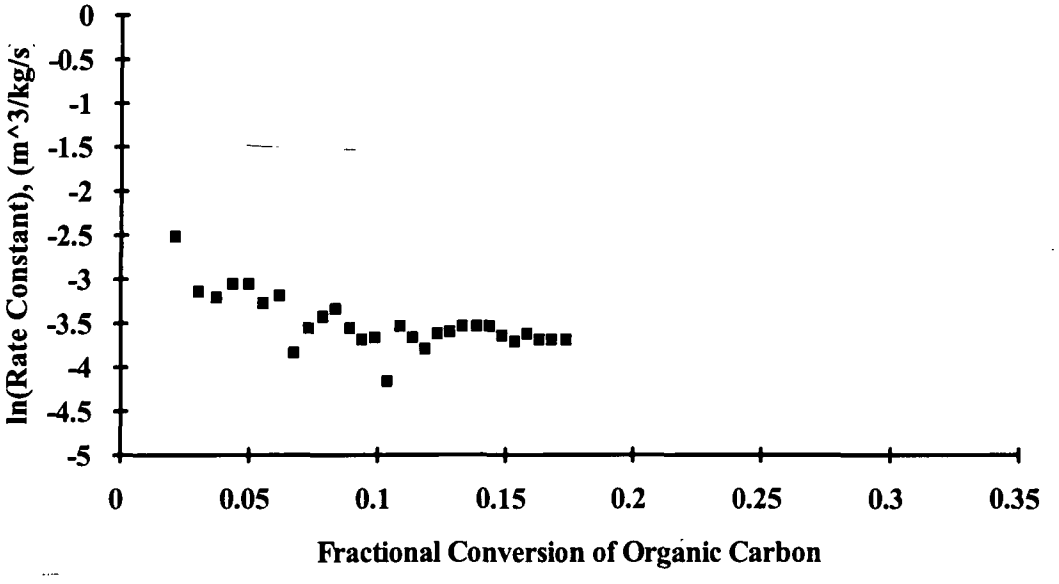


**Figure A13-12.** First Order Rate Constant vs. Fractional Burnout of Organic Carbon for Gasification Experiment 4974 (697°C, 5.0%$CO_2$, 5.3 slpm, $N_2$ Carrier Gas).

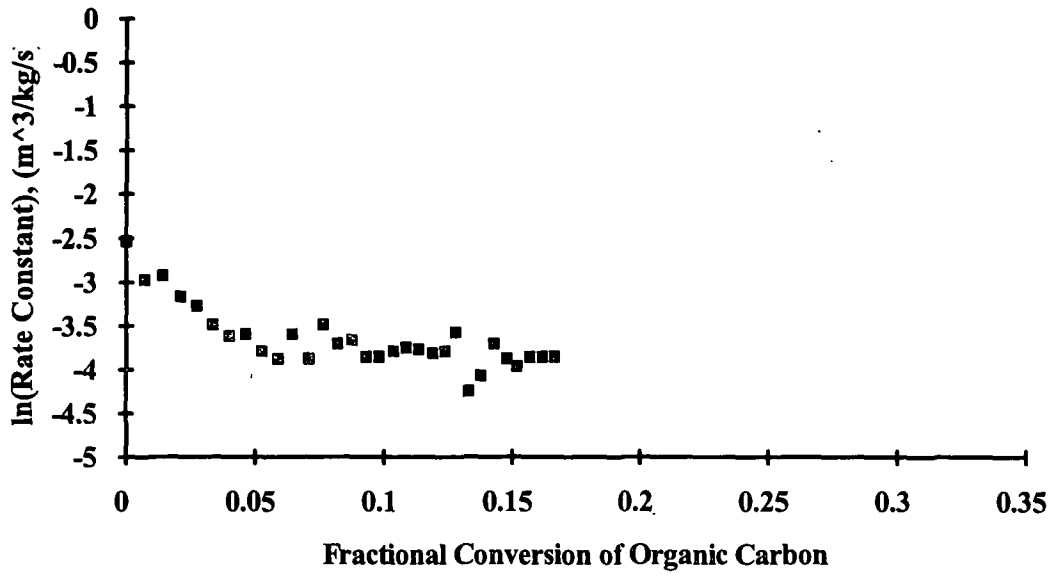


**Figure A13-13.** First Order Rate Constant vs. Fractional Burnout of Organic Carbon for Gasification Experiment 4983 (698°C, 4.8%$CO_2$, 5.5 slpm, He Carrier Gas).

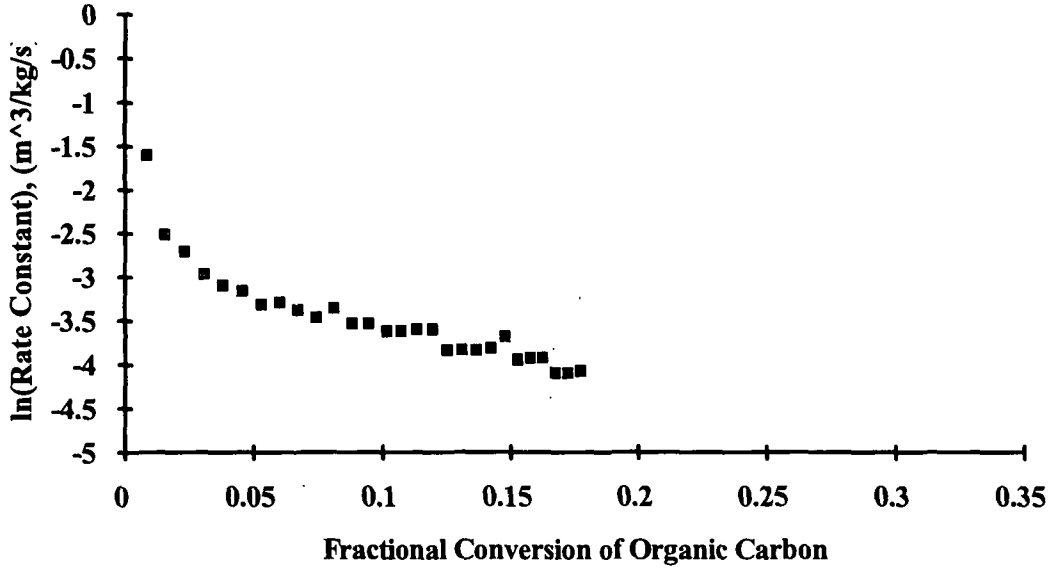


**Figure A13-14.** First Order Rate Constant vs. Fractional Burnout of Organic Carbon for Gasification Experiment 4984 (699°C, 4.9%$CO_2$, 5.4 slpm, He Carrier Gas).

# APPENDIX XIV: UNCERTAINTY ANALYSIS

The degree of certainty associated with the parameters derived from the experimental data is determined. The ASME measurement uncertainty methodology[109] is employed for this analysis. Rudemiller's[110] Ph.D. dissertation also proved to be a reliable source.

Since no measurement is perfectly accurate, means for describing inaccuracies are necessary. The appropriate concept for expressing inaccuracies is an "uncertainty", the value of which is determined by "uncertainty analysis". Inaccuracies are composed of a bias error component (systematic error which is considered to remain constant during a given test) and a precision error component (random error). The error in measurement is the difference between the true value and the recorded value, and uncertainty is the possible value that the error might assume in a given experiment; thus, error is a fixed number, and uncertainty is a statistical variable. In essence, the value reported for a measurement describes the central tendency, usually in terms of a parameter associated with a stated probability level, such as the standard deviation.

## The Method of Determining Uncertainty

The accuracy of a given number will depend on the accuracy of the data used to generate the number. For instance, the accuracy of the rate constant calculated from the thermocouple readings, gas analyzer readings, gas flow meter readings, and mass balance readings depends on the extent to which inaccuracies in these measured parameters are propagated through the calculations. To maximize accuracy of the dependent parameter, the error components of the measurements must be minimized. Bias error can be eliminated by calibration of the measuring instruments, and precision error can be minimized statistically by taking a number of measurements of the same parameter. Thus, attention to the error components of measured data ensures acceptable accuracy of the final calculated data.

Errors in measurements of various parameters (P) are propagated into a derived result (r) through the functional relationship between the result and its independent parameters. The relationship provides the sensitivity factors ($\theta_i$), which indicate the error propagated to the result because of unit error in the parameter. Thus if

$$r = f(P_1, P_2 \ldots\ldots P_j) \qquad \text{eqn. A14-1}$$

where J is the number of parameters involved, then

$$\theta_i = \frac{\partial r}{\partial P_i}. \qquad \text{eqn. A14-2}$$

The bias and precision errors of the parameters are kept separate until the last step of computing the uncertainty of a result. Thus, the precision index of a result is given by

$$S_r = \left[ \sum_{i=1}^{j} (\theta_i S_{P_i})^2 \right]^{\frac{1}{2}} \qquad \text{eqn. A14-3}$$

and the bias limit of a result is given by

$$B_r = \left[ \sum (\theta_i B_{P_i})^2 \right]^{\frac{1}{2}}. \qquad \text{eqn. A14-4}$$

The precision index ($S_{P_i}$) of an independent parameter can be reduced further to the statistical expression of standard deviation (S) of a number of readings (N),

$$S_{p_i} = \frac{S}{\sqrt{N}}. \qquad \text{eqn. A14-5}$$

The bias error is the systematic error which is considered to remain constant during a given test. Thus, in repeated measurements of a given set, each measurement has the same bias. There is no statistical equation to define the bias limit, B. Instead, it must be estimated, and this is not an easy matter since the

true value is not known. Calibrations help, as does a comparison of measurements by independent methods, but in general the estimate of bias must be based on judgement.

If a single number ($U$) is needed to express a reasonable limit of error for a given parameter, then some model for combining the bias and precision errors must be adopted, where the interval

$$\bar{X} \pm U \qquad \text{eqn. A14-6}$$

represents a band within which the true value of the parameter is expected to lie, for a specified coverage.

While no rigorous confidence level can be associated with the uncertainty ($U$), coverages analogous to the 95 percent and 99 percent confidence levels can be given for the two recommended uncertainty models. Thus

$$U_{r_{ADD}} = B_r + tS_r \ @99\% \qquad \text{eqn. A14-7}$$

and

$$U_{r_{RSS}} = [B_r^2 + (tS_r^2)]^{\frac{1}{2}} \ @95\%. \qquad \text{eqn. A14-8}$$

The Student $t$ value is a function of the degrees of freedom used in calculating $S_r$.

Tables A14-1-A14-3 list the functional relationships used to determine the derived parameters from the same experimental data. Also listed are the sensitivity factor equations used in eqns. A14-2, A14-3, and A14-4 to determine the propogated error components of the independent parameters.

Table A14-4 lists the magnitude of uncertainty, and the precision and bias indices used for each independent parameter. The values of the bias indices are subjectively selected based on experience with the experiments. The magnitude of uncertainty for each of the derived parameters is very small.

**Table A14-1.** The Functional Relationships and Sensitivity Factors Used in the Uncertainty Analysis for the Parameters Derived from the Experimental Data.

| Derived Parameter | Independent Parameters | Equations | Functional Relationship or Sensitivity Factors |
|---|---|---|---|
| Kinetic Rate Constant | | $k = \frac{uA}{m} \ln \frac{(C_{CO_2})_{feed}}{(C_{CO_2})_{exit}}$ | Functional Relationship |
| | Gas Velocity | $\frac{\partial k}{\partial u} = \frac{A}{m} \ln \frac{(C_{CO_2})_{feed}}{(C_{CO_2})_{exit}}$ | Sensitivity Factor |
| | Cross Sectional Area of Fixed Bed | $\frac{\partial k}{\partial A} = \frac{u}{m} \ln \frac{(C_{CO_2})_{feed}}{(C_{CO_2})_{exit}}$ | Sensitivity Factor |
| | Mass of Organic Carbon | $\frac{\partial k}{\partial m} = -\frac{uA}{m^2} \ln \frac{(C_{CO_2})_{feed}}{(C_{CO_2})_{exit}}$ | Sensitivity Factor |
| | Initial $CO_2$ Concentration | $\frac{\partial k}{\partial C_{CO_{2_{feed}}}} = \frac{uA}{m} \frac{1}{C_{CO_{2_{feed}}}}$ | Sensitivity Factor |
| | Final $CO_2$ Concentration | $\frac{\partial k}{\partial C_{CO_{2_{exit}}}} = -\frac{uA}{m} \frac{1}{C_{CO_{2_{exit}}}}$ | Sensitivity Factor |

**Table A14-2.** The Functional Relationships and Sensitivity Factors Used in the Uncertainty Analysis for the Parameters Derived from the Experimental Data.

| Derived Parameter | Independent Parameters | Equations | Functional Relationship or Sensitivity Factors |
|---|---|---|---|
| Thiele Modulus | | $M_{TM} = \frac{d_p}{6}\left[\frac{k\rho_{bed}}{\varepsilon_{bed}\varepsilon_{part}D_{AB}}\right]^{0.5}$ | Functional Relationship |
| | Char Particle Diameter | $\frac{\partial M_{TM}}{\partial d_p} = \frac{1}{6}\left[\frac{k\rho_{bed}}{\varepsilon_{bed}\varepsilon_{part}D_{AB}}\right]^{0.5}$ | Sensitivity Factor |
| | Density of Char Bed | $\frac{\partial M_{TM}}{\partial \rho_{bed}} = -\frac{d_p}{12}\left[\frac{k}{\rho_{bed}\varepsilon_{bed}\varepsilon_{part}D_{AB}}\right]^{0.5}$ | Sensitivity Factor |
| | Diffusivity of $CO_2$ through $N_2$ or He | $\frac{\partial M_{TM}}{\partial D_{AB}} = -\frac{d_p}{12D_{AB}^{1.5}}\left[\frac{k\rho_{bed}}{\varepsilon_{bed}\varepsilon_{part}}\right]^{0.5}$ | Sensitivity Factor |
| | Void Fraction of the Char Bed | $\frac{\partial M_{TM}}{\partial \varepsilon_{bed}} = -\frac{d_p}{12\varepsilon_{bed}^{1.5}}\left[\frac{k\rho_{bed}}{\varepsilon_{part}D_{AB}}\right]^{0.5}$ | Sensitivity Factor |
| | Void Fraction of the Char Particle | $\frac{\partial M_{TM}}{\partial \varepsilon_{part}} = -\frac{d_p}{12\varepsilon_{part}^{1.5}}\left[\frac{k\rho_{bed}}{\varepsilon_{bed}D_{AB}}\right]^{0.5}$ | Sensitivity Factor |
| | Rate Constant at Specified Temperature | $\frac{\partial M_{TM}}{\partial k} = \frac{d_p}{12}\left[\frac{\rho_{bed}}{k\varepsilon_{bed}\varepsilon_{part}D_{AB}}\right]^{0.5}$ | Sensitivity Factor |

**Table A14-3.** The Functional Relationships and Sensitivity Factors Used in the Uncertainty Analysis for the Parameters Derived from the Experimental Data.

| Derived Parameter | Independent Parameters | Equations | Functional Relationship or Sensitivity Factors |
|---|---|---|---|
| Mass Transfer Coefficient | | $k_m = \left(\frac{0.455}{\varepsilon_{bed}}\right)\left(\frac{ud_p\rho}{\mu}\right)^{-0.407}\left(\frac{\mu}{\rho D_{AB}}\right)^{-0.667} u$ | Functional Relationship |
| | Void Fraction of the Char Bed | $\frac{\partial k_m}{\partial \varepsilon_{bed}} = -\left(\frac{0.455}{\varepsilon_{bed}^2}\right)\left(\frac{ud_p\rho}{\mu}\right)^{-0.407}\left(\frac{\mu}{\rho D_{AB}}\right)^{-0.667} u$ | Sensitivity Factor |
| | Gas Velocity | $\frac{\partial k_m}{\partial u} = 0.593\left(\frac{0.455}{\varepsilon_{bed}}\right)\left(\frac{ud_p\rho}{\mu}\right)^{-0.407}\left(\frac{\mu}{\rho D_{AB}}\right)^{-0.667}$ | Sensitivity Factor |
| | Char Particle Diameter | $\frac{\partial k_m}{\partial d_p} = -0.407 d_p^{-1.407}\left(\frac{0.455}{\varepsilon_{bed}}\right)\left(\frac{u\rho}{\mu}\right)^{-0.407}\left(\frac{\mu}{\rho D_{AB}}\right)^{-0.667} u$ | Sensitivity Factor |
| | Gas Density | $\frac{\partial k_m}{\partial \rho} = 0.26\rho^{-0.74}\left(\frac{0.455}{\varepsilon_{bed}}\right)\left(\frac{ud_p}{\mu}\right)^{-0.407}\left(\frac{\mu}{D_{AB}}\right)^{-0.667} u$ | Sensitivity Factor |
| | Gas Viscosity | $\frac{\partial k_m}{\partial \mu} = -0.260\mu^{-1.26}\left(\frac{0.455}{\varepsilon_{bed}}\right)\left(ud_p\rho\right)^{-0.407}(\rho D_{AB})^{0.667} u$ | Sensitivity Factor |
| | Diffusivity of $CO_2$ through $N_2$ or He | $\frac{\partial k_m}{\partial D_{AB}} = 0.667 D_{AB}^{-0.333}\left(\frac{0.455}{\varepsilon_{bed}}\right)\left(\frac{ud_p\rho}{\mu}\right)^{-0.407}\left(\frac{\mu}{\rho}\right)^{-0.667} u$ | Sensitivity Factor |

**Table A14-4.** Uncertainties for the Parameters Derived from the Experimental Data.

| Derived Parameter | Independent Parameters | Value of Bias Error Indices | Value of Precision Error Indices | Uncertainty ADD (eqn. A14-7) | Uncertainty RSS (eqn. A14-8) |
|---|---|---|---|---|---|
| Kinetic Rate Constant | Gas Velocity | 7E-4m/s | 2.6E-5m/s | 0.24% | 0.16% |
| | Cross Sectional Area of Fixed Bed | 4E-4$m^2$ | 0 | | |
| | Mass of Organic Carbon | 1.0E-4kg | 0 | | |
| | Initial $CO_2$ Concentration | 2.4E-4kg/$m^3$ | 1.28E-4kg/$m^3$ | | |
| | Final $CO_2$ Concentration | 2.4E-4kg/$m^3$ | 2.9E-4kg/$m^3$ | | |
| Thiele Modulus | Char Particle Diameter | 7.0E-4m | 1.7E-4m | 0.061% | 0.045% |
| | Char Density | 2.49kg/$m^3$ | 1.02kg/$m^3$ | | |
| | Diffusivity of $CO_2$ through $N_2$ or He | 1.47E-6$m^2$/s | 0 | | |
| | Void Fraction of the Char Bed | 0.1 | 0 | | |
| | Void Fraction of the Char Particle | 0.1 | 0 | | |
| | Rate Constant at Specified Temperature | 0.04 | 0.04 | | |
| Mass Transfer Coefficient | Void Fraction of the Char Bed | 0.1 | 0 | 0.014% | 0.013% |
| | Gas Velocity | 7E-4m/s | 2.6E-5 | | |
| | Char Particle Diameter | 7E-4m | 1.7E-4 | | |
| | Gas Density | 3.3E-3kg/$m^3$ | 0 | | |
| | Gas Viscosity | 4.6E-7kg/ms | 0 | | |
| | Diffusivity of $CO_2$ through $N_2$ or He | 1.47E-6$m^2$/s | 0 | | |

APPENDIX XV. EXPERIMENTAL DATA FOR $O_2$ OXIDATION OF KRAFT BLACK LIQUOR CHAR PREPARED ACCORDING TO THE MAXIMUM TEMPERATURE PREHEAT PROCEDURE

Figs. 15-1-15-9 are the complete sets of CO, $CO_2$, and $O_2$ concentration profiles recorded at the various experimental conditions outlined in Table 8.

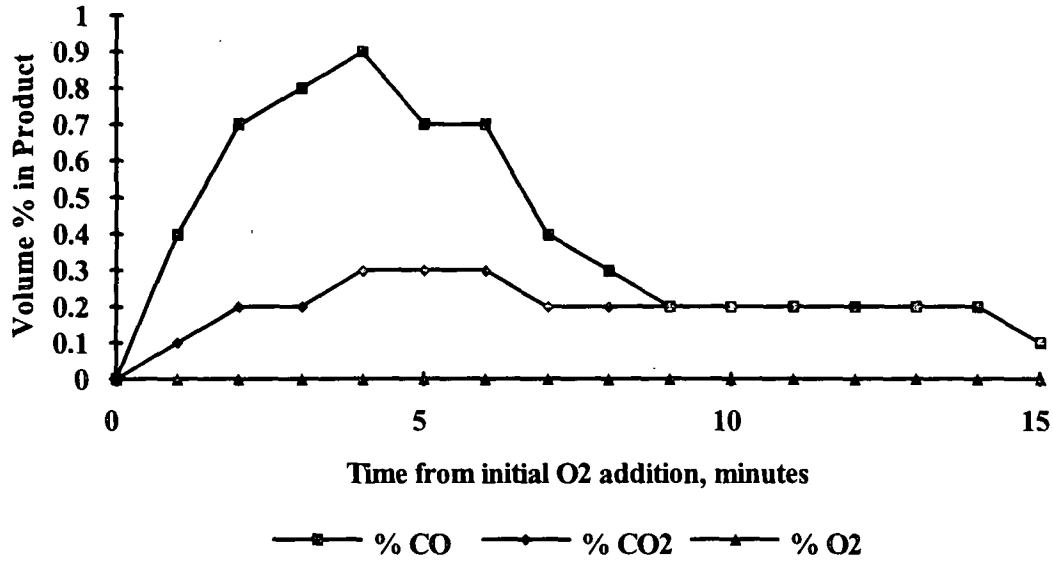


**Figure A15-1.** %CO, $\%CO_2$, and $\%O_2$ in Product Gas as a Function of Time for Combustion Experiment 4993 (694°C, 2.0%$O_2$, 5.3 slpm, $N_2$ Carrier Gas).

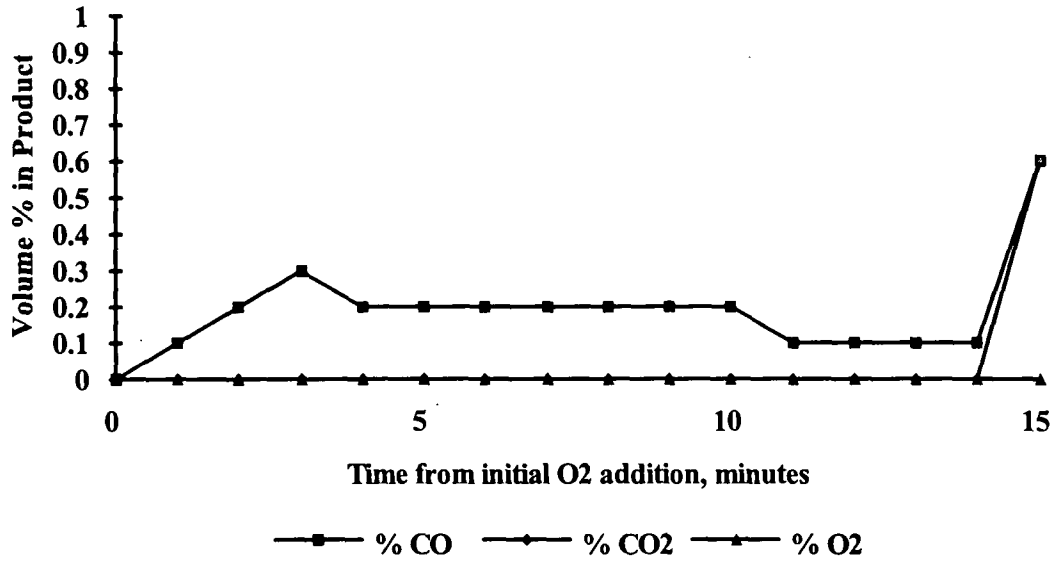


**Figure A15-2.** %CO, $\%CO_2$, and $\%O_2$ in Product Gas as a Function of Time for Combustion Experiment 4994 (703°C, 2.4%$O_2$, 5.3 slpm, $N_2$ Carrier Gas).

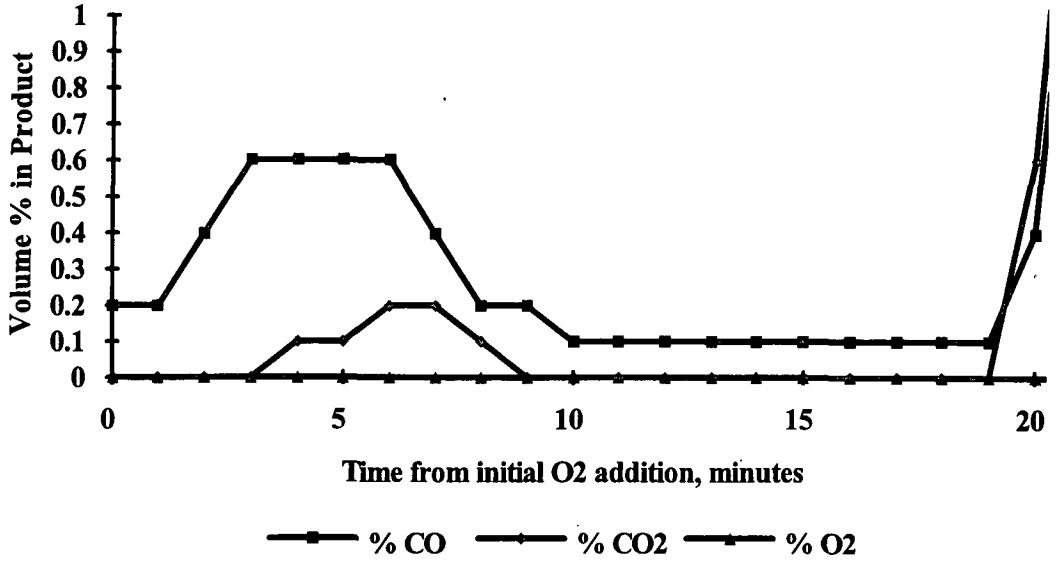


**Figure A15-3.** %CO, $\%CO_2$, and $\%O_2$ in Product Gas as a Function of Time for Combustion Experiment 5002 (702°C, 2.2%$O_2$, 5.4 slpm, $N_2$ Carrier Gas).

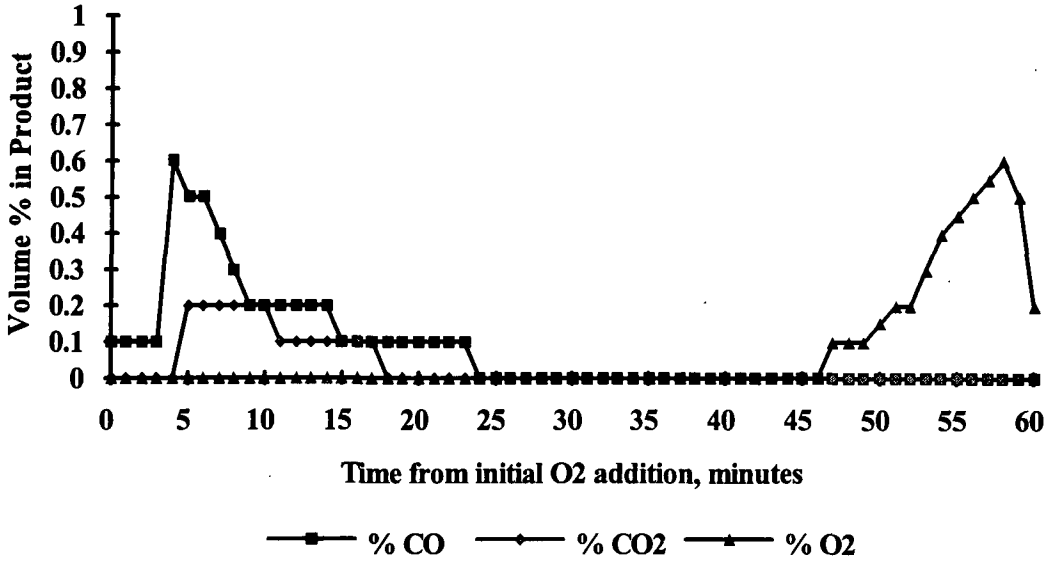


**Figure A15-4.** %CO, $\%CO_2$, and $\%O_2$ in Product Gas as a Function of Time for Combustion Experiment 5001 (696°C, 2.2%$O_2$, 5.3 slpm, $N_2$ Carrier Gas).

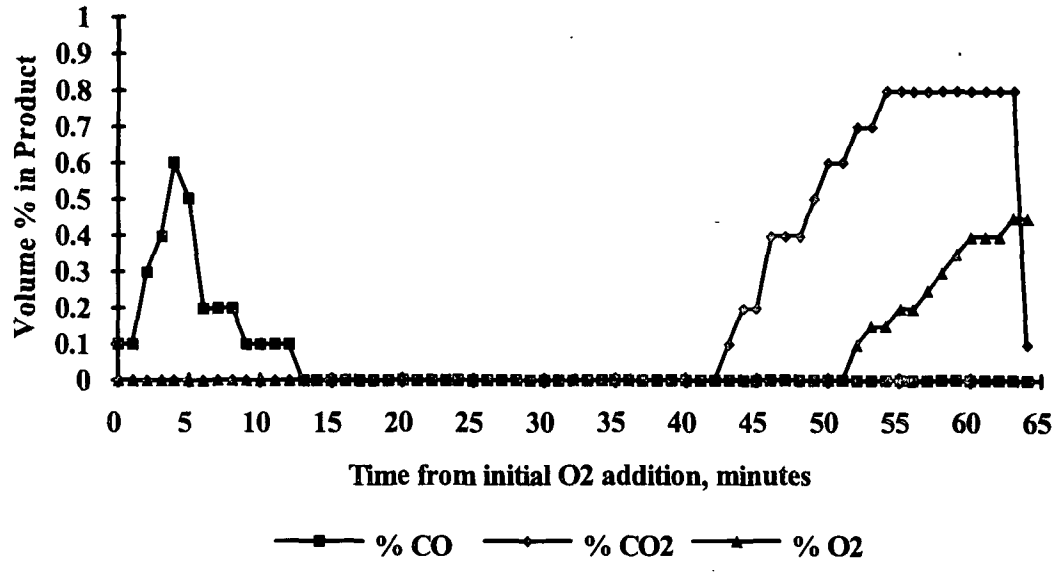


**Figure A15-5.** %CO, $\%CO_2$, and $\%O_2$ in Product Gas as a Function of Time for Combustion Experiment 4996 (704°C, 1.97%$O_2$, 5.3 slpm, $N_2$ Carrier Gas).

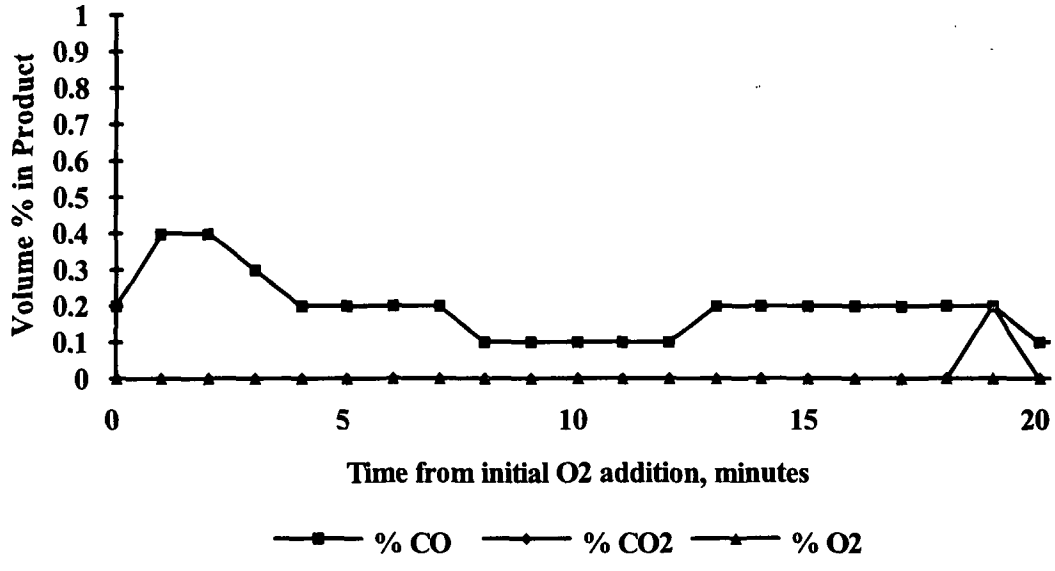


**Figure A15-6.** %CO, $\%CO_2$, and $\%O_2$ in Product Gas as a Function of Time for Combustion Experiment 4999 (698°C, 4.7%$O_2$, 5.5 slpm, $N_2$ Carrier Gas).

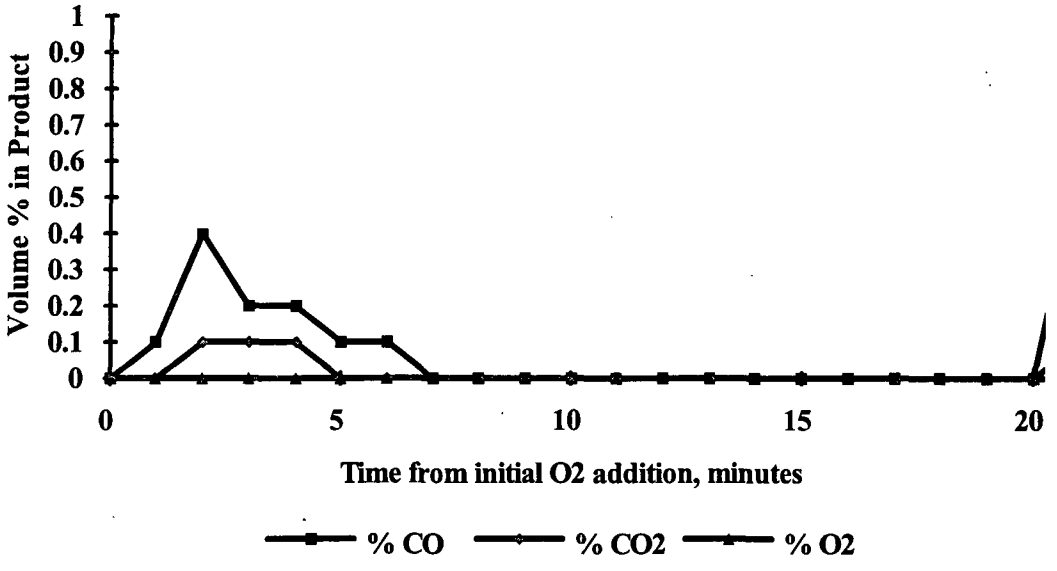


**Figure A15-7.** %CO, $\%CO_2$, and $\%O_2$ in Product Gas as a Function of Time for Combustion Experiment 5000 (697°C, 4.5%$O_2$, 5.4 slpm, $N_2$ Carrier Gas).

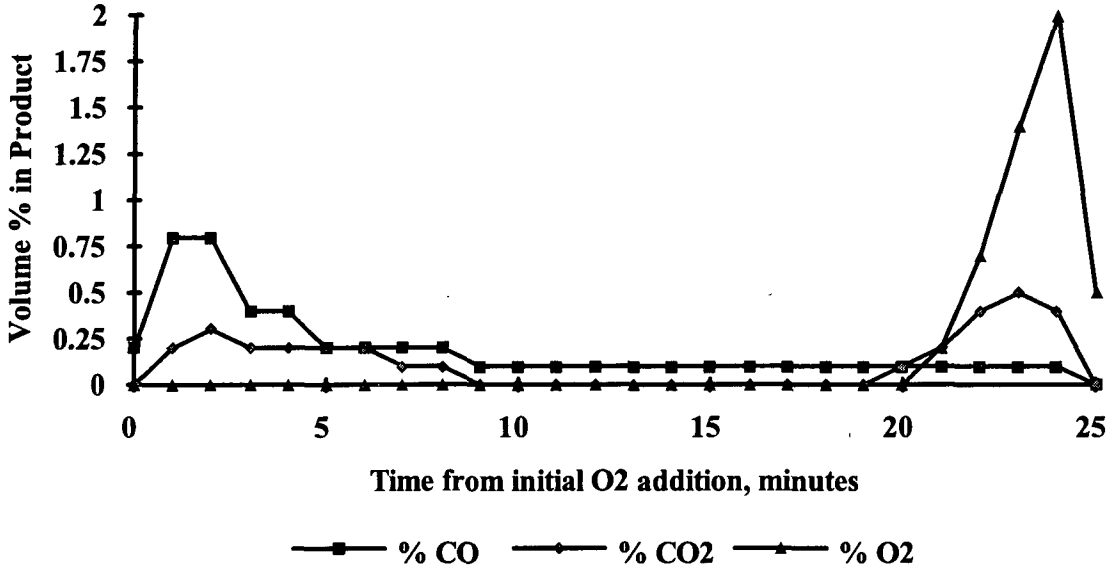


**Figure A15-8.** %CO, $\%CO_2$, and $\%O_2$ in Product Gas as a Function of Time for Combustion Experiment 4998 (709°C, 4.6%$O_2$, 5.5 slpm, $N_2$ Carrier Gas).

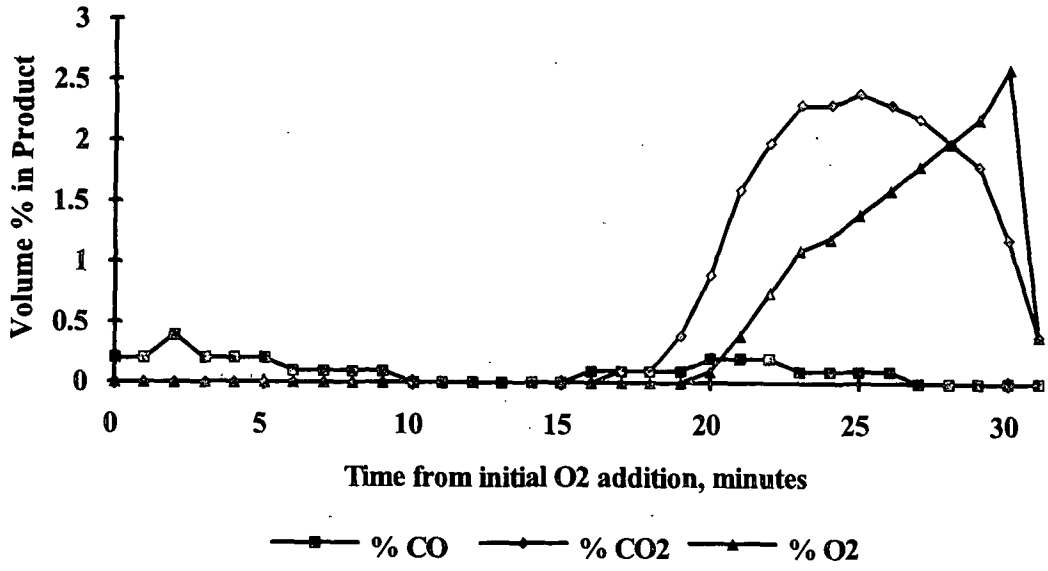


**Figure A15-9.** %CO, $\%CO_2$, and $\%O_2$ in Product Gas as a Function of Time for Combustion Experiment 4997 (697°C, $4.6\%O_2$, 5.4 slpm, $N_2$ Carrier Gas).

APPENDIX XVI: EXPERIMENTAL DATA FOR COMBINATION OXIDATION/GASIFICATION OF KRAFT BLACK LIQUOR CHAR PREPARED ACCORDING TO THE MAXIMUM TEMPERATURE PREHEAT PROCEDURE

Figs. A16-1-A16-5 are the complete sets of CO, $CO_2$, and $O_2$ concentration profiles recorded at the various experimental conditions outlined in Table 9.

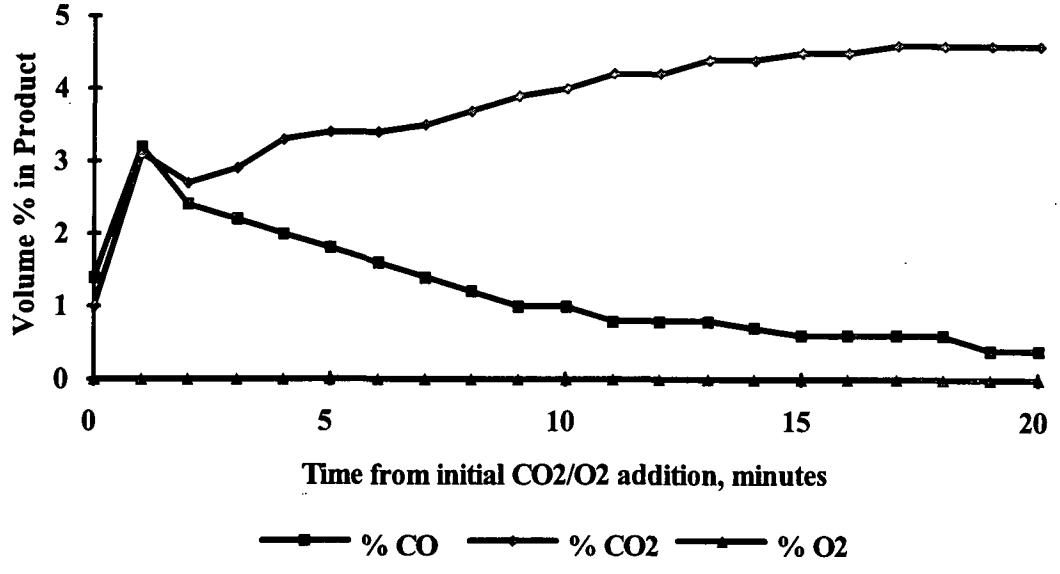


**Figure A16-1.** %CO, %$CO_2$, and %$O_2$ in Product Gas as a Function of Time for Oxidation Experiment 5006 (701°C, 2.0%$O_2$, 5.0%$CO_2$, 5.4 slpm, $N_2$ Carrier Gas).

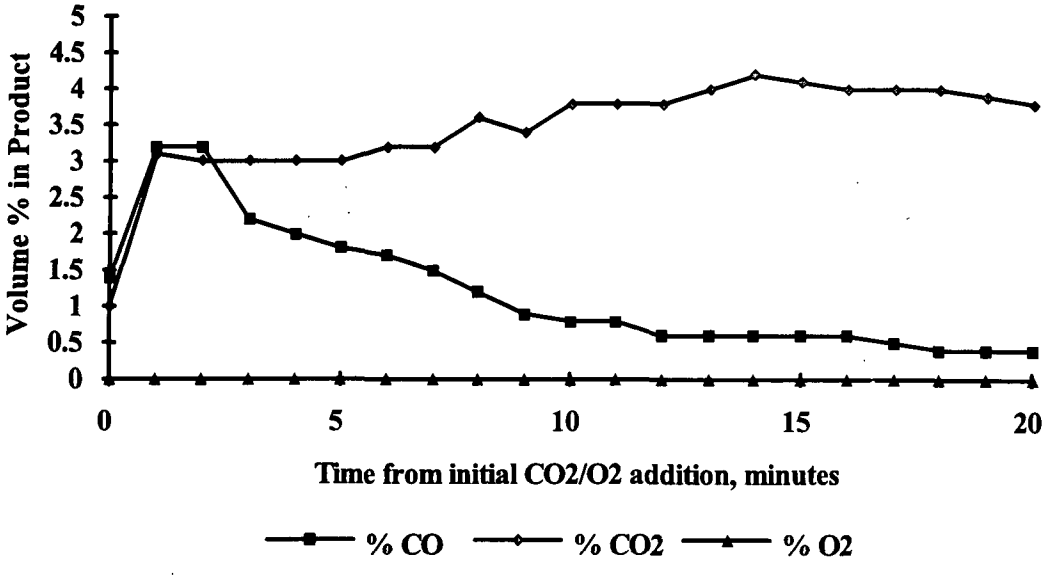


**Figure A16-2.** %CO, %$CO_2$, and %$O_2$ in Product Gas as a Function of Time for Oxidation Experiment 5008 (700°C, 2.2%$O_2$,4.9 % $CO_2$, 5.6 slpm, $N_2$ Carrier Gas).

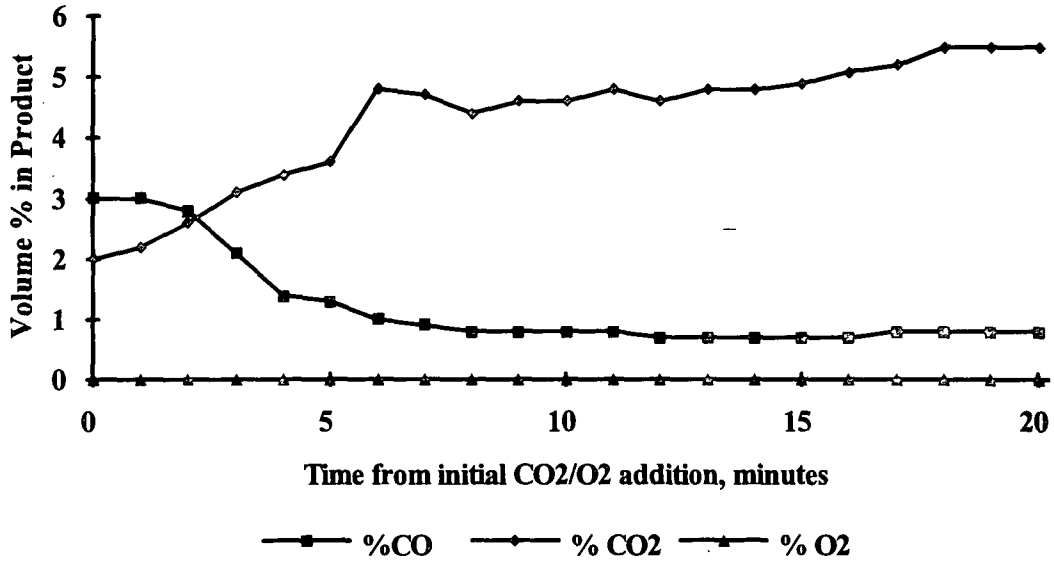


**Figure A16-3.** %CO, $\%CO_2$, and $\%O_2$ in Product Gas as a Function of Time for Oxidation Experiment 5003 (711°C, $4.9\%O_2$, 4.9 % $CO_2$, 5.3 slpm, $N_2$ Carrier Gas).

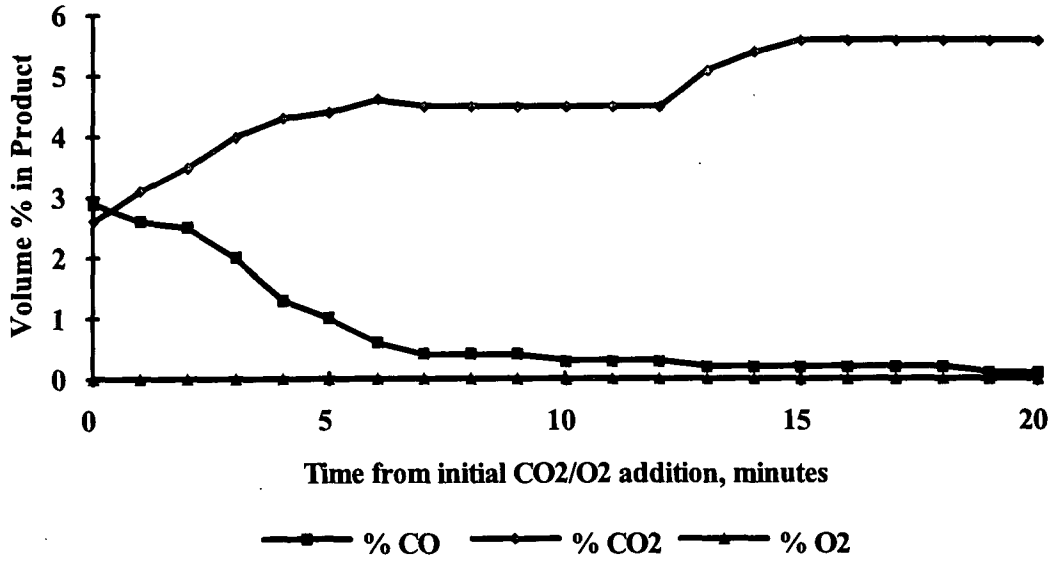


**Figure A16-4.** %CO, $\%CO_2$, and $\%O_2$ in Product Gas as a Function of Time for Oxidation Experiment 5004 (708°C, $4.8\%O_2$, 4.8 $CO_2$, 5.4 slpm, $N_2$ Carrier Gas).

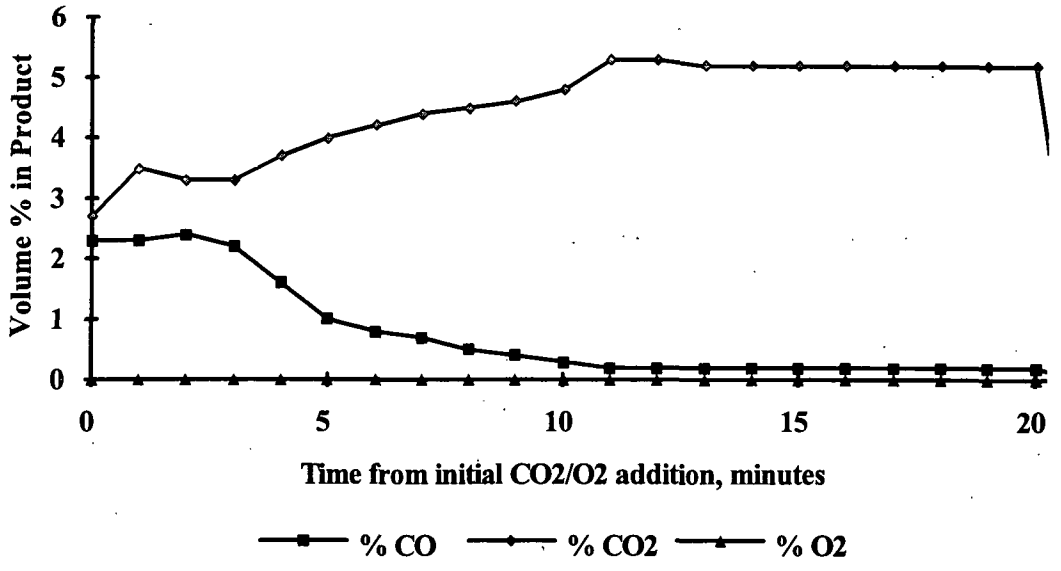


**Figure A16-5.** %CO, $\%CO_2$, and $\%O_2$ in Product Gas as a Function of Time for Oxidation Experiment 5005 (706°C, 4.7%$O_2$, 4.9% $CO_2$, 5.5 slpm, $N_2$ Carrier Gas).

## ADDITIONAL LITERATURE CITED


105. Laun, L.F. The Dictionary of Paper. Fourth Edition. The American Paper Institute, New York, New York (1980).

106. Swalin, R.A. Thermodynamics of Solids. John Wiley & Sons, New York, New York, pp. 104-118 (1972).

107. Snoeyink, V.L.; and Jenkins, D. Water Chemistry. John Wiley & Sons, New York, New York, pp. 60-71 (1980).

108. Outokumpu HSC Chemistry for Windows. Chemical Reaction and Equilibrium Software with extensive Thermochemical Database. Version 1.10. 1993.

109. Abernethy, R.B.; Benedict, R.P.; and Dowdell, R.B. ASME Measurement Uncertainty. Journal of Fluids Engineering 107(6):161-164(1985).

110. Rudemiller, G.R. A Fundamental Study of Boiling Heat Transfer Mechanisms Related to Impulse Drying. Doctoral Dissertation. Atlanta, GA, The Institute of Paper Science and Technology, 1989.